A CONTINUOUS-TIME FORMULATION FOR SPATIAL CAPTURE-RECAPTURE MODELS

Greg Distiller

A Thesis Submitted for the Degree of PhD
at the
University of St Andrews

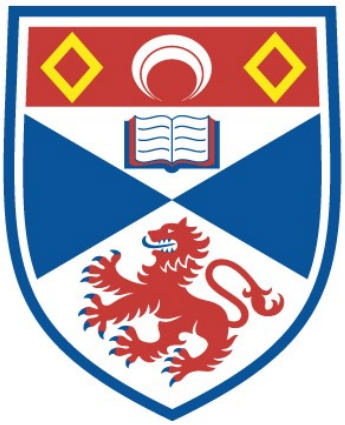

2017

A Continuous-Time Formulation for Spatial Capture-Recapture Models

Greg Distiller

A thesis presented for the degree of
Doctor of Philosophy

University of
St Andrews

FOUNDED
1413

[1] Department of Statistical Sciences
Statistics in Ecology, Environment and Conservation (SEEC)
University of Cape Town, South Africa

[2] School of Mathematics and Statistics
Centre for Research into Ecological and Environmental Modelling (CREEM)
University of St Andrews, United Kingdom

December 2, 2016

1. **Candidate's declarations:**

I, G B Distiller hereby certify that this thesis, which is approximately 44,000 words in length, has been written by me, and that it is the record of work carried out by me, or principally by myself in collaboration with others as acknowledged, and that it has not been submitted in any previous application for a higher degree.

I was admitted as a research student in January, 2012 and as a candidate for the degree of Doctor of Philosophy in January 2013; the higher study for which this is a record was carried out in the University of St Andrews and the University of Cape Town between 2013 and 2016.

Date: 9th June 2017 signature of candidate

2. **Supervisor's declaration:**

I hereby certify that the candidate has fulfilled the conditions of the Resolution and Regulations appropriate for the degree of Doctor of Philosophy in the University of St Andrews and that the candidate is qualified to submit this thesis in application for that degree.

Date 9th June 2017 signature of supervisor

3. **Permission for publication:** (*to be signed by both candidate and supervisor*)

In submitting this thesis to the University of St Andrews I understand that I am giving permission for it to be made available for use in accordance with the regulations of the University Library for the time being in force, subject to any copyright vested in the work not being affected thereby. I also understand that the title and the abstract will be published, and that a copy of the work may be made and supplied to any bona fide library or research worker, that my thesis will be electronically accessible for personal or research use unless exempt by award of an embargo as requested below, and that the library has the right to migrate my thesis into new electronic forms as required to ensure continued access to the thesis. I have obtained any third-party copyright permissions that may be required in order to allow such access and migration, or have requested the appropriate embargo below.

The following is an agreed request by candidate and supervisor regarding the publication of this thesis:

PRINTED COPY
a) No embargo on print copy

ELECTRONIC COPY
a) No embargo on electronic copy

ABSTRACT AND TITLE EMBARGOES

An embargo on the full text copy of your thesis in the electronic and printed formats will be granted automatically in the first instance. This embargo includes the abstract and title except that the title will be used in the graduation booklet.

If you have selected an embargo option indicate below if you wish to allow the thesis abstract and/or title to be published. If you do not complete the section below the title and abstract will remain embargoed along with the text of the thesis.

a)	I agree to the title and abstract being published	YES
b)	I require an embargo on abstract	NO
c)	I require an embargo on title	NO

Date 9th June 2017 signature of candidate signature of supervisor

Please note initial embargos can be requested for a maximum of five years. An embargo on a thesis submitted to the Faculty of Science or Medicine is rarely granted for more than two years in the first instance, without good justification. The Library will not lift an embargo before confirming with the student and supervisor that they do not intend to request a continuation. In the absence of an agreed response from both student and supervisor, the Head of School will be consulted. Please note that the total period of an embargo, including any continuation, is not expected to exceed ten years.
Where part of a thesis is to be embargoed, please specify the part and the reason.

A Continuous-Time Formulation for Spatial Capture-Recapture Models

Greg Distiller

Abstract

Spatial capture-recapture (SCR) models are relatively new but have become the standard approach used to estimate animal density from capture-recapture data. It has in the past been impractical to obtain sufficient data for analysis on species that are very difficult to capture such as elusive carnivores that occur at low density and range very widely. Advances in technology have led to alternative ways to virtually "capture" individuals without having to physically hold them. Some examples of these new non-invasive sampling methods include scat or hair collection for genetic analysis, acoustic detection and camera trapping.

In traditional capture-recapture (CR) and SCR studies populations are sampled at discrete points in time leading to clear and well defined occasions whereas the new detector types mentioned above sample populations continuously in time. Researchers with data collected continuously currently need to define an appropriate occasion and aggregate their data accordingly thereby imposing an artificial construct on their data for analytical convenience.

This research develops a continuous-time (CT) framework for SCR models by treating detections as a temporal non homogeneous Poisson process (NHPP) and replacing the usual SCR detection function with a continuous detection hazard function. The general CT likelihood is first developed for data from passive (also called "proximity") detectors like camera traps that do not physically hold individuals. The likelihood is then modified to produce a likelihood for single-catch traps (traps that are taken out of action by capturing an animal) that has proven difficult to develop with a discrete-occasion approach.

The lack of a suitable single-catch trap likelihood has led to researchers using a discrete-time (DT) multi-catch trap estimator to analyse single-catch trap data. Previous work has found the DT multi-catch estimator to be robust despite the fact that it is known to be based on the wrong model for single-catch traps (it assumes that the traps continue operating after catching an individual). Simulation studies in this work confirm that the multi-catch estimator is robust for estimating density when density is constant or does not vary much in space. However, there are scenarios with

non-constant density surfaces when the multi-catch estimator is not able to correctly identify regions of high density. Furthermore, the multi-catch estimator is known to be negatively biased for the intercept parameter of SCR detection functions and there may be interest in the detection function in its own right. On the other hand the CT single-catch estimator is unbiased or nearly so for all parameters of interest including those in the detection function and those in the model for density.

When one assumes that the detection hazard is constant through time there is no impact of ignoring capture times and using only the detection frequencies. This is of course a special case and in reality detection hazards will tend to vary in time. However when one assumes that the effects of time and distance in the time-varying hazard are independent, then similarly there is no information in the capture times about density and detection function parameters. The work here uses a detection hazard that assumes independence between time and distance. Different forms for the detection hazard are explored with the most flexible choice being that of a cyclic regression spline.

Extensive simulation studies suggest as expected that a DT proximity estimator is unbiased for the estimation of density even when the detection hazard varies though time. However there are indirect benefits of incorporating capture times because doing so will lead to a better fitting detection component of the model, and this can prevent unexplained variation being erroneously attributed to the wrong covariate. The analysis of two real datasets supports this assertion because the models with the best fitting detection hazard have different effects to the other models. In addition, modelling the detection process in continuous-time leads to a more parsimonious approach compared to using DT models when the detection hazard varies in time.

The underlying process is occurring in continuous-time and so using CT models allows inferences to be drawn about the underlying process, for example the time-varying detection hazard can be viewed as a proxy for animal activity. The CT formulation is able to model the underlying detection hazard accurately and provides a formal modelling framework to explore different hypotheses about activity patterns. There is scope to integrate the CT models developed here with models for space usage and landscape connectivity to explore these processes on a finer temporal scale.

SCR models are experiencing a rapid growth in both application and method development. The data generating process occurs in CT and hence a CT modelling approach is a natural fit and opens up several opportunities that are not possible with a DT formulation. The work here makes a contribution by developing and exploring the utility of such a CT SCR formulation.

Publications resulting from this PhD dissertation

- Distiller, G. and Borchers, D. (2015) *A spatially explicit capture-recapture estimator for single-catch traps.* Ecology and Evolution 5 (21): 5075-5087.
- Borchers, D., Distiller, G., Foster, R., Harmsen, B., and Milazzo, L. (2014) *Continuous-time spatially explicit capture-recapture models, with an application to a jaguar camera-trap survey.* Methods in Ecology and Evolution 5 (7): 656-665. doi: 10.1111/2041-210X.12196

Acknowledgements

I have learnt a great deal over the course of this research and my heartfelt thanks go out to my primary supervisor Prof David Borchers for all his input and wisdom. Without him this project would never have been conceived and made a reality. I would also like to thank my local supervisor Dr Birgit Erni for always being prepared to listen to my obscure questions and for providing assistance wherever she could.

Thanks are due to Rebecca Foster and Bart Harmsen for making the jaguar camera-trap data available for this study. Collection of camera-trap data was funded by Panthera, with field and logistical assistance provided by the University of Belize's Environmental Research Institute and the Belize Audubon Society. Thanks also to Phil Cowan and Landcare Research Manaaki Whenua, New Zealand for making the possum timing data available.

I also thank the Engineering and Physical Sciences Research Council (EPSRC) for funding this work (EPSRC grant EP/I000917/1).

Last but not least I acknowledge my wife Suki for all the support she has given me and for putting up with me during the difficult moments, and to my beautiful children Amy and Ruben who bring so much light into my life.

Contents

List of Figures

List of Tables

Chapter 1

Introduction

1.1 Estimating animal density

Estimating population size is a crucial component of ecological research and conservation management (Silver et al., 2004; Dillon and Kelly, 2007; Gardner et al., 2009; Royle et al., 2009b; Ivan et al., 2013b). Capture-recapture (CR) methods are well established and have been used for several decades to fit both closed-population models that estimate abundance, and open-population models that estimate demographic vital rates such as survival and recruitment (Cormack, 1965; Jolly, 1965; Seber, 1965; White et al., 1982).

Closed population CR models estimate animal abundance but animal density is a vital parameter in wildlife management and conservation (Buckland et al., 1993; Marques et al., 2013), and is often preferable to abundance since density estimates can be compared across space and time (Gerber et al., 2012; Ivan et al., 2013a). Furthermore there is often interest in understanding how and why density varies in space (Gaston, 2003).

An estimate of density is obtained by dividing the estimate of abundance N by the size of the sampled area. In addition to demographic closure, conventional closed-population CR models assume geographic closure, an assumption which hardly ever holds (White et al., 1982; Royle et al., 2009a,b; Gardner et al., 2009; Gerber et al., 2012). Movement of animals results in the effective trapping area (ETA) being larger than the actual trapping area (also know as the "edge effect"), and leads to negative bias in detection probabilities and positive bias in abundance and density estimates (White et al., 1982; Williams et al., 2002; Karanth and Nichols, 1998; Royle et al., 2009b; Foster and Harmsen, 2012; Ivan et al., 2013b). It is widely acknowledged that it is difficult and usually problematic to estimate the ETA (Royle et al., 2009b;

Gardner et al., 2009; Obbard et al., 2010; Gerber et al., 2012; Noss et al., 2012).

Typically the ETA is estimated by adding a buffer to the sampling area that represents the additional area outside the trapping grid used by captured individuals. The size of this buffer is usually based on capture data from the trap array and approaches tend to use half the Mean Maximum Distance Moved (MMDM) as advocated by Dice (1938) (Karanth and Nichols, 1998; Karanth et al., 2004; Maffei et al., 2004; Silver et al., 2004; Maffei and Noss, 2008; Noss et al., 2012) though some also use full MMDM (Soisalo and Cavalcanti, 2006; Trolle et al., 2007; Obbard et al., 2010) or some variant of this (Dillon and Kelly, 2007; Gerber et al., 2012). MMDM type measures are viewed as a proxy for home range diameter but tend to underestimate home ranges since the movement data is truncated at the edge of the sampling array (Maffei and Noss, 2008; Obbard et al., 2010; Foster and Harmsen, 2012). When abundance is fixed and the area occupied by the population unknown, apparent density is a linear function of the assumed area. Hence the particular method used will affect density estimates and consequently this approach is not robust (Maffei et al., 2004; Dillon and Kelly, 2007; Maffei and Noss, 2008; Foster and Harmsen, 2012; Gerber et al., 2012).

It is well established that using survey areas that are too small leads to inflated estimates of density (Maffei and Noss, 2008; Foster and Harmsen, 2012). Studies that compare radio-telemetry data with MMDM methods confirm that the latter underestimate the size of an animal's home range (Dillon, 2005; Soisalo and Cavalcanti, 2006) unless the survey area is large (a factor of at least four) relative to the average home range size (Maffei and Noss, 2008) which is unlikely for wide-ranging animals. Furthermore these ad hoc boundary-strip methods do not incorporate uncertainty in the estimation of the sampling area and result in density estimates that assume the effective sampling area is known with certainty (Gardner et al., 2009; Obbard et al., 2010; Gerber et al., 2012).

The advent of spatially explicit capture-recapture (SECR), or more briefly spatial capture-recapture (SCR), methods that incorporate spatial information on where captures are made resolves this problem. SCR models allow inference about the underlying point process that determines the locations of individuals thereby relaxing the assumption of geographic closure and directly estimating density without requiring an ad hoc ETA estimate (Efford, 2004; Royle and Young, 2008; Borchers and Efford, 2008; Royle et al., 2009a,b; Efford et al., 2009a). The addition of spatial information also means that SCR models are able to account for trap failure and spatially varying effort.

SCR models embed a detection function in the observation process that depends on the distance between an individual's activity centre and the detector location.

Consequently SCR models recognise that individuals that tend to roam far from a particular detector will be less likely to be detected compared to those that are closer to the detector, and hence model individual heterogeneity in detection probability. SCR models are still relatively new but over the past few years have experienced rapid growth in both method development and application (Efford et al., 2009b; Gardner et al., 2010; Kery et al., 2011; Borchers, 2012; Foster and Harmsen, 2012; Borchers, 2016; Borchers and Marques, 2016). The inclusion of spatial information means that SCR models make use of more information in the data compared to non-spatial CR studies, and this is particularly beneficial when studying the type of species where small data sets are the norm.

Recent studies that compare results from SCR models to those that use conventional CR techniques with ad hoc boundary strip methods confirm that the latter tend to underestimate the effective sampling area and overestimate density, and recommend the use of the spatially explicit methods to estimate density (Obbard et al., 2010; Gerber et al., 2012; Noss et al., 2012). Ivan et al. (2013b) used a range of simulations to compare the performance of the maximum likelihood SCR approach with MMDM methods and a method that uses telemetry data (Ivan et al., 2013a). They found that overall the SCR estimator was the most consistent and also the most robust to changes in parameter levels (for detection probability, number of occasions, and abundance). The maximum likelihood SCR outperformed the other methods when capture probability was low, and outperformed MMDM approaches in almost all cases except where the home range was highly asymmetric or elongated in which case the methods performed similarly.

1.2 Capturing in continuous-time

The monitoring of secretive species that occur at low densities and range over wide areas has proven to be difficult (Kery et al., 2011; Goldberg et al., 2015). These characteristics exacerbate two central problems with sampling animal populations, namely being unable to survey the entire area occupied by the population and being unable to detect all individuals within the surveyed area (Karanth et al., 2006; Royle et al., 2009a). These sorts of species are also often of the highest conservation concern (Thompson, 2004; Stuart et al., 2004). Similar problems occur with species that are difficult to detect visually and difficult to trap.

Technological advances in non-invasive sampling methods such as scat or hair collection for genetic analysis, camera trapping, and acoustic detection have led to new ways of "capturing" individuals that are particularly useful for species that are difficult to survey using more conventional methods (Carbone et al., 2001; Karanth

et al., 2006; Dillon and Kelly, 2007; Gardner et al., 2010; Kery et al., 2011; Foster and Harmsen, 2012; Noss et al., 2012). Camera trap arrays in particular have become one of the most important tools for assessment and management of species that are hard to detect by other means (Rowcliffe and Carbone, 2008).

Griffiths and van Schaik (1993) first used camera traps to survey elusive rainforest mammals and they recommended a CR framework to estimate abundance. Karanth (1995) then used camera traps to obtain photographic captures of tigers that were analysed in a traditional CR framework. This pilot study used two to three camera traps that were rotated over different sites, and was limited by a small sample of ten individuals and 31 captures. The photographic capture approach has become an important monitoring tool since Karanth and Nichols (1998) extended the initial study and estimated tiger densities at four different sites (Foster and Harmsen, 2012). The same approach has since been used for other species that are also individually identifiable from photographs, including felids, canids, ursids, hyaenids, procynoids, tapirids and dasypodids (Silver et al., 2004; Maffei et al., 2004; Soisalo and Cavalcanti, 2006; Trolle et al., 2007; Dillon and Kelly, 2007; Maffei and Noss, 2008; Balme et al., 2009; Gardner et al., 2010; Noss et al., 2012; Gerber et al., 2012) and are increasingly used with SCR methods. Data from camera trap surveys have also been used for studies on species richness (Tobler et al., 2008) and occupancy (Linkie et al., 2007).

Cameras are almost always placed in optimal locations to maximise capture probabilities (Karanth, 1995; Karanth and Nichols, 1998; Karanth et al., 2004; Silver et al., 2004; Karanth et al., 2006; Soisalo and Cavalcanti, 2006; Foster and Harmsen, 2012). Doing so can result in non-random, biased placement if the locations are only optimal for a subset of the population (Foster and Harmsen, 2012). For cats in dense habitat these optimal locations are usually along trails (Gerber et al., 2012). Harmsen et al. (2010a) studied differential use of trails by different mammal species and found very few captures of jaguars and no captures of pumas at off trail locations. Furthermore all jaguars caught off trail were also captured by on trail cameras which suggests that placing cameras on trails should not lead to much bias, at least in the case of this population of jaguars.

Photographic captures differ fundamentally from traditional physical captures in that they are continuously sampled and record the exact time of capture (Foster and Harmsen, 2012). Spatial and non-spatial application of classic CR typically involves physically capturing and marking individuals at discrete sampling occasions in time, and the survey process generates well-defined sampling occasions. But when there is no physical capture and release, as in the case of camera trap studies or acoustic CR surveys that record times of detection, there is no well-defined sampling occasion.

In such cases, aggregating data into capture occasions introduces subjectivity (the occasion length chosen by the analyst) and discards some information (the exact times of capture).

Summarizing the data from camera trap CR studies into discrete capture occasions imposes an artificial construction on the data for reasons of analytic convenience. It is always a better policy to find a statistical formulation that fits the data than to shoehorn the data into a form that fits statistical formulations that happen to be available. The tendency with camera trap data has been towards the latter, typically camera trap studies aggregate the data into sampling occasions so that the data are then suitable for analysis. This approach is not necessarily the best approach for SCR analysis of camera trap studies.

CR methods typically assume independence across occasions (model M_b relaxes this assumption) and SCR methods also assume independence between traps, i.e. the probability of being caught at a particular trap is not affected by a capture elsewhere. In general, the only benefit to imposing the artificial construct of occasions on continuous data is to remove correlation in the capture times so that the independence assumption is not violated, although there may be cases in which discrete summary statistics by occasion are sufficient statistics. There is also likely to be little additional information in multiple captures in a short time (Royle et al., 2009a,b).

However, binning the data into occasions does not allow the inclusion of continuous covariates (for example weather) and limits the potential inferences that can be made regarding underlying biological processes that occur in continuous-time (CT). Furthermore, the use of occasions often leads to the assumption of equal occasion lengths so that the interpretation of the capture probabilities are comparable across different periods. Such an assumption is questionable when factors like trap failure exist. It is common to aggregate the data into 24 hour periods (Maffei et al., 2004; Foster and Harmsen, 2012) which can lead to the so called "midnight problem" (Jordan et al., 2011) where an animal photographed either side of midnight counts as two encounters as opposed to only counting as one encounter when captured twice during the same day. If animals are most active around the cutoff then capture probability will be positively biased, and this is likely to be true for nocturnal cats. Capture histories that use daily occasions for low density animals also tend to have many zeros (Foster and Harmsen, 2012).

1.3 Continuous-time models

CT models avoid the problems mentioned above but are far less developed compared to discrete-time (DT) models (Chao, 2001; Xi et al., 2007; Barker et al., 2014). The

earliest CR CT models are probably those of Craig (1953) and Darroch (1958) that assume equal catchability for all individuals at all times, but have been extended to include individual heterogeneity (Boyce et al., 2001).

Becker (1984) first established a counting process framework for CT models that uses a martingale estimator. His model allowed time variation in the intensity or λ parameter and most of the subsequent development in CR CT models extend his approach to come up with more general models (Becker, 1984; Yip, 1989; Becker and Heyde, 1990; Yip et al., 1995, 1999; Lin and Yip, 1999; Yip and Wang, 2002; Hwang and Chao, 2002). Most of these models do not estimate detectability and abundance simultaneously. Nayak (1988), Becker and Heyde (1990), Hwang et al. (2002) and Xi et al. (2007) developed maximum likelihood estimators (MLEs) and Chao and Lee (1993) developed a CT estimator based on sample coverage.

More recently Barker et al. (2014) developed a CR model for the sampling of DNA fragments in CT. The authors link their model with the earlier CT models and show that the earlier models can be written in terms of probability distributions and modelled within a Bayesian framework. Like the other CT models mentioned above, this model is not parameterised in terms of density and does not include spatial information on detections.

There is no consensus on the utility of CT estimators. Some authors conclude that the use of a DT model to analyze a CT dataset will bias estimates (Yip and Wang, 2002; Barbour et al., 2013) and can result in a loss of efficiency (Xi et al., 2007; Chao and Huggins, 2005); while others find no benefit over discrete-occasion estimators (e.g. Chao and Lee, 1993; Wilson and Anderson, 1995). Chapter 2 shows that Chao & Lee's (1993) conclusion that capture times are uninformative about abundance does not hold in general.

1.4 Single-catch traps

The majority of studies of small mammals use single-catch traps that catch and hold a single animal at a time (Efford et al., 2009a; Krebs et al., 2011; Gerber and Parmenter, 2015). The use of single-catch traps results in captures that are not independent and the likelihood for such models is complex. Efford (2004) used simulation and inverse prediction to fit single-catch trap models but the likelihood for such models remains to be developed under the discrete-occasion setup (Efford et al., 2009a; Royle et al., 2013c). This research began with a particular focus on data from camera traps but it soon became apparent that using a CT framework also facilitates the development of a single-catch trap estimator.

1.5 Applications

CR and SCR methods are increasingly used with camera traps for rare and elusive carnivores that are difficult to monitor with traditional methods (Dillon, 2005; Gerber et al., 2012), and camera traps yield CT capture data that are appropriate for CT models. The CT single-catch trap estimator that is developed in this research is appropriate for single-catch trap data with observed capture times.

Jaguars are an example of a large carnivore that is notoriously difficult to study and possums are the type of small mammal that are often live-trapped with cage traps. The models that are developed in this research are therefore applied to two quite different datasets, one from a camera trap survey of jaguars and the other from a live-trapping study of possums where timing devices were fixed to the cages.

1.5.1 Jaguars in Belize

Jaguars (*Panthera onca*) are near threatened and their global population is declining (Caso et al., 2008), and population monitoring is difficult because they occur at low densities, range widely and are elusive, often inhabiting thick habitat. Over the past decade, the challenge of detecting jaguars for population estimation has been facilitated by camera traps, following the work of Silver et al. (2004); however, reliable and robust density estimates of jaguars are rarely obtained (see Foster and Harmsen, 2012; Tobler and Powell, 2013).

Study site and camera trapping of jaguars

The Cockscomb Basin Wildlife Sanctuary in Belize encompasses 490 km^2 of secondary tropical moist broadleaf forest at various stages of regeneration following anthropogenic and natural disturbance (for more details see Harmsen et al., 2010b). To the west, the sanctuary forms a contiguous forest block with the protected forests of the Maya Mountain Massif ($\approx$ 5,000 km^2 of forest). To the east the sanctuary is partially buffered by unprotected forest beyond which is a mosaic of pine savannah, shrub land and broadleaf forest, inter-dispersed with villages and farms. Jaguars are found throughout this landscape (Foster et al., 2010). There are 65 km of trails, all within the eastern part of the sanctuary (see Figure 1.1 and Figure 1.2).

Few female jaguars were detected and since females have very different home ranges and possibly density, the analyses only use male detections. Male jaguars routinely walk the trail system and trail use overlaps extensively. Although they frequently leave the trails to move through the forest they are rarely detected off-trail by camera traps (Harmsen et al., 2010a). Nineteen paired camera stations

Figure 1.1: Camera trap survey sites within Cockscomb Basin Wildlife Sanctuary, Belize.

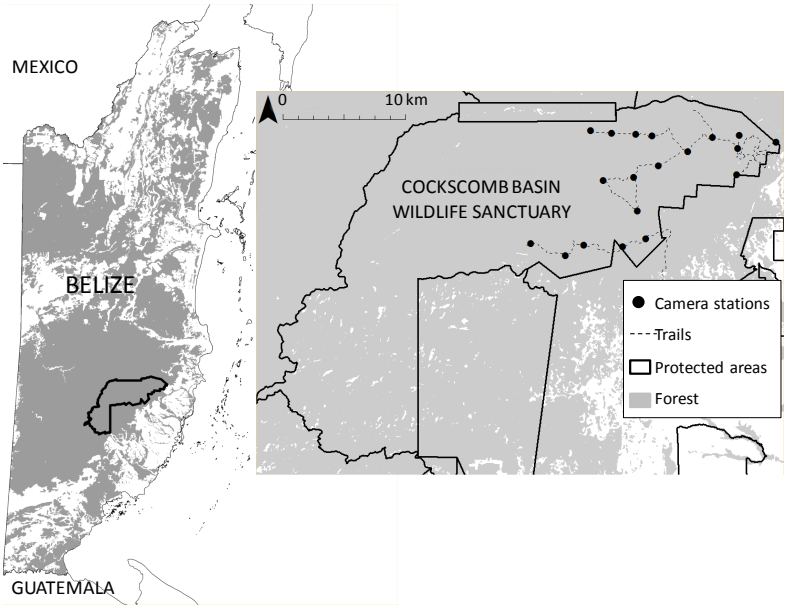

(Pantheracam v3) were deployed along the trail network within the eastern basin and maintained for 90 days (April to July 2011) producing 207 captures of 17 individuals. Neighbouring stations had an average spacing of 2.0 km (1.1 to 3.1 km). Digital photographic data were downloaded every two weeks.

1.5.2 Brushtail possums in New Zealand

Possums (*Trichosurus vulpecula*) were introduced to New Zealand in the nineteenth century to establish a fur industry (Efford and Cowan, 2004). Their selective browsing and predation on indigenous birds and invertebrates has caused them to become major pests (Campbell, 1990; Sadleir, 2000).

Study site and trapping of possums

The study site is in a mixed podocarp-hardwood forest in Orongorongo Valley on the North island of New Zealand (for more details see Efford and Cowan, 2004; Cowan and Forrester, 2012). Possums were live-trapped in a grid of wire mesh cage traps spaced 30 meters apart from each other that were baited with pieces of apple coated in flour and mixed with aniseed oil. The trapping ran for three consecutive days each month and traps were checked and reset daily.

The trapping grid is bounded to the north and west by the Orongorongo River. Apart from the river the habitat surrounding the trapping grid for several kilometers is similar to that covering the grid. Figure 1.2 shows the study area used in the possum analysis which has the river and the area across the river excluded as potential areas where activity centres could occur.

Timing devices (accurate to within five minutes) were fitted to the door frames of the traps and were activated when the door closed. Occasionally other non-targeted species such as rats (*Rattus rattus*), mice (*Mus musculus*) and hedgehogs (*Erinaceus europeus*) triggered the traps. In these cases the timing devices still recorded the time that the trap was triggered and these events are referred to as "DG" events (door **D**own and bait **G**one).

In this population females breed once a year in May - June, young become independent during October to December, and juvenile dispersal occurs mostly from February to April but can happen from December to May. There may also be some additional movement of animals during the mating period (April-June) (Cowan, personal communication, 2015). In order to maintain the assumption of a closed population, the months of August, September and October (from 1982) are selected for analysis. The data were received in hand written timing sheets (see Figure 1.3) and were transcribed and formatted appropriately for analysis. From August to October 70 unique possums were trapped over 57 cage traps and there were 286 capture events. Trap saturation can be calculated as the average proportion of traps that are occupied at the end of an occasion, and in these data the average trap saturation was 58%.

1.6 Objective and overview

The research presented here develops CT SCR likelihoods and MLEs which, unlike any existing CT models, are parameterised in terms of population density rather than abundance, and crucially, incorporate a model for (unobserved) individual activity centres. These models are obtained by formulating the SCR survey process as a type of recurrent event process, in which events are detections (see Cook and Lawless, 2007, for a comprehensive overview of recurrent event processes). The combination of recurrent event processes and CR methods was identified by Chao and Huggins (2005, p85) as "a fruitful area for future research". Simulations are used extensively in this research as a tool for investigating how different estimators perform under different conditions.

Chapter 2 presents the theory underlying the formulation of the CT SCR models. The first section provides methodological context by reviewing the existing DT SCR

Figure 1.2: Study areas for the jaguar and possum analyses.

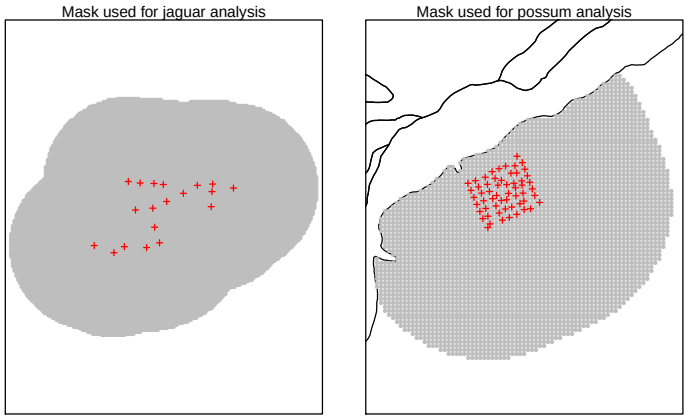

Notes: Traps are indicated with red crosses. For the jaguar analysis, the total area is 114,218.8 ha and consists of 18,275 grid cells, each one being 6.25 ha (250m x 250m). The possum analysis has a total area of 79.9 ha and consists of 3,551 grid cells, each one being 0.0225 ha (15m x 15m)

Figure 1.3: Example of a handwritten timing sheet with possum capture data that needed to be transcribed and formatted.

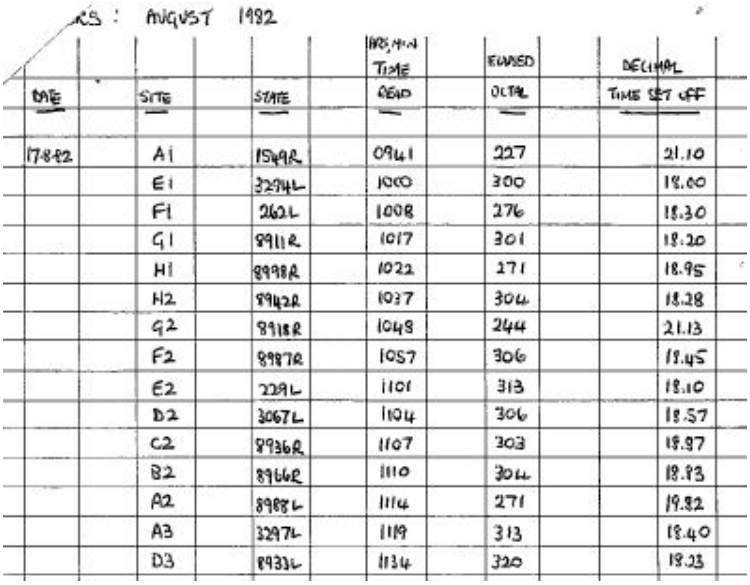

models. The second and third section modify the usual likelihood by incorporating a continuous detection hazard, and likelihoods are developed for both passive (or "proximity") detectors and single-catch traps. The chapter ends by providing more detail on the hazard function.

Chapter 3 develops CT proximity detector and single-catch trap models under the fairly common assumption that the detection hazard is constant through time, and the jaguar dataset is analysed under this assumption. This chapter, as well as the next chapter (Chapter 4), are broadly broken into two parts, one that deals with data from proximity detector surveys and another that deals with data from single-catch trap surveys. Both CT and DT proximity detector models assume independent detections within individuals but this assumption is likely to be unrealistic for camera trap studies over short time intervals. The first set of simulations in Chapter 3 examines the properties of the proximity detector estimators with a constant hazard for camera trap surveys both when the independence assumption holds and when it does not hold. The second set of simulations explores and contrasts the performance of the CT single-catch trap and the DT multi-catch trap estimators across a range of different scenarios.

Models that use a detection hazard that is not constant in time are developed in Chapter 4. Two different forms for a non-constant detection hazard are considered including a cosine form and a more flexible cyclic regression spline form. In addition, the simulations in Chapter 4 explore how a DT estimator performs when hazard cycle lengths are not an integer multiple of occasion length. These models are applied to both of the datasets described in Section 1.5.

The final chapter summarises the research, discusses the findings and makes concluding remarks.

The statistical computing language `R` (R Core Team, 2015) was used for the analysis and the R package `secr` (Efford, 2016) used to fit the DT models. Parameters and standard errors were estimated using a Newton-type algorithm with function `nlm` in R. Computations were performed using facilities provided by the University of Cape Town's ICTS High Performance Computing team (http://hpc.uct.ac.za).

Chapter 2

A continuous-time spatial capture-recapture formulation

The objective of this research is to develop a continuous-time (CT) spatial capture-recapture (SCR) formulation and this chapter introduces the general framework for analysing SCR studies in CT. The first section reviews the traditional discrete-time (DT) or discrete-occasion (these two terms are used interchangeably) SCR model specification. From this starting point the CT likelihoods are developed for proximity detectors and single-catch traps in the second and third section respectively. Detection hazard functions are at the heart of the CT framework and the chapter concludes with a more thorough discussion on the detection hazard function.

The terms "detector" and "detection" can be used interchangeably with the terms "trap" and "capture", although the convention used here is to refer to a detector that holds an animal as a "trap" and a detector that records an animal's presence without holding it as a "detector".

2.1 Spatial capture recapture: discrete-time formulation

SCR models can be fitted using maximum likelihood (Borchers and Efford, 2008), inverse prediction (Efford, 2004), or using Bayesian inference (Royle et al., 2009a,b; Gardner et al., 2009). The latter would require setting up a full probability model for all unknown quantities including parameters. The developments in this research occur within a maximum likelihood framework. The maximum likelihood DT SCR models are reviewed here and the material in this section is based on papers by

Borchers and Efford (2008) and Efford et al. (2009a).

SCR models directly model density by including both an underlying state process and an observation or capture process. The state process deals with the density or abundance and distribution of activity centres of individuals in space. An activity centre is the centre of gravity of an individual's locations over the duration of the survey. It may have a biological interpretation, e.g. as a home range centre, but need not. The observation process incorporates a spatial detection function whereby the probability of detecting an individual at a particular detector is a function of the distance between that individual's activity centre and the detector. This distance is a latent variable since it depends on unobserved activity centres and hence can be viewed as a type of individual random effect. SCR models therefore include a source of individual heterogeneity and are a special case of the model M_h.

2.1.1 Notation

The objective is to estimate the density of a closed population of animals where it is assumed that the animals have fixed activity centres for the duration of the survey period. There are n unique animals detected at K detectors over J trapping occasions. The capture history for individual i is of length J and denoted with $\boldsymbol{\omega}_i$, and $\omega_{ij} = k$ if animal i is detected at detector k during occasion j (and zero otherwise) so that $\boldsymbol{\omega}_i = (\omega_{i1}, \ldots, \omega_{iJ})$ and $\omega_{i\cdot} = 1$ if the animal was caught at all during the study and zero otherwise. The two-dimensional coordinate of the ith individual's activity centre is notated as $\boldsymbol{s}_i$ and $\boldsymbol{S} = (\boldsymbol{s}_1, \ldots, \boldsymbol{s}_n)$. The distance from an individual's activity centre to the kth detector ($d_k(\boldsymbol{s}_i)$) affects detectability but for notational brevity the dependence of detection on distance through $\boldsymbol{s}$ is not always made explicit. The two-dimensional coordinate of any location in the study area is notated as $\boldsymbol{x}$.

The parameter $p_{kj}(\boldsymbol{s}_i; \boldsymbol{\theta})$ is the probability that an individual with activity centre at $\boldsymbol{s}_i$ is caught in trap k during occasion j, and $\boldsymbol{\theta}$ is a vector of detection function parameters. The parameter $p_{\cdot j}(\boldsymbol{s}_i; \boldsymbol{\theta})$ is the probability the animal is detected at any of the K traps on occasion j, and similarly $p_{\cdot}(\boldsymbol{s}_i; \boldsymbol{\theta})$ is the probability that the animal is detected at all during the study, i.e. $p_{\cdot}(\boldsymbol{s}_i; \boldsymbol{\theta}) = \Pr(\omega_{i\cdot} = 1 | \boldsymbol{s}_i; \boldsymbol{\theta})$. In addition to $\boldsymbol{\theta}$, $\boldsymbol{\phi}$ is the vector of parameters related to the spatial point process that determines animal density and distribution. For example, $D(\boldsymbol{x}; \boldsymbol{\phi})$ indicates that the density at a point in space depends on both the $\boldsymbol{\phi}$ parameters and the spatial coordinate $\boldsymbol{x}$. If density follows an exponential east-west gradient then $D(\boldsymbol{x}; \boldsymbol{\phi}) = e^{\beta_0 + \beta_1 \times X}$ where X is the distance east and $\boldsymbol{\phi} = (\beta_0, \beta_1)$. In the simplest case, the spatial point process is homogeneous i.e. there are no covariates on density and it is constant.

2.1.2 General likelihood

The appropriate likelihood for $\boldsymbol{\phi}$ and $\boldsymbol{\theta}$ is the joint distribution of the number of animals captured n and their capture histories $(\boldsymbol{\omega}_i)$. The likelihood can be written in terms of the marginal distribution of n and the conditional distribution of $\boldsymbol{\omega}_1, \ldots, \boldsymbol{\omega}_n$ given n.

$$L(\boldsymbol{\theta}, \boldsymbol{\phi} \mid n, \boldsymbol{\omega}_1, \ldots, \boldsymbol{\omega}_n) = \Pr(n \mid \boldsymbol{\phi}, \boldsymbol{\theta}) \Pr(\boldsymbol{\omega}_1, \ldots, \boldsymbol{\omega}_n \mid n, \boldsymbol{\theta}, \boldsymbol{\phi}) \tag{2.1}$$

The first component concerns the number of animals captured (n), and assumes that the (unobserved) activity centres of detected individuals are realisations of a filtered, spatial non homogeneous Poisson process (NHPP). The NHPP has intensity $D(\boldsymbol{x}; \boldsymbol{\phi})$ at $\boldsymbol{x}$ with the filter at $\boldsymbol{x}$ being the detection probability at that location. If individuals are detected independently, the number of individuals detected is therefore a Poisson random variable:

$$\Pr(n \mid \boldsymbol{\phi}, \boldsymbol{\theta}) = \frac{e^{-\lambda(\boldsymbol{\theta}, \boldsymbol{\phi})} \lambda(\boldsymbol{\theta}, \boldsymbol{\phi})^n}{n!} \tag{2.2}$$

where

$$\lambda(\boldsymbol{\theta}, \boldsymbol{\phi}) = \int_{\mathbb{A}} D(\boldsymbol{x}; \boldsymbol{\phi}) p_\cdot(\boldsymbol{x}; \boldsymbol{\theta}) \, d\boldsymbol{x} \tag{2.3}$$

and $p_\cdot(\boldsymbol{x}; \boldsymbol{\theta})$ is the probability of being detected during the survey and the integral is over all points $\boldsymbol{x}$ in the area A in which activity centres occur. These activity centres are assumed to be fixed over the duration of the survey. The state model is essentially the model for the abundance and distribution of animals in space, and the observation model includes the filtering of this process that results in n observed captures and n capture histories.

The second component in Equation 2.1 is modelled with a multinomial distribution where each possible combination for a capture history of length J is treated as a category:

$$\begin{aligned} \Pr(\boldsymbol{\omega}_1, \ldots, \boldsymbol{\omega}_n \mid n, \boldsymbol{\phi}, \boldsymbol{\theta}) &= \Pr(\boldsymbol{\omega}_1, \ldots, \boldsymbol{\omega}_n \mid \omega_{1\cdot} > 0, \ldots, \omega_{n\cdot} > 0, \boldsymbol{\theta}, \boldsymbol{\phi}) \\ &= \binom{n}{n_1, \ldots, n_C} \prod_{i=1}^{n} \Pr(\boldsymbol{\omega}_i \mid \omega_{i\cdot} > 0, \boldsymbol{\theta}, \boldsymbol{\phi}) \end{aligned} \tag{2.4}$$

where $n_1, \ldots, n_C$ are the frequencies of the C unique observed capture histories.

Note that Equation 2.1 is general and other assumptions could be made about the form of the two components in that equation. Both these components are also conditional on the location of the activity centres $\boldsymbol{S}$, and it is possible to evaluate the likelihood without knowing $\boldsymbol{S}$ by integrating over possible locations. When integrating the unobserved activity centres out of the likelihood, it is important that the area that the integration is carried out over is large enough to ensure that it contains the locations of any animals that have a non zero probability of being caught anywhere in the trap array over the duration of the study. It is better to use an area that is bigger than necessary rather than one that is too small as increasing the area will only affect computational efficiency.

Since detectability depends on $\boldsymbol{S}$, and $\boldsymbol{S}$ is unobserved and needs to be integrated out, the probability of observing capture history $\boldsymbol{\omega}_i$ for the ith individual, given that it was caught is:

$$\Pr(\boldsymbol{\omega}_i \mid \omega_{i\cdot} > 0, \boldsymbol{\theta}, \boldsymbol{\phi}) = \int_A \Pr(\boldsymbol{\omega}_i \mid \omega_{i\cdot} > 0, \boldsymbol{s}_i; \boldsymbol{\theta}) f(\boldsymbol{s}_i \mid \omega_{i\cdot} > 0; \boldsymbol{\theta}, \boldsymbol{\phi})\, d\boldsymbol{s} \tag{2.5}$$

The terms in the integral above can be written in terms of the detection function $p_{kj}(\boldsymbol{s}; \boldsymbol{\theta})$ and the non homogenous Poisson process rate $D(\boldsymbol{x}; \boldsymbol{\phi})$. The first term can be written as:

$$\Pr(\boldsymbol{\omega}_i \mid \omega_{i\cdot} > 0, \boldsymbol{s}_i; \boldsymbol{\theta}) = p_{\cdot}(\boldsymbol{s}_i; \boldsymbol{\theta})^{-1} \prod_{j=1}^{J} [1 - p_{\cdot j}(\boldsymbol{s}_i; \boldsymbol{\theta})^{1-\delta_{\cdot}(\omega_{ij})}] \prod_{k=1}^{K} p_{kj}(\boldsymbol{s}_i; \boldsymbol{\theta})^{\delta_k(\omega_{ij})} \tag{2.6}$$

where $\delta_k(\omega_{ij}) = 1$ if $\omega_{ij} = k$ and zero otherwise, $\delta_{\cdot}(\omega_{ij}) = 1$ if $\delta_k(\omega_{ij}) > 0$ for any $k = 1, \ldots, K$ and zero otherwise, and $p_{\cdot}(\boldsymbol{s}_i; \boldsymbol{\theta}) = 1 - \prod_{j=1}^{J} [1 - p_{\cdot j}(\boldsymbol{s}_i; \boldsymbol{\theta})]$.

The second term can be written as:

$$f(\boldsymbol{s}_i \mid \omega_{i\cdot} > 0; \boldsymbol{\theta}, \boldsymbol{\phi}) = \frac{D(\boldsymbol{s}_i; \boldsymbol{\phi}) p_{\cdot}(\boldsymbol{s}_i; \boldsymbol{\theta})}{\int_{\mathbb{A}} D(\boldsymbol{x}; \boldsymbol{\phi}) p_{\cdot}(\boldsymbol{x}; \boldsymbol{\theta})\, d\boldsymbol{x}} = \frac{D(\boldsymbol{s}_i; \boldsymbol{\phi}) p_{\cdot}(\boldsymbol{s}_i; \boldsymbol{\theta})}{\lambda(\boldsymbol{\theta}, \boldsymbol{\phi})} \tag{2.7}$$

Hence the general likelihood becomes:

$$
\begin{aligned}
L(\boldsymbol{\phi}, \boldsymbol{\theta} \mid n, \boldsymbol{\omega}_1, \ldots, \boldsymbol{\omega}_n) = & \frac{\lambda(\boldsymbol{\phi}, \boldsymbol{\theta})^n e^{-\lambda(\boldsymbol{\phi}, \boldsymbol{\theta})}}{n!} \prod_{i=1}^{n} \int_{\mathbb{A}} \frac{D(\boldsymbol{s}_i; \boldsymbol{\phi})}{\lambda(\boldsymbol{\phi}, \boldsymbol{\theta})} \\
& \prod_{j=1}^{J} [1 - p_{\cdot j}(\boldsymbol{s}_i; \boldsymbol{\theta})^{1-\delta_\cdot(\omega_{ij})}] \prod_{k=1}^{K} p_{kj}(\boldsymbol{s}_i; \boldsymbol{\theta})^{\delta_k(\omega_{ij})} \, d\boldsymbol{s} \\
= & \frac{e^{-\lambda(\boldsymbol{\phi}, \boldsymbol{\theta})}}{n!} \prod_{i=1}^{n} \int_{\mathbb{A}} D(\boldsymbol{s}_i; \boldsymbol{\phi}) \prod_{j=1}^{J} [1 - p_{\cdot j}(\boldsymbol{s}_i; \boldsymbol{\theta})^{1-\delta_\cdot(\omega_{ij})}] \prod_{k=1}^{K} p_{kj}(\boldsymbol{s}_i; \boldsymbol{\theta})^{\delta_k(\omega_{ij})} \, d\boldsymbol{s}
\end{aligned}
\tag{2.8}
$$

Equation 2.8 is general and can be reduced to simpler forms, e.g. if detection probability is constant across occasions. Note that n can also be viewed as the number of activity centres (one per captured individual), and this model assumes that the activity centres occur independently of one another (such an assumption would not hold for territorial animals), and that captures are independent both between and within animals. Note also that Equation 2.8 corresponds to a model where the total number of animals in the sampled area N is a random variable. The likelihood can also be modelled with N as a fixed but unknown parameter, rather than with D as the unknown parameter (Borchers and Efford, 2008).

2.1.3 The spatial detection function

The observation process is modelled with a detection function $p_{kj}(\boldsymbol{s}; \boldsymbol{\theta})$ that models the probability of capturing an individual at detector k during occasion j as a function of distance $d_k(\boldsymbol{s})$ from that individual's activity centre to the kth detector. A variety of forms can be used for the detection function and Figure 2.1 depicts three examples of different detection functions.

The $\boldsymbol{\theta}$ parameter vector depends on the type of detection function used. These parameters control the efficiency of detection and also the spatial scale of the detection function, which is expected to increase with home range size. For example the commonly used "half-normal" form is used in this work and uses two parameters:

$$p_{kj} = g_0 \times \exp\left(\frac{-d_k(\boldsymbol{s})^2}{2\sigma^2}\right)$$

The g_0 parameter determines the detection function height and is the probability that an individual with an activity centre located at detector k (at a distance of zero)

is detected during occasion j, while σ is the standard deviation of the half-normal detection function and determines the range over which an individual is detectable. The half-normal detection function produces a circular bivariate normal shape for the detection surface around a detector.

Other examples include the exponential form that also uses two parameters:

$$p_{kj} = g_0 \times \exp\left(\frac{-d_k(\boldsymbol{s})}{\sigma}\right)$$

and the hazard rate form that uses three parameters:

$$p_{kj} = g_0 \times \left(1 - \exp\left(\frac{-d_k(\boldsymbol{s})}{\sigma}\right)^{-z}\right)$$

Figure 2.1: Three different possible forms for the spatial detection function.

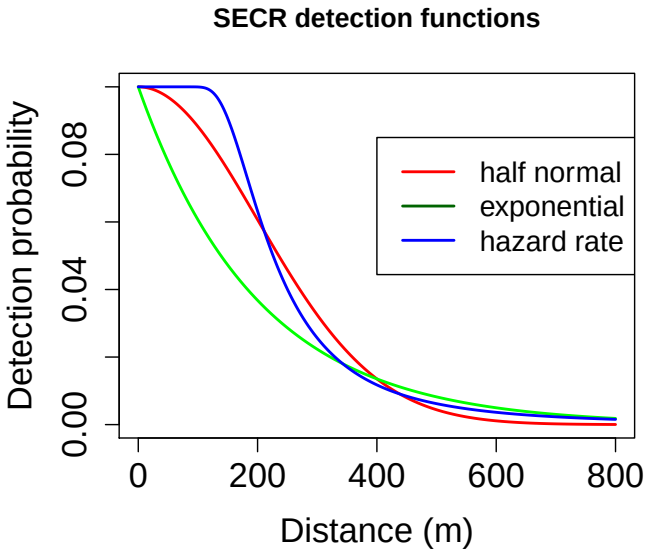

The capture process needs to take into account the characteristics of the different types of detectors that can be used. Passive detectors (also called "proximity" detectors) refer to traps or detectors that "catch" an animal without holding them such as camera traps, acoustic devices and devices that collect DNA samples without limiting movement. "Multi-catch" traps refer to traps that physically hold an animal

once it is caught, but that are capable of holding multiple animals at a time such as mist nets for birds and pitfall traps for lizards. Lastly, "single-catch" traps refer to traps that also physically hold an individual but the difference from multi-catch traps is that these traps can only hold a single animal and so "fill up" once they catch an individual.

The general likelihood (Equation 2.8) above remains the same but the difference arises with how the capture histories are modelled. The general form is:

$$\Pr(\boldsymbol{\omega}_i \mid \boldsymbol{s}_i; \boldsymbol{\theta}) = \prod_j [1 - p_{\cdot j}(\boldsymbol{s}_i; \boldsymbol{\theta})]^{1-\delta_\cdot(\omega_{ij})} \prod_k p_{kj}(\boldsymbol{s}_i; \boldsymbol{\theta})^{\delta_k(\omega_{ij})} \tag{2.9}$$

where $\delta_k(\omega_{ij}) = 1$ if $\omega_{ij} = k$ and zero otherwise, $\delta_\cdot(\omega_{ij}) = 1$ if $\delta_k(\omega_{ij}) > 0$ for any $k = 1, \ldots, K$ and zero otherwise.

2.1.4 Detector types

Passive (proximity) detectors

Passive detectors do not hold individuals and so an individual can be caught at more than one site during an occasion. Camera traps, acoustic devices and hair snares are all examples of proximity detectors. Capture histories are necessarily more complicated and can be thought of as a 3-dimensional array where there is a $n \times J$ matrix for each of the k detectors. Detections at different detectors during an occasion are assumed to be independent. The `secr` library (Efford, 2016) defines a "count" detector as a proximity detector that can detect an individual multiple times during an occasion (such as for a camera trap) as opposed to a proximity detector that can only register one capture event (such as a hair snare).

The pdf of the detection histories, given detection can be written as

$$P_\Omega(\boldsymbol{\Omega} \mid \boldsymbol{S}, \omega_{i\cdot} > 0; \boldsymbol{\theta}) = \prod_{i=1}^{n} \prod_{j=1}^{J} \prod_{k=1}^{K} P(\omega_{ikj} \mid \boldsymbol{s}_i, \omega_{i\cdot} > 0; \boldsymbol{\theta}) \tag{2.10}$$

where $\boldsymbol{\Omega} = \{\boldsymbol{\omega}_{ik}\}$ $(i = 1, \ldots, n; k = 1, \ldots, K)$ and $\boldsymbol{\omega}_{ik} = (\omega_{ik1}, \ldots, \omega_{ikJ})$ is individual i's detection history on detector k over the J occasions.

Two forms of $P_\Omega(\boldsymbol{\Omega} \mid \boldsymbol{S}; \boldsymbol{\theta})$ have been proposed for proximity detectors under the assumption that detections are conditionally independent (given the location): one in which ω_{ikj} is binary, indicating detection or not of individual i at detector k on

occasion j (as shown in Equation 2.9), and one in which ω_{ikj} is a count of the number of times individual i was detected by detector k on occasion J:

$$P(\omega_{ikj} \mid \boldsymbol{s}_i; \boldsymbol{\theta}) = \prod_j \prod_k \frac{H_{jk}(\boldsymbol{s}_i; \boldsymbol{\theta})^{\omega_{ijk}} e^{-H_{jk}(\boldsymbol{s}_i; \boldsymbol{\theta})}}{\omega_{ijk}!} \tag{2.11}$$

where $H_{jk}(\boldsymbol{s}_i; \boldsymbol{\theta})$ is modeled as a function of distance in a similar way as the occasion-specific capture probability, except that, in the case of a half-normal form, g_0 is no longer constrained to lie between 0 and 1 and so can take on any value > 0.

Unlike conventional CR methods that require multiple occasions, it is possible to obtain density estimates from spatial data for a single time interval when individuals may be seen at more than one location. Data with these characteristics may arise from photographic captures over an extended period or from collapsing binary detection data across multiple intervals when capture probability is constant. In the former case a Poisson model may be used with a rate parameter applicable to the study duration, and in the latter case a binomial model is appropriate and is identical to a model for data from multiple intervals where the detection probability is constant.

Barker et al. (2014) use a non-spatial CR model for DNA fragments drawn one at a time in CT that is based on Poisson sampling. Their model formulation also allows abundance to be estimated from capture frequencies from what is essentially a single session.

Multi-catch traps

Capture in a multi-catch trap precludes capture elsewhere for the remainder of the occasion and leads to a competing risks formulation being used to model the probability that an individual with activity centre at $\boldsymbol{s}$ is caught during occasion j at trap k. In typical competing risks survival analysis applications there are several possible causes of "death" but only one that will eventually cause death. If one considers an individual being caught as the event of interest ("death"), the different traps can be thought of as competing with one another to cause the event.

A hazard function that specifies the expected detection rate per unit time is associated with each of the k detectors for occasion j and depends on the distance $d_k(\boldsymbol{s})$ from that individual's activity centre to the kth detector. Given this distance, the hazard of detection is assumed to remain constant throughout the occasion of length T_j leading to the following expression for the probability of capture during occasion j in any of the K detectors:

$$p_{\cdot j}(\boldsymbol{s};\boldsymbol{\theta}) = 1 - \exp\left\{-T_j \sum_{k=1}^{K} h_j(d_k(\boldsymbol{s}))\right\} = 1 - e^{-T_j h_{\cdot j}(\boldsymbol{s})}$$

where $h_j(d_k(\boldsymbol{s}))$ is the hazard function for trap k during occasion j at distance $d_k(\boldsymbol{s})$ from $\boldsymbol{s}$ and $h_{\cdot j}(\boldsymbol{s}) = \sum_{k=1}^{K} h_j(d_k(\boldsymbol{s}))$ is the total hazard during occasion j of the individual being caught, from all K traps, given $\boldsymbol{s}$.

The expression for the probability of being caught in trap k during occasion j can be constructed by combining the term that relates to the probability of being caught anywhere during occasion j with the term for the relative hazard that represents the probability that the capture event took place specifically at trap k:

$$p_{kj}(\boldsymbol{s};\boldsymbol{\theta}) = \frac{\left\{1 - e^{-T_j h_{\cdot j}(\boldsymbol{s})}\right\} h_j(d_k(\boldsymbol{s}))}{h_{\cdot j}(\boldsymbol{s})}$$

Single-catch traps

When animals are physically detained by traps they can only be detected by one trap per occasion. Traps holding an animal are also effectively taken out of action after catching an individual. This means that capture probability is affected by the presence of other individuals, and so both other traps and other individuals "compete" for a capture. The assumption of animals being caught independently is therefore violated and the likelihoods above are not appropriate. A likelihood for single-catch traps can be formulated with a CT framework and is presented in Section 2.3.1 below.

2.2 Spatial capture recapture: continuous-time formulation for proximity detectors

The CT framework involves modelling the process generating detections as a temporal NHPP in which the events are detections. This approach assumes that the hazard of detection for the ith individual at the kth detector at any time is independent of the individual's capture history up to that time, and a model and estimator is developed under this assumption. Note that the model is easily extended to be of type M_b by estimating different hazard levels before and after first capture.

2.2.1 Notation

The notation is similar to that presented in Section 2.1.1. As is typical for SCR models, it is assumed that the individuals have fixed activity centre locations for the duration of the survey period: $\boldsymbol{s}_i$ for the ith individual, which is a distance $d_k(\boldsymbol{s}_i)$ from trap k. The primary difference from the DT setup is that there are no longer J occasions but rather an SCR survey of duration T with an array of continuously-sampling proximity detectors. For the ith detected individual, instead of a capture history of length J there are ω_{ik} captures at detector k at times $\boldsymbol{t}_{ik} = (t_{ik1}, \ldots, t_{ik\omega_{ik}})$ where ω_{ik} is an integer, and $\boldsymbol{t} = \{\boldsymbol{t}_{ik}\}$ $(i = 1, \ldots, n; k = 1, \ldots, K)$ denotes the set of all detection times. An individual's overall detection frequency is $\omega_{i\cdot} = \sum_{k=1}^{K} \omega_{ik}$ and the event $\omega_{i\cdot}>0$ indicates detection by some detector.

In a CT formulation, the discrete-occasion expression for the probability of detecting individual i at detector k during an occasion is replaced by a detection hazard function. The hazard function for the ith individual and the kth trap at time t is denoted as $h_k(t, \boldsymbol{s}_i; \boldsymbol{\theta})$ and can depend on both space (in terms of the distance from the trap to the activity centre $d_k(\boldsymbol{s}_i)$) and time while $\boldsymbol{\theta}$ is an unknown vector of hazard function parameters. As before, the dependence of detection on the distance from detector k to the individual's activity centre ($d_k(\boldsymbol{s}_i)$ is not always made explicit for notational brevity.

In the absence of other traps and other individuals, the "survivor function" for individual i at trap k over the whole survey (the probability of individual i not being detected by the trap by time T) is

$$S_k(T, \boldsymbol{s}_i; \boldsymbol{\theta}) = \exp\left(-\int_0^T h_k(t, \boldsymbol{s}_i; \boldsymbol{\theta})\, dt\right)$$

and hence $1 - S_k(T, \boldsymbol{s}_i; \boldsymbol{\theta})$ is the probability of detection in $(0, T)$. Similarly the combined detection hazard over all traps at time t is $h_\cdot(t, \boldsymbol{s}_i; \boldsymbol{\theta}) = \sum_{k=1}^{K} h_k(t, \boldsymbol{s}_i; \boldsymbol{\theta})$, and the overall probability of detection in $(0, T)$ over all detectors is $p_\cdot(\boldsymbol{s}_i; \boldsymbol{\theta}) = 1 - S_\cdot(T, \boldsymbol{s}_i; \boldsymbol{\theta})$, where $S_\cdot(T, \boldsymbol{s}_i; \boldsymbol{\theta}) = \exp\left(-\int_0^T h_\cdot(t, \boldsymbol{s}_i; \boldsymbol{\theta})\, dt\right)$ is the overall survivor function.

In addition to $\boldsymbol{\theta}$, $\boldsymbol{\phi}$ is a vector of unknown parameters that govern the intensity and hence the distribution of activity centres.

2.2.2 General likelihood

The development of the likelihood begins by considering a single individual (the ith individual), with activity centre at $\boldsymbol{s}_i$, and a single detector (the kth detector). By

considering $\boldsymbol{t}_{ik}$ to be a realisation of a NHPP in time, an expression for the probability density function (pdf) of $\boldsymbol{t}_{ik}$ is obtained. This is analogous to the probability of obtaining a capture history at detector k for individual i in a DT formulation, but it is worth noting that both the length of $\boldsymbol{t}_{ik}$ (i.e. ω_{ik}) and the times that it contains are random variables, whereas for a discrete-occasion survey the length of a capture history is fixed by the number of occasions used.

The pdf of $\boldsymbol{t}_{ik}$

Using a result from Poisson process theory (see Cook and Lawless, 2007, Theorem 2.1 on page 30, and Equation (2.13) on page 32), and assuming that, conditional on the activity centre location, the times of detections are independent, the detection times for individual i at detector k can be modelled as a NHPP with pdf:

$$f_k(\boldsymbol{t}_{ik} \mid \boldsymbol{s}_i; \boldsymbol{\theta}) = S_k(T, \boldsymbol{s}_i; \boldsymbol{\theta}) \prod_{r=1}^{\omega_{ik}} h_k(t_{ikr}, \boldsymbol{s}_i; \boldsymbol{\theta}) \tag{2.12}$$

(I omit ω_{ik} from the LHS for brevity, because given $\boldsymbol{t}_{ik}$, ω_{ik} is known.) Equation 2.12 is a generalisation of the expression obtained by Hwang et al. (2002, p43) for their model M_t (given by their expression for L_i), and of the expression of Chao and Huggins (2005, p80) for the case in which $h_k(t_{ikr}, \boldsymbol{s}_i; \boldsymbol{\theta})$ is constant. Both these sets of authors use λ for the hazard, whereas $h(\,)$ is used here. In addition to locating these models in the Poisson process literature, the generalisation involves the inclusion of $\boldsymbol{s}$ as a latent variable, and extension to multiple detectors.

Following the same logic as in Section 2.1.2, since detectability depends on $\boldsymbol{s}$ which needs to be integrated out, the probability density function of $\boldsymbol{t}_{ik} = (t_{ik1}, \ldots, t_{ik\omega_{ik}})$ for the ith individual at the kth detector, given that it was caught during the survey, can be written as:

$$f_k(\boldsymbol{t}_{ik} \mid \omega_{i\cdot} > 0; \boldsymbol{\theta}, \boldsymbol{\phi}) = \int_{\mathbb{A}} f_k(\boldsymbol{t}_{ik} \mid \omega_{i\cdot} > 0, \boldsymbol{s}_i; \boldsymbol{\theta}) f(\boldsymbol{s}_i \mid \omega_{i\cdot} > 0; \boldsymbol{\theta}, \boldsymbol{\phi})\, d\boldsymbol{s} \tag{2.13}$$

The first term in the integral above is Equation 2.12 above but conditional on being caught during the survey and so becomes:

$$f_k(\boldsymbol{t}_{ik} \mid \omega_{i\cdot} > 0, \boldsymbol{s}_i; \boldsymbol{\theta}) = p_\cdot(\boldsymbol{s}_i; \boldsymbol{\theta})^{-1} S_k(T, \boldsymbol{s}_i; \boldsymbol{\theta}) \prod_{r=1}^{\omega_{ik}} h_k(t_{ikr}, \boldsymbol{s}_i; \boldsymbol{\theta}) \tag{2.14}$$

The second term that relates to the density of the activity centre is the same as shown in Equation 2.7 above.

Multiple detectors and individuals

Using the survivor function, an expression for the probability of detecting individual i at all is obtained. Then, as in Section 2.1 above, the number of individuals detected is a Poisson random variable with parameter $\lambda(\boldsymbol{\theta}, \boldsymbol{\phi}) = \int_A D(\boldsymbol{x}; \boldsymbol{\phi}) p_\cdot(\boldsymbol{x}; \boldsymbol{\theta})\, d\boldsymbol{x}$.

This gives rise to a joint probability model for the number of individuals detected (n) and the density of the outcomes "ω_{ik} events, at times $t_{ik1} < \ldots < t_{ik\omega_{ikr}}$" for all i and all k. When considered as a function of the unknown model parameters, this is the CT SCR likelihood function. The likelihood can be written in terms of the marginal distribution of n and the conditional distribution of $\boldsymbol{t}$ given n.

$$L(\boldsymbol{\theta}, \boldsymbol{\phi} \mid n, \boldsymbol{t}) = \Pr(n \mid \boldsymbol{\phi}, \boldsymbol{\theta}) f_t(\boldsymbol{t} \mid n, \boldsymbol{\theta}, \boldsymbol{\phi}) \tag{2.15}$$

It follows that the general likelihood becomes:

$$L(\boldsymbol{\phi}, \boldsymbol{\theta} \mid n, \boldsymbol{t}) = \frac{e^{-\lambda(\boldsymbol{\phi}, \boldsymbol{\theta})}}{n!} \prod_{i=1}^{n} \int_{\mathbb{A}} D(\boldsymbol{s}_i; \boldsymbol{\phi}) \prod_{k=1}^{K} S_k(T, \boldsymbol{s}_i; \boldsymbol{\theta}) \prod_{r=1}^{\omega_{ik}} h_k(t_{ikr}, \boldsymbol{s}_i; \boldsymbol{\theta})\, d\boldsymbol{s} \tag{2.16}$$

It is sometimes useful (see below) to write this likelihood in terms of the marginal distribution of the detection frequency at detector k (ω_{ik}) and the conditional distribution of $\boldsymbol{t}_{ik}$ given ω_{ik}. The capture frequency ω_{ik} has a Poisson distribution with parameter $H_k(\boldsymbol{s}_i; \boldsymbol{\theta}) = \int_0^T h_k(t, \boldsymbol{s}_i; \boldsymbol{\theta})\, dt$ leading to the following probability mass function (pmf):

$$P_k(\omega_{ik} \mid \boldsymbol{s}_i; \boldsymbol{\theta}) = \frac{H_k(\boldsymbol{s}_i; \boldsymbol{\theta})^{\omega_{ik}} e^{-H_k(\boldsymbol{s}_i; \boldsymbol{\theta})}}{\omega_{ik}!} = \frac{H_k(\boldsymbol{s}_i; \boldsymbol{\theta})^{\omega_{ik}} S_k(T, \boldsymbol{s}_i; \boldsymbol{\theta})}{\omega_{ik}!} \tag{2.17}$$

(see Cook and Lawless, 2007, Equation (2.15) on page 32). It follows from this and Equation 2.12 that the conditional pdf of detection times $\boldsymbol{t}_{ik}$, given ω_{ik}, for the ith animal is

$$f_{t|\omega,k}(\boldsymbol{t}_{ik} \mid \omega_{ik}, \boldsymbol{s}_i; \boldsymbol{\theta}) = \omega_{ik}! \prod_{r=1}^{\omega_{ik}} \frac{h_k(t_{ikr}, \boldsymbol{s}_i; \boldsymbol{\theta})}{H_k(\boldsymbol{s}_i; \boldsymbol{\theta})}. \tag{2.18}$$

The general likelihood (Equation 2.16) above can therefore also be written as

$$L(\boldsymbol{\phi}, \boldsymbol{\theta} \mid n, \boldsymbol{t}) = \frac{e^{-\lambda(\boldsymbol{\theta},\boldsymbol{\phi})}}{n!} \prod_{i=1}^{n} \int_{\mathbb{A}} D(\boldsymbol{s}_i; \boldsymbol{\phi}) \prod_{k=1}^{K} P_k(\omega_{ik}|\boldsymbol{s}_i; \boldsymbol{\theta}) \prod_{r=1}^{\omega_{ik}} f_{t|\omega,k}(\boldsymbol{t}_{ik}|\omega_{ik}, \boldsymbol{s}_i; \boldsymbol{\theta})\, d\boldsymbol{s} \tag{2.19}$$

2.2.3 Lack of sufficiency of detection frequencies

The use of capture times raises the question of what additional value they have for inference. At a very basic level, if detection frequencies are sufficient statistics for $\boldsymbol{\theta}$ then capture times add no value. To investigate the sufficiency of the detection frequencies ($\boldsymbol{\Omega}$) for the unknown parameters $\boldsymbol{\theta}$ and $\boldsymbol{\phi}$, we consider the term $f_k(\boldsymbol{t}_{ik}|\boldsymbol{s}_i; \boldsymbol{\theta})$ in a discrete-occasion setting. As shown in Equation 2.19 this density can be factorised into the pmf for the count and the pdf for the detection times, given the count:

$$\begin{aligned} f_k(\boldsymbol{t}_{ikj} \mid \boldsymbol{s}_i; \boldsymbol{\theta}) &= \prod_{j=1}^{J} \frac{H_{kj}(\boldsymbol{s}_i; \boldsymbol{\theta})^{\omega_{ikj}} e^{-H_{kj}(\boldsymbol{s}_i;\boldsymbol{\theta})}}{(\omega_{ikj}!)} \left[\omega_{ikj}! \prod_{r=1}^{\omega_{ikj}} \frac{h_k(t_{ikr}|\boldsymbol{s}_i; \boldsymbol{\theta})}{H_{kj}(\boldsymbol{s}_i; \boldsymbol{\theta})} \right] \\ &= \prod_{j=1}^{J} P_k(\omega_{ikj} \mid \boldsymbol{s}_i; \boldsymbol{\theta}) f_{t_j}(\boldsymbol{t}_{ik}^{(j)}|\omega_{ikj}, \boldsymbol{s}_i; \boldsymbol{\theta}) \end{aligned} \tag{2.20}$$

For a discrete-occasion setup the likelihood can therefore be written as follows

$$L(\boldsymbol{\phi}, \boldsymbol{\theta} \mid n, \boldsymbol{t}) = \frac{e^{-\lambda(\boldsymbol{\phi},\boldsymbol{\theta})}}{n!} \prod_{i=1}^{n} \int_{A} D(\boldsymbol{s}_i; \boldsymbol{\phi}) \prod_{k=1}^{K} \prod_{j=1}^{J} P_k(\omega_{ikj} \mid \boldsymbol{s}_i; \boldsymbol{\theta}) f_{t_j}(\boldsymbol{t}_{ik}^{(j)} \mid \omega_{ikj}, \boldsymbol{s}_i; \boldsymbol{\theta})\, d\boldsymbol{s} \tag{2.21}$$

The likelihood for the Poisson count model proposed by Efford et al. (2009b) is this likelihood with a single occasion ($J = 1$) and without $f_{t_j}(\boldsymbol{t}_{ik}^{(j)}|\omega_{ikj}, \boldsymbol{s}_i; \boldsymbol{\theta})$). It ignores the times of detection and because $f_{t_j}(\boldsymbol{t}_{ik}^{(j)}|\omega_{ikj}, \boldsymbol{s}_i; \boldsymbol{\theta})$ involves $\boldsymbol{\theta}$, the detection frequencies alone (without the times of detection) are not in general sufficient for $\boldsymbol{\theta}$. And because $\boldsymbol{\phi}$ occurs in a product inside the integral in Equation 2.21, the likelihood can't be factorised into a component with $\boldsymbol{\phi}$ and without $\boldsymbol{t}_{ik}^{(j)}$, so that (by the Fisher-Neyman Factorization Theorem) the detection frequencies alone are neither sufficient for $\boldsymbol{\theta}$ nor $\boldsymbol{\phi}$. Finally, because neither the binomial nor the Bernoulli models involve the detection times, $\boldsymbol{\Omega}$ is not sufficient for $\boldsymbol{\theta}$ and $\boldsymbol{\phi}$ with any of these models either.

There are notable exceptions. The first is when $h_k(t_{ikr}, \boldsymbol{s}; \boldsymbol{\theta})$ is constant within intervals (see Chapter 3). In this case $f_{t_j}(\boldsymbol{t}_{ik}^{(j)} | \omega_{ikj}, \boldsymbol{s}_i; \boldsymbol{\theta}) = \omega_{ikj}! / T_s^{\omega_{ikj}}$, which does not involve $\boldsymbol{\theta}$ (or the detection times) and so integer counts with the Poisson model are sufficient for $\boldsymbol{\theta}$ and $\boldsymbol{\phi}$. The second is when density is constant, i.e. $D(\boldsymbol{s}; \boldsymbol{\phi}) = D$. In this case D can be factorised out of the integral and n is conditionally sufficient for $\boldsymbol{\phi}$, given $\boldsymbol{\theta}$.

Apart from these cases, if it is assumed that the effect of t and $\boldsymbol{s}$ are independent in the hazard $h_k(.)$ and that the $\boldsymbol{\theta}$ parameter vector can be split into two vectors $(\boldsymbol{\psi}, \boldsymbol{\theta})$, then the hazard can be factored (suppressing the subscripts) as:

$$h(t, \boldsymbol{s}; \boldsymbol{\theta}) = h(t; \boldsymbol{\psi}) \times \gamma(\boldsymbol{s}; \boldsymbol{\theta})$$

Then:

$$\begin{aligned} \int h(t, \boldsymbol{s}; \boldsymbol{\theta})\, dt &= \int h(t; \boldsymbol{\psi}) \times \gamma(\boldsymbol{s}; \boldsymbol{\theta})\, dt \\ &= \gamma(\boldsymbol{s}; \boldsymbol{\theta}) \int h(t; \boldsymbol{\psi})\, dt \\ &= \gamma(\boldsymbol{s}; \boldsymbol{\theta}) \nu(T, \boldsymbol{\psi}) \end{aligned}$$

It then follows that the conditional density of capture times (Equation 2.18) can be written so that it does not depend on $\boldsymbol{s}$:

$$\begin{aligned} f_{t|\omega}(\boldsymbol{t} \mid \omega, \boldsymbol{s}; \boldsymbol{\theta}) &= \omega! \prod_{r=1}^{\omega} \frac{h(t; \boldsymbol{\psi}) \gamma(\boldsymbol{s}; \boldsymbol{\theta})}{\gamma(\boldsymbol{s}; \boldsymbol{\theta}) \nu(T, \boldsymbol{\psi})} \\ &= \omega! \prod_{r=1}^{\omega} \frac{h(t; \boldsymbol{\psi})}{\nu(T, \boldsymbol{\psi})} \end{aligned} \tag{2.22}$$

The density for $\boldsymbol{t}$ can then be factored out of Equation 2.21 which means that the statistics $\boldsymbol{t}$ are S-ancillary for the parameters $\boldsymbol{\phi}$ and $\boldsymbol{\theta}$ with respect to the $\boldsymbol{\psi}$ parameters and can be safely ignored unless one is interested in making inference about $\boldsymbol{\psi}$.

2.2.4 Latent capture times

Barker et al. (2014) develop a non-spatial CR model parameterised in terms of abundance, rather than density, where the captures are identified from DNA samples. This

model accommodates multiple captures in an occasion and hence the scenario is essentially the same as one that uses passive or proximity detectors with ω_{ikj} being a count of the capture frequency for individual i at detector k during occasion j. However the times of capture are unknown and are thus latent variables that are integrated out of the likelihood.

The work in this dissertation does not deal with latent times of capture but a similar approach can be taken if such a need arises, for example if the timestamps attached to images from a camera-trap survey are faulty. The derivation below shows that applying a similar approach to that taken by Barker et al. (2014), but in a CT SCR context, leads to a SCR Poisson likelihood if the order in which individuals are captured is ignored.

Assuming one had the actual capture times, the appropriate density is $f(\boldsymbol{t}_{i\cdot}|\boldsymbol{s}_i;\boldsymbol{\theta})$ the joint distribution of capture times from K detectors for the ith individual over a study with duration $= T$. For brevity the subscript i is omitted in the derivation below as well as the dependence on $\boldsymbol{s}$ which gets integrated out from the full likelihood.

Let $\omega_\cdot = \sum_{k=1}^{K} \omega_k$ be the total capture frequency across the K detectors, $\boldsymbol{\omega} = \{\omega_1, \ldots, \omega_K\}$ be a vector of the capture frequencies at each of the k detectors, $H_\cdot = \sum_k^K H_k$ be the total integrated hazard across all K detectors where as before $H_k = \int_T h_k(t)\ dt$, $\boldsymbol{H} = \{H_1, \ldots, H_K\}$ be a vector of the K cumulative hazards, $h_\cdot = \sum_k h_k(t)$ be the total hazard rate across all K detectors at time t, and $\boldsymbol{y} = \{y_1, \ldots, y_{\omega\cdot}\}$ be a vector giving the ordered sequence of captures across detectors where $y_j \in \{1, \ldots, K\}$. Note that $\boldsymbol{y}, \boldsymbol{\omega}$ and $\omega_\cdot$ are all summaries of $\boldsymbol{t}$ and may be observed even if $\boldsymbol{t}$ is not recorded.

The density of capture times can be written as:

$$f(\boldsymbol{t} \mid \boldsymbol{\theta}) = f(\boldsymbol{t} \mid \boldsymbol{y}, \boldsymbol{\theta}) P(\boldsymbol{y} \mid \boldsymbol{\omega}, \boldsymbol{\theta}) P(\boldsymbol{\omega} \mid \omega_\cdot, \boldsymbol{\theta}) P(\omega_\cdot \mid \boldsymbol{\theta}) \tag{2.23}$$

Then:

$$\int_{\boldsymbol{t}} f(\boldsymbol{t} \mid \boldsymbol{y}, \boldsymbol{\theta}) P(\boldsymbol{y} \mid \boldsymbol{\omega}, \boldsymbol{\theta}) P(\boldsymbol{\omega} \mid \omega_\cdot, \boldsymbol{\theta}) P(\omega_\cdot \mid \boldsymbol{\theta})\ d\boldsymbol{t} = P(\boldsymbol{y} \mid \boldsymbol{\omega}, \boldsymbol{\theta}) P(\boldsymbol{\omega} \mid \omega_\cdot, \boldsymbol{\theta}) P(\omega_\cdot \mid \boldsymbol{\theta}) \tag{2.24}$$

and hence the required integral can be found from the three components: $P(\boldsymbol{y}|\boldsymbol{\omega}, \boldsymbol{\theta})$, $P(\boldsymbol{\omega}|\omega_\cdot, \boldsymbol{\theta})$ and $P(\omega_\cdot|\boldsymbol{\theta})$.

Starting with the third component $P(\omega_\cdot|\boldsymbol{\theta})$, $\omega_\cdot$ is the observed number of detections across all K traps which under the assumption of independent nonhomogeneous Poisson processes is a Poisson random variable with rate equal to the sum of the rates

for each detector $h_\cdot(t) = \sum_K h_k(t)$ and a cumulative hazard equal to $H_\cdot = \int_T h_\cdot(t)\, dt$. Therefore:

$$P(\omega_\cdot \mid \boldsymbol{\theta}) = \frac{e^{-H_\cdot}(H_\cdot)^{\omega_\cdot}}{\omega_\cdot!} \tag{2.25}$$

The second component $P(\boldsymbol{\omega}|\omega_\cdot, \boldsymbol{\theta})$ is the distribution of the observed capture frequencies conditional on the overall sum $\omega_\cdot$. Since the conditional distribution, given $\omega_\cdot$, of k independent Poisson(H_k) random variables follows a multinomial distribution with parameter vector $\boldsymbol{\pi} = \frac{\boldsymbol{H}}{H_\cdot}$, this term is:

$$P(\omega_\cdot \mid \boldsymbol{\theta}) = \frac{\omega_\cdot!}{\prod_{k=1}^K \omega_k!} \prod_{k=1}^K \pi_k^{\omega_k} \tag{2.26}$$

Lastly, if the sum of two independent k-dimensional random variables follows a multinomial distribution then the summands are individually multinomial random variables with the same parameter vector. Therefore $y_1, \ldots, y_{\omega_\cdot}$ are i.i.d multinomial observations with index 1 and parameter vector $\boldsymbol{\pi}$. Then:

$$\begin{aligned} P(\boldsymbol{y} \mid \boldsymbol{\omega}, \boldsymbol{\theta}) &= \frac{P(\boldsymbol{y}, \boldsymbol{\omega} \mid \omega_\cdot, \boldsymbol{\theta})}{P(\boldsymbol{\omega} \mid \omega_\cdot, \boldsymbol{\theta})} \\ &= \frac{P(\boldsymbol{y} \mid \omega_\cdot, \boldsymbol{\theta})}{P(\boldsymbol{\omega} \mid \omega_\cdot, \boldsymbol{\theta})} \\ &= \frac{\prod_{k=1}^K \pi_k^{\omega_k}}{\frac{\omega_\cdot!}{\prod_{k=1}^K \omega_k!} \prod_{k=1}^K \pi_k^{\omega_k}} \\ &= \frac{\prod_{k=1}^K \omega_k!}{\omega_\cdot!} \end{aligned} \tag{2.27}$$

Multiplying these 3 components together gives the following expression:

$$\frac{\prod_{k=1}^K \omega_k!}{\omega_\cdot!} \times \frac{\omega_\cdot!}{\prod_{k=1}^K \omega_k!} \prod_{k=1}^K \pi_k^{\omega_k} \times \frac{e^{-H_\cdot}(H_\cdot)^{\omega_\cdot}}{\omega_\cdot!} = \frac{1}{\omega_\cdot!} \times \prod_{k=1}^K e^{-H_k} H_k^{\omega_k} \tag{2.28}$$

and so the full likelihood for proximity detectors when capture times are latent is:

$$L(\boldsymbol{\phi}, \boldsymbol{\theta} \mid n, \boldsymbol{\omega}) = \frac{e^{-\lambda(\boldsymbol{\phi},\boldsymbol{\theta})}}{n!} \prod_{i=1}^{n} \int_{\mathbb{A}} D(\boldsymbol{s}_i; \boldsymbol{\phi}) \frac{1}{\omega_i.!} \prod_{k=1}^{K} e^{-H_{ik}(T,\boldsymbol{s}_i;\boldsymbol{\theta})} H_{ik}(T, \boldsymbol{s}_i; \boldsymbol{\theta})^{\omega_{ik}} \, d\boldsymbol{s} \tag{2.29}$$

If the derivation ignores the first term that corresponds to the ordering of captures, then the multinomial coefficient does not cancel in Equation 2.28 and the expression becomes:

$$\frac{\omega.!}{\prod_{k=1}^{K} \omega_k!} \prod_{k=1}^{K} \pi_k \times \frac{e^{-H.}(H.)^{\omega.}}{\omega.!} \tag{2.30}$$

Equation 2.30 is the product of two factors, one being the Poisson distribution for the overall total, and the second being a multinomial distribution for where the captures occurred given the overall total. This expression is equivalent to a product of k Poisson distributions and hence is equivalent to the usual SCR Poisson likelihood.

2.2.5 Relationship to DT proximity detector SCR models

The DT models for the capture histories can be easily derived from the CT formulation. The likelihood for $\boldsymbol{\phi}$ and $\boldsymbol{\theta}$ for the discrete-occasion proximity detector case in which there are K detectors and J occasions can be written in terms of Equation 2.10 as follows:

$$L(\boldsymbol{\phi}, \boldsymbol{\theta} \mid \boldsymbol{\Omega}) = P(n \mid \boldsymbol{\phi}, \boldsymbol{\theta}) \int_{A} P_{\Omega}(\boldsymbol{\Omega} \mid \boldsymbol{S}, \boldsymbol{\omega}.{>}0; \boldsymbol{\theta}) f(\boldsymbol{S} \mid \boldsymbol{\omega}.{>}0; \boldsymbol{\phi}, \boldsymbol{\theta}) d\boldsymbol{S}. \tag{2.31}$$

When a CT detection process is discretised into discrete occasions this gives rise to a Bernoulli model in the case of binary data, and to binomial and Poisson SCR models in the case of count data. To do this, divide the time interval $(0, T)$ into J subintervals with interval j running from t_{j-1} to t_j, of length $T_j = t_j - t_{j-1}$, and with $t_0 = 0$. With a CT model, the probability of detecting individual i at least once in detector k over an occasion j is $p_{kj}(\boldsymbol{s}_i; \boldsymbol{\theta}) = 1 - e^{-H_{kj}(\boldsymbol{s}_i;\boldsymbol{\theta})}$, where $H_{kj}(\boldsymbol{s}_i; \boldsymbol{\theta}) = \int_{t_{j-1}}^{t_j} h_k(u, \boldsymbol{s}_i; \boldsymbol{\theta}) \, du$.

The link between the integrated hazard and the DT response for the ith individual at the kth detector over the jth occasion ($P(\omega_{ijk}|\boldsymbol{s_i}; \boldsymbol{\theta})$) is given below for different types of DT response data.

Bernoulli (binary) model This is obtained from a CT model as

$$P_{Bern}(\omega_{ikj} \mid \boldsymbol{s}_i; \boldsymbol{\theta}) = p_{kj}(\boldsymbol{s}_i; \boldsymbol{\theta})^{\omega_{ikj}} \{1 - p_{kj}(\boldsymbol{s}_i; \boldsymbol{\theta})\}^{1-\omega_{ikj}}$$

with $p_{kj}(\boldsymbol{s}_i; \boldsymbol{\theta}) = 1 - e^{-H_{kj}(\boldsymbol{s}_i;\boldsymbol{\theta})}$ and binary ω_{ikj}.

Binomial count model Efford et al. (2009b) proposed this for the case in which the J original intervals are collapsed into $J^*(< J)$ intervals and ω_{ikj^*} is the count in the new interval j^*, which comprises N_{j^*} adjacent original intervals. In this case

$$P_{binom}(\omega_{ikj^*} \mid \boldsymbol{s}_i; \boldsymbol{\theta}) = \binom{N_{j^*}}{\omega_{ikj^*}} p_{kj^*}(\boldsymbol{s}_i; \boldsymbol{\theta})^{\omega_{ikj^*}} \{1 - p_{kj^*}(\boldsymbol{s}_i; \boldsymbol{\theta})\}^{1-\omega_{ikj^*}}$$

where $p_{kj^*}(\boldsymbol{s}_i; \boldsymbol{\theta}) = 1 - e^{-H_{kj^*}(\boldsymbol{s}_i;\boldsymbol{\theta})}$, and $H_{kj^*}(\boldsymbol{s}_i; \boldsymbol{\theta}) = \sum_{l=1}^{N_{j^*}} H_{kj}(\boldsymbol{s}_i; \boldsymbol{\theta})$.

Poisson count model A NHPP with intensity $h_k(t, \boldsymbol{s}_i; \boldsymbol{\theta})$ at time t gives rise to an event count (ω_{ikj}) in a time interval (t_{j-1}, t_j) that has the Poisson pmf

$$P_P(\omega_{ikj} \mid \boldsymbol{s}_i; \boldsymbol{\theta}) = \frac{H_{kj}(\boldsymbol{s}_i; \boldsymbol{\theta})^{\omega_{ikj}} e^{-H_{kj}(\boldsymbol{s}_i;\boldsymbol{\theta})}}{(\omega_{ikj}!)}$$

where event counts in non-overlapping intervals are independent.

2.3 Spatial capture recapture: continuous-time formulation for single-catch traps

As explained in Section 2.1.3, a variety of different detectors or traps are used in CR or SCR studies and their different characteristics determine the specification of the detection process component of the SCR model (Efford et al., 2009a). Capture in either a multi or single-catch trap precludes capture in any other trap during that occasion. The competition between traps for individuals leads to a competing risks formulation for multi-catch traps but single-catch traps have the additional complexity that, once they are full, they are effectively unable to catch any other individuals. A suitable capture model for single-catch traps therefore needs to account for a second kind of competing risk, that of competition amongst individuals for traps (Efford et al., 2009a).

The nature of single-catch traps induces a dependence in captures between individuals and compared to multi-catch traps it is considerably more complicated to construct a suitable likelihood (Borchers, 2012, 2016). To date no DT likelihood function for single-catch traps exists (Efford et al., 2009a; Royle et al., 2013c; Borchers, 2016; Borchers and Marques, 2016) and consequently the DT multi-catch trap estimator is typically used for the analysis of single-catch trap data.

For situations in which actual capture times are recorded, the CT setup enables the construction of an appropriate single-catch trap likelihood with only small modifications to the general CT likelihood (Equation 2.16). Traditionally, data from live-trapping studies do not contain actual capture times however devices that record times when a trap is triggered are available and have been used by Cowan and Forrester (2012) to study the activity patterns of possums. This dataset on possums is described in Section 1.5 and analysed later in Chapter 4.

Following Barker et al. (2014), if we were dealing with proximity detectors it would be straight forward to handle latent times of capture by integrating times out of the likelihood as shown in Section 2.2.4. However the fact that single-catch traps induce a dependence between individuals complicates matters and means that a high dimensional integral would need to be solved.

The CT single-catch trap likelihood is presented below in Section 2.3.1. Simulations are used in both Chapters 3 and 4 to explore the performance of this new estimator and compare it with that of the DT multi-catch estimator, in the first case with a constant hazard and in the second with a time-varying hazard function.

2.3.1 A CT likelihood for single-catch traps with observed times

Assuming that the actual times of capture in single-catch traps are available, the process generating detections can be modelled as a competing hazards survival process (Borchers and Efford, 2008) in which "death" corresponds to being caught and all individuals become "alive" again after release. There are K traps and once caught an animal remains in the detector until it is released. Traps are regularly checked and the period of time preceding a detector check is an occasion, i.e. an interval of time rather than an instantaneous point in time. If release times are the same for all traps then this leads to a natural definition of occasions (for DT SCR models) and the survey duration T can be divided into J occasions. Each individual is exposed to trap-specific hazards that we assume are at any time independent of the individual's capture history up to that time (though the model is easily extended to estimate different hazard levels before and after first capture as per model M_b).

As before, the likelihood for $\boldsymbol{\phi}$ and $\boldsymbol{\theta}$ is the joint distribution of the number of individuals captured n, and the density of the outcomes "ω_{ik} events, at times $t_{ik1} < \ldots < t_{ik\omega_{ikr}}$", for all i and k. The appropriate likelihood is the same expression as that given for proximity detectors (Equation 2.16) with a slight change to the term representing the density of capture times, which is $f_k(\boldsymbol{t}_{ik} \mid \boldsymbol{s}_i; \boldsymbol{\theta}) = S_k(T \mid \boldsymbol{s}_i; \boldsymbol{\theta}) \prod_r h_k(t_{ikr} \mid \boldsymbol{s}_i; \boldsymbol{\theta})$. The survival function term $S_k(T \mid \boldsymbol{s}_i; \boldsymbol{\theta})$ involves integrating the detection hazard at the kth trap over the survey duration to produce the cumulative hazard, which can be thought of as accumulating the exposure to capture at that trap over time.

The likelihood for single-catch traps needs to account for the consequences of a trap catching and holding an individual. The first consequence is that the trapped individual cannot be caught at any other trap until it is released, i.e. the individual's exposure to detection by all other traps is zero for the remaining period of capture. The second consequence is that the trap in which the individual is held cannot catch any other individuals until the time of release, i.e. exposure to that trap for all other individuals is zero. The DT multi-catch estimator accounts for the first consequence but not the second.

The proximity detector survival function therefore needs to be modified as follows to be suitable for data from single-catch traps:

1. when a particular individual is caught in a particular trap, the hazard of that individual being caught anywhere else is zero for the period of time that the individual is held in the trap, i.e. until release.

2. once a trap captures an animal, the hazard to all other uncaught individuals of being caught at that trap must be zero until the trap is reset.

To construct a likelihood with these features, we define an indicator variable $a_k(t)$ that is 1 if trap k is unoccupied at time t and zero otherwise ($k = 1, \ldots, K$), and we define another indicator variable $v_i(t)$ to be 1 if individual i is not in a trap at time t, and zero otherwise ($i = 1, \ldots, n$). (These variables are readily calculated from the observed capture and release times of individuals at each trap.) The hazard function for individual i for trap k at time t is then conveniently written as $v_i(t)a_k(t)h_k(t, \boldsymbol{s}_i; \boldsymbol{\theta})$ from which it can be seen how the two indicator functions "switch" the hazard of detection on and off so that it is zero when capture is not possible.

The survivor function across all traps for individual i to time t is therefore defined to be

$$S_{\cdot}^{*}(t, \boldsymbol{s}_i; \boldsymbol{\theta}) = \exp\left(- \int_0^t v_i(u) \sum_{k=1}^{K} a_k(u) h_k(u, \boldsymbol{s}_i; \boldsymbol{\theta}) \, du \right) \tag{2.32}$$

Further details of how the survival function calculation is implemented can be found in Appendix A.

The likelihood for $\boldsymbol{\phi}$ and $\boldsymbol{\theta}$ for single-catch trap SCR surveys then becomes:

$$L(\boldsymbol{\phi}, \boldsymbol{\theta} \mid n, \boldsymbol{t}) = \frac{e^{-\lambda(\boldsymbol{\phi},\boldsymbol{\theta})}}{n!} \prod_{i=1}^{n} \int_A D(\boldsymbol{s}_i; \boldsymbol{\phi}) S_{\cdot}^{*}(T, \boldsymbol{s}_i; \boldsymbol{\theta}) \times \prod_{k=1}^{K} \prod_{r=1}^{\omega_{ik}} h_k(t_{ikr}, \boldsymbol{s}_i; \boldsymbol{\theta})\, d\boldsymbol{s} \quad (2.33)$$

where $\lambda(\boldsymbol{\phi}, \boldsymbol{\theta}) = \int_A D(\boldsymbol{x}; \boldsymbol{\phi}) p_{\cdot}(\boldsymbol{x}; \boldsymbol{\theta})\, d\boldsymbol{x}$, and the integral is over all possible activity centre locations that could have led to a detection on the survey. The term $p_{\cdot}(\boldsymbol{x}; \boldsymbol{\theta})$ is the overall probability of being caught during the survey, which depends on the combined detection hazard $h_{\cdot}(t, \boldsymbol{x}; \boldsymbol{\theta})$ over the duration of the survey. This in turn depends on $a_k(t)$ $(k = 1, \ldots, K)$, which depend on random variables (the times of capture in each trap). Calculating $p_{\cdot}(\boldsymbol{x}; \boldsymbol{\theta})$ requires taking expectation over these K random variables, and since they are dependent for single-catch traps a K dimensional integral would need to be evaluated – something that is prohibitively computationally expensive. The estimator therefore involves maximising the above likelihood equation with $\lambda(\boldsymbol{\phi}, \boldsymbol{\theta})$ replaced by $\lambda(\boldsymbol{\phi}, \boldsymbol{\theta}) = \int_A D(\boldsymbol{s}; \boldsymbol{\phi}) \exp\left(-\int_0^T \sum_{k=1}^{K} a_k(u) h_{\cdot}(u, \boldsymbol{s}; \boldsymbol{\theta})\, du\right) d\boldsymbol{s}$, which depends on the observed $a_k(t)$ $(k = 1, \ldots, K)$. Consequently the proposed estimator may not be an MLE and may not enjoy the asymptotic properties of MLEs and hence the bias of the estimator and the coverage of a confidence interval estimator based on the observed information is evaluated by simulation in Section 3.2.1.

2.4 Summary of models

Table 2.1 summarises the different models that are applied in this research. It is included for reference purposes to help a reader easily understand what model is being applied and what the key differences between the model types are.

Table 2.1: Summary of the different models used in this research. Time formulation refers to the use of either a discrete-time (DT) model or a continuous-time (CT) model.

Time Formulation	Response Type	Detector Type	Independence	
			between detectors within individual?	between individuals at each detector?
DT	Proximity	Binary	Yes	Yes
DT	Proximity	Count	Yes	Yes
CT	Proximity	Times	Yes	Yes
DT	Multi-catch	Binary	No	Yes
CT	Single-catch	Times	No	No

2.5 More about the hazard function

As shown in Section 2.2, the key difference between the DT models and the CT models is that the usual detection function that models detection during an occasion is replaced with a detection hazard. This section begins by discussing different forms for modelling a non-constant detection hazard through time, shows how to link the DT detection function with the CT detection hazard, and touches on the use of a hazard function in DT SCR models with varying effort.

2.5.1 Forms for the hazard function

When the hazard function varies through time, the hazard of individual i being detected at trap k depends as before on the distance between trap k and individual i's activity centre, but also depends on time. This scenario is more realistic as most animals are more likely to be caught at certain times rather than others depending on their behaviour and activity patterns.

The non-constant hazards have been parameterised in this work to contain a component that depends on distance ($h(\boldsymbol{s};\boldsymbol{\theta})$) and a component that depends on time ($h(t;\boldsymbol{\psi})$). As before the dependence of the first component on distance through $\boldsymbol{s}(d_k(\boldsymbol{s}))$ is not always made explicit for notational brevity. Note that the two components do not interact and hence the effect of time is independent of the effect of distance (and vica versa).

$$h(t,\boldsymbol{s};\boldsymbol{\theta},\boldsymbol{\psi}) = h(\boldsymbol{s};\boldsymbol{\theta}) \times h(t;\boldsymbol{\psi}) \tag{2.34}$$

The second component $h(t, \boldsymbol{\psi})$ determines the hazard shape over time which is scaled by a factor that depends on the distance from the individuals' activity centre to the detector ($h(\boldsymbol{s}; \boldsymbol{\theta})$). This scaling factor depends on the parameters that appear in the usual detection function, i.e. for the half-normal form the parameters in $\boldsymbol{\theta}$ include detectability (g_0) and dispersion characteristics (σ). It is only $h(t; \boldsymbol{\psi})$ that changes form for different selected hazard shapes over time and two forms for $h(t; \boldsymbol{\psi})$ are given below.

The detection hazards used in this work are conceived as cyclical hazards that repeat over time after a specified cycle length. This approach facilitates the modeling of a daily pattern to detectability that, for example, can result in nocturnal animals being very unlikely to be captured during the day. Using a cyclical hazard means that the hazard is constrained to begin and end at the same point each cycle. Note that the CT hazard results in a model in which variation in detectability is modelled at a finer resolution than DT models with occasions. Further details are given below for both a cosine and a regression spline hazard form.

Cosine hazard function

The standard cosine function (Figure 2.2) produces a cyclical pattern that varies in height between -1 and 1. The function is connected to revolutions of a circle and can be parameterised in either degrees or radians. The latter approach is implemented in R and applied in this work.

The angular frequency is denoted as α and converts times into radians according to a specified cycle frequency. The angular frequency can be calculated as $\alpha = \frac{2\pi}{\text{cycle frequency}}$. For example if the cycle frequency is 24 hours, $\alpha = 0.26$ and so a time of 36 hours would be equivalent to 9.42 radians or 3π. Given that a full cycle is equal to 2π or 6.28 radians, 36 hours would be 3.14 or π radians into the second cycle, i.e. halfway into the second cycle.

Figure 2.2: Standard cosine function with the number of radians in terms of π on the x axis.

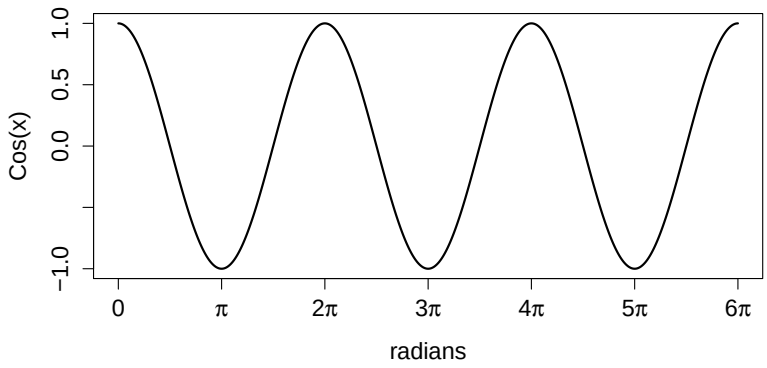

The standard cosine curve has a peak at zero radians and a minimum value of -1. The parameterisation below includes two parameters to shift the curve vertically and horizontally.

$$h(t;\boldsymbol{\psi}) = \cos(\alpha \times (t + \psi_1)) + \psi_2 \tag{2.35}$$

The parameter ψ_1 shifts the curve horizontally to control when the cycle peak occurs. For example if a 24 hour cycle started at midnight and an animal was most detectable at 2am then the curve should be shifted two units to the right. Similarly ψ_2 shifts the curve vertically and since hazard rates cannot be negative must be parameterised appropriately to ensure that this constraint holds:

$$\psi_2 = 1 + e^{\psi_*}$$

where ψ_* is an unconstrained parameter estimate.

Regression spline hazard function

Regression splines are a form of less rigid parametric fitting that can be thought of as fitting piecewise polynomials to segments of the data. A regression spline takes the form of a weighted sum of smooth functions of the data, and these functions of the data are known as basis functions. The flexibility of regression splines increases with the degrees of freedom or knots, i.e. increasing the knots increases the number of parameters that need to be estimated and increases the function's flexibility.

An array of different types of basis functions are available that produce splines with different features. Cyclic cubic regression splines are used in this work to produce hazard cycles of a specified length that repeat over time.

The $h(t;\boldsymbol{\psi})$ component with a flexible shape is parameterised as follows:

$$h(t;\boldsymbol{\psi}) = e^{f(t;\boldsymbol{\psi})} \tag{2.36}$$

where $f(t;\boldsymbol{\psi}) = \beta_1 b_1(t) + \beta_2 b_2(t) + \ldots + \beta_p b_p(t)$, the $b_p(t)$ refer to p basis functions, p is determined by the specified degrees of freedom (denoted as K), and the log link ensures a positive detection hazard. The R package *mgcv* (Wood, 2016) is used to construct the necessary basis functions. Specifying "fit = FALSE" in the *gam* function returns the basis functions that can then be used as ordinary covariates in the hazard model. Note that the intercept of the spline coefficients is redundant because its role is effectively subsumed by the $h(\boldsymbol{s};\boldsymbol{\theta})$ scaling factor. Plots that depict the detection hazards are focusing on the shape through time and hence are scaled so that they integrate to 1. Furthermore, a degree of freedom is lost when specifying hazards with a cyclic cubic spline form. The number of degrees of freedom for different spline hazards that are reported in this work matches the number given to the *gam* function in package *mgcv*. Therefore the actual number of parameters estimated in the reported models is two less than the value given for K.

Figure 2.3 depicts three fictitious examples of different possible hazard shapes that can be modelled with regression splines. The top panel shows a simple detection hazard that rises to a peak about halfway through the cycle and then falls away again. The second example is similar but remains around its peak for a longer time. The final example shows a hazard that has two peaks, if one considers the 24 hour hazard cycle to be in sync with a 24 hour daily cycle then these peaks occur roughly at dawn and dusk. These shapes are produced by making up a series of data points that follow a certain pattern, extracting the basis functions, and then using the basis functions as covariates for fitting a generalised linear model with a log link. For example the fitted model for the hazard shape for the first shape with K = 4 is $h(t;\boldsymbol{\psi}) = e^{1.145 b_1(t) + 1.284 b_2(t)}$.

A large number (500,000) of first capture times from a hypothetical study lasting 56 hours are simulated from different detection hazards and plotted in Figure 2.4 with both the underlying hazards (in blue) and the theoretical distribution of times (in red). It is apparent from the top plot that as expected a constant hazard leads to exponentially distributed first capture times, and that in general, later capture times are less likely due to the accumulation of the detection hazard, i.e. the hazard of detection accumulates through time making it less likely to "survive" to later times.

Figure 2.3: Three examples of possible detection hazard shapes that can be modelled using regression splines of increasing complexity. From top to bottom the degrees of freedom are 4, 8 and 10.

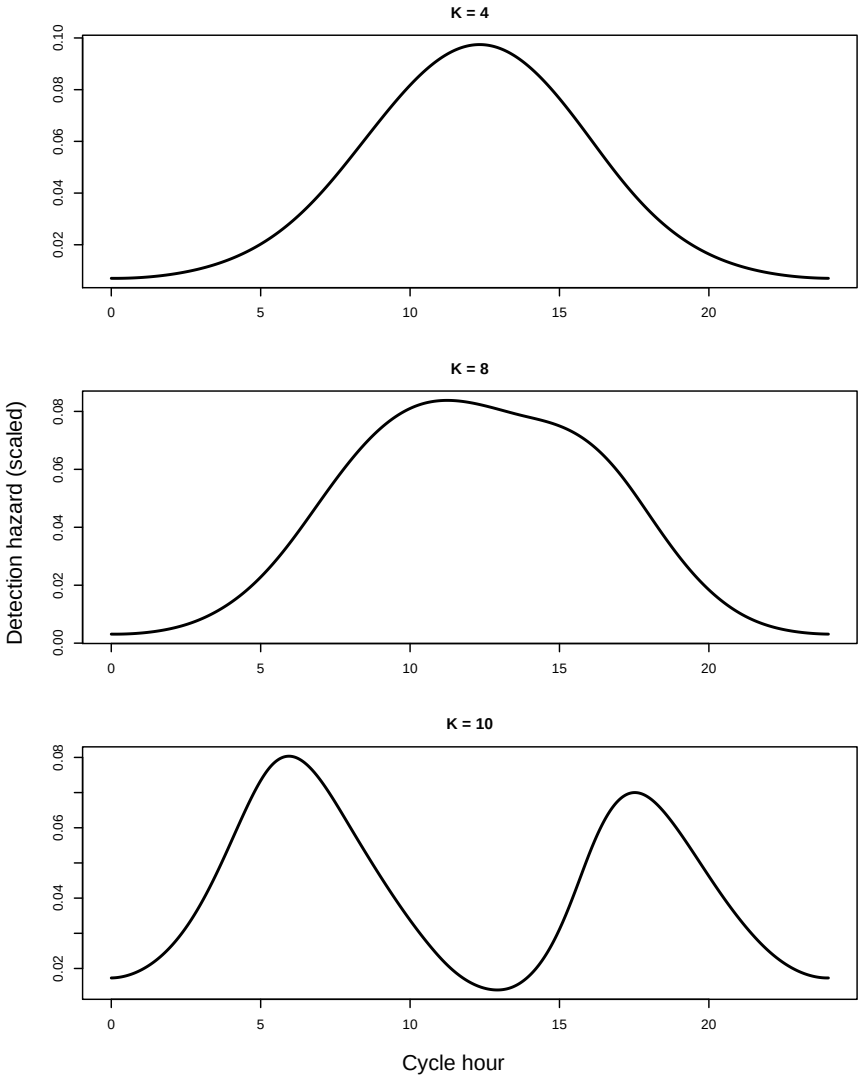

Figure 2.4: Plots of 500,000 simulated first capture times from a hypothetical study lasting 56 hours and using three different underlying 24 hour hazards. The underlying hazards (blue) and the theoretical distribution of first capture times (red) are scaled appropriately and overlaid on the simulated times (grey).

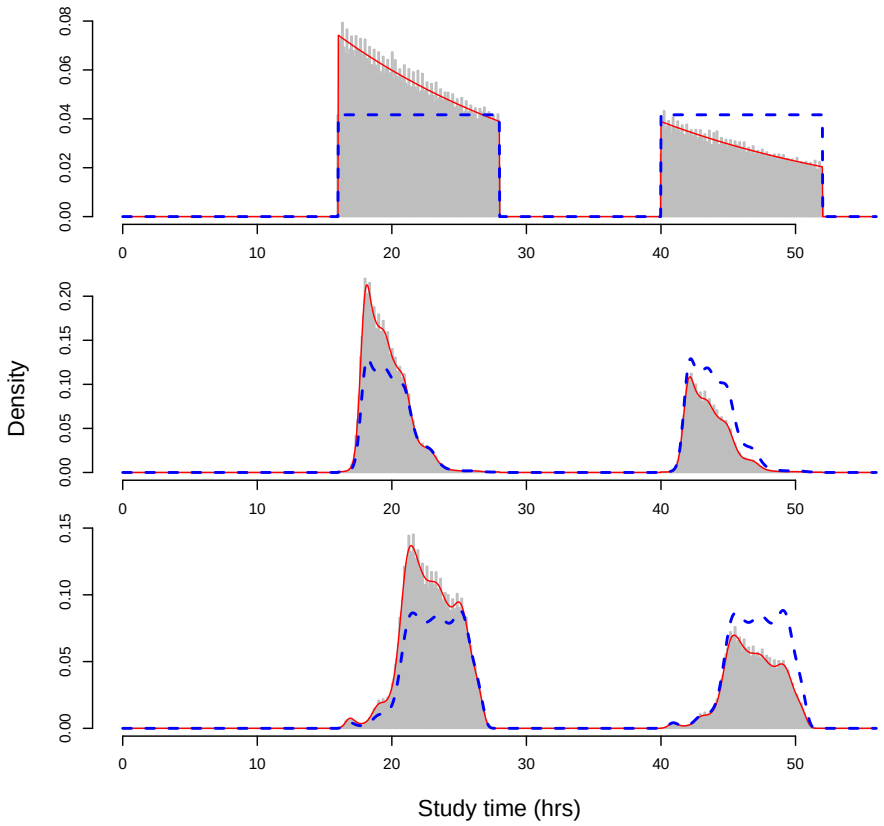

Alternative parameterisation

Below is an alternative way of parameterising the time-varying hazard function that resembles a GLM setup with a linear predictor and a link function:

$$h(t, \boldsymbol{s}; \boldsymbol{\psi}) = e^{\beta_0} \times e^{\beta_1 \times \text{ distance}} \times e^{f(t)} \dots$$

The first component can be thought of as the equivalent of g_0 on the hazard scale, i.e. it gives the appropriate scaling of the time-varying hazard when distance is equal to zero. The second component gives the effect of distance and the third component the effect of time. If these are the only factors involved then this parameterisation amounts to the same thing as the initial parameterisation. This can be seen if we let $e^{\beta_0 + \beta_1 \times \text{ distance}} = h(\boldsymbol{s}; \boldsymbol{\theta})$ and $e^{f(t)} = h(t, \boldsymbol{\psi})$. The primary advantage of this alternative parameterisation is that it can readily accommodate other covariates for the hazard as well as interaction effects. This paramaterisation is akin to using a complementary log log link as can be seen below:

$$\begin{aligned}
p_{kj}(\boldsymbol{s}, t_0, t_1; \boldsymbol{\theta}) &= 1 - \exp\left(-\int_{t_0}^{t_1} h(u, \boldsymbol{s}; \boldsymbol{\psi})\, du\right) \\
&= 1 - \exp\left(-\int_{t_0}^{t_1} e^{\beta_0} \times e^{\beta_1 \times \text{ distance}} \times e^{f(t)}\, d\text{time}\right) \\
&= 1 - \exp\left(-e^{\beta_0} \times e^{\beta_1 \times \text{ distance}} \int_{t_0}^{t_1} e^{f(t)}\, d\text{time}\right) \\
&= 1 - \exp\left(-e^{\beta_0} \times e^{\beta_1 \times \text{ distance}} \times H_{t_0}^{t_1}\right) \\
\exp\left(-e^{\beta_0} \times e^{\beta_1 \times \text{ distance}} \times H_{t_0}^{t_1}\right) &= (1 - p_{kj}(\boldsymbol{s}, t_0, t_1; \boldsymbol{\theta})) \\
e^{\beta_0 + \beta_1 \times \text{ distance}} \times H_{t_0}^{t_1} &= -log(1 - p_{kj}(\boldsymbol{s}, t_0, t_1; \boldsymbol{\theta})) \\
\beta_0 + \beta_1 \times \text{ distance} + log(H_{t_0}^{t_1}) &= log(-log(1 - p_{kj}(\boldsymbol{s}, t_0, t_1; \boldsymbol{\theta})))
\end{aligned}$$

where the term on the right is the cloglog transformation of p_{kj}. Note that for brevity the notation for the hazard function that includes the $\boldsymbol{\psi}$ parameter vector will only be used when explicitly referring to a non-constant hazard and not in general.

2.5.2 Linking the CT hazard function with the DT detection function

The estimators from CT and DT models are compared later on in several simulation studies. The data for these studies are simulated in CT using a CT detection hazard but this hazard needs to be linked with the DT detection function to ensure that the detection process is not misspecified for the DT models. In other words we need the CT data to be in sync with a DT detection function that has particular parameter values. If $T_j = t_j - t_{j-1}$ where t_{j-1} is the start of occasion j and t_j the end, then this is accomplished by specifying the detection probability for detector k in occasion j of duration T_j in terms of the hazard function as follows.

$$p_{kj}(\boldsymbol{s};\boldsymbol{\theta}) = 1 - \exp\left(-\int_{t_{j-1}}^{t_j} h_k(u,\boldsymbol{s};\boldsymbol{\theta})\, du\right) \tag{2.37}$$

Under the assumption of a constant hazard $\int_{t_{j-1}}^{t_j} h_k(u,\boldsymbol{s};\boldsymbol{\theta})\, du = h_k(\boldsymbol{s};\boldsymbol{\theta}) \times T_j$ and hence solving Equation 2.37 for $h_k(\boldsymbol{s};\boldsymbol{\theta})$ leads to a hazard with the following form:

$$h_k(\boldsymbol{s};\boldsymbol{\theta}) = \frac{-\log(1 - p_{kj}(\boldsymbol{s};\boldsymbol{\theta}))}{T_j} \tag{2.38}$$

As explained in Section 2.5.1, the paramaterisation used when the hazard function is not constant through time has a component that depends on distance $h(\boldsymbol{s};\boldsymbol{\theta}))$ and a component that depends on time $h(t;\boldsymbol{\psi})$. Since $h(\boldsymbol{s};\boldsymbol{\theta}))$ does not depend on time, $\int h(t,\boldsymbol{s};\boldsymbol{\theta},\boldsymbol{\psi})\, dt = h(\boldsymbol{s};\boldsymbol{\theta}) \int h(t;\boldsymbol{\psi})\, dt$ and as before $h(\boldsymbol{s};\boldsymbol{\theta})$ can be specified so that the CT detection hazard links with the DT detection function as follows:

$$h_k(\boldsymbol{s};\boldsymbol{\theta}) = \frac{-log(1 - p_{kj}(\boldsymbol{s};\boldsymbol{\theta}))}{\int_{T_j} h(t;\boldsymbol{\psi})\, dt} \tag{2.39}$$

Note that for the cosine hazard, if the integration $\int h(t;\boldsymbol{\psi})\, dt$ is carried out over a period that is equal to a multiple of the cycle length, the first cosine component of $h(t;\boldsymbol{\psi})$ $(cos(\alpha \times (t + \psi_1)))$ integrates to zero, and in such cases the integration in the denominator will become $T_j \times \psi_2$.

It may be helpful to think about this linkage for a given distance. In other words, for a given distance from a trap, integrating the associated hazard over the duration of the jth occasion will lead to the probability of capture during that occasion for an individual with an activity centre that given distance away from the trap. If the hazard is specified according to Equation 2.37, and probabilities are calculated for a

range of distances, then the probabilities will follow the same shape as the detection function used in the specification ($p_{kj}(\boldsymbol{s};\boldsymbol{\theta})$).

In subsequent analyses, I use hazard functions in which $p_{kj}(\boldsymbol{s};\boldsymbol{\theta})$ has a half-normal form:

$$p_{kj}(\boldsymbol{s};\boldsymbol{\theta}) = g_{0,T_j} \exp\left(\frac{-d_k(\boldsymbol{s})^2}{(2\sigma^2)}\right)$$

where as before $d_k(\boldsymbol{s})$ is the distance from $\boldsymbol{s}$ to detector k and g_{0,T_j} and σ are parameters to be estimated. The parameter g_{0,T_j} is the probability that an individual with activity centre located at a detector is detected in a time period of length T_j.

Specifying a model for $p_{kj}(\boldsymbol{s};\boldsymbol{\theta})$ implies a model for $h_k(t,\boldsymbol{s};\boldsymbol{\theta},\boldsymbol{\psi})$, although not a unique one. The mean value of the detection hazard in interval j must be $\bar{h}_{kj}(\boldsymbol{s};\boldsymbol{\theta},\boldsymbol{\psi}) = -\log\{1-p_{kj}(\boldsymbol{s};\boldsymbol{\theta})\} / \int h(t;\boldsymbol{\psi})\,dt$ and any $h_k(t,\boldsymbol{s};\boldsymbol{\theta},\boldsymbol{\psi})$ with this mean is consistent with $p_{kj}(\boldsymbol{s};\boldsymbol{\theta})$. When the hazard is constant in the interval there is a one-to-one relationship between the detection hazard and the detection probability.

As shown above, the hazard function specified in this way will produce a detection function with a half-normal shape when it is integrated over a specific period of time (for example $H_{t_0}^{t_1}$ would be the integrated or cumulative hazard for the length of the first interval from t_0 to t_1). When the hazard varies across time, integrating the hazard over some other interval of time will give a different integrated hazard to $H_{t_0}^{t_1}$ and consequently the detection function will have a shape that is different to the half-normal, i.e. the effect of distance will change over time. The discrete-occasion model can only achieve a similar degree of flexibility if occasion-specific parameters are estimated (although the shape of the detection function will still be constrained to be half-normal in each interval).

This can be seen mathematically for occasion j that runs from t_0 to t_1 as follows:

$$\begin{aligned}
p_{kj}(\boldsymbol{s},t_0,t_1;\boldsymbol{\theta}) &= 1-\exp\left(-\int_{t_0}^{t_1} h(u,\boldsymbol{s};\boldsymbol{\theta},\boldsymbol{\psi})\,du\right)\\
&= 1-\exp\left(-h(\boldsymbol{s};\boldsymbol{\theta})\int_{t_0}^{t_1} h(u;\boldsymbol{\psi})\,du\right)\\
&= 1-\exp\left(-h(\boldsymbol{s};\boldsymbol{\theta})H_{t_0}^{t_1}\right)\\
&= 1-\exp\left(-h(\boldsymbol{s};\boldsymbol{\theta})\right)^{H_{t_0}^{t_1}}
\end{aligned}$$

Hence, when the cumulative hazard is equal to $H_{t_0}^{t_1}$ the detection function will have the form of $p_{kj}(\boldsymbol{s};\boldsymbol{\theta})$ (half-normal in this work but need not be), but this will

not hold for different values of $H_{t_j}^{t_j+1}$. If a time-varying cyclic hazard has the same cycle length as the occasions used then the integrated hazard for each occasion will be the same.

2.5.3 Models with varying effort

CT models readily accommodate detectors that are operational for different periods of time by setting the detection hazard at a detector to zero while the detector is out of operation (i.e. $h_k(t, \boldsymbol{s}; \boldsymbol{\theta}, \boldsymbol{\psi}) = 0$ if detector k was not operating at time t). This is the basis of the varying effort model for binary detectors and counts in Efford et al. (2013).

However it should be noted that in that case it was assumed that the effect on the hazard is proportional to a standard unit of effort, i.e. if the effort for a given occasion is twice that of a standard unit of effort then the detection hazard gets doubled. The varying effort model can therefore accommodate occasions that are of different lengths but in order to do this it implicitly assumes that the hazard is constant through time.

The CT framework generalises this idea and can for example recognise that a detector failing for a period of time during the day will have little effect on the detectability of a nocturnal species. The ability of the CT model to properly handle varying trap exposure is what leads to the construction of the single-catch trap likelihood. It is more difficult to accommodate detectors when their time of failing is unknown, and that problem is not addressed here.

Chapter 3

Models with a constant detection hazard

This chapter presents models under the assumption of a constant detection hazard through time, firstly in the context of proximity detectors and secondly for single-catch traps. The first section illustrates how the general continuous-time (CT) proximity likelihood reduces to a discrete-time (DT) Poisson count model when the detection hazard is constant through time. Both a DT binary proximity detector model and a CT proximity detector model with a constant hazard are applied to the Belize jaguar dataset followed by two simulation studies that compare these estimators when captures are firstly independent of each other, and secondly when there is spatio-temporal correlation in captures.

The second section again uses two simulation studies to explore the robustness of the DT multi-catch estimator when it is incorrectly applied to single-catch trap data, and to assess the performance of the correct CT single-catch trap likelihood (Equation 2.33) presented in Chapter 2. The first simulation study examines and compares the performance of the estimators when the density component of the model is incorrectly specified. The second set of simulations is similar but has density correctly specified in the models.

3.1 Proximity detectors

3.1.1 Simplified CT proximity likelihood

When one assumes that activity centres occur according to a homogeneous Poisson process, the rate parameter $D(\boldsymbol{x};\boldsymbol{\theta})$ becomes a constant D. Hence $\lambda(\boldsymbol{\theta},\boldsymbol{\phi}) = Da(\boldsymbol{\theta})$

where $a(\boldsymbol{\theta}) = \int_A p.(\boldsymbol{x};\boldsymbol{\theta})\, d\boldsymbol{x}$ can be thought of as the effective survey area. In addition to this, if the detection hazards do not change with time $h_k(t, \boldsymbol{s}_i;\boldsymbol{\theta}) = h_k(\boldsymbol{s}_i;\boldsymbol{\theta})$, and so $H_k(\boldsymbol{s}_i;\boldsymbol{\theta}) = T \times h_k(\boldsymbol{s}_i;\boldsymbol{\theta})$ and consequently $f_{t|\omega,k}(\boldsymbol{t}_{ik}|\omega_{ik}) = \omega_{ik}! \prod_{r=1}^{\omega_{ik}} T^{-1}$.

As a result, the likelihood (Equation 2.16) simplifies to

$$L(D, \boldsymbol{\theta} \mid n, \boldsymbol{t}) \;=\; \left(\frac{D^n e^{-Da(\boldsymbol{\theta})}}{n!} \prod_{i=1}^{n} \int_A \prod_{k=1}^{K} P_k(\omega_{ik}|\boldsymbol{s}_i;\boldsymbol{\theta})\, d\boldsymbol{s}\right)\left(\omega_{ik}! \prod_{r=1}^{\omega_{ik}} \frac{1}{T}\right) \quad (3.1)$$

The second term in large brackets is the pdf of the detection times $\boldsymbol{t}$, given the detection frequencies $\{\omega_{ik}\}$ $(i = 1, \ldots, n; k = 1, \ldots, K)$. Since this term does not contain any model parameters, and the term in the first large brackets contains the parameters and the detection frequencies $\{\omega_{ik}\}$ but not the detection times, it follows (from the Fisher-Neyman Factorization Theorem for sufficiency) that in this case the detection frequencies are sufficient statistics for the parameters $\boldsymbol{\theta}$ and D, i.e. that no information about D is lost by discarding the detection times. This is the same result as was obtained by Chao and Lee (1993) (from a similar likelihood, albeit with a single trap and parameterised in terms of abundance N rather than density D), but the result does not hold in general with non-constant hazards in time, as discussed in the previous chapter.

Recall that the overall survivor function $S.(T, \boldsymbol{s}_i;\boldsymbol{\theta}) = \exp\left(-\int_0^T h.(t, \boldsymbol{s}_i;\boldsymbol{\theta})\, dt\right)$, and from Equation 2.17 that $P_k(\omega_{ik} \mid \boldsymbol{s}_i;\boldsymbol{\theta}) = \frac{H_k(\boldsymbol{s}_i;\boldsymbol{\theta})^{\omega_{ik}} S_k(T,\boldsymbol{s}_i;\boldsymbol{\theta})}{\omega_{ik}!}$. After writing $H_k(\boldsymbol{s}_i;\boldsymbol{\theta})$ as $T \times h_k(\boldsymbol{s}_i;\boldsymbol{\theta})$, and cancelling the ω_{ik}!s and $T^{\omega_{ik}}$s, the reduced likelihood (3.1) can be written as:

$$L(D, \boldsymbol{\theta} \mid n, \boldsymbol{t}) = \frac{D^n e^{-Da(\boldsymbol{\theta})}}{n!} \prod_{i=1}^{n} \int_A \prod_{i=1}^{n} S.(T, \boldsymbol{s}_i;\boldsymbol{\theta}) \prod_{k=1}^{K} \prod_{r=1}^{\omega_{ik}} h_k(\boldsymbol{s}_i;\boldsymbol{\theta})\, d\boldsymbol{s} \quad (3.2)$$

3.1.2 Relationship to Poisson count models

One can see from Equation (3.1) that under the above assumptions, the CT model gives rise to a Poisson count model since $P_k(\omega_{ik})$ is a Poisson pmf. If we consider the data as occuring during one long interval of duration T, the rate parameter is $Th_k(\boldsymbol{s};\boldsymbol{\theta})$. The term in the second large bracket can be neglected because it is constant with respect to the parameters.

This model was proposed in Appendix A of Efford et al. (2009b), and a similar model was proposed by Royle et al. (2009a). The CT model provides an interpretation of the Poisson rate parameter of these models as the cumulative detection hazard, $Th_k(\boldsymbol{s}_i;\boldsymbol{\theta})$. Both Efford et al. (2009b) and Royle et al. (2009a) proposed

modelling $Th_k(\boldsymbol{s}_i;\boldsymbol{\theta})$ using the same functional forms as are used for the probability of detecting an individual within an occasion, but allowing an intercept greater than 1. This may be a reasonable strategy but modellers should be aware that $p_{kj}(\boldsymbol{s};\boldsymbol{\theta})$ and $h_{kj}(\boldsymbol{s};\boldsymbol{\theta})$ necessarily have different shapes because $p_{kj}(\boldsymbol{s};\boldsymbol{\theta}) = 1 - e^{-T_j h_{kj}(\boldsymbol{s};\boldsymbol{\theta})}$. So for example, assuming a half-normal shape for the Poisson rate parameter (as do Royle et al., 2009a): $T_j h_{kj}(\boldsymbol{s};\boldsymbol{\theta}) = \lambda_0 \exp\left(-d_k(\boldsymbol{s})^2/\sigma^2\right)$ generates a shape for the detection function $p_{kj}(\boldsymbol{s};\boldsymbol{\theta})$ that is not half-normal.

Note that for this scenario, the multi-occasion ($J > 1$) likelihood is identical to a single-occasion likelihood with occasion duration $T = \sum_{j=1}^{J} T_j$ (the only difference being the multiplicative constant $\omega_{ikj}!/T_j^{\omega_{ikj}}$). A consequence of this is that when detection hazards do not change with time (or change after first capture as per model M_b), the notion of occasion is redundant when using a Poisson count model – since the likelihood is identical whether or not it involves occasions.

Lack of sufficiency of detection frequencies

I showed in Section 2.2.5 that the discrete-occasion Bernoulli, binomial and Poisson models are reduced-data versions of the CT model and that the detection histories or detection frequencies $\boldsymbol{\Omega} = \{\omega_{ikj}\}$ ($i = 1,\ldots,n; k = 1,\ldots,K; j = 1,\ldots,J$, where J is the number of occasions in the survey) are not in general sufficient statistics for $\boldsymbol{\theta}$ and $\boldsymbol{\phi}$, i.e. that in general detection time is informative.

As mentioned there, a notable exception is when the detection hazard is constant within occasions. In this case, discarding detection times does not discard information about population density. Reducing counts to a binary event does however discard information and the consequences of this reduction are explored in the first set of simulations below.

3.1.3 Jaguar application

The Belize jaguar dataset is analysed with both a DT binary proximity detector model, and a CT proximity detector model. Density is assumed to be constant with a constant probability of detection across occasions in the first case, and a constant detection hazard across time in the second case. As shown above, the CT model reduces to a Poisson count model under these assumptions and so comparisons are essentially between a model that uses binary data and a model that uses count data for the detection histories.

A total of 207 detections of 17 identifiable males were made, of which six males (35%) were detected at least twice in a day at the same detector. Not all detectors

operated for the 90 days of the survey and hence the appropriate detection hazard is set to zero for all of the failed days in the case of the CT model, and by removing a detector from occasions on which it was out of action in the case of the DT model.

In addition to models with no covariates, models with a behavioural response in the form of separate g_0 and/or σ parameters before and after first detection were considered. This led to models with a behavioural response for g_0 but not σ being selected on the basis of AIC_c (see Table 3.1). Estimates from a discrete-occasion model with $T_j = 24$ hours are shown in Table 3.2, together with estimates from the comparable CT model.

Since no bait or lure was used, it is unlikely that the behavioural response in g_0 is a true trap-happiness effect. The camera stations are located on trails resulting in a higher probability of detecting the individuals that habitually use those trails. Royle et al. (2009a) and Soisalo and Cavalcanti (2006) hypothesise that the behavioural response parameter in this context may be acting as a proxy for individual heterogeneity whereby animals that regularly use the trail network are more likely to be captured.

Table 3.1: Model selection summary for the jaguar data. All models specify a constant density.

Model	ΔAIC_c	wt	npar
Discrete-occasion models			
D(.) g_0(b) σ(.)	0.00	0.53	4
D(.) g_0(.) σ(.)	1.29	0.28	3
D(.) g_0(b) σ(b)	3.04	0.12	5
D(.) g_0(.) σ(b)	3.83	0.08	4
CT models			
D(.) g_0(b) σ(.)	0.00	0.81	4
D(.) g_0(b) σ(b)	3.16	0.17	5
D(.) g_0(.) σ(b)	8.18	0.01	4
D(.) g_0(.) σ(.)	8.97	0.01	3

Notes: The brackets in the "Model" column indicate which parameter has a behavioural effect included where "(.)" indicates no effect and "(b)" indicates a behavioural. ΔAIC_c is the difference in AIC_c between the current and the best model (AIC_c is Akaike Information Criterion corrected for small sample size), wt denotes the Akaike weight, npar denotes the number of estimated parameters.

Table 3.2: Estimates (and 95% confidence intervals) from the DT binary and the CT proximity detector models fitted to the male jaguar data with constant density specified and different behavioural effects. The best fitting models are marked in bold.

Model	$\hat{D}$ (95% CI)	$\hat{g}_{01}$ (95% CI)	$\hat{g}_{02}$ (95% CI)	$\hat{\sigma_1}$ (95% CI)	$\hat{\sigma_2}$ (95% CI)
DT proximity model ($T_j = 24$)					
D(.) g_0(.) σ(.)	3.12 (1.90;5.13)	0.066 (0.051;0.084)	NA	2.74 (2.42;3.10)	NA
D(.) g_0(b) σ(.)	**3.60 (2.14;6.05)**	**0.034 (0.016;0.068)**	**0.067 (0.055;0.094)**	**2.74 (2.42;3.10)**	**NA**
D(.) g_0(.) σ(b)	3.40 (2.01;5.74)	0.065 (0.051;0.084)	NA	2.56 (2.13;3.08)	2.78 (2.44;3.15)
D(.) g_0(b) σ(b)	3.34 (1.94;5.76)	0.025 (0.010;0.061)	0.070 (0.054;0.090)	3.09 (2.37;4.03)	2.68 (2.36;3.05)
CT model with constant hazard					
D(.) g_0(.) σ(.)	2.80 (1.71;4.58)	0.074 (0.058;0.092)	NA	2.95 (2.63;3.31)	NA
D(.) g_0(b) σ(.)	**3.26 (1.95;5.45)**	**0.035 (0.018;0.07)**	**0.075 (0.060;0.094)**	**2.95 (2.63;3.31)**	**NA**
D(.) g_0(.) σ(b)	3.15 (1.88;5.30)	0.073 (0.058;0.091)	NA	2.68 (2.25;3.19)	3.00 (2.66;3.38)
D(.) g_0(b) σ(b)	3.05 (1.78;5.23)	0.027 (0.011;0.063)	0.078 (0.061;0.098)	3.27 (2.53;4.22)	2.90 (2.58;3.27)

Notes: The DT models use 90 occasions of 24 hours and the CT models a survey duration of T =2,160 hours. The CT models use a constant hazard that is consistent with a half-normal detection function shape over an interval of 24 hours. Results are reported on the natural scale. The brackets in the "Model" column indicate which parameter has a behavioural effect included where "(.)" indicates no effect and "(b)" indicates a behavioural effect. Estimated density ($\hat{D}$) is individuals per 100 km^2, $\hat{\sigma}$ is in km, and $\hat{g}_{01}$, $\hat{g}_{02}$, $\hat{\sigma}_1$ and $\hat{\sigma}_2$ are estimated detection function parameters before and after initial detection, respectively.

3.1.4 Simulation studies

These simulations compare the performance of the DT binary proximity detector estimator and the CT proximity detector estimator when captures are firstly independent of each other, and secondly when there is spatio-temporal correlation in captures.

Data with observed capture times from an array of proximity detectors are simulated and two estimators (namely the DT binary proximity detector estimator and the CT proximity detector estimator) used to estimate the parameters of interest. As shown in Section 3.1.2, the CT proximity detector model is effectively equal to a DT Poisson (count) proximity detector model with a single occasion when hazards are constant through time. The simulations presented here investigate the properties of the CT proximity detector estimator with a constant hazard, and compare this estimator with the estimator from a DT binary proximity detector model (in which ω_{ikj} is binary). The effects of aggregating the data in different ways are also explored by varying the number and length of the occasions used in the DT models.

The proximity detector models presented assume independent detections within individuals. If animals are detected as a consequence of their moving close to a detector, the expected detection rate of the animal at any given detector depends on when and where the animal was last detected, because animals' locations are temporally correlated. But if times between detections are sufficiently long that the pdf of an animal's location at time t is independent of where it was last detected, then the process generating detection times can be modelled using the model derived above. The first set of simulations corresponds to the case when the independence assumption holds (referred to as "independence simulations"), and the second set of simulations to the case when a model for animal movement is used to generate captures that have spatio-temporal correlation, i.e. the assumption of independent captures within individuals is violated (referred to as "correlated simulations").

Except where stated otherwise, all simulations are from a study of duration 2,160 hours with a 5×4 array of proximity detectors. Three different levels of trap spacings are used in the independence simulations: 1,500 m (0.625 σ), 3,000 m (1.25 σ), and 4,500 m (1.875 σ). The correlated simulations use the larger two spacing levels (3,000 m and 4,500 m). A range of aggregation levels is used to collapse the data into binary capture events for the DT models: (i) 360 occasions of length $T_j = 6$ hours (ii) 90 occasions of length $T_j = 24$ hours (iii) 30 occasions of length $T_j = 72$ hours, and (iv) 18 occasions of length $T_j = 120$ hours. In all cases the data are simulated from a constant density in the survey region and the models are appropriately specified to estimate a constant level of density. The density estimates from the jaguar survey data (Table 3.2) are used to inform the simulation scenarios and lead to the use of

$D = 4$ individuals per 100 km^2 in these simulations.

Independence simulation

Separate detection hazards are used to simulate data for the different aggregation levels, so as to have discrete-occasion detection functions with half-normal forms at each level (to facilitate DT estimation with the secr package). The corresponding CT model estimator is also applied to each simulated dataset. Following Section 2.5.2, for an occasion of length T_j, $h_{kj}(\boldsymbol{s}_i; \boldsymbol{\theta}_{T_j}) = -\log\left\{1 - p_{kj}(\boldsymbol{s}_i; \boldsymbol{\theta}_{T_j})\right\}/T_j$, where $p_{kj}(\boldsymbol{s}_i; \boldsymbol{\theta}_{T_j}) = g_{0,T_j} \exp\{-d_k(\boldsymbol{s}_i)^2/(2\sigma^2)\}$, $\boldsymbol{\theta}_6 = (g_{0,6} = 0.01, \sigma = 2,400)$, $\boldsymbol{\theta}_{24} = (g_{0,24} = 0.05, \sigma = 2,400)$, $\boldsymbol{\theta}_{72} = (g_{0,72} = 0.15, \sigma = 2,400)$ and $\boldsymbol{\theta}_{120} = (g_{0,120} = 0.25, \sigma = 2,400)$. The movement model described below is not parameterised in terms of the parameters g_0 and σ. In order to facilitate comparison of results across the two kinds of simulations, the specific values chosen for these parameters are based on estimates obtained by fitting the CT proximity detector model to data from the movement simulations.

Function sim.popn from the R package secr (Efford, 2016) was used to simulate populations of N individuals with activity centres $\boldsymbol{s}_1, \ldots, \boldsymbol{s}_N$ (see Fewster and Buckland, 2004, for details of the simulation method). For proximity detectors the detections between individuals are assumed to be independent and hence capture times for the ith individual at the kth trap are simulated according to Equation 2.20 by first simulating the total number of detections (ω_{ik}) and secondly simulating the actual detection times. As stated in Equation 2.17, the capture frequency ω_{ik} is a Poisson distributed random variable with rate parameter $H_k(\boldsymbol{s}_i; \boldsymbol{\theta}) = \int_0^T h_k(t, \boldsymbol{s}_i; \boldsymbol{\theta})\, dt$ which is just equal to $T \times h_k(\boldsymbol{s}_i; \boldsymbol{\theta})$ for a constant hazard. The detection times (given the capture frequency ω_{ik}) were generated by independent draws from a uniform distribution on $(0, T)$. This is equivalent to using the conditional distribution of times (see Equation 2.20) where times are drawn in proportion to their respective hazards.

Correlated simulation

Independence can be violated in any number of ways. Because the initial focus is on the application of CT estimators to jaguar camera trap survey data, dependence is modeled by constructing individual movement models that are plausible for jaguar movement. Activity centres are simulated as above. Animals are moved independently in time steps of one hour according to the movement model described below. Whenever a path crosses a 250 × 250 m grid cell containing a detector, detection occurs with probability P_{GC} (where subscript GC stands for "Grid Cell" as these probabilities operate at the level of grid cells). The lower P_{GC}, the less clustered

are detections and the closer the data conform to the independence model. This is because a correlated time series becomes less correlated when randomly thinned.

The movement model: a mixture of random walks There is considerable literature on the modelling of animal movement using various types of random walks (Morales et al., 2004; Codling et al., 2008; Smouse et al., 2010; Langrock et al., 2012). Movement can conveniently be simulated by generating a step length and a turning angle from appropriate distributions at each time step (Morales et al., 2004). Different turning angle distributions produce different types of random walks. For example, for a biased random walk (BRW) the turning angle for the next step is drawn from a distribution with mean oriented towards some focal point whereas for a correlated random walk (CRW) the mean is the current direction of movement.

In order to reproduce both the tendency of individuals to persist in the direction in which they are currently moving and the tendency not to stray too far from their activity centre, we constructed a movement model in which individuals transition stochastically between two states. In the first state (state $s = 0$) they follow a CRW, and in the second state (state $s = 1$) a BRW with bias towards an activity centre. The probability of being in a particular state depends on the distance the individual is from its activity centre. Specifically, the state s of an individual at distance d from its activity centre has the following Bernoulli distribution $s|d \sim \gamma(d)^s(1-\gamma(d))^{1-s}$, where $\gamma(d)$ is the probability of being in state 1, which is modelled as a logistic function of distance: $\gamma(d) = (1 + \exp\{\alpha + \beta d\})^{-1}$. For example, the parameter values used in the simulation (Table 3.3) result in a probability of being in state 0 (CRW) of 0.95 at a distance of zero, 0.5 at a distance of 2,500 m, and 0.05 at a distance of 5,000 m from the activity centre.

The size of each movement step (l) is a draw from a gamma distribution (using the shape and scale parameterization) with mean step length a and standard deviation b: $l \sim \text{Gamma}(\frac{a^2}{b^2}, \frac{b^2}{a})$. The turning angle ($\phi$), given that the individual is in state s, is drawn from a Von Mises distribution $\phi|s \sim \text{von Mises}(\mu(s), \kappa(s))$ where $\mu(s)$ is the mean and $\kappa(s)$ the concentration parameter. Values for $\kappa(s)$ close to zero generate something close to a uniform distribution on the circle, whereas larger values will place increasing mass around the mean value. Table 3.3 shows the movement model parameter values used in the movement simulations and Figure 3.1 shows a realisation of the model over $T = 2,160$ hours (90 days) for a single individual. Because the objective is to generate correlated detection times rather than to make inferences about the underlying behaviour, a large standard deviation for step length was used to represent movement of a range of behavioural states (resting, hunting, travelling etc).

Figure 3.1: Simulated movement for a single individual for a 90 day period in hourly steps, showing the number of times each cell is visited in the period and smoothed with a nonparametric smoother.

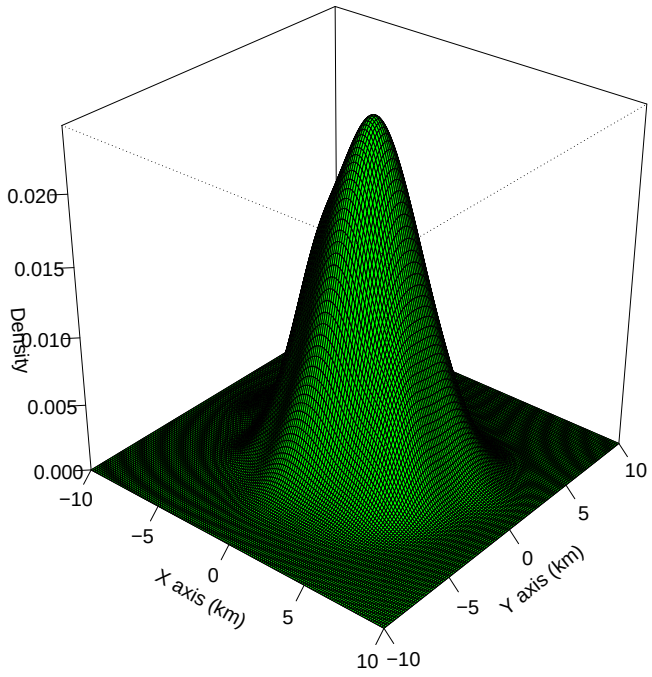

Table 3.3: Movement model parameter values used in the movement simulations.

Parameter	CRW (state $s = 0$)	BRW (state $s = 1$)
α	3	3
β	-0.0012	-0.0012
a	750	750
b	450	450
$\kappa(s)$	6	0.5
$\mu(s)$	0^o	ϕ_t

Notes: Only the Von Mises parameters ($\mu(s)\kappa(s)$) are state dependent. CRW refers to a Correlated Random Walk and BRW to a Biased Random Walk. 0^o indicates movement in the same direction while ϕ_t represents a turning angle from the current location back towards the activity centre.

3.1.5 Simulation results

The estimated biases of estimators as a percentage of true parameter values (or relative bias (RB)) are shown together with their standard errors for the different detector spacings in Tables 3.4 and 3.5.

Independence simulations

The number of detections was consistently higher for the CT models because reducing capture frequencies to binary data in the discrete-occasions models discards some detections. The number of individuals detected per survey increased with detector spacing because greater spacing leads to a larger area being sampled. There is substantial bias in density for the discrete-occasion models when traps are spaced closely together relative to σ, more so when many short occasions were used. This result appears to be caused by convergence issues as discussed in more detail below.

On average, with 1,500 m detector spacing 12% of individuals were detected at least twice a day at the same detector. This reduced to 9% and 6% with spacing of 3,000 m and 4,500 m, respectively. These values are substantially lower than the 35% observed in the jaguar survey data.

Correlated simulations

Table 3.5 summarises the results from the movement simulations. Recall that a lower P_{GC} results in more thinning and less spatio-temporal correlation. Longer occasions also thin detections and hence should reduce autocorrelation. When $P_{GC} = 0.3$ the estimators of density are approximately unbiased for all cases apart from the scenario when many, short occasions of 6 hours are used with a spacing of 3,000 m

Table 3.4: Relative bias (RB) of density and detection parameters estimated by the DT binary and the CT proximity detector models with a constant hazard. The data are simulated for a survey duration of T = 2,160 hours under the independence assumption with constant density and a constant hazard.

Detector spacing (m)	T_j (hrs)	$\text{RB}_{\hat{D}}(\%)$	$\text{RB}_{\hat{g}_0}(\%)$	$\text{RB}_{\hat{\sigma}}(\%)$	Detections	Unique	Reps
0.625 σ (1,500m)	6	85.43 (2.51)	-41.13 (0.69)	-25.43 (0.44)	103.7	10.0	979
	CT (6)	8.35 (1.31)	-3.01 (0.75)	-2.28 (0.46)	103.8	9.9	1000
	24	69.35 (2.21)	-36.94 (0.73)	-21.62 (0.41)	130.6	10.6	988
	CT (24)	8.69 (1.16)	-4.10 (0.65)	-2.49 (0.38)	132.3	10.5	998
	72	36.15 (1.66)	-21.17 (0.77)	-13.49 (0.43)	129.6	10.4	995
	CT (72)	6.64 (1.19)	-3.40 (0.64)	-1.92 (0.41)	134.7	10.4	999
	120	21.75 (1.39)	-11.99 (0.75)	-8.01 (0.41)	130.0	10.5	998
	CT (120)	6.42 (1.15)	-3.55 (0.62)	-1.27 (0.40)	139.1	10.5	1000
1.25 σ (3,000m)	6	1.81 (0.81)	-2.97 (0.53)	-1.35 (0.25)	101.8	16.0	995
	CT (6)	-0.51 (0.79)	-0.01 (0.54)	0.10 (0.25)	102.0	16.0	1000
	24	0.01 (0.82)	-0.31 (0.44)	-0.68 (0.22)	128.1	16.7	991
	CT (24)	-0.95 (0.81)	0.61 (0.44)	-0.14 (0.22)	129.5	16.6	1000
	72	-0.84 (0.78)	0.42 (0.46)	-0.05 (0.23)	127.6	16.7	981
	CT (72)	-1.14 (0.77)	0.17 (0.44)	-0.06 (0.23)	132.4	16.6	1000
	120	-0.24 (0.81)	0.23 (0.43)	0.15 (0.22)	128.0	16.8	950
	CT (120)	-0.86 (0.80)	0.24 (0.40)	0.06 (0.21)	136.6	16.7	1000
1.875 σ (4,500m)	6	1.25 (0.67)	1.22 (0.52)	-0.02 (0.23)	105.2	24.6	994
	CT (6)	1.18 (0.67)	1.18 (0.51)	-0.02 (0.23)	105.4	24.6	1000
	24	0.89 (0.65)	0.74 (0.45)	-0.09 (0.20)	130.9	25.6	982
	CT (24)	0.84 (0.64)	0.84 (0.44)	-0.11 (0.20)	132.8	25.6	1000
	72	1.07 (0.68)	-0.02 (0.45)	0.29 (0.19)	130.9	25.8	924
	CT (72)	0.89 (0.65)	0.22 (0.41)	0.12 (0.18)	136.3	25.7	1000
	120	1.51 (0.69)	1.29 (0.46)	-0.20 (0.21)	131.6	25.9	865
	CT (120)	1.15 (0.64)	1.16 (0.41)	-0.25 (0.19)	141.0	25.8	1000

Notes: Relative % bias is shown for each parameter followed by the standard error in parentheses. "CT (t)" indicates a CT model with a constant hazard that is consistent with a half-normal detection function shape over an interval of t hours. The DT models use occasion lengths ranging from $T_j = 6$ to $T_j = 120$ hours. True density is 4 individuals per 100 km^2, $\sigma = 2,400$, $g_0 = 0.01$ for $T_j = 6$, $g_0 = 0.05$ for $T_j = 24$, $g_0 = 0.15$ for $T_j = 72$, $g_0 = 0.25$ for $T_j = 120$. Twenty detectors spaced 1,500m, 3,000m and 4,500m apart are used. Results are reported on the natural scale. "Detections" is mean number of detections per survey, "Unique" is mean number of individuals detected per survey, and "Reps" is number of replications out of 1000 where any replications that did not converge or estimated negative or very large variances for any parameter were excluded.

which results in slight positive bias of around 8%. The bias is worse when P_{GC} is high, especially when $T_j = 6$ hrs although the extent of this bias reduces considerably when the spacing is increased to 4,500 m (35% to 5%).

Reducing P_{GC} in the movement simulation effectively thins the detection time process and consequently reduces temporal correlation. For spacing of 3,000 m, when $P_{GC} = 0.9$, on average 85% of individuals were detected at least twice in a day at the same detector and this proportion drops to 52% when $P_{GC} = 0.3$. Results were similar for the larger detector spacing.

3.2 Single-catch traps

Efford et al. (2009a) conducted simulations that explored the performance of the DT multi-catch trap estimator when applied to single-catch trap data. As explained in Section 2.1.3 multi-catch traps assume that traps do not fill up after catching an individual and hence the extent to which this assumption is violated depends on the degree of trap saturation. The multi-catch estimator is therefore expected to perform well at low levels of trap saturation. Three distributions for the activity centres were considered: a homogeneous Poisson distribution (constant density), a Neyman-Scott distribution (with clustered centres), and an inhomogeneous Poisson distribution with an east-west linear gradient in density. The fitted models assumed constant density and a half-normal detection function. They reported that in all cases, even at high levels of trap saturation (of around 86%), the multi-catch estimator of both the density and σ parameters performed well. There was negative bias in the g_0 parameter that increased with increasing trap saturation. The only scenario that exhibited slight bias in density (of around -5%) was that with a gradient in the density of activity centres and a high degree of trap saturation. The tentative conclusion was that the multi-catch estimator may be sufficiently robust to use with single-catch traps as long as extreme trap saturation is avoided.

It should be noted that the models evaluated in the simulations mentioned above fitted a constant density model in all cases, used a single set of parameter values for the Neyman-Scott distribution, and assessed a single gradient in density. The simulation studies presented in this section further explore the robustness of the DT multi-catch estimator for other kinds of non-constant density surfaces, and contrast its performance with that of the CT single-catch estimator.

When fitting these models it is necessary to specify both the detection function and the model for density. The first set of simulations involves models that always have a constant density model specified irrespective of the underlying density surface used to simulate the data. Therefore, for this simulation set, the density model for

Table 3.5: Relative bias (RB) of density estimated by the DT binary and the CT proximity detector models with a constant hazard. All models specify a constant density. The data are simulated for a survey duration of T =2,160 hours with constant density and from an animal movement model that induces spatio-temporal correlation.

Detector spacing (m)	T_j (hrs)	$\text{RB}_{\hat{D}}(\%)$	Detections	Unique	Reps
		$\boldsymbol{P_{GC} = 0.9}$			
3000m	6	35.33 (1.21)	367.2	19.8	990
	24	13.76 (0.90)	332.1	19.8	997
	72	3.82 (0.76)	303.6	19.8	995
	120	0.82 (0.81)	283.5	19.8	865
	CT (24)	-4.33 (0.71)	468.2	19.8	1000
		$\boldsymbol{P_{GC} = 0.3}$			
	6	8.00 (0.86)	143.2	17.2	992
	24	2.48 (0.81)	138.1	17.3	998
	72	1.49 (0.81)	133.2	17.3	995
	120	1.50 (0.81)	129.4	17.3	990
	CT (24)	0.38 (0.85)	153.6	17.3	898
		$\boldsymbol{P_{GC} = 0.9}$			
4500m	6	5.39 (0.64)	361.7	29.2	997
	24	-0.03 (0.60)	327.1	29.1	976
	72	-0.12 (0.60)	299.3	29.2	987
	120	-0.98 (0.62)	278.1	28.9	853
	CT (24)	-4.45 (0.57)	461.9	29.2	1000
		$\boldsymbol{P_{GC} = 0.3}$			
	6	-0.91 (0.64)	142.0	25.6	1000
	24	-0.26 (0.65)	137.0	25.7	960
	72	-0.47 (0.64)	131.9	25.6	988
	120	-0.47 (0.65)	128.1	25.6	969
	CT (24)	-1.83 (0.64)	153.6	25.6	986

Notes: Relative % bias (RB) in density is followed by the standard error in parentheses. P_{GC} is the probability that an individual is detected when it is in a 250m×250m cell containing a camera and two levels of P_{GC} are used. The CT model uses a constant hazard that is consistent with a half-normal detection function shape over an interval of 24 hours. The DT models use occasion lengths ranging from $T_j = 6$ to $T_j = 120$ hours. True density is 4 individuals per 100 km^2 and twenty detectors spaced 3,000m and 4,500m apart are used. Results are reported on the natural scale, "Detections" is mean number of detections per survey, "Unique" is mean number of individuals detected per survey, and "Reps" is number of replications out of 1000 where any replications that did not converge or estimated negative or very large variances for any parameter were excluded.

both estimators is misspecified in all cases except for the constant density scenario. The second set of simulations differs from the first in that the two estimators being compared are from models where the model for density is correctly specified for different exponential gradients and quadratic density surfaces. The detection function for the DT multi-catch estimator is misspecified in all cases due to the violation of the assumption that traps continue to operate after catching an individual.

3.2.1 Simulation studies

Except where stated otherwise, all simulations are over 5×24 hour occasions (all trapped individuals are released simultaneously after each 24-hour period) with a 5×4 array of traps and use a σ of 100 m, trap spacings of 100 m, and a g_0 of 0.2. For all scenarios, single-catch trap data with observed capture times are simulated and two estimators (namely the DT multi-catch trap estimator and the CT single-catch trap estimator proposed in Section 2.3) used to estimate the parameters of interest. The hazard function is specified so that links it with the DT model to allow the same detection function to be fitted when the performance of the two models is compared.

Recall that it is better to use an integration area that is bigger than necessary as the only effect is on computational efficiency. The model parameters are therefore estimated using an integration area (or integration mask) constructed with a buffer equal to $4 \times \sigma$ placed around the convex hull of the trap array. However in order to avoid extrapolating estimated density too far from the trap array, the estimated density surfaces are evaluated within the convex hull of the trap array with a buffer of width $2 \times \sigma$ added. The spatial east-west X coordinate was standardised in the models with non-constant density to stabilise the estimation. Density values are given per hectare (ha) unless stated otherwise.

Simulating single-catch trap data

The approach used to simulate single-catch trap detection times is adapted from a method for simulating competing risks data (Beyersmann et al., 2009). Individuals compete for traps and hence the capture of one individual changes the relative hazards of capture elsewhere for all other individuals. For this reason the simulation cannot generate capture times for each individual in isolation and needs to move forward with time rather than loop over individuals. The steps of the simulation are summarised below:

1. A density surface is constructed from a linear, exponential or quadratic formula that contains the east-west coordinate corresponding to each cell in the mask.

The activity centres for a population of individuals is simulated as a realisation from the given density surface using function sim.popn from the R package secr (Efford, 2016). It is not necessary to construct and supply a density surface for the scenarios with constant density in which case just the density level is required, or in the case of clustered distributions where the `sim.popn` function has an option to use a Neyman-Scott distribution (through the "model2D = 'cluster' " argument).

2. The total hazard across all traps for each individual is calculated and used to generate a vector of capture times (one time for each individual). In this chapter a constant hazard through time is assumed which leads to the density of capture times following an exponential distribution.

3. The minimum capture time from this vector is taken and the rest discarded. If this time is greater than the end of the study the simulation ends, if not the time is taken to be the capture time. The time of release is also calculated and is based on the assumption that all traps are checked and reset on a set time each day (08:00 used in these simulations).

4. The particular trap where the capture event took place is then drawn from a multinomial distribution using the relative hazard at each as yet unfilled trap as the appropriate vector of probabilities, where the relative hazard for the kth trap is $\frac{h_k}{\sum_K h_k}$, and the sum is over all unfilled traps at the given capture time.

5. The total hazard from the remaining traps and the revised trap-specific relative hazards are recalculated. A new vector of capture times is simulated and the minimum of these times added to the last capture time to generate the next capture time. If this new capture time exceeds the release time from step 3 the time is discarded and step 2 restarted from the release time, if not it becomes the next capture time and this step is repeated.

Simulation scenarios

As mentioned earlier Efford et al. (2009a) found that the multi-catch estimator exhibited slight bias when there was a gradient in density. The simulations here explore this issue further by examining a range of density distributions including a homogeneous Poisson distribution (where I expect to confirm the results found by Efford et al. (2009a)), a Neyman-Scott distribution but with different parameter values to that used in Efford et al. (2009a), and different gradients in density as a function of distance east with either linear, exponential or quadratic rate parameters. The aim

is to examine density surfaces with different gradients that produce capture histories with varying degrees of trap saturation.

Further details for the different density surfaces are given below.

1. Constant density:
   Four different levels of constant density are used including 4, 2, 1, and 0.5 per ha.

2. Neyman-Scott distribution (see Figures 3.2 and 3.3):
   Five different density levels are chosen (0.0625, 0.125, 0.5, 2, 4) and for each level four different parameter combinations for μ_c (the fixed number of individuals per cluster) and σ_c (the spread of the individuals in a cluster) are used ($\mu_c = 5, 8$ and $\sigma_c = 25, 50$). Figures 3.2 and 3.3 show example realisations from a Neymann-Scott distribution with D = 0.5 and 2 per hectare respectively. The plots show in particular how lower values for σ_c increase the degree of clustering.

3. Linear density gradient (see Figure 3.4):
   Four scenarios with linear gradients in density are explored. All the gradients start with a density of zero at the western edge of the integration mask ($D_{min} = 0$ at coordinate x_{min}) and rise to a maximum at the eastern edge of the integration mask (D_{max} at coordinate x_{max}). The first scenario reaches a maximum density of 2, the second is the same as that used in Efford et al. (2009a) and reaches a maximum density of 4, the third reaches a maximum density of 6, and the fourth a maximum density of 8 per ha. The respective intercepts and slopes are found by solving a set of simple equations:

$$\beta_0 + \beta_1 \times x_{min} = 0 \qquad \beta_0 + \beta_1 \times x_{max} = D_{max}$$

$$\beta_0 = -\beta_1 \times x_{min} \qquad \beta_1 = \frac{D_{max}}{(x_{max} - x_{min})}$$

4. Exponential density gradient (see Figure 3.4):
   Different exponential gradients are chosen based on the density level at the western edge of the trap array (D_{start} at coordinate x_{start}) and the maximum density reached at the eastern edge of the integration mask (D_{max} at coordinate x_{max}). Again a set of equations are solved for the β values used in the simulations:

Figure 3.2: Four realisations from different Neyman-Scott distributions with density = 0.5 per ha.

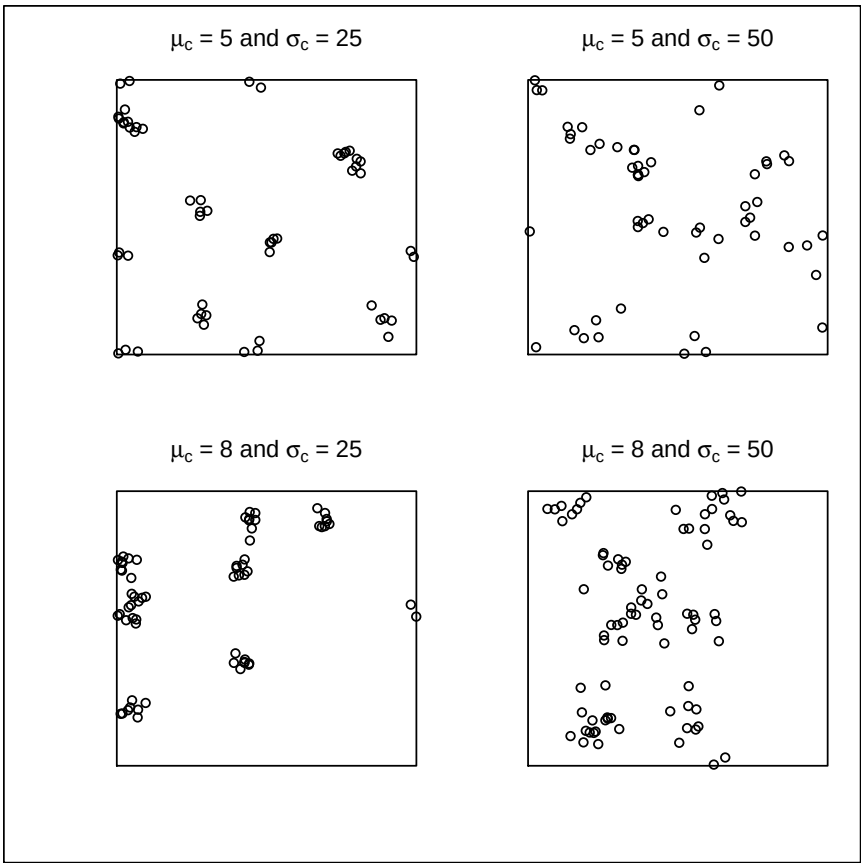

Figure 3.3: Four realisations from different Neyman-Scott distributions with density = 2 per ha.

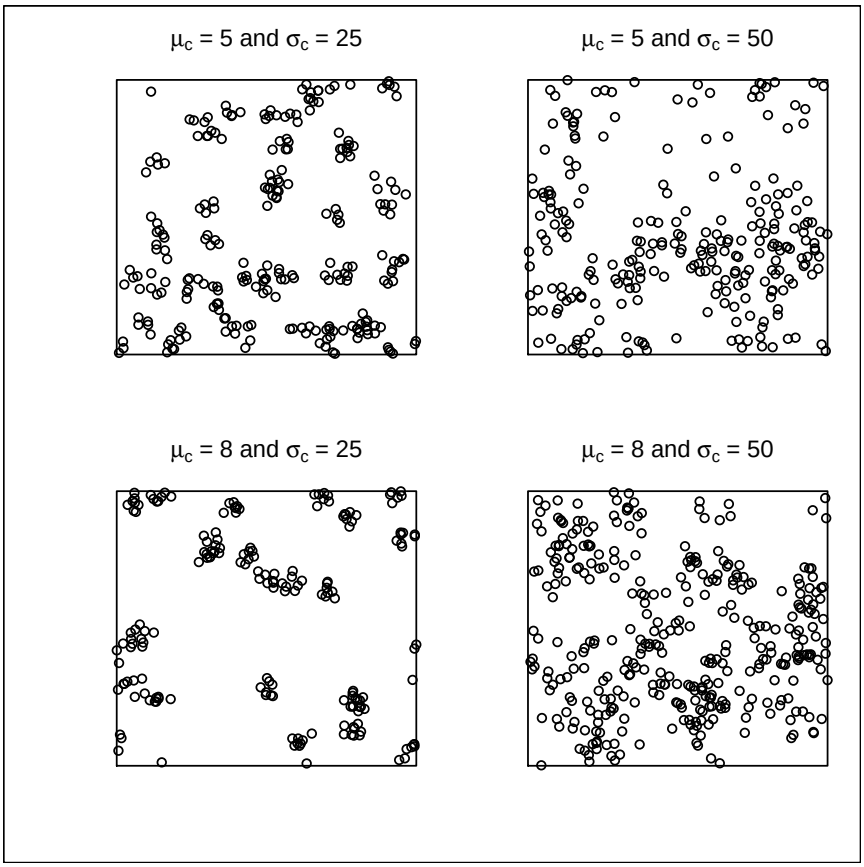

$$\beta_0 + \beta_1 \times x_{start} = log(D_{start}) \qquad \beta_0 + \beta_1 \times x_{max} = log(D_{max})$$

$$\beta_0 = log(D_{start}) - \beta_1 \times x_{start} \qquad \beta_1 = \frac{log(D_{max}) - log(D_{start})}{(x_{max} - x_{start})}$$

5. Quadratic surfaces (see Figure 3.4):
   The quadratic density surface is calculated from the east-west x coordinate $\beta_0 + \beta_1 \times x + \beta_2 \times x^2$. Trial and error is used to choose a set of coefficients that produce quadratic surfaces with varying levels of maximum density and steepness in gradients.

These scenarios are named with a "Sc." prefix (for "single-catch") followed by the letter C, N, L, E, or Q corresponding to the type of density surface, and end with

Figure 3.4: Simulated density surfaces used in the linear, exponential and quadratic density scenarios for single-catch trap data. The vertical dashed red lines indicate the borders of the trap array.

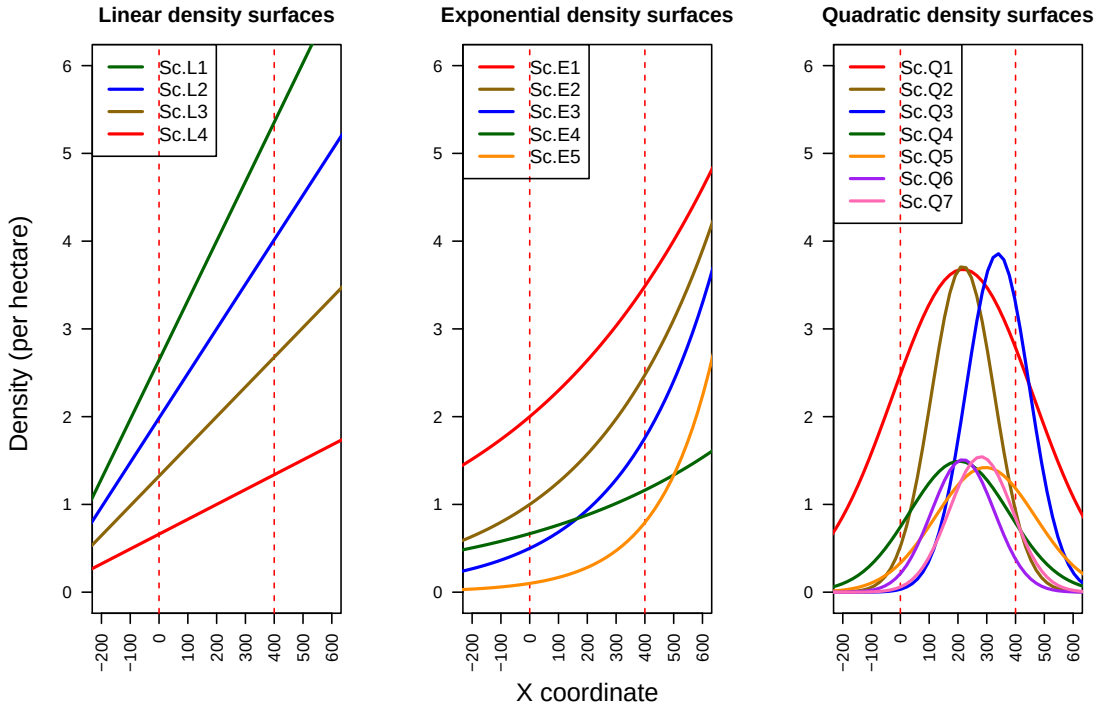

the scenario number, e.g. Sc.N1 indicates the single-catch Neyman-Scott distribution with the first density level of 0.0625. Figure 3.4 illustrates the density surfaces used in the linear, exponential and quadratic cases. Note that scenario 3 in the quadratic simulations (Sc.Q3) is similar to scenario 2 (Sc.Q2) but with the maximum density being shifted from the centre of the trap array to the right hand side of the array area.

Tables 3.6 and 3.7 provide further details for all the simulation scenarios including the mean trap saturation and mean number of unique individuals from 100 simulated capture histories. These latter numbers are provided to give an idea of what sort of sample sizes can be expected from the different scenarios and for the sake of brevity are not included in the various tables of simulation results that are found in Appendix B. The density values reported in Table 3.6 are calculated over an east-west range that corresponds to using the convex hull of the trap array with a buffer of width $2 \times \sigma$, i.e. it is a shorter range compared to the full integration mask that uses a

buffer of $4 \times \sigma$.

Note that with single-catch traps there is an upper limit on the total number of captures over the survey that is equal to the number of traps multiplied by the number of occasions, i.e. with 20 traps and five occasions there are a maximum of 100 captures and consequently the mean number of captures for these simulations is equal to the mean trap saturation.

Table 3.6: Details of the different density surfaces used in the single-catch trap simulations.

Simulation Type	Scenario	D_{Max}	D_S	$\bar{D}$	Unique	Trap %
Constant	Sc.C1	4.00	4.00	4.00	76.3	98.9%
	Sc.C2	2.00	2.00	2.00	55.9	88.5%
	Sc.C3	1.00	1.00	1.00	35.0	64.7%
	Sc.C4	0.50	0.50	0.50	19.5	40.0%
Linear	Sc.L1	6.67	2.65	4.00	74.3	98.2%
	Sc.L2	5.00	1.98	3.00	66.9	94.8%
	Sc.L3	3.33	1.32	2.00	54.1	86.1%
	Sc.L4	1.67	0.66	1.00	33.5	62.4%
Exponential	Sc.E1	4.50	2.00	2.77	64.4	93.7%
	Sc.E2	3.76	1.00	1.79	49.9	81.0%
	Sc.E3	3.14	0.50	1.20	35.1	61.3%
	Sc.E4	1.50	0.67	0.92	31.0	58.1%
	Sc.E5	2.06	0.10	0.52	16.9	31.0%
Quadratic	Sc.Q1	3.68	2.48	2.56	66.3	95.6%
	Sc.Q2	3.71	0.52	1.30	47.6	81.9%
	Sc.Q3	3.86	0.03	1.33	41.8	69.6%
	Sc.Q4	1.49	0.74	0.80	32.1	62.8%
	Sc.Q5	1.42	0.33	0.75	29.3	58.2%
	Sc.Q6	1.51	0.21	0.53	23.0	49.9%
	Sc.Q7	1.54	0.06	0.54	23.0	48.0%

Notes: All density values are given per hectare (ha) and calculated using a buffer of $2 \times \sigma$. D_{Max} is the maximum density, D_S refers to the density at the start of the trap array, $\bar{D}$ the mean density, "Unique" is the mean number of unique individuals captured and "Trap %" refers to mean trap saturation from 100 simulated capture histories with 5 occasions.

Table 3.7: Details of the different Neyman-Scott clustered distributions used in the single-catch trap simulations.

Scenario	μ_c	σ_c	Unique	Trap %
Sc.N1 (D=0.0625)	5	50	2.1	4.9%
	5	25	2.3	4.8%
	8	50	1.7	3.3%
	8	25	2.2	3.9%
Sc.N2 (D=0.125)	5	50	5.1	10.4%
	5	25	4.8	9.4%
	8	50	5.5	10.7%
	8	25	5.0	10.3%
Sc.N3 (D=0.5)	5	50	18.4	36.2%
	5	25	18.6	34.4%
	8	50	17.6	32.5%
	8	25	19.3	35.2%
Sc.N4 (D=2)	5	50	55.8	85.9%
	5	25	53.8	82.2%
	8	50	55.2	84.3%
	8	25	52.8	81.4%
Sc.N5 (D=4)	5	50	75.1	98.1%
	5	25	74.2	97.7%
	8	50	73.9	96.8%
	8	25	75.1	97.4%

Notes: μ_c and σ_c refer to the parameters used in the Neyman-Scott distribution, "Unique" is the mean number of unique individuals captured and "Trap %" refers to mean trap saturation from 100 simulated capture histories with 5 occasions.

Evaluating the estimators from models where non-constant density is specified.

It is straightforward to evaluate the bias in the density parameter ($\hat{D}$) for the simple case of constant density. The performance of the estimators from models with non-constant density is evaluated in a variety of ways starting with a visual examination of plots that show the estimated density surface from each simulation overlaid on the true density surface.

Secondly the relative biases of the predicted mean density over some area ($\hat{D}_A$) and of the detection function parameters ($\hat{g}_0$ and $\hat{\sigma}$) for both exponential and quadratic simulations, and of the density slope parameter ($\hat{D}_{slope}$) for the exponential simulations are calculated. The density slope parameter referred to is the coefficient for the west-east coordinate from the exponential density model. The estimated parameters of the quadratic coefficients are not reported since they are correlated and are more difficult to interpret than the slope parameter from the exponential density model.

Lastly, two measures of overall model performance that are based on predicted density at each mask point are calculated and reported, namely the root mean squared prediction error (RMSPE), and the root mean squared bias (RMSB). These measures of model performance are calculated for two different areas: the "full" area which extends 2σ beyond the trap array, and the "reduced" area which is defined as the area encompassed by the convex hull of the trap array.

The RMSPE and RMSB are calculated as follows:

$$\text{RMSPE} = \sqrt{\frac{1}{R}\sum_{r=1}^{R}(\text{MSPE}_r)}$$

where

$$\text{MSPE}_r = \frac{1}{M}\sum_{m=1}^{M}(\hat{D}_{mr} - D_m)^2 \times \text{cell area}$$

$$\text{RMSB} = \sqrt{\frac{1}{M}\sum_{m=1}^{M}(\hat{\bar{D}}_m - D_m)^2 \times \text{cell area}}$$

where $\hat{\bar{D}}_m$ is the mean estimated density at the mth mask point ($m = 1, \ldots, M$) averaged over the R simulations, and the "cell area" is the area of each of the M mask points, i.e. the measures are integrated over space.

Standard errors

Coverage is explored for all parameters of interest. The Delta method is used to estimate the variance of the estimates of mean density from non-constant density surfaces that are functions of more than one model parameter.

$$Var[g(\hat{\boldsymbol{\beta}})] = g'(\hat{\boldsymbol{\beta}})^T \Sigma(\hat{\boldsymbol{\beta}}) g(\hat{\boldsymbol{\beta}})$$

Further details of the relevant first partial derivatives for different functions are given below. Note that the expressions are evaluated at $\hat{\boldsymbol{\beta}}$ from a given simulation, and that X_m refers to the mth mask point and gives the distance east.

- Exponential density

$$g(\hat{\boldsymbol{\beta}}) = \frac{\sum_m \hat{D}_m(\hat{\boldsymbol{\beta}})}{m} = \bar{D}(\hat{\boldsymbol{\beta}}) = \frac{\exp(\hat{\beta}_0 + \hat{\beta}_1 \times X_1) + \ldots + \exp(\hat{\beta}_0 + \hat{\beta}_1 \times X_m)}{m}$$

  The first derivatives for the β's are:

$$g_{\beta_0}(\hat{\boldsymbol{\beta}}) = \frac{\exp(\hat{\beta}_0 + \hat{\beta}_1 \times X_1) + \ldots + \exp(\hat{\beta}_0 + \hat{\beta}_1 \times X_m)}{m}$$
$$g_{\beta_1}(\hat{\boldsymbol{\beta}}) = \frac{X_1 \exp(\hat{\beta}_0 + \hat{\beta}_1 \times X_1) + \ldots + X_m \exp(\hat{\beta}_0 + \hat{\beta}_1 \times X_m)}{m}$$

- Quadratic density

$$g(\hat{\boldsymbol{\beta}}) = \bar{D}(\hat{\boldsymbol{\beta}}) = \frac{\exp(\hat{\beta}_0 + \hat{\beta}_1 \times X_1 + \hat{\beta}_2 \times (X_1)^2) + \ldots + \exp(\hat{\beta}_0 + \hat{\beta}_1 \times X_m + \hat{\beta}_2 \times (X_m)^2)}{m}$$

  The first derivatives for the β's are:

$$g_{\beta_0}(\hat{\boldsymbol{\beta}}) = \frac{\exp(\hat{\beta}_0 + \hat{\beta}_1 \times X_1 + \hat{\beta}_2 \times (X_1)^2) + \ldots + \exp(\hat{\beta}_0 + \hat{\beta}_1 \times X_m + \hat{\beta}_2 \times (X_m)^2)}{m}$$
$$g_{\beta_1}(\hat{\boldsymbol{\beta}}) = \frac{X_1 \exp(\hat{\beta}_0 + \hat{\beta}_1 \times X_1 + \hat{\beta}_2 \times (X_1)^2)) + \ldots + X_m \exp(\hat{\beta}_0 + \hat{\beta}_1 \times X_m + \hat{\beta}_2 \times (X_m)^2)}{m}$$
$$g_{\beta_2}(\hat{\boldsymbol{\beta}}) = \frac{(X_1)^2 \exp(\hat{\beta}_0 + \hat{\beta}_1 \times X_1 + \hat{\beta}_2 \times (X_1)^2) + \ldots + (X_m)^2 \exp(\hat{\beta}_0 + \hat{\beta}_1 \times X_m + \hat{\beta}_2 \times (X_m)^2)}{m}$$

- The variance in the RMSPE measure is estimated from the Delta method with the square root transformation that produces the following first derivative where x is the mean MSPE across the R simulations.

$$g'(x) = 1/2x^{-1/2}$$

- The variance in the RMSB measure is estimated with bootstrapping. This is done by resampling the $R \times M$ matrix of estimated densities from the simulation results. In each case an entire row that corresponds to the estimated density at m points in space from a single simulation is selected to correctly capture the dependence in the spatial density estimates.

3.2.2 Simulation results

The tables that summarise these simulation results are found in Appendix B to improve readability.

Simulation I: Comparing the two estimators when density is incorrectly specified

Tables B.1 to B.6 present the results from the simulations where constant density models are fitted to data that are simulated from the range of density surfaces given above. Specifically Table B.1 presents the results from the simulations where the true density is in fact constant in space and hence the density component of the model is correctly specified. Other constant density scenarios with higher levels of density and higher values for g_0 that produced 100% trap saturation were also run for 10 occasions. The results were similar to those shown in Table B.1 although when both g_0 and density are high the DT multi-catch estimator also exhibits negative bias of just over 10% for σ.

The results from simulations where data are generated from a linear gradient in density are presented in Table B.2, from an exponential gradient in density in Table B.3, and from a quadratic density surface in Table B.4. Consistent with the results from the simulations done by Efford et al. (2009a), the multi-catch estimator of the g_0 parameter is negatively biased and depends on the degree of trap saturation. There is also slight positive bias in the multi-catch estimator of σ for the quadratic scenarios with the steepest changes in density (for example Sc.Q2). Apart from that there are some scenarios where both estimators exhibit slight bias in mean density

but more importantly the performance of the DT multi and CT single-catch trap density estimators is similar when the density model is misspecified.

Clustered density surfaces The results from simulations with clustered density surfaces are presented in Tables B.5 to B.7. Table B.5 presents the results from simulations with 5 occasions and it is apparent that there is severe positive bias in density for the scenarios with low levels of density. Table B.6 contains results from rerunning the low density scenarios with twice the number of occasions (10) and the extra data from using more occasions does not have much of an effect on the bias in density. Increasing the μ_c parameter in the Neyman-Scott distribution will increase the degree of clustering and Table B.7 summarises the results from extra scenarios where the data are simulated using a distribution with a higher value for μ_c of 15.

With $D < 0.5$ the sample sizes are so small (around 5 unique animals or less) that it is not surprising that the estimators perform poorly (with bias of between about 80% and 300%). With larger sample sizes (between 50 and 75 unique individuals), the estimators that specify constant density perform well even with high trap saturations (around 98%). With moderate sample sizes (around 18 individuals) the estimators also perform well with the exception of the scenarios with higher clustering ($\mu_c = 8; \sigma_c = 25$ and the various scenarios with $\mu_c = 15$) where the level of bias in density ranges between 30% and 60%. It appears that the underlying clustering process becomes difficult to distinguish when density is high enough and in these cases assuming a constant density provides a good approximation.

The multi-catch estimator is also negatively biased for the g_0 parameter, and the extent of this bias depends on the degree of trap saturation. For example the bias ranges between about 25% and 75% for corresponding trap saturations of between 35% to 98%. Doubling the number of occasions results in more data and generally leads to a reduction in the level of bias for the density parameter but not the g_0 parameter.

Simulation II: Comparing the two estimators with density correctly specified

The results from simulations where the correct density model is specified for exponential and quadratic density surfaces are now presented. As explained in Section 3.2.1 the results are evaluated by examining plots of the estimated density surfaces and of the root mean square error and bias, and by tabulating the relative biases for the relevant model parameters.

Exponential simulations Figures 3.5 - 3.9 present a set of plots from the exponential simulations that show the estimated density surface from each simulation scenario overlaid on the true density surface. It is apparent that at high levels of trap saturation (see Table 3.6) the multi-catch estimator has a tendency to flatten out the estimated density surface. Table B.8 and Figure 3.10 show that the multi-catch model underestimates the exponential slope parameter and that the extent of the bias depends on trap saturation.

Table B.8 also shows that the relative bias in mean density is similar for the two models. As expected the the multi-catch estimator of the g_0 parameter is negatively biased and again depends on trap saturation, while the estimators of σ are unbiased. Figure 3.11 shows that the single-catch trap model has lower bias in all cases except Sc.E4 and Sc.E5. With five occasions the RMSPE for the single-catch trap estimator across the full area is slightly worse than the multi-catch estimator due to the increased variance of the single-catch trap estimator though there is no difference between the two models when not extrapolating beyond the trap array. The simulations with 10 occasions show how the increased sample size helps to reduce the variance in the single-catch trap estimator.

Quadratic simulations For the quadratic simulations, Figures 3.12 - 3.18 present the estimated density surface plots, Figure 3.19 the RMSPE's and RMSB's, and Table B.9 the relative biases of the detection function parameters and the mean density estimates. The results are similar to those from the exponential simulations although, in addition to the estimator of g_0 being negatively biased, the multi-catch trap estimator of σ tend to be slightly positively biased in Sc.Q2 and Sc.Q3 where the gradient in density is steeper than the other scenarios. The RMSPE for the single-catch trap estimator is noticeably higher then that for the multi-catch trap estimator for Sc.Q1 which has the flattest quadratic bump, and for Sc.Q3 when the peak in density is shifted to the side of the trap array.

Note that while in general the multi-catch trap estimator again performs worse for higher levels of trap saturation, scenario Sc.Q2 (and Sc.Q3 over the reduced area) has more bias than Sc.Q1 despite having lower trap saturation (81% vs 96%). This suggests that the performance of the estimator is affected by the underlying density surface in addition to the level of trap saturation.

It should be noted that the sample sizes produced by these simulations are not large (between about 23 and 66 unique individuals). The simulations are rerun with 10 occasions and the results in Table B.9 and Figure 3.19 confirm that both the RMSPE and the slight bias reduces with larger sample sizes.

Figure 3.5: Estimated density surfaces from the simulation scenario Sc.E1 for single-catch trap data with a constant hazard.

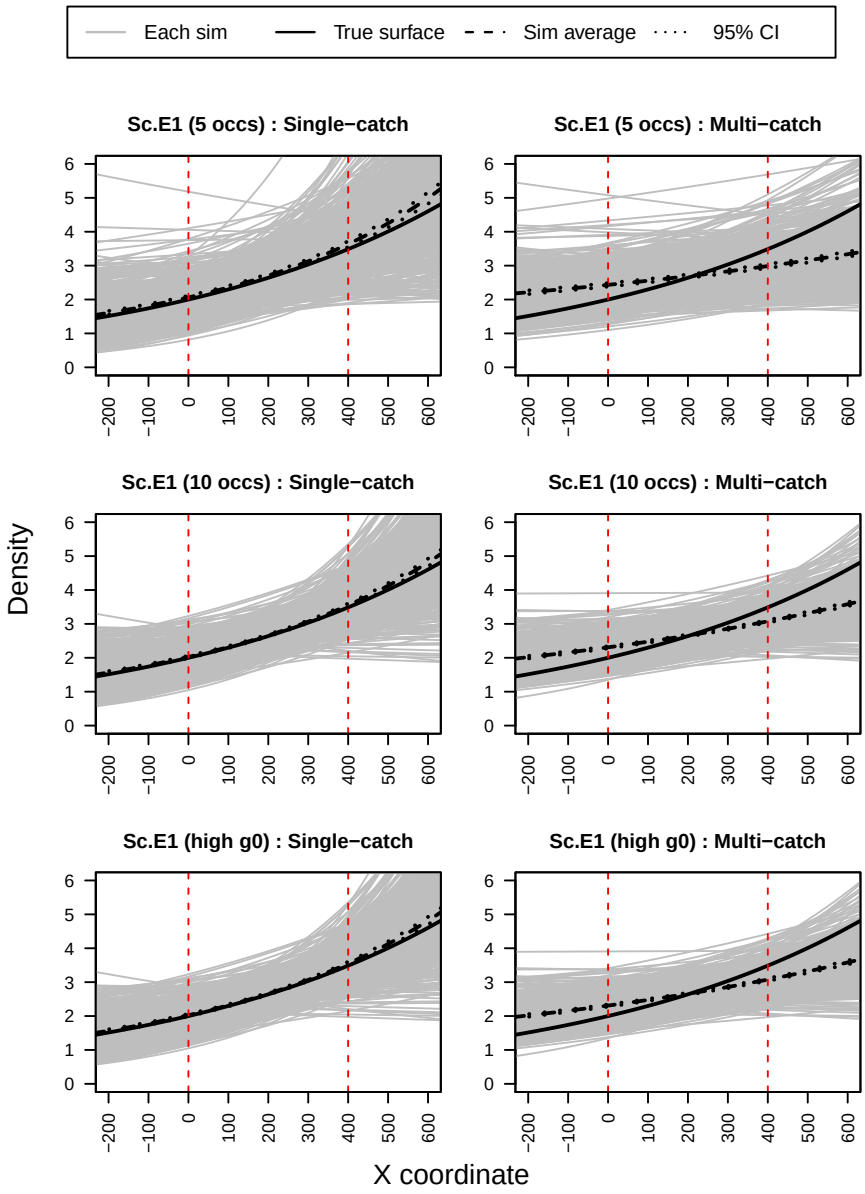

Notes: The black line depicts the true density surface, the grey lines the estimated density surface from each simulation, and the dashed black line the average of the simulations. The vertical dashed red lines indicate the borders of the trap array. The top row uses the standard simulation parameters, the 2nd row uses 10 occasions, and the bottom row uses a higher g_0.

Figure 3.6: Estimated density surfaces from the simulation scenario Sc.E2 for single-catch trap data with a constant hazard.

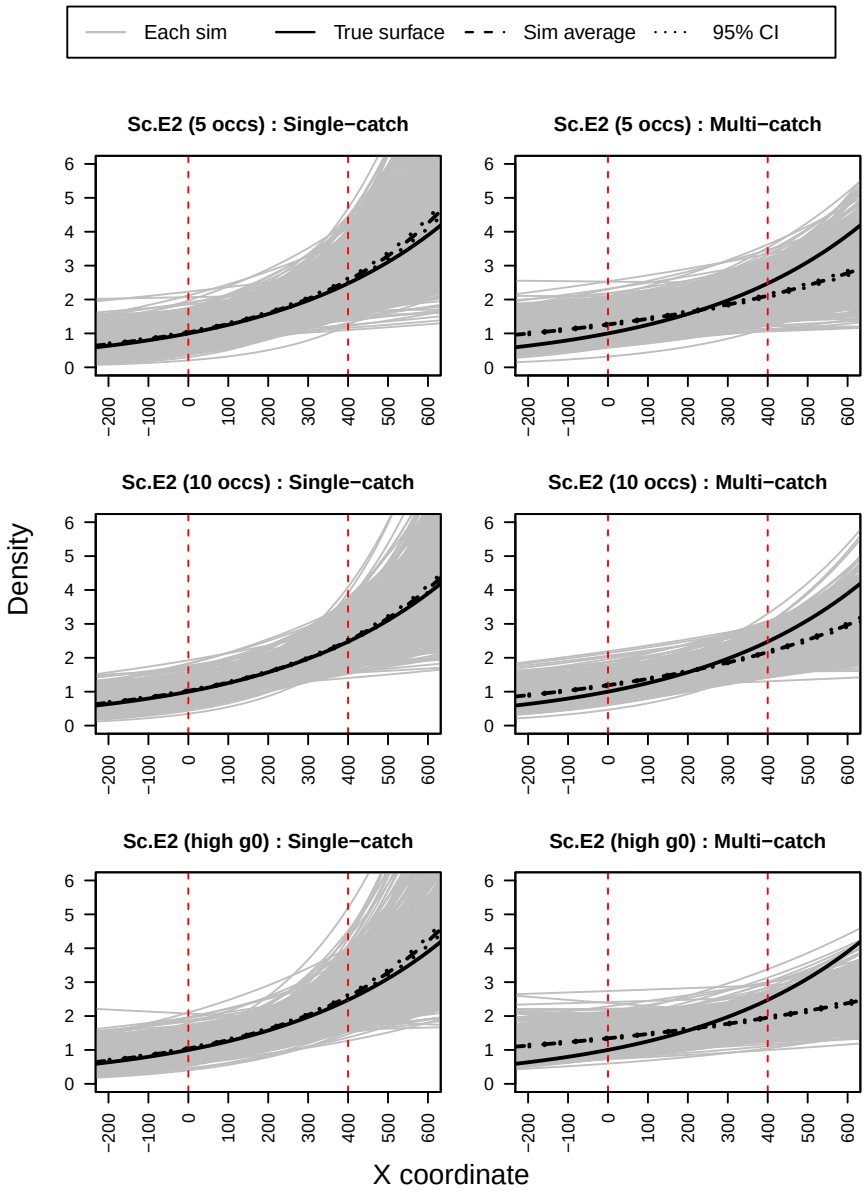

Notes: The black line depicts the true density surface, the grey lines the estimated density surface from each simulation, and the dashed black line the average of the simulations. The vertical dashed red lines indicate the borders of the trap array. The top row uses the standard simulation parameters, the 2nd row uses 10 occasions, and the bottom row uses a higher g_0.

Figure 3.7: Estimated density surfaces from the simulation scenario Sc.E3 for single-catch trap data with a constant hazard.

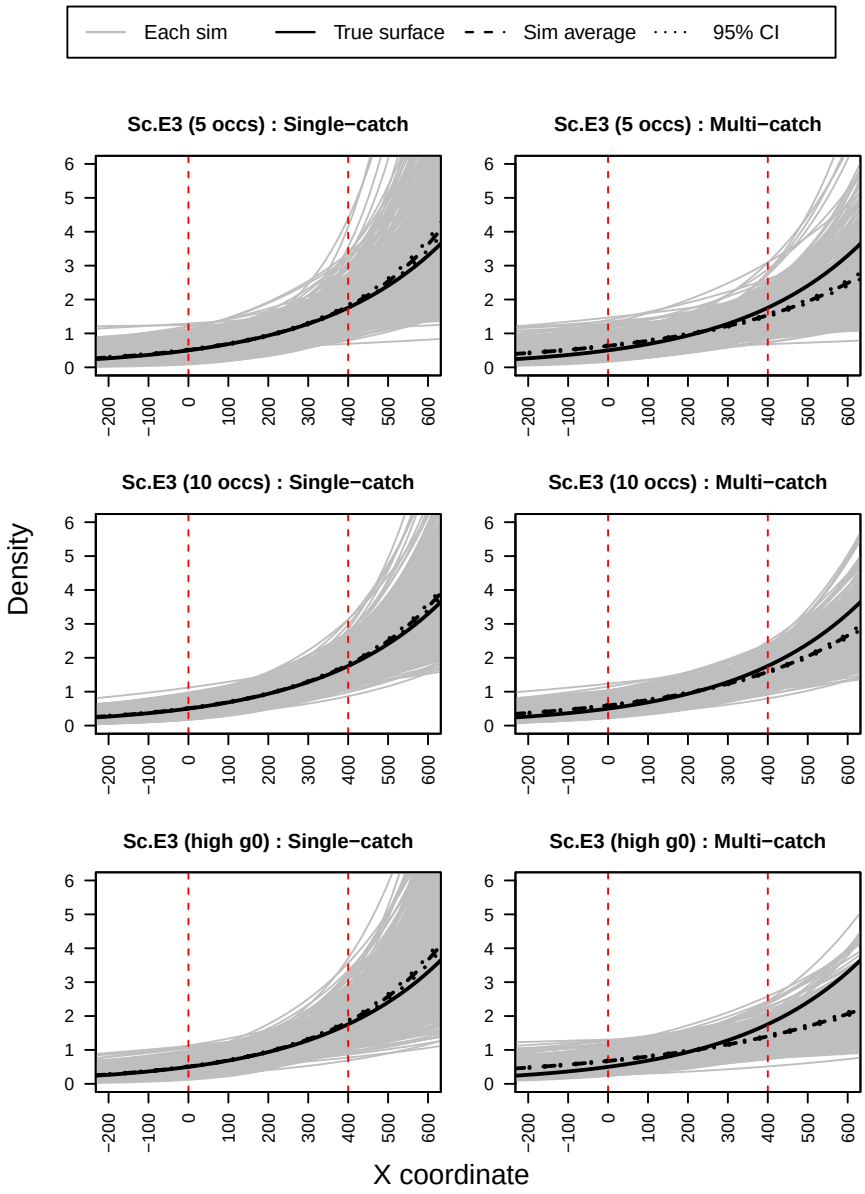

Notes: The black line depicts the true density surface, the grey lines the estimated density surface from each simulation, and the dashed black line the average of the simulations. The vertical dashed red lines indicate the borders of the trap array. The top row uses the standard simulation parameters, the 2nd row uses 10 occasions, and the bottom row uses a higher g_0.

Figure 3.8: Estimated density surfaces from the simulation scenario Sc.E4 for single-catch trap data with a constant hazard.

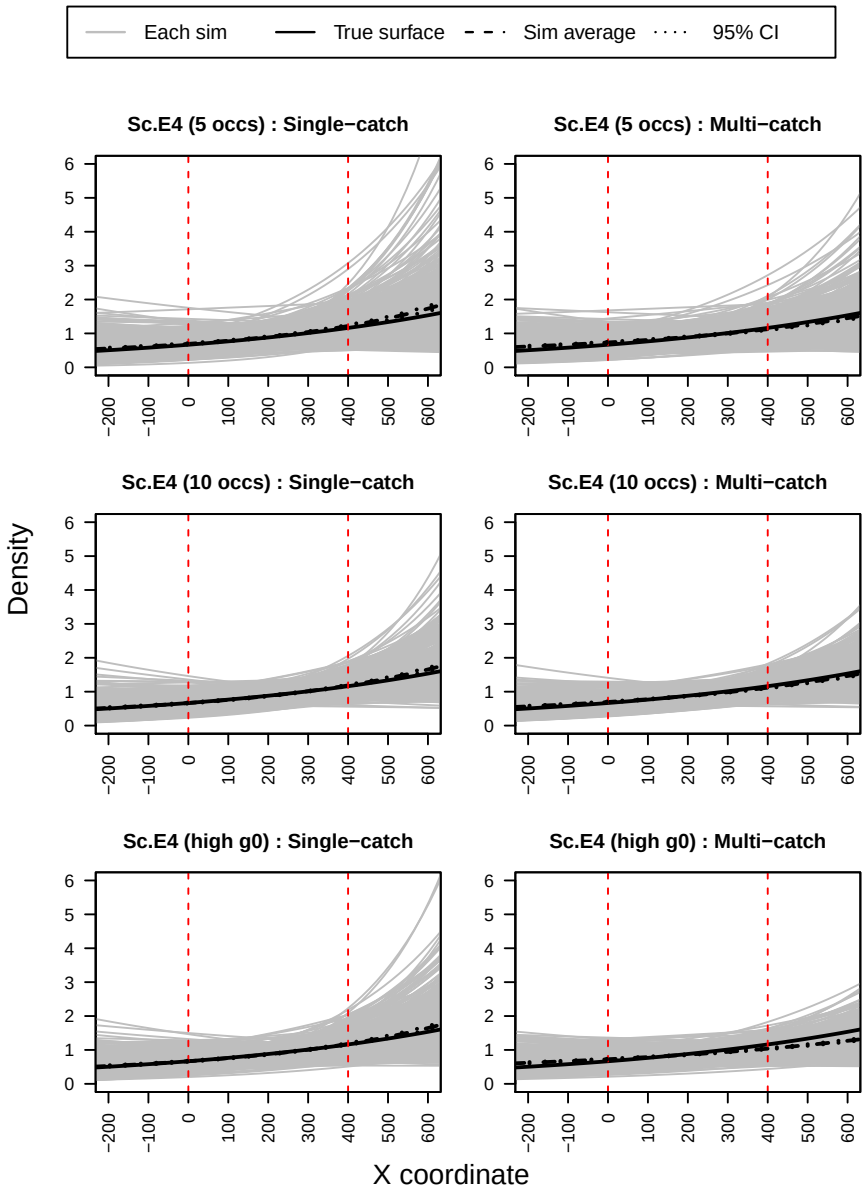

Notes: The black line depicts the true density surface, the grey lines the estimated density surface from each simulation, and the dashed black line the average of the simulations. The vertical dashed red lines indicate the borders of the trap array. The top row uses the standard simulation parameters, the 2nd row uses 10 occasions, and the bottom row uses a higher g_0.

Figure 3.9: Estimated density surfaces from the simulation scenario Sc.E5 for single-catch trap data with a constant hazard.

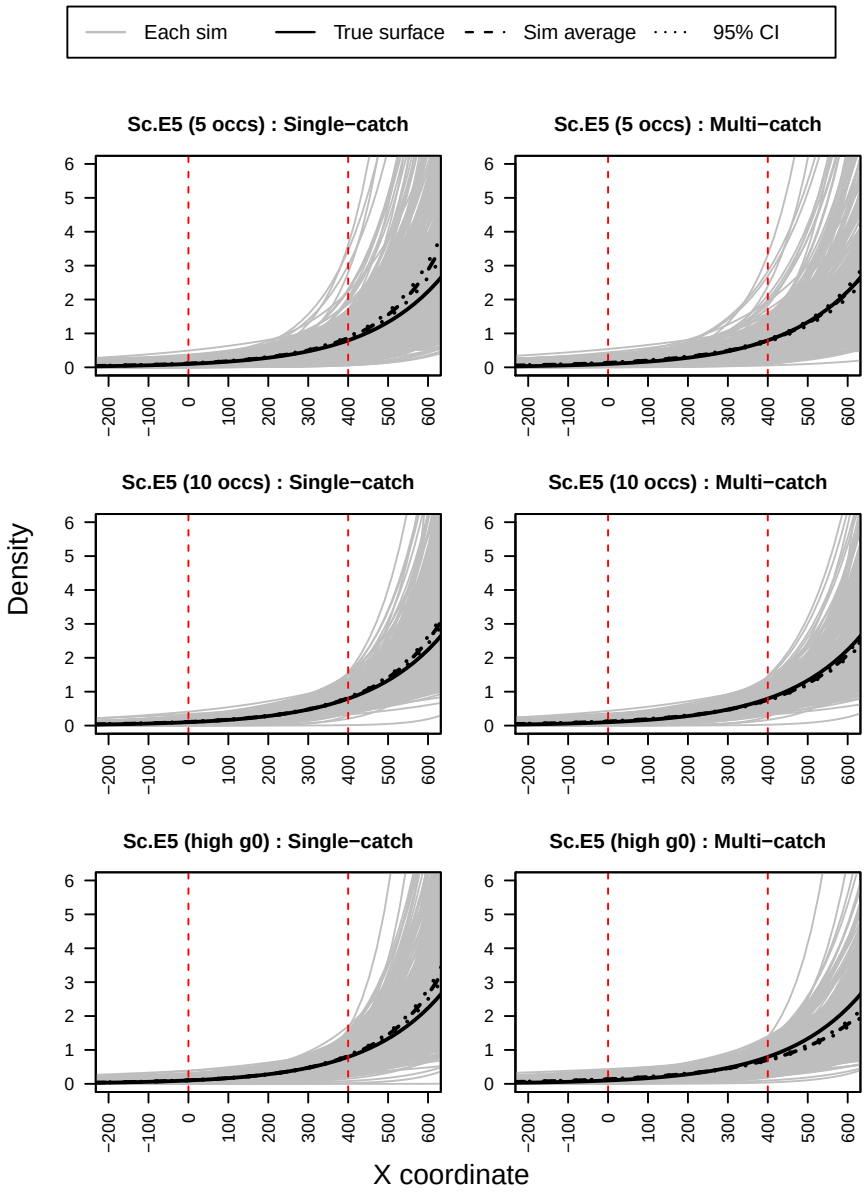

Notes: The black line depicts the true density surface, the grey lines the estimated density surface from each simulation, and the dashed black line the average of the simulations. The vertical dashed red lines indicate the borders of the trap array. The top row uses the standard simulation parameters, the 2nd row uses 10 occasions, and the bottom row uses a higher g_0.

Figure 3.10: Sampling distributions of the estimates for the slope in the exponential density model for both the multi and single-catch trap estimators for single-catch trap data with a constant hazard.

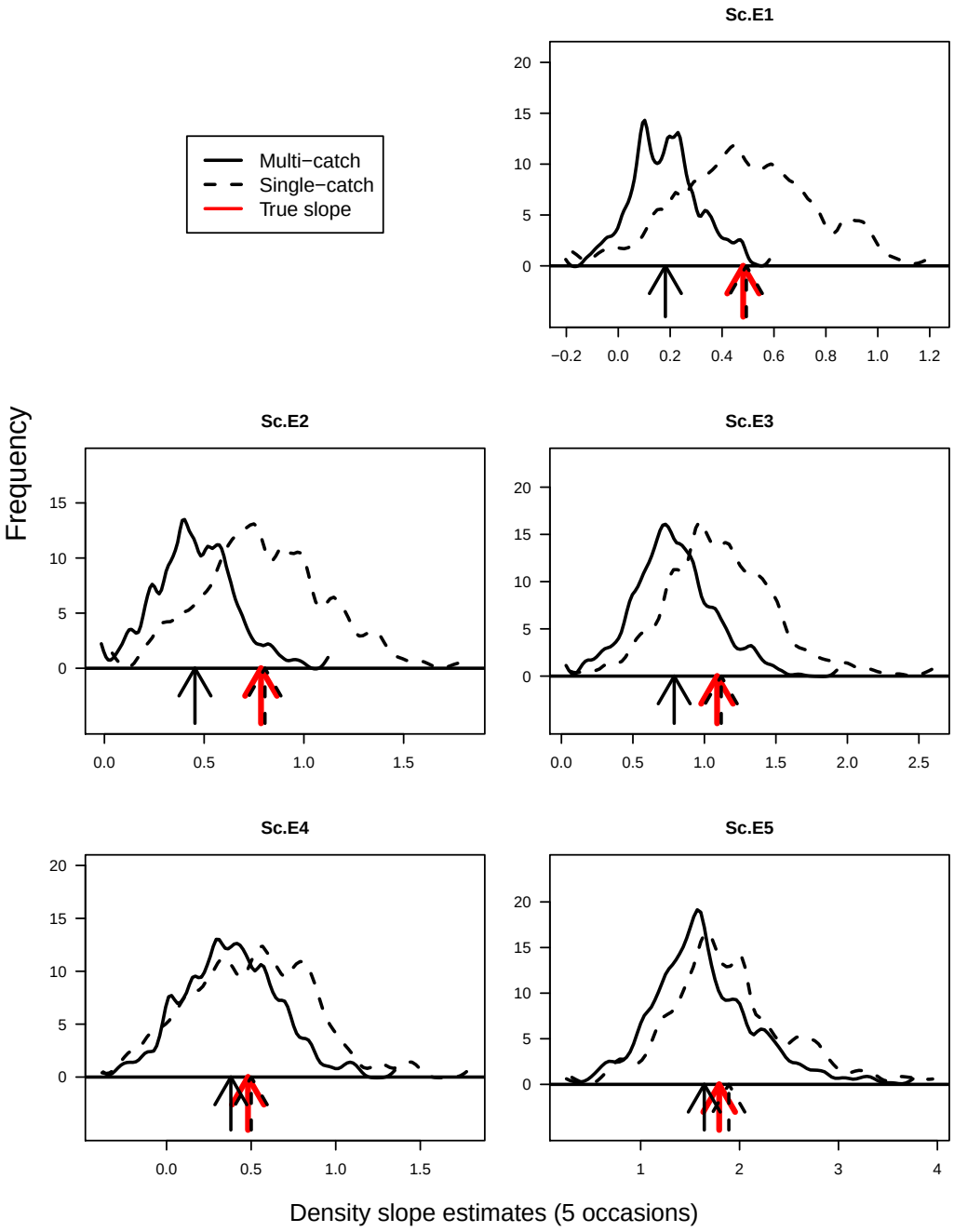

Notes: The arrows mark the position of the mean values for the multi (solid) and single-catch (dashed) estimators, and the red arrows show the true values of the slope parameters.

Figure 3.11: Measures of model performance based on predicted density from the exponential density simulations for single-catch trap data with a constant hazard.

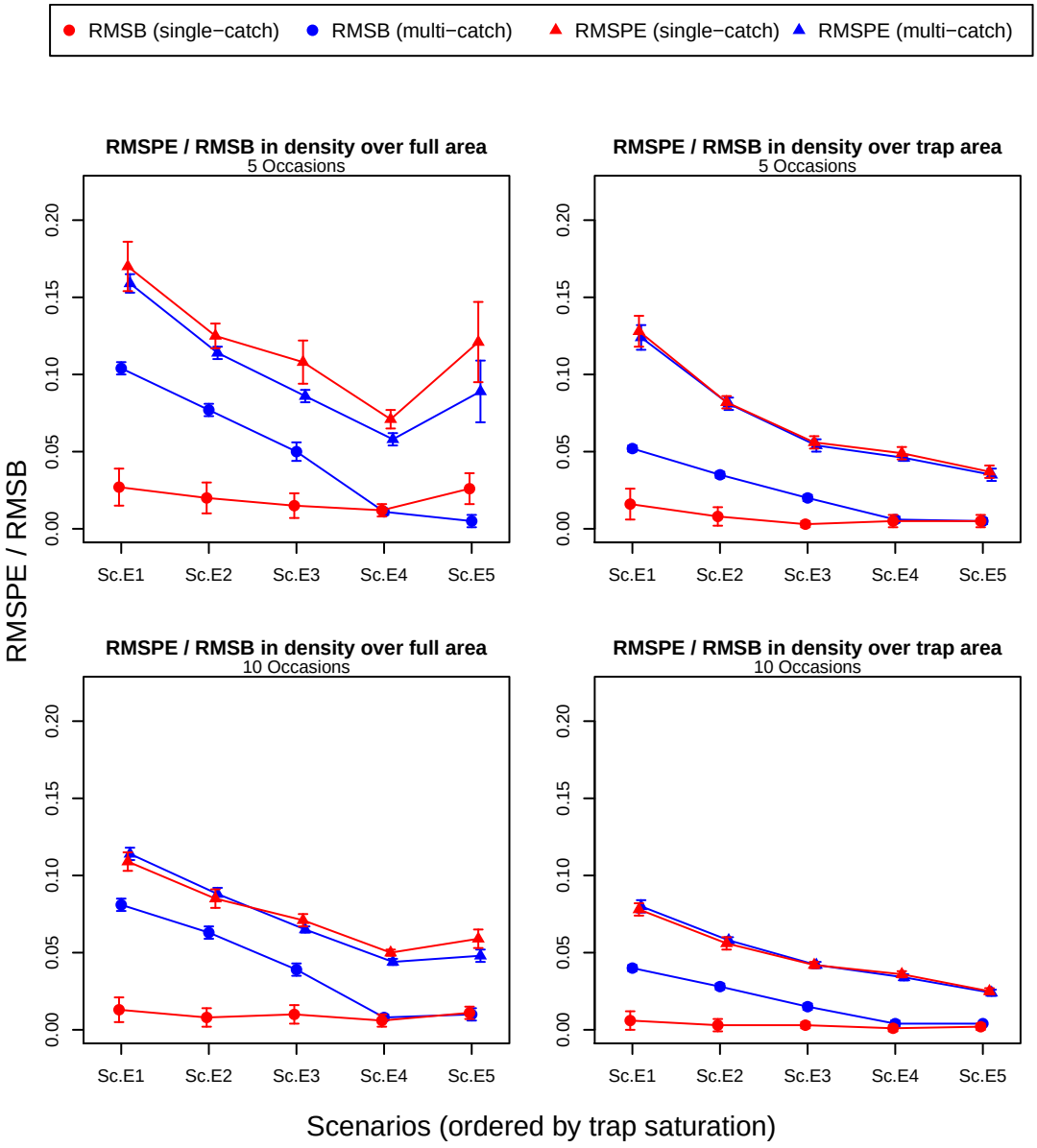

Notes: Results are given for both the full area (top left and bottom left plots) and the area spanning the trap array (top right and bottom right plots). The top row is from simulations with 5 occasions and the bottom row from simulations with 10 occasions. Standard errors are calculated using the Delta method for the RMSPE and bootstrapping for the RMSB, and error bars are plotted using 2 standard errors. The x-axis is ordered by trap saturation (94%, 81%, 61%, 58%, 31%)

Figure 3.12: Estimated density surfaces from the simulation scenario Sc.Q1 for single-catch trap data with a constant hazard.

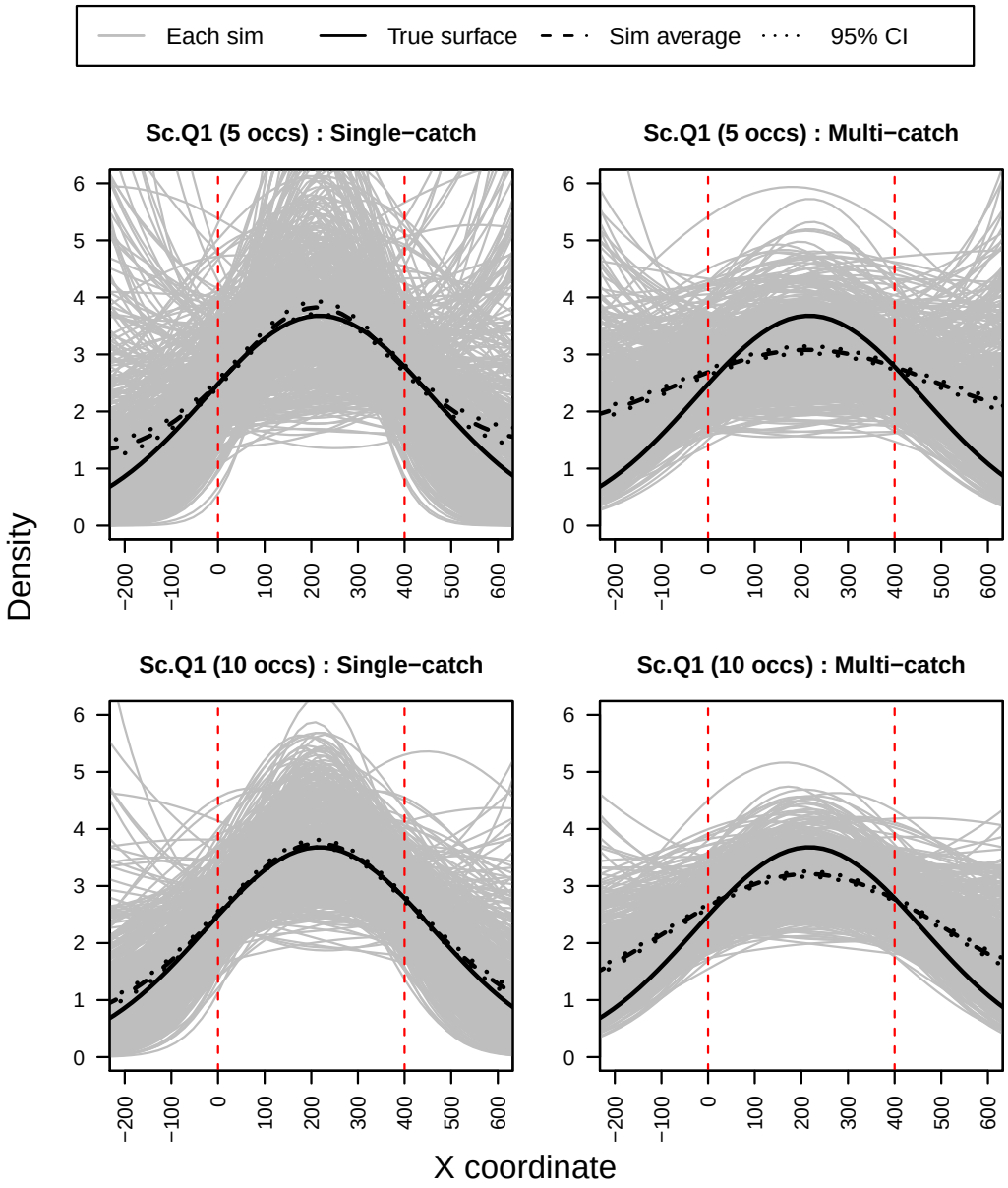

Notes: The black line depicts the true density surface, the grey lines the estimated density surface from each simulation, and the dashed black line the average of the simulations. The vertical dashed red lines indicate the borders of the trap array. The top row uses the standard simulation parameters and the 2nd row uses 10 occasions.

Figure 3.13: Estimated density surfaces from the simulation scenario Sc.Q2 for single-catch trap data with a constant hazard.

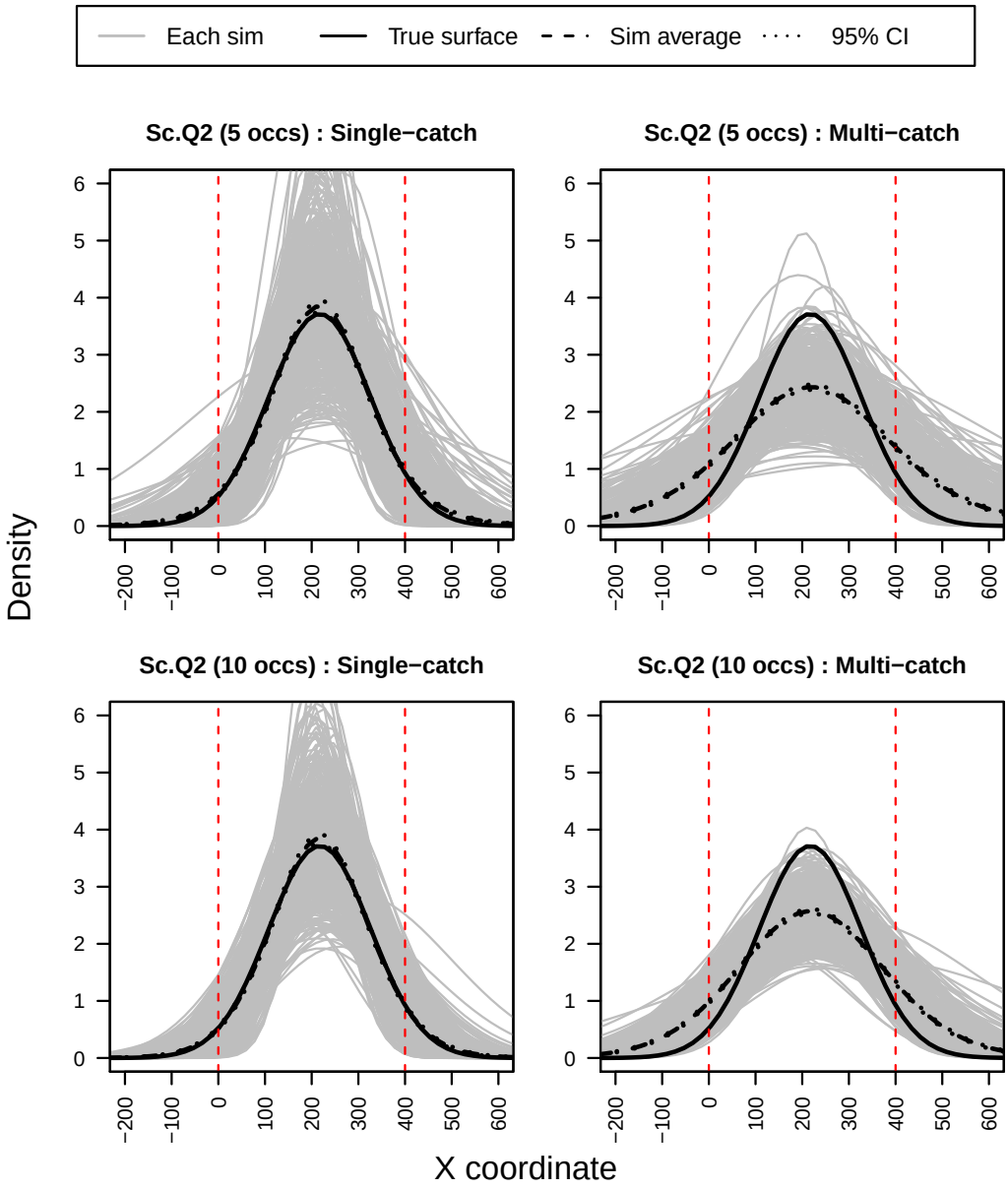

Notes: The black line depicts the true density surface, the grey lines the estimated density surface from each simulation, and the dashed black line the average of the simulations. The vertical dashed red lines indicate the borders of the trap array. The top row uses the standard simulation parameters and the 2nd row uses 10 occasions.

Figure 3.14: Estimated density surfaces from the simulation scenario Sc.Q3 for single-catch trap data with a constant hazard.

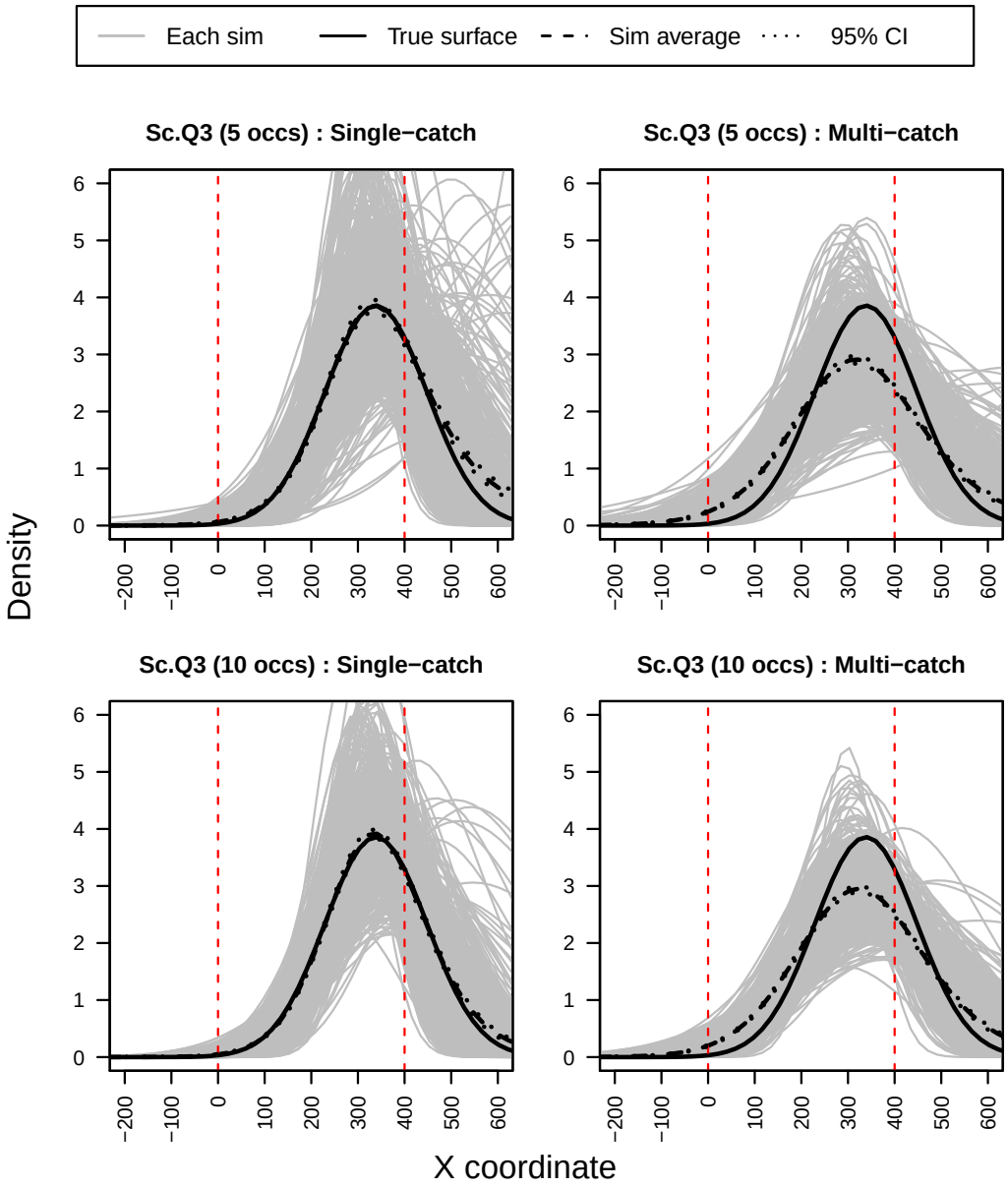

Notes: The black line depicts the true density surface, the grey lines the estimated density surface from each simulation, and the dashed black line the average of the simulations. The vertical dashed red lines indicate the borders of the trap array. The top row uses the standard simulation parameters and the 2nd row uses 10 occasions.

Figure 3.15: Estimated density surfaces from the simulation scenario Sc.Q4 for single-catch trap data with a constant hazard.

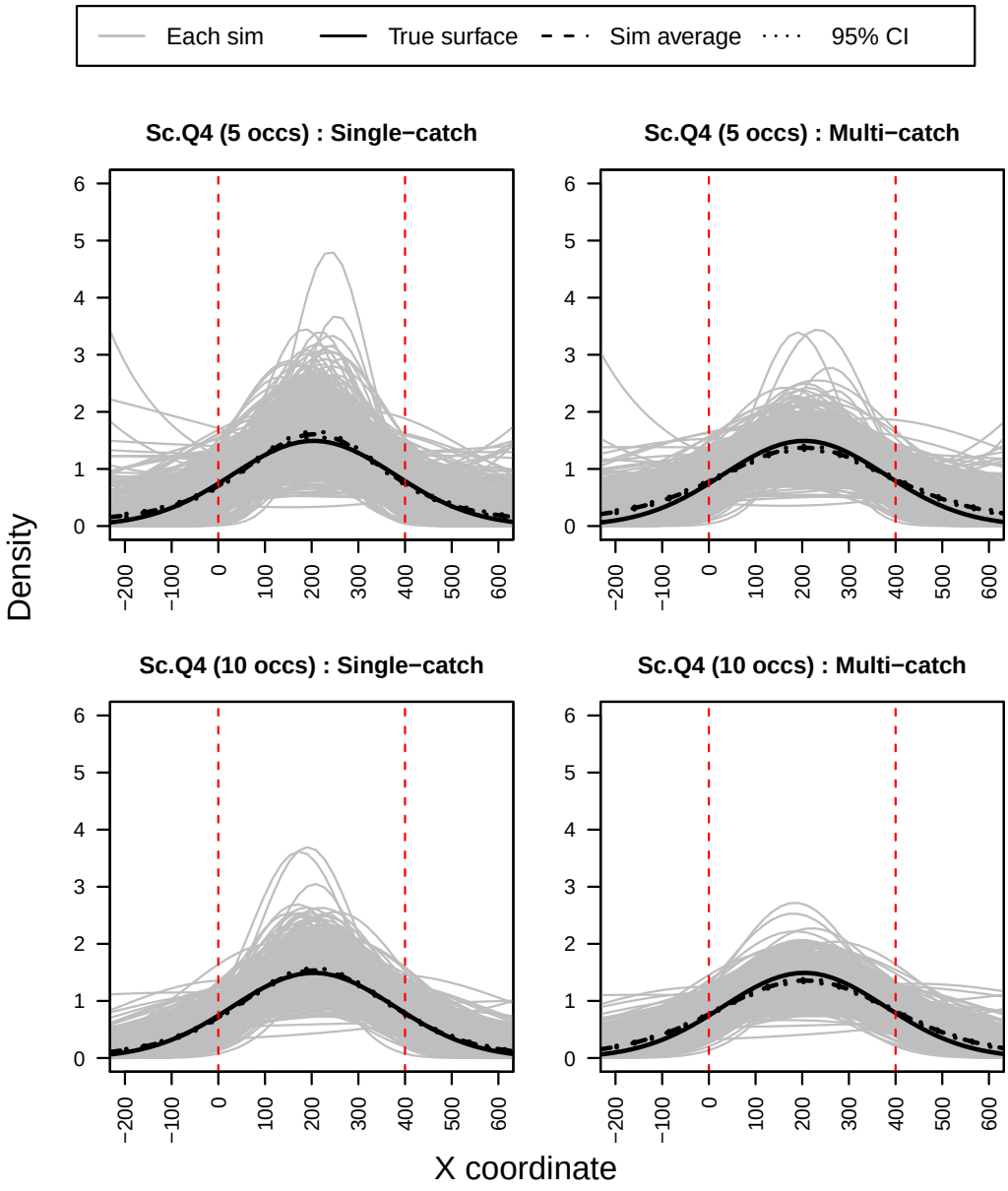

Notes: The black line depicts the true density surface, the grey lines the estimated density surface from each simulation, and the dashed black line the average of the simulations. The vertical dashed red lines indicate the borders of the trap array. The top row uses the standard simulation parameters and the 2nd row uses 10 occasions.

Figure 3.16: Estimated density surfaces from the simulation scenario Sc.Q5 for single-catch trap data with a constant hazard.

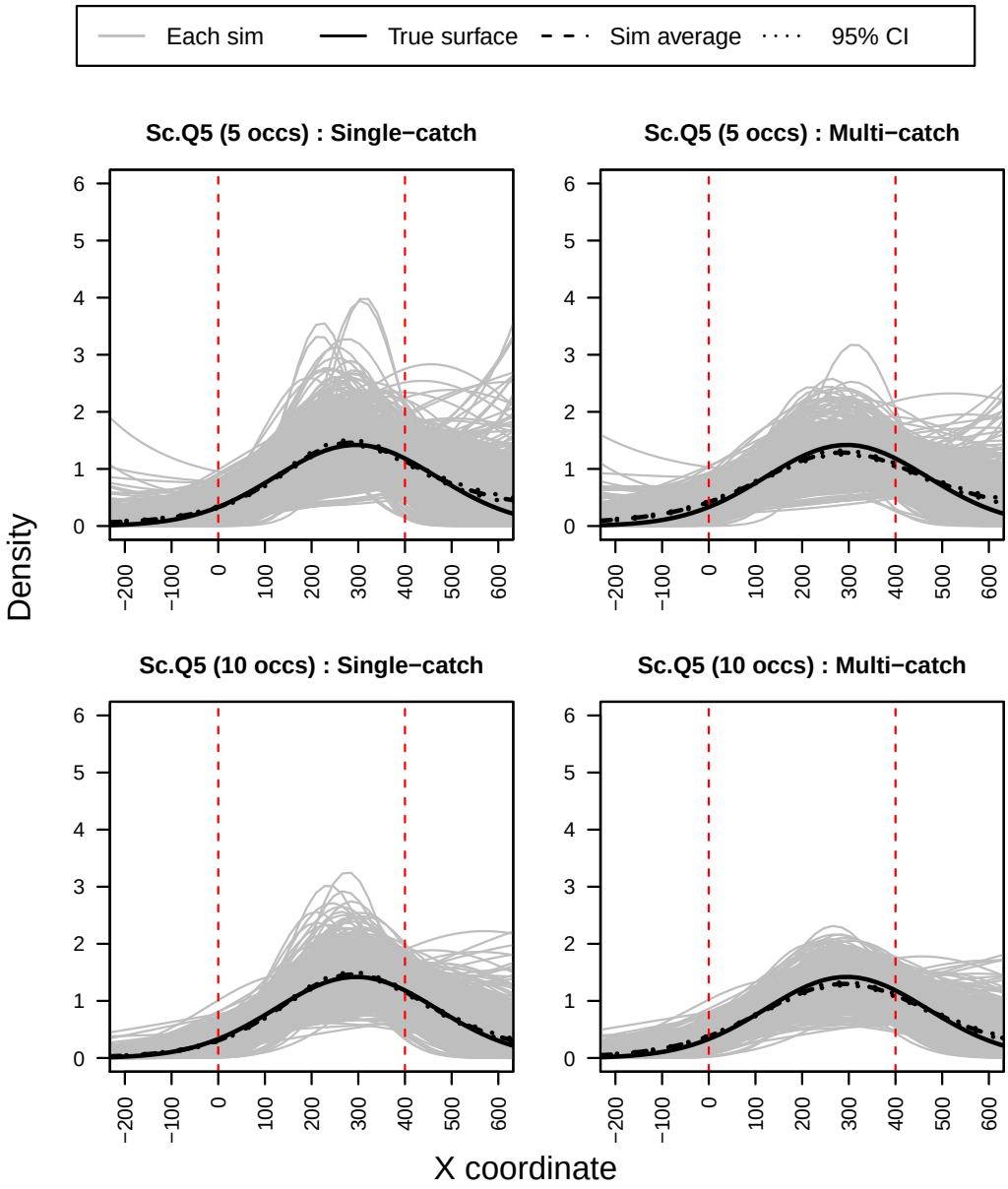

Notes: The black line depicts the true density surface, the grey lines the estimated density surface from each simulation, and the dashed black line the average of the simulations. The vertical dashed red lines indicate the borders of the trap array. The top row uses the standard simulation parameters and the 2nd row uses 10 occasions.

Figure 3.17: Estimated density surfaces from the simulation scenario Sc.Q6 for single-catch trap data with a constant hazard.

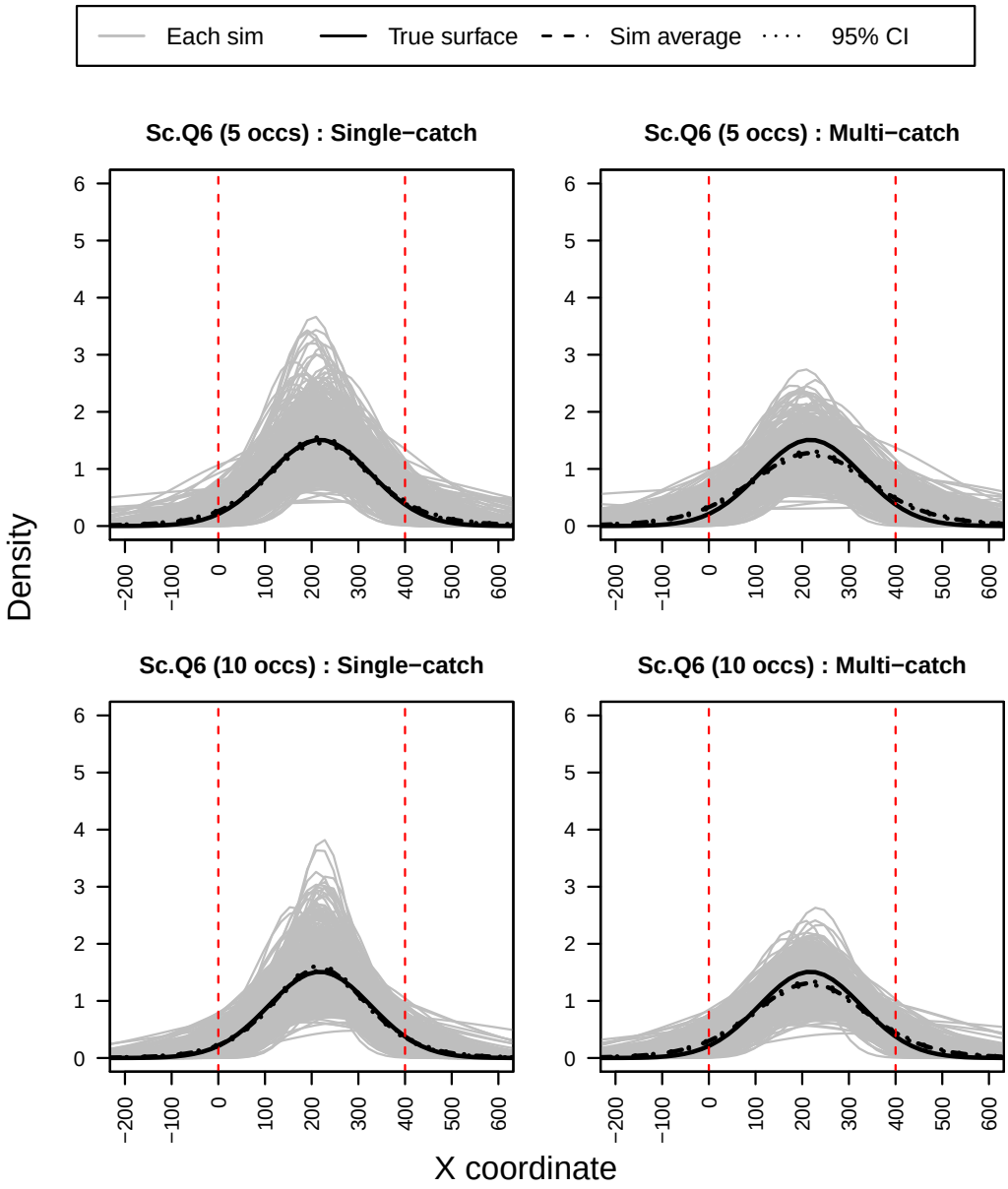

Notes: The black line depicts the true density surface, the grey lines the estimated density surface from each simulation, and the dashed black line the average of the simulations. The vertical dashed red lines indicate the borders of the trap array. The top row uses the standard simulation parameters and the 2nd row uses 10 occasions.

Figure 3.18: Estimated density surfaces from the simulation scenario Sc.Q7 for single-catch trap data with a constant hazard.

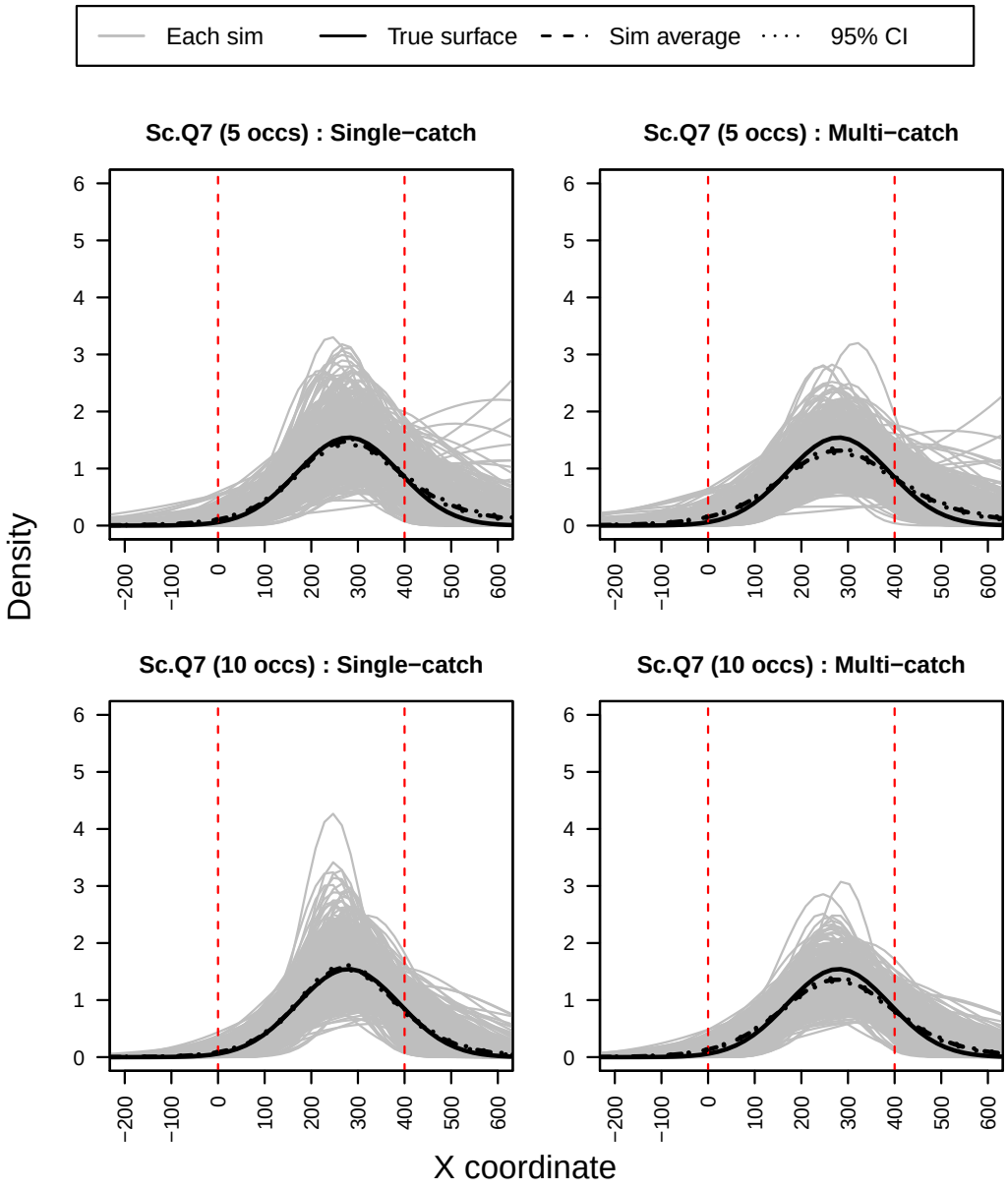

Notes: The black line depicts the true density surface, the grey lines the estimated density surface from each simulation, and the dashed black line the average of the simulations. The vertical dashed red lines indicate the borders of the trap array. The top row uses the standard simulation parameters and the 2nd row uses 10 occasions.

Figure 3.19: Measures of model performance based on predicted density from the quadratic density simulations for single-catch trap data with a constant hazard.

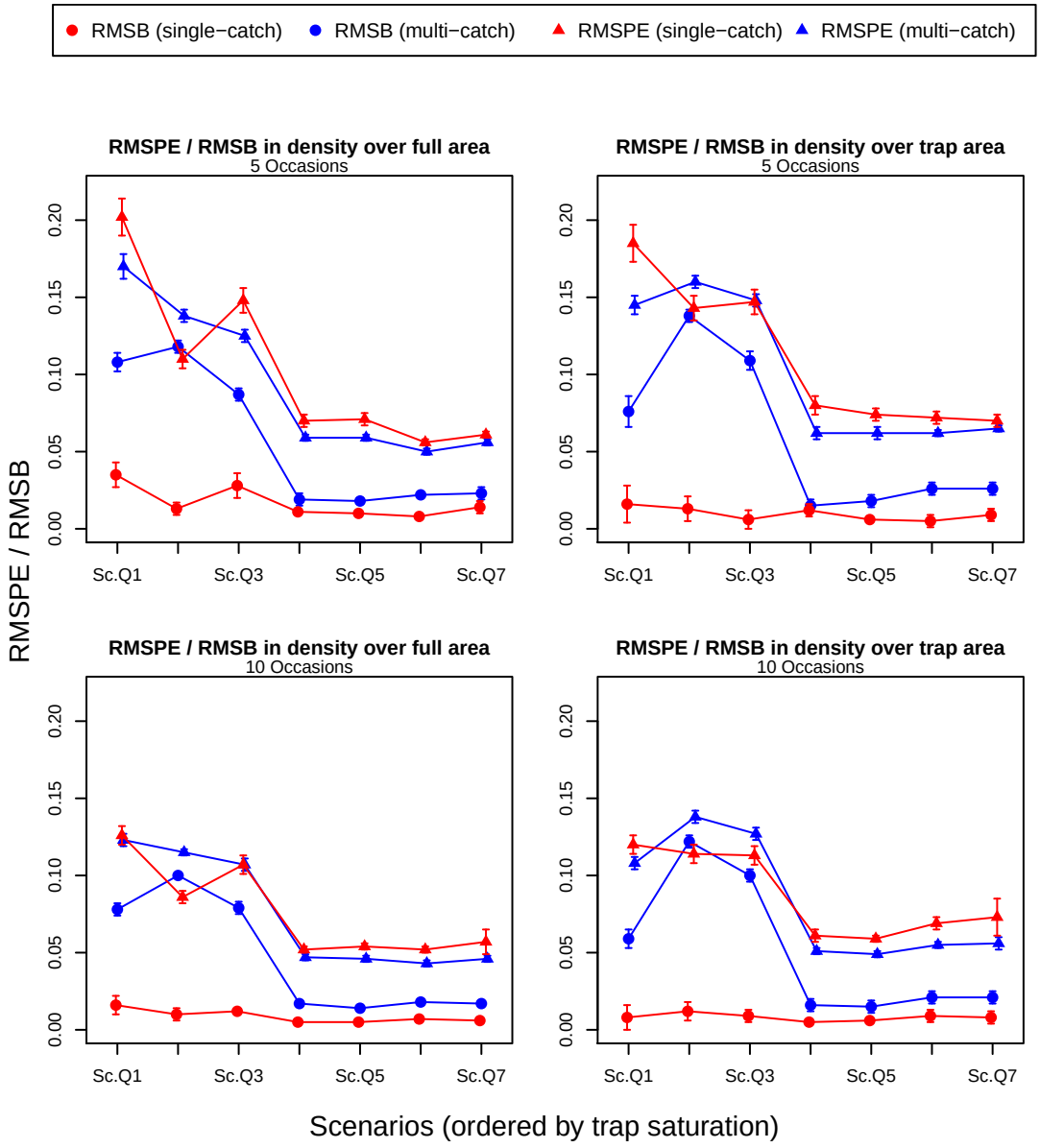

Notes: Results are given for both the full area (top left and bottom left plots) and the area spanning the trap array (top right and bottom right plots). The top row is from simulations with 5 occasions and the bottom row from simulations with 10 occasions. Standard errors are calculated using the Delta method for the RMSPE and bootstrapping for the RMSB, and error bars are plotted using 2 standard errors. The x-axis is ordered by trap saturation (96%, 82%, 70%, 63%, 58%, 50%, 48%)

3.3 Discussion

3.3.1 Proximity detectors

Belize jaguar survey results

The percentage of individuals that are detected at least twice in a day at the same camera gives a rough indication of spatio-temporal clustering within individuals. The differences in this percentage between the real jaguar data (35%) and the simulated movement data (52% and 85%) suggest that the Belize jaguar data are closer to satisfying the independence assumptions of the CT model than are either of the movement simulation scenarios.

Although the assumption of independent activity centre distribution is not realistic for territorial species, the "repulsive" effect that activity centres of territorial species exert on one another's activity centres is difficult to model and the vast majority of SCR studies assume independence between activity centres. Reich and Gardner (2014) developed a SCR model that relaxes the assumption of activity centre independence by using a Strauss process for the spatial point process of the state component of the model. The process includes a parameter for the strength of repulsion. However this model is developed for constant density only (Borchers, 2016), and while it has potential there are in the words of the authors "computational challenges". Efford et al. (2009a) found SCR estimators of density to be robust to violation of the independent activity centre distribution assumption in the form of clustering (overdispersion), and they may also be robust to violation in the form of underdispersion. In contrast, Reich and Gardner (2014) found via simulation that accounting for the tendency of territorial animals to repel each other's activity centres can improve the accuracy of the estimates for abundance. In either case there is evidence from a range of metrics that male jaguars in this population do not have exclusive territories and so this violation is unlikely to have severe consequences on density estimates (Harmsen et al., 2009). Royle et al. (2013c) have developed a test for complete spatial randomness that tests for deviation from a random distribution of activity centres.

Since no bait or lure was used, it is unlikely that the behavioural response in g_0 is a true trap-happiness effect. The camera stations are located on trails resulting in a higher probability of detecting the individuals that habitually use those trails, and hence the behavioural response parameter may be acting as a proxy for individual heterogeneity (Royle et al., 2009a; Soisalo and Cavalcanti, 2006).

Estimator properties

Recall that when assuming a constant detection hazard through time, the CT proximity detector estimator is essentially equivalent to a DT Poisson count estimator with a single occasion. Like Efford et al. (2009b), we found that a Poisson count model estimator with a single sampling interval can give precise and unbiased density estimates. In general, information is lost if exact detection times are discarded, although this is not the case if the hazard of detection is constant through time and count data are retained. There is a loss if count data are reduced to binary data although Efford et al. (2009b) found the loss to be small in the scenarios they considered. Similarly we found little difference between the performance of DT binary proximity detector estimators and CT proximity detector estimators with a constant detection hazard when using detector spacings of 1.25σ and 1.88σ.

When detector spacing was reduced to 0.625σ, the CT proximity detector estimator performed substantially better than the binary discrete-occasion proximity estimators. However, when rerunning these simulations under a new version of `secr` (Efford, 2016) it became apparent that the observed bias that was originally observed for the low detector spacing setup was a convergence issue. From `secr` version 2.9.5 a default setting in the `secr.fit` function(`details$minprob`) was changed to improve the optimisation, and rerunning these simulations no longer results in the same bias. The fact that the optimisation was slightly unstable does however suggest that it can be more difficult to optimise the binary likelihood which has less data compared to a count model.

Data aggregation

Except in some special cases, data aggregation involves information loss. Aggregation can be useful when modelling unaggregated data is difficult, but aggregation without good reason is not good practice. When SCR data are recorded in continuous time, there is no good reason (apart from convenience) not to use a CT model.

When there is spatio-temporal correlation in detections (e.g. due to movement) and a design with adequate detector spacing, there may be merit in aggregating data across time and using binary discrete-occasion models with appropriate occasion lengths. However, our simulations suggest that (a) the convergence of binary discrete-occasion density estimators can be sensitive to the length of occasions when detectors are too close together, and (b) that the CT estimator of density is moderately robust to inadequate detector spacing and levels of spatio-temporal correlation that are substantially higher than is apparent in the jaguar field data.

The results from the correlated simulations also suggest that aggregating the

data into many, short occasions, and using a DT model, may result in positive bias in density. However the extent of this bias appears to reduce with an increase in sample size - it drops from around 35% to 5% when using greater trap spacing that results in more unique individuals being caught.

3.3.2 Single-catch traps

The multi-catch trap estimator ignores the fact that occupied single-catch traps are out of action until they are reset. The estimator appears to compensate for this by underestimating the g_0 parameter and as expected the extent to which this happens increases with trap saturation. As stated by Efford et al. (2009a) this compensator mechanism results in a surprisingly robust estimator of density though the incorrect estimation of g_0 would still have implications if the estimated detection function is used in movement or space-use models. In most cases σ is well estimated.

Comparing the multi-catch and single-catch trap estimators from models with constant density

When the true density is constant in space both the estimators are unbiased or nearly so even when the multi-catch estimator of the g_0 parameter is badly negatively biased (Efford et al., 2009a). Both estimators of density exhibit slight positive bias of around 10% for the scenario with the highest density level (and very high levels of trap saturation) and with 5 occasions, however when the number of occasions are doubled and the data contain more recaptures there is no longer any bias evident.

When a constant density is incorrectly specified there is no gain in terms of density estimation from using the single-catch trap estimator. However it is obviously not desirable to misspecify the density model in this way and essentially just estimate mean density as shown in Figure 3.20.

If the true distribution of activity centres follows a clustered distribution, the simulations show that a constant density model is a good approximation when density is high enough so that there are not many areas with no animals. Density estimates are positively biased with both estimators for very patchy distributions. The single-catch trap likelihood does however have the advantage of providing unbiased estimates of the detection function parameters except when there is very little data, in which case no estimator is likely to perform well.

Figure 3.20: Results from two of the single-catch trap simulations where the data are from non-constant density surfaces (exponential and quadratic) and the models specify a constant density.

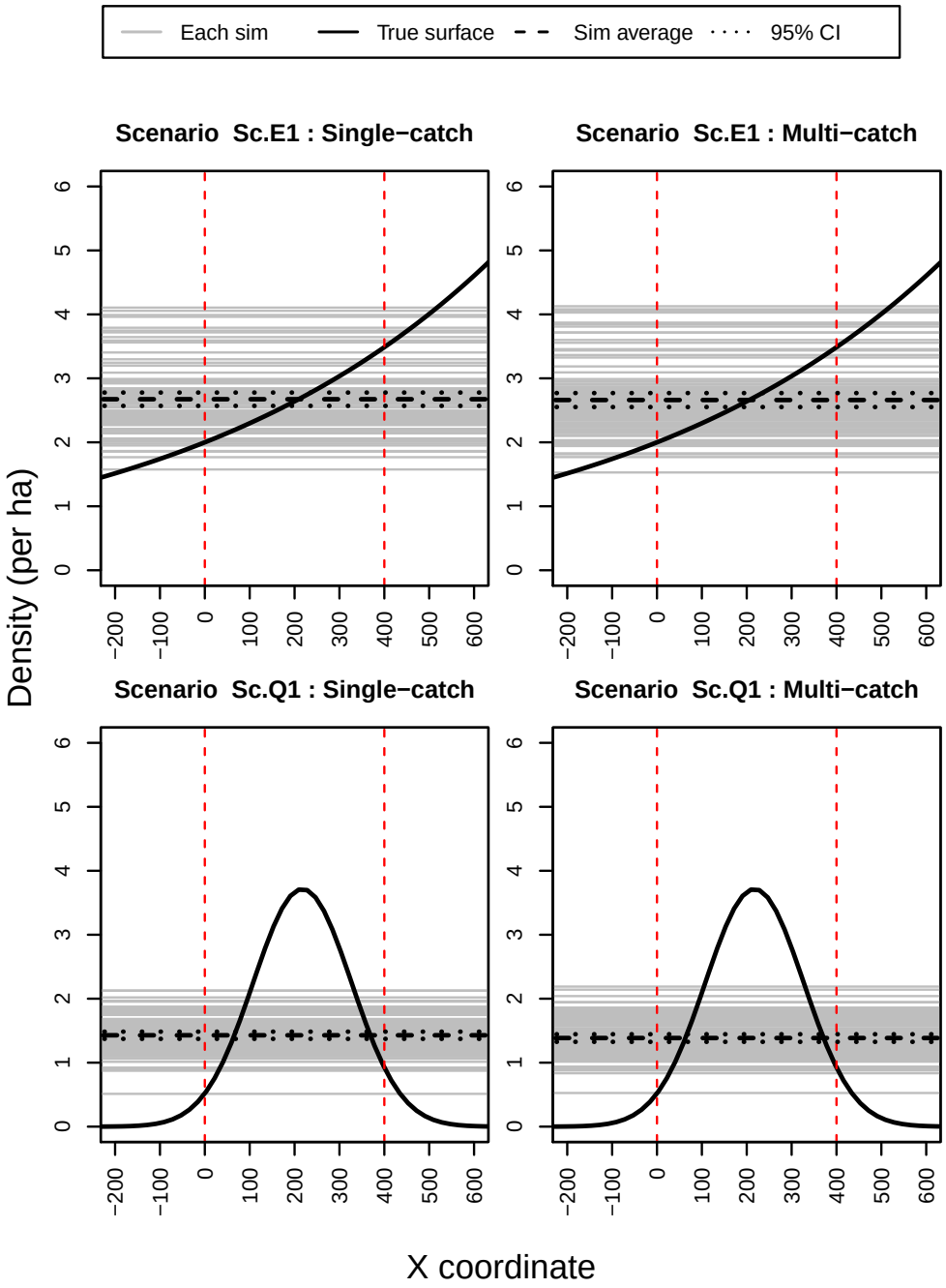

Notes: The black line depicts the true density surface, the grey lines the estimated density surface from each simulation, and the dashed black line the average of the simulations. The vertical dashed red lines indicate the borders of the trap array.

Comparing the estimators from models that do not assume constant density

A non-constant density surface can lead to high trap saturation in areas of high density but not in low density areas. The assumption implicit in the multi-catch trap model that traps continue to operate after catching an individual can therefore be badly violated in the high density areas leading to density being underestimated in those areas. The consequent underestimation of g_0 also gets applied to the traps in low density areas where trap saturation may not be high, resulting in density being overestimated in low density areas.

When density follows a west-east exponential gradient, the multi-catch trap estimator overestimates density where density is low in the west and underestimates density where it is high in the east. These two errors tend to cancel each other out and the estimator of mean density is nearly unbiased. A slight negative bias is evident when evaluating density over the full area due to the steep exponential increase in the eastern part of the true density surface.

A similar thing happens with a quadratic bump in density whereby the multi-catch trap estimator underestimates density around its peak and overestimates density at the edges resulting in a reasonably unbiased estimate of mean density over the full area. However the estimator is negatively biased for mean density if evaluated over the reduced area since then the error from underestimating density dominates the corresponding error from overestimating density at the edges. This bias is worst when the peak in density is centered on the trap array as in scenarios Sc.Q1 and Sc.Q2.

Trap saturation affects the extent that the multi-catch trap estimator underestimates g_0, however the steepness of the change in density also plays an important part and can lead to overestimation in σ and to the deterioration of the robustness of the multi-catch estimator. When the gradient is slight the multi-catch estimator performs well.

The single-catch trap estimator is approximately unbiased for the parameters of interest and the confidence interval estimator has reasonably good coverage for the parameters of interest (see Table 3.8). Figures 3.5 to 3.9 and 3.12 to 3.18 show that the single-catch trap estimator accurately estimates the true density surface over the area of the trap array, but that in most scenarios there is slight positive bias in the estimated density over the regions at the edges of the plots where no sampling occurs. The extent of this positive bias at the edges of the plots appears to be related to the gradient in density at the boundaries of the trap array, e.g. scenario Sc.Q4 has a fairly flat density gradient at the boundaries and the estimator is unbiased over that region whereas Sc.Q1 has a much steeper decline in density at the boundaries and

Table 3.8: Coverage of the parameter and derived density estimates from the single-catch trap estimator for both the exponential and quadratic simulations, and for both 5 and 10 occasions of 24 hours. The Delta method was used to calculate the variance in the derived density estimates.

# Occasions	Scenario	Exponential					Quadratic			
		$\hat{D}_F$	$\hat{D}_R$	$\hat{D}_{slope}$	$\hat{g}_0$	$\hat{\sigma}$	$\hat{D}_F$	$\hat{D}_R$	$\hat{g}_0$	$\hat{\sigma}$
5 Occasions	1	0.94	0.94	0.93	0.96	0.95	0.95	0.96	0.97	0.95
	2	0.95	0.95	0.97	0.97	0.95	0.97	0.97	0.96	0.95
	3	0.94	0.94	0.93	0.96	0.95	0.95	0.96	0.97	0.95
	4	0.94	0.94	0.93	0.96	0.95	0.95	0.96	0.97	0.95
	5	0.92	0.92	0.96	0.97	0.90	0.96	0.95	0.95	0.95
	6	NA	NA	NA	NA	NA	0.94	0.93	0.96	0.94
	7	NA	NA	NA	NA	NA	0.96	0.94	0.97	0.95
10 Occasions	1	0.94	0.93	0.95	0.95	0.95	0.95	0.93	0.96	0.94
	2	0.96	0.95	0.95	0.97	0.94	0.93	0.92	0.94	0.95
	3	0.94	0.94	0.98	0.96	0.95	0.95	0.95	0.96	0.98
	4	0.95	0.95	0.94	0.97	0.96	0.95	0.94	0.96	0.96
	5	0.94	0.92	0.96	0.96	0.95	0.95	0.95	0.94	0.95
	6	NA	NA	NA	NA	NA	0.94	0.93	0.97	0.96
	7	NA	NA	NA	NA	NA	0.96	0.95	0.94	0.95

the estimator exhibits positive bias at the edges. However overall, it is clear that the single-catch trap estimator has lower bias than the multi-catch estimator for trap saturations above about 60%, and the estimators have similar RMSPE's.

3.3.3 Summary of model performance

When proximity detectors are used and detectability does not change through time there is no need for multiple occasions and a CT proximity detector / Poisson count model produces precise and unbiased estimates. This model assumes independent captures and hence it is possible that the estimator does not perform as well if the capture times have a higher degree of spatio-temporal correlation than what is typically found in data from the type of species that tend to be monitored with camera traps.

A binary DT model also performs well despite the fact that reducing counts to binary capture events results in some data loss. There does however appear to be some instability in the estimation, and sensitivity to the length or number of occasions, when the spacing between traps is low relative to σ.

For data from single-catch trap surveys, the multi-catch estimator tends to be

negatively biased for the g_0 parameter but surprisingly robust when it comes to the estimation of density. There do appear to be scenarios with spatially varying density surfaces that result in the multi-catch estimator being unable to accurately identify areas of low and high density whereas the single-catch trap estimator is unbiased in all cases.

Chapter 4

Models with a time-varying detection hazard

This chapter again uses simulations to compare the performance of the discrete-time (DT) and the continuous-time (CT) estimators when the detection hazard is not constant through time, for a range of density surfaces. The ability of the CT estimator to model underlying activity patterns is also explored by applying these methods to the jaguar data (for proximity detectors) and to the possum data (for single-catch traps).

Both the cosine hazard and the cyclic spline hazard forms are used in the proximity detector simulations in the first section of this chapter. In contrast the single-catch trap simulations in the second section only use the cyclic spline form.

A particular hazard is termed a "synchronous" hazard when the hazard cycle length matches the occasion length used in a DT model, for example if each occasion is defined as a 24 hour day and the hazard cycle repeats every 24 hours. In such a case, integrating the hazard over any occasion will give the same cumulative hazard and consequently the same detection function. Equation 2.37 shows how to link the detection hazard with the detection function for a specified period of time. If the hazard is synchronous then any occasion could be used when specifying the hazard function in this way.

In contrast, an "asynchronous" hazard is when the duration of the hazard cycle is different to the occasion length and hence will result in different integrated hazards for different intervals of time. In such a case, the interpretation of g_0 and σ (or other detection function parameters) will specifically be for the particular occasion used in the hazard specification. In the simulations below the hazard has always been specified so that integrating it over the first occasion will produce the half-normal

detection function, i.e. the interpretation of g_0 and σ is specifically with reference to the period of time that corresponds to the first occasion.

The estimators are evaluated in a similar way to that outlined in Section 3.2.1. The relative biases of the parameters of interest are presented in tables and both the estimated hazards and the estimated density surfaces (in the case of non-constant density) for each simulation are plotted over the true surface. In order to improve readability the tables displaying the relative biases are found in Appendix C. Furthermore many of the figures depicting the estimated hazard and density surfaces are similar to each other. The first of each of these plots for the cosine and spline hazard (including the asynchronous hazard with longer cycle durations) is included in the main report and subsequent figures are found in Appendix D.

Following the approach used in Chapter 3 when exponential and quadratic density surfaces are used, relative bias in mean density is reported over two areas (D_F and D_R), the relative bias of the density "slope" parameter is reported for the exponential scenarios, and the relative biases of the quadratic coefficients are not reported. In addition, the relative biases of the spline hazard coefficients are also omitted from the tables for brevity and the adequacy of the hazard cycle estimation is gauged visually from plots. The focus with these plots is on the shape of the detection hazard through time or the $h(t;\boldsymbol{\psi})$ component of the hazard, and hence the plots exclude the $h(\boldsymbol{s};\boldsymbol{\theta})$ scaling component and show the "scaled hazard", i.e. the area under all the hazard curves is equal.

4.1 Proximity detectors

This section presents extensive simulations where data are generated from a variety of density surfaces with a time-varying hazard and an array of proximity detectors. The simulations include synchronous hazards with a cosine hazard and cyclic spline hazard form, and asynchronous hazards with a cyclic spline form. In both cases cyclic spline hazards with two different degrees of freedom (K = 4 and K = 8) are used. The proximity detector simulation scenario is again based on the jaguar dataset and uses a similar setup to the proximity detector simulations with a hazard that is constant in time presented in the previous chapter (Section 3.1.4).

CT models assuming various non-constant hazards are then applied to the jaguar dataset.

4.1.1 Simulation studies

Except where stated otherwise, all simulations are from a study of duration 2,160 hours that for the DT models is divided up into 90×24 hour occasions with a 5×4 array of proximity detectors spaced $3,000$ m apart. For all scenarios, proximity detector data with observed capture times are simulated and two estimators (namely the DT binary proximity detector estimator and the CT proximity detector estimator) used to estimate the parameters of interest. The hazard function is specified so that it produces a half-normal detection function with $g_0 = 0.05$ and $\sigma = 2400$ for the first occasion. The trap spacing of 3,000 m is hence equivalent to a spacing of $1.25\ \sigma$.

Capture times are simulated in the same manner outlined in Section 3.1.4 where the count of events is first simulated and then followed by the actual capture times themselves. The first step requires, for each individual, the simulation of trap-specific counts of capture events from the whole study. Consequently the hazard function needs to be integrated over the full study period and this can be accomplished numerically over a fine mesh for the spline hazard. A probability integral transform is used to simulate actual capture times by simulating a random probability between 0 and 1 from the uniform distribution and using the cumulative distribution function (CDF) for capture times (conditional on ω_{ik}) to solve for t. Further details for the cosine and spline hazards are given in their respective sections below.

Simulation scenarios

The simulation scenarios that use non-constant density surfaces presented in Section 3.2.1 are for single-catch trap studies that usually involve small mammals. Proximity detectors (camera traps) are typically used for animals with different characteristics that occur at lower densities and range widely. A survey with proximity detectors tends to cover a much larger area. If I used the same density surfaces as in Section 3.2.1 but effectively sampled the surface over a much larger range I may not have obtained the required degree of variation in density. Consequently the density surfaces used in the single-catch trap simulations cannot be reused for the proximity detector simulations and a new set of surfaces are used here.

Figure 4.1 illustrates the density surfaces used in the exponential and quadratic cases, and Table 4.1 provides further details of the scenarios, including the mean number of unique individuals from 100 simulated capture histories. The scenarios follow the same convention as in Chapter 3 and are ordered in descending order with respect to the average number of captures that each scenario simulates, and named with a "Px." prefix (for "proximity") followed by the letter C, E, or Q corresponding

Figure 4.1: Simulated density surfaces used in the exponential and quadratic density scenarios for proximity detectors. The vertical dashed red lines indicate the borders of the trap array.

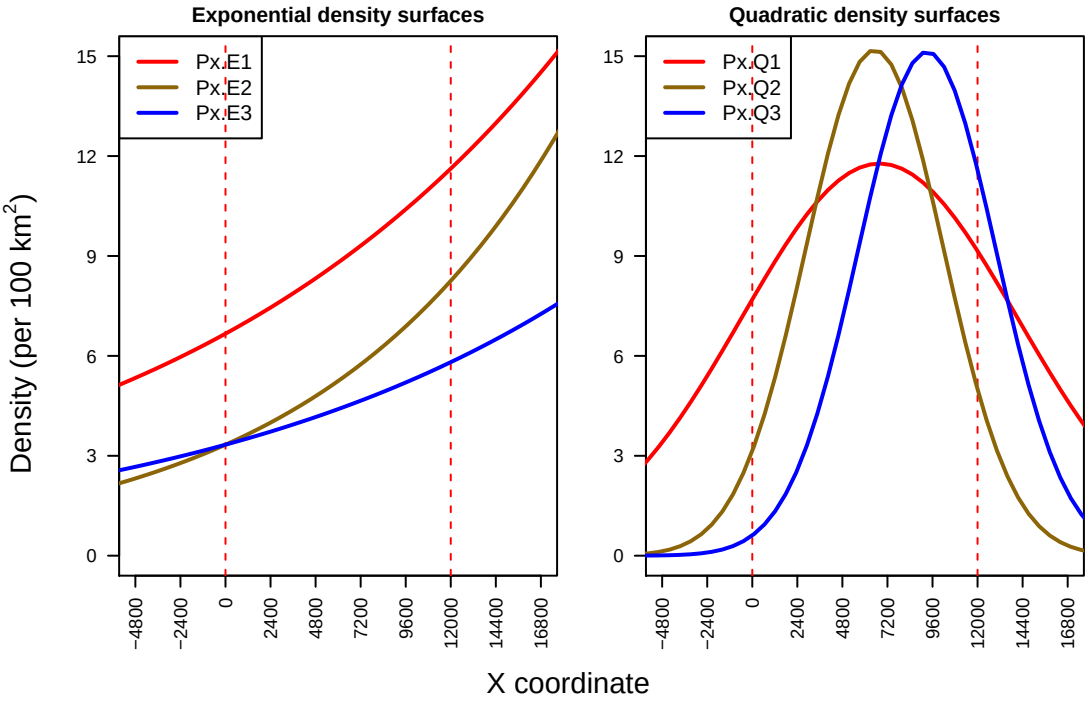

to the type of density surface and ending with the scenario number.

Simulating capture times from a cosine hazard

As explained in Section 4.1 the capture times from proximity detectors are simulated in two steps. Firstly the count of capture events for each individual at each detector is generated, and then the appropriate number of actual times is simulated. The cosine hazard needs to be integrated over the study period to simulate the ω_{ik} random variables and the integrated hazard can be written as follows:

Table 4.1: Details of the different density surfaces used in the proximity detector simulations.

Simulation Type	Scenario	D_{Max}	D_S	$\bar{D}$	Unique	Captures
Constant	Px.C1	8.00	8.00	8.00	34.5	272.2
	Px.C2	4.00	4.00	4.00	16.4	127.3
	Px.C3	2.00	2.00	2.00	8.8	70.1
Exponential	Px.E1	13.89	6.67	9.03	39.4	302.1
	Px.E2	11.03	3.33	5.68	24.6	182.8
	Px.E3	6.94	3.33	4.51	18.9	144.9
Quadratic	Px.Q1	11.77	7.69	8.74	38.0	332.0
	Px.Q2	15.15	3.15	6.68	28.1	286.1
	Px.Q3	15.10	0.61	6.48	27.3	265.3

Notes: All density values are given per 100 km^2 and calculated using a buffer of $2 \times \sigma$. D_{Max} is the maximum density, D_S refers to the density at the start of the trap array, $\bar{D}$ the mean density, "Unique" is the mean number of unique individuals captured and "Captures" is the mean number of captures from 100 simulated capture histories over a 90 day period using a non-constant hazard that is consistent with a half-normal detection function with $g_0 = 0.05$ and $\sigma = 2400$.

$$\begin{aligned} H_k(\boldsymbol{s}_i;\boldsymbol{\theta},\boldsymbol{\psi}) &= \int_0^T h_k(t, s_i;\boldsymbol{\theta},\boldsymbol{\psi})\, dt \\ &= \int_0^T h_k(\boldsymbol{s_i};\boldsymbol{\theta}) \times (\cos(\alpha \times (t+\psi_1)) + \psi_2)\ dt \\ &= h_k(\boldsymbol{s_i};\boldsymbol{\theta}) \times \int_0^T \cos(\alpha \times (t+\psi_1)) + \psi_2\, dt \end{aligned} \tag{4.1}$$

where ψ_1 is the parameter that shifts the cosine curve horizontally and ψ_2 the parameter that shifts it vertically.

The conditional density of the detection times (Equation 2.18) is then used to simulate the ω_{ik} times. The hazard is setup with t and $\boldsymbol{s}$ being independent and hence, as shown in Equation 2.22 the density simplifies to the following expression: $f_{t|\omega,k}(\boldsymbol{t}_{ik} \mid \omega_{ik}, \boldsymbol{s}_i;\boldsymbol{\theta},\boldsymbol{\psi}) = \omega_{ik}! \prod_{r=1}^{\omega_{ik}} \frac{h_k(t_{ikr};\boldsymbol{\psi})}{\int h_k(t_{ikr};\boldsymbol{\psi})\, dt}$ which is then used to simulate the ω_{ik} times. The probability integral transfer method is used as follows, noting that both the integrated hazard ($H(\boldsymbol{s};\boldsymbol{\theta},\boldsymbol{\psi})$) and the component of the hazard that depends on distance ($h(\boldsymbol{s};\boldsymbol{\theta})$) are constant with respect to time:

$$
\begin{aligned}
P(T < t) &= p \\
\int_0^t \frac{h_k(u_{ik};\boldsymbol{\psi})}{\int h_k(v_{ik};\boldsymbol{\psi})\, dv}\, du &= p \\
\int_0^t (\cos(\alpha \times (u + \psi_1)) + \psi_2)\ du &= \int h_k(v_{ikr};\boldsymbol{\psi})\, dv \times p
\end{aligned}
\tag{4.2}
$$

The expression on the left hand side can be solved analytically leading to the following expression:

$$
1/\alpha\,(\sin[\alpha(t+\psi_1)] - \sin\alpha\psi_1) + \psi_2 t = \int h_k(v_{ikr};\boldsymbol{\psi})\, dv \times p
$$

A uniform probability is simulated and the expression above is then solved for t (using the `uniroot` function in R) to generate a detection time.

The method described above to simulate data from the cosine hazard is verified by simulating a large dataset (205 individuals, 7,407 captures over 90 days) and plotting the capture times. The detection times can be displayed over time in two different ways, either collapsed over a single cycle or else over the actual study period (Figure 4.2). For example, if the cosine period is 24 hours then the first approach would convert all detection times into hours since midnight and then plot them over a single 24 hour period.

Simulated detection times will be from multiple traps and across a range of distances and therefore a visual comparison of the simulated data with the hazard function requires firstly that distance be integrated out of the $h(\boldsymbol{s},\boldsymbol{\theta})$ component of the hazard function. Secondly a visual comparison of the underlying detection hazard with the data requires the hazard curve to be overlaid on to the histograms. In order to do this the two plots need to be on the same scale and this requires the area under the hazard curve to be equal to the area under the histogram. This scaling is achieved by calculating the two areas and working out an appropriate scale factor to be applied to the hazard curve. Figure 4.2 shows these plots for the simulated dataset (only 10 cycles are shown for the lower plot). Kolmogorov-Smirnov goodness-of-fit tests were conducted in both cases and the test statistics were not significant at the 5% level.

Figure 4.2: Histograms of simulated capture times from a survey with proximity detectors and a cosine detection hazard. The top panel collapses all captures (7,407 captures) into one cycle and the bottom panel plots the first ten cycles (798 captures).

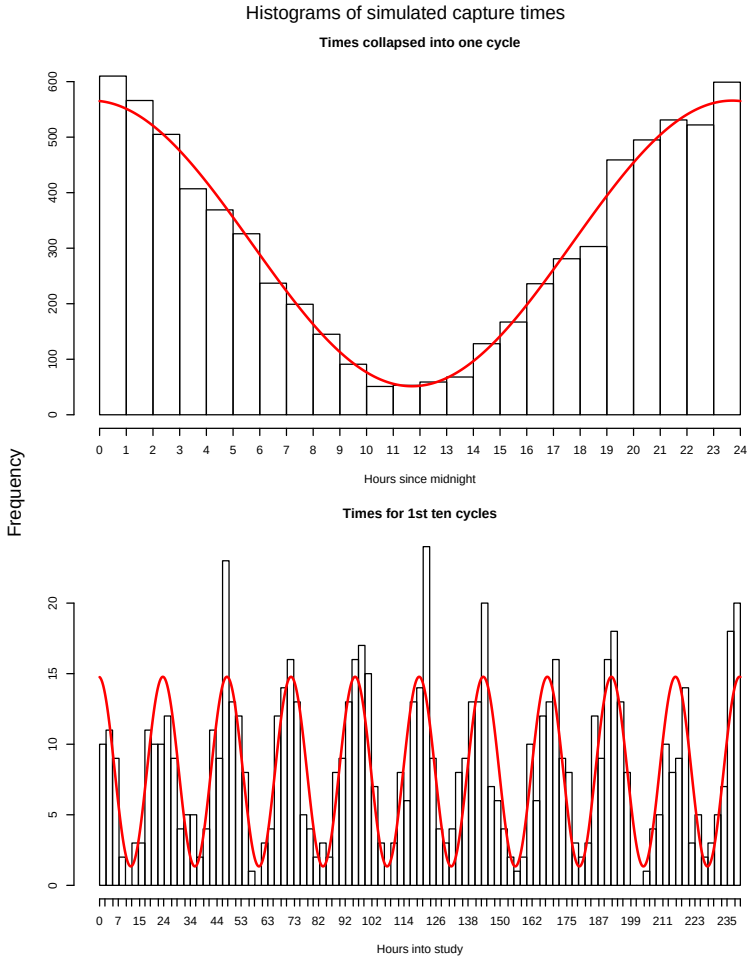

Notes: The red line is the true cosine hazard used in the simulation and has been scaled to have the same area under the curve as the histograms.

Simulating capture times from a cyclic regression spline

The CDF of the detection times is required to simulate the ω_{ik} times but this cannot be done analytically for a hazard with a regression spline form. However it is apparent from Equation 2.20 that the conditional distribution of capture times ($f(\boldsymbol{t}_{ik} \mid \omega_{ik})$) is proportional to the hazard. It is easy to therefore estimate $f(\boldsymbol{t}_{ik} \mid \omega_{ik})$ across a

fine mesh of time points, and then it is straight forward to calculate $F(\boldsymbol{t}_{ik} \mid \omega_{ik})$ and simulate $\boldsymbol{t}_{ik}$, using the probability integral transform.

4.1.2 Simulation results

The results from simulations using synchronous hazards are presented first followed by those using asynchronous hazards. The primary focus is on the comparison between the DT binary proximity detector estimator and the CT proximity detector estimator with a time-varying hazard, though the first set of simulations with the cosine hazard also includes a constant hazard or count model for comparison.

Synchronous cosine simulations

The performance of three estimators is compared here, namely the DT binary proximity detector estimator where multiple capture events at a detector during an occasion are collapsed into a binary indicator, and CT proximity detector models where firstly a constant hazard and secondly where the correct cosine hazard is specified. The results including the relative biases for the parameters of interest are summarised in Tables C.1 to C.4.

For constant density, Table C.1 presents the results for three levels of density (8, 4, and 2 per 100 km^2) and Table C.2 displays the results for different levels of detectability by varying g_0 (with density kept at the middle level of 4 per 100 km^2). The results from the non-constant density scenarios are summarised in Table C.3 for exponential density and Table C.4 for quadratic density.

All three estimators are unbiased or nearly so for all parameters of interest, including ψ_1 and ψ_2 for the correctly specified cosine hazard model. Note that the relative biases for the $\boldsymbol{\psi}$ parameters are not shown in Table C.3 and Table C.4 for brevity, but Figure 4.3 confirms visually that the estimator manages to estimate the underlying cosine hazard well in all cases.

Figure 4.4 plots the true density surface overlaid on the estimated density surfaces from each simulation for the first of the non-constant density scenarios Px.E1 and Px.Q1. It is clear that the estimated density surfaces from the three estimators are virtually indistinguishable from each other and consequently the RMSB and RMSPE's are not reported.

Figure 4.3: Estimated hazard surfaces from the proximity detector simulation scenarios with both constant and non-constant density and a 24 hour cosine hazard.

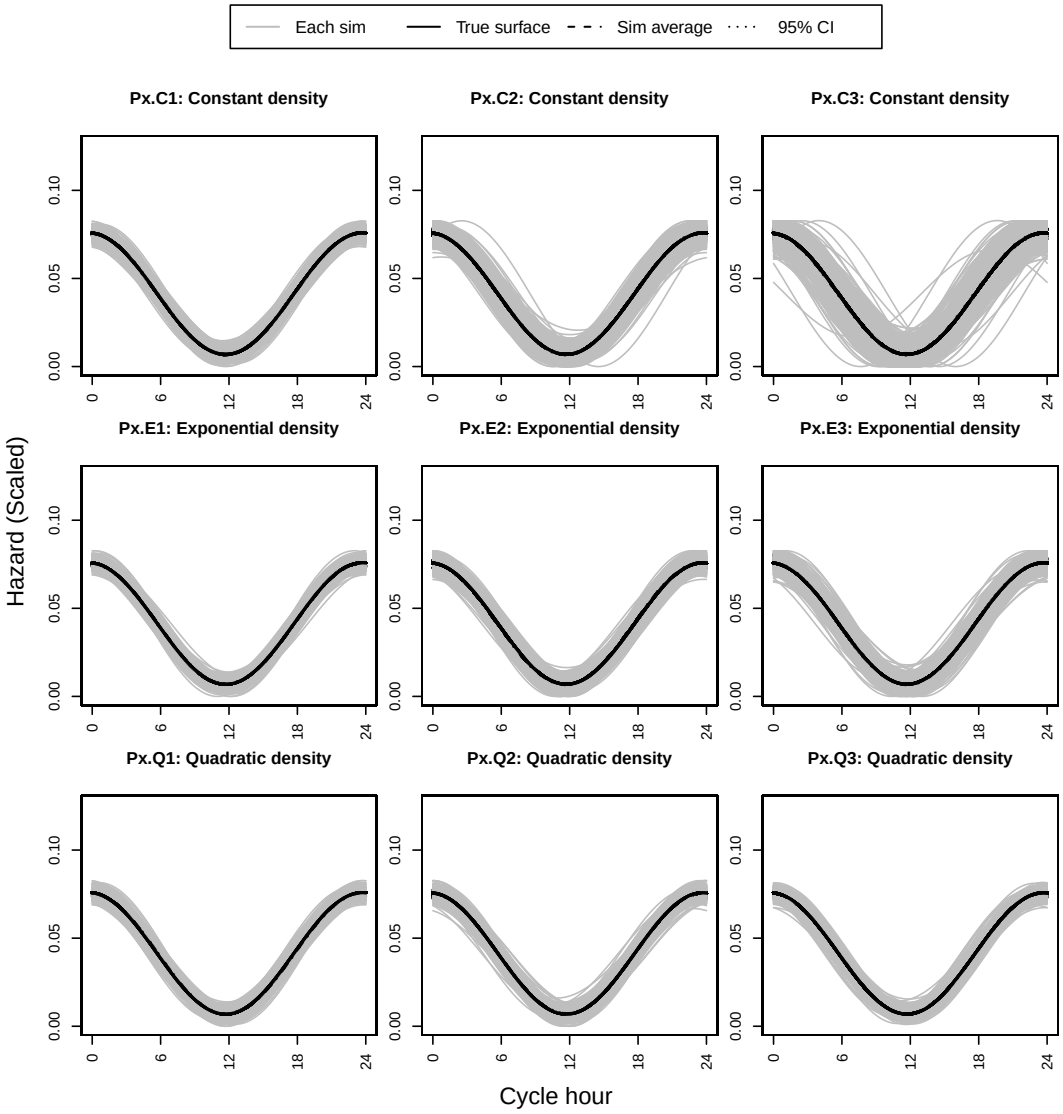

Notes: The black line depicts the true hazard function, the grey lines the estimated hazard functions from each simulation, and the dashed black line the average of the simulations.

Figure 4.4: Estimated density surfaces from the proximity detector simulation scenarios Px.E1 and Px.Q1 with a 24 hour cosine hazard.

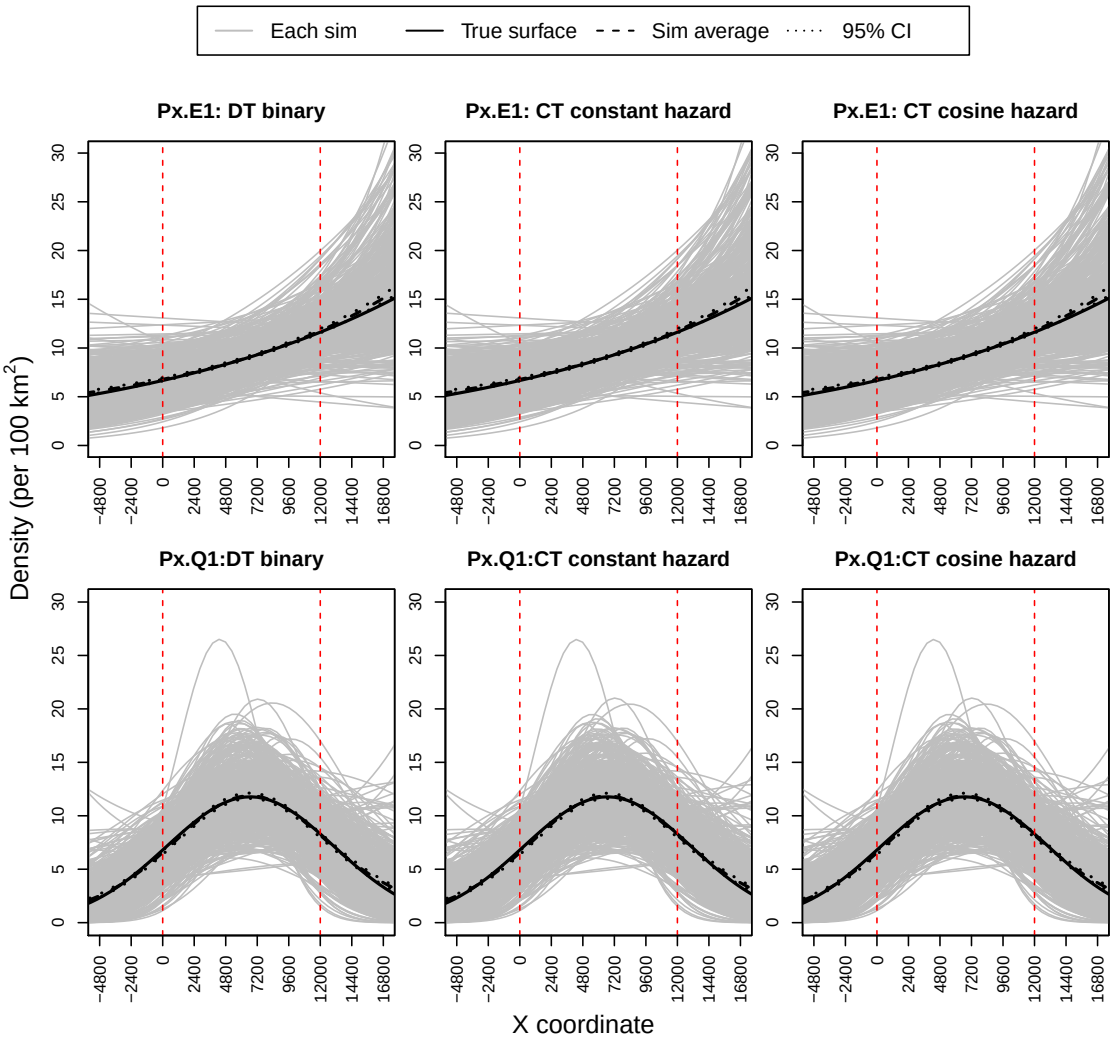

Notes: The black line depicts the true density gradient, the grey lines the estimated density from each simulation, and the dashed black line the average of the simulations.

Synchronous spline simulations

Figure 2.3 on page 38 shows three examples of cyclic spline detection hazards with a cycle duration of 24 hours and different degrees of freedom. The proximity simulations with a synchronous cyclic hazard make use of the top two hazards in that figure.

The first hazard form begins at a low level, rises to its peak at around the middle of the cycle, and then falls away again. This fairly simple shape can be produced with a spline that has 4 degrees of freedom (K = 4). The second hazard is similar but rises to its peak earlier on in the cycle and stays around this peak for several hours before falling away again. Additional parameters are required to capture this shape (K = 8). The same three constant and non-constant density scenarios used in the cosine simulations are again used here (Px.C1-3, Px.E1-3, Px.Q1-3) together with the two different detection hazards mentioned above.

Tables C.5 to C.7 present the relative biases for the parameters of interest for the three types of density surfaces considered. Figures 4.5, D.1 and D.2 plot the estimated detection hazards with the two levels of K from each of the three scenarios for constant, exponential and quadratic density surfaces respectively. The estimated density surfaces from the first scenario of the exponential and quadratic density types (Px.E1 and Px.Q1) are shown in Figures 4.6 and D.3.

The results are similar to those from the cosine hazard simulations and show that both estimators are unbiased or nearly so for all parameters of interest across the different density surfaces considered. Similarly the underlying spline hazards and non-constant density surfaces are estimated accurately. The estimated density surfaces from the different estimators are again very similar to each other and hence the RMSB and RMSPE's are not shown.

Asynchronous spline simulations

The objective of the simulations with asynchronous hazards is to explore how the DT binary proximity detector model performs when there is variation in detectability across occasions that is not modelled. Three types of asynchronous hazards are considered starting with a hazard cycle duration of 30 hours that repeats 72 times over the duration of the study.

Figure 4.7 plots two further detection hazards with a 30 day (720 hour) and a 90 day (2,160 hour) cycle. In the first case the hazard cycle repeats itself three times over the simulated study duration of 90 days, and in the second the hazard has the same shape but extends over the full period and hence does not repeat. These two extra hazards aim to increase the variation in the integrated hazards across occasions (as shown by the red lines in Figure 4.7) and do not strive for realism.

The 30 hour hazard is used in a repeat of the simulations conducted above, i.e. for the same three scenarios for each type of density surface (Px.C1-3, Px.E1-3, Px.Q1-3) and for K = 4 and K = 8. The relative biases from these simulations are presented in Tables C.8 to C.10, the estimated hazard plots in Figures D.4, D.5, and D.7, and the

Figure 4.5: Estimated hazard surfaces from the proximity detector simulation scenarios with constant density and a 24 hour spline hazard (K = 4 in the top panel and K = 8 in the bottom panel).

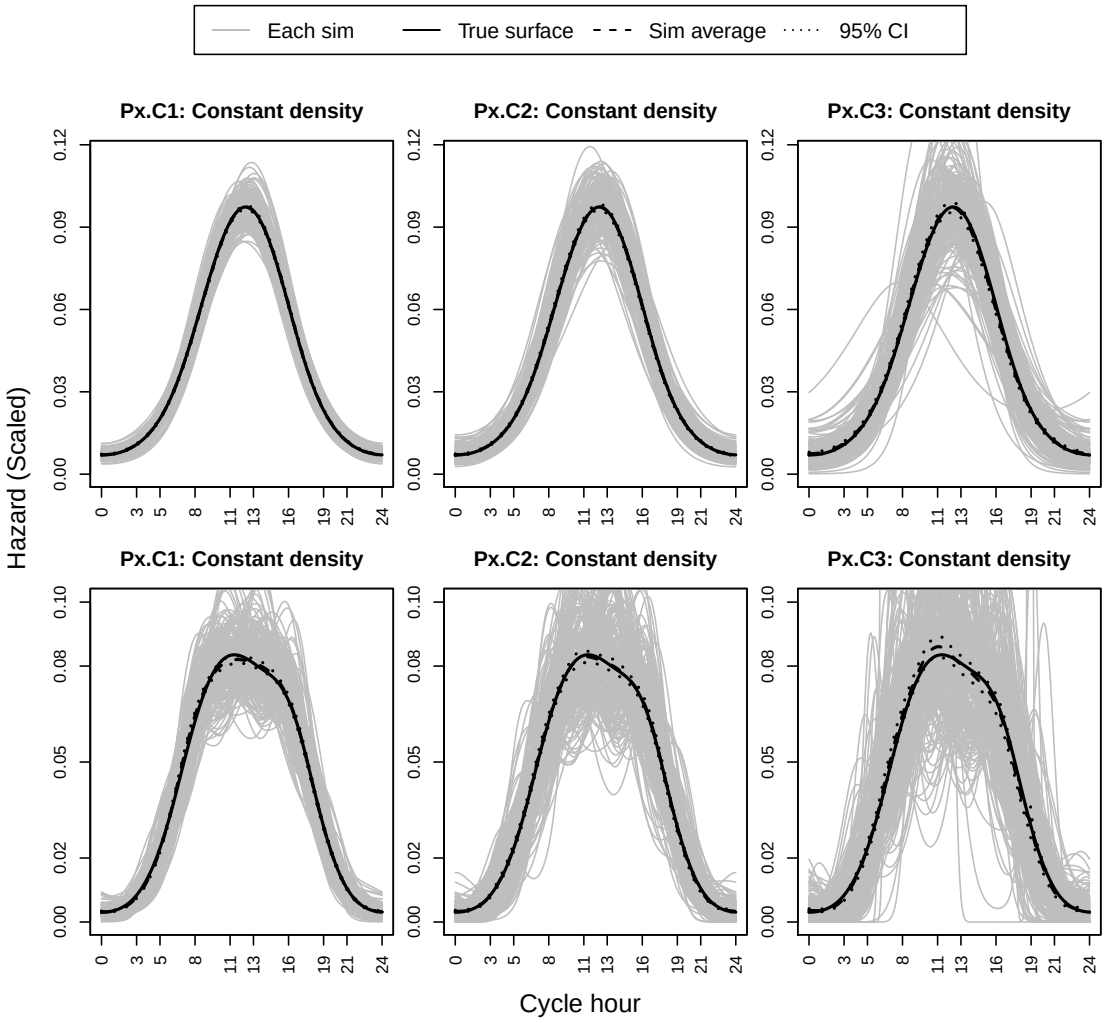

Notes: The black line depicts the true hazard function, the grey lines the estimated hazard functions from each simulation, and the dashed black line the average of the simulations.

Figure 4.6: Estimated density surfaces from the proximity detector simulation scenario Px.E1 with a 24 hour spline hazard (K = 4 in the top panel and K = 8 in the bottom panel).

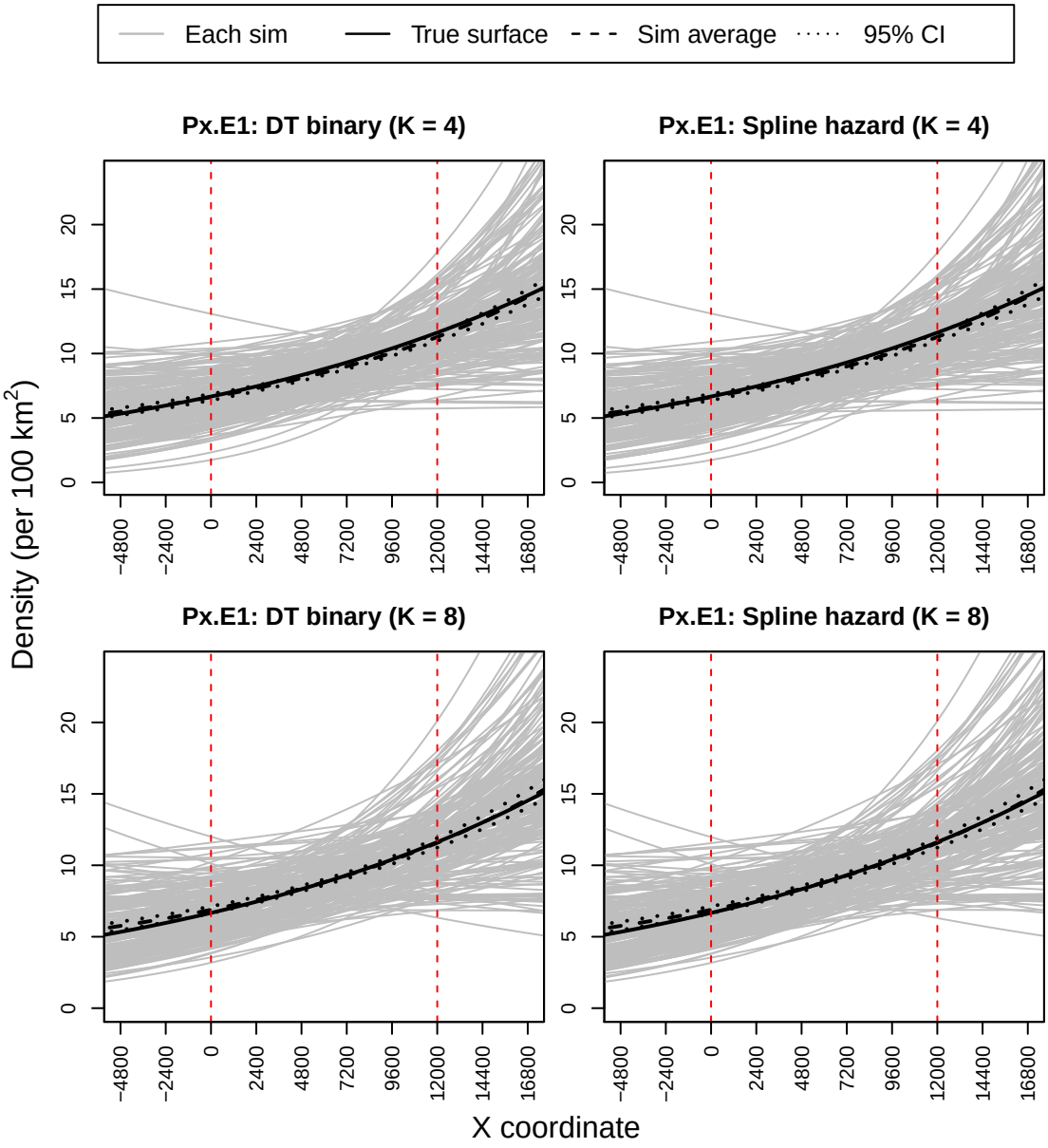

Notes: The black line depicts the true density gradient, the grey lines the estimated density from each simulation, and the dashed black line the average of the simulations.

estimated density surface plots in Figure D.6 (for the exponential density scenario Px.E2) and Figure D.8 (for the quadratic density scenario Px.Q1).

The estimator with the correctly specified 30 hour spline hazard is unbiased or nearly so for all parameters of interest, and the DT binary proximity detector estimator is also approximately unbiased with regards to estimating density and σ but underestimates g_0 by approximately 15%. The figures confirm that on average the spline hazard model estimates the underlying hazard well and that both estimators do a good job of estimating the non-constant density surface if it is correctly specified.

One slight anomaly in the tabulated results in Table C.9 is the 13% bias in the estimate of the density slope for the exponential density scenario Px.E2 with K = 4. Figure D.6 illustrates the density plots from this scenario and it is clear that both models on average estimate the density surface accurately, and that there are a small number of repetitions where the exponential increase in density is overestimated in the region east of the trap array which affects the mean performance. Apart from this the only case where slight positive bias in density is evident for both estimators is for the constant density scenario with the lowest level of density that on average only had about eight unique individuals.

The second and third asynchronous hazards are used with K = 8 in one scenario from each type of density surface namely: D = 4 per 100 km^2 for the constant density scenario, and the second scenario for each of the exponential and quadratic density simulations (Px.E2, Px.Q2). The average sample sizes from each of these scenarios are presented in Table 4.2. These numbers are not the same as those in Table 4.1 due to the fact that the hazard function is consistent with the specified half-normal detection function only when integrated over the first occasion, and in these two cases the hazard is at a low level for this period of time (the first 24 hours). For this reason this set of simulations simulate captures using a g_0 of 0.01.

The relative biases from this set of simulations appear in Table C.11, the hazard plots in Figure 4.8, and the density plots in Figures 4.9 and D.9. These results are in agreement with those from the 30 hour asynchronous hazard and it is noticeable how the negative bias in g_0 does not affect the estimation of density. The primary difference from the 30 hour asynchronous hazard results is that the negative bias in the g_0 parameter appears to be much worse (approximately 850%). This will be discussed further in Section 4.3 below.

Figure 4.7: A 30 day (720 hours) hazard that repeats three times over the simulated study duration and a 90 day (2,160 hours) hazard with the same shape that does not repeat.

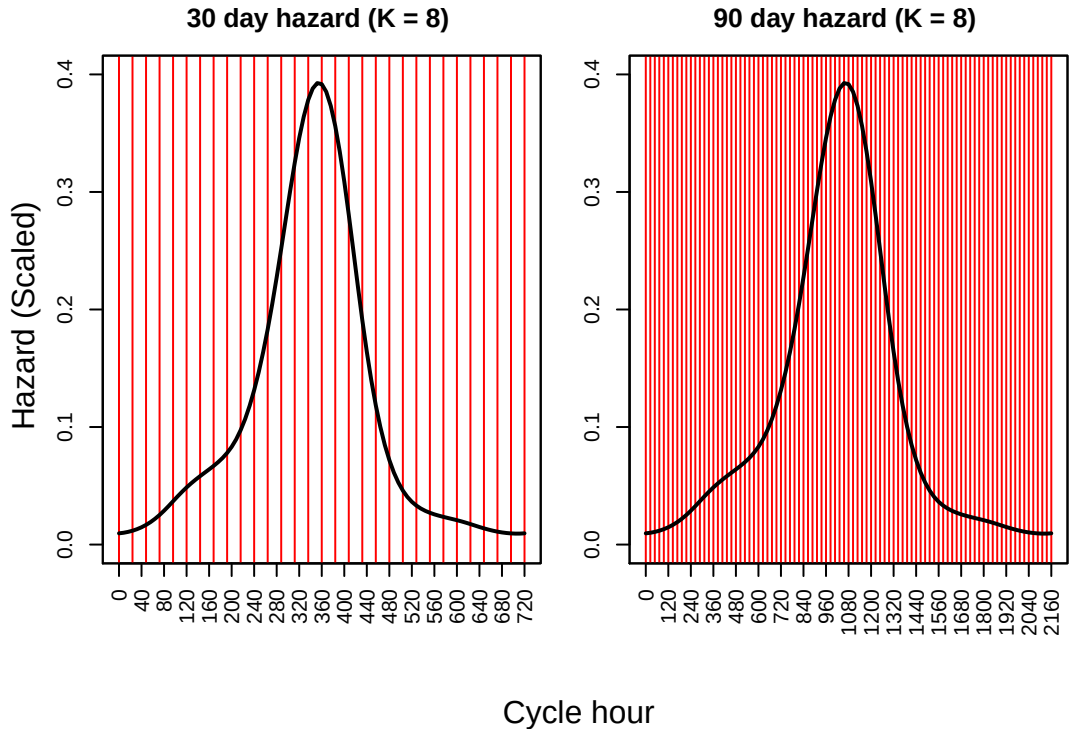

Notes: The vertical red lines demarcate the 24 hour occasions to show the variation in the integrated hazard between occasions.

Table 4.2: Details of the different density surfaces used in the proximity detector simulations with the second and third asynchronous hazards.

Simulation Type	Scenario	D_{Max}	D_S	$\bar{D}$	Unique	Captures
Constant	Px.C2	4.00	4.00	4.00	19.2	262.6
Exponential	Px.E2	11.03	3.33	5.68	28.5	384.3
Quadratic	Px.Q2	15.15	3.15	6.68	29.0	553.1

Notes: All density values are given per 100 km^2. D_{Max} is the maximum density, D_S refers to the density at the start of the trap array, $\bar{D}$ the mean density over a region extending 2σ from the trap array, "Unique" is the mean number of unique individuals captured and "Captures" the mean number of captures from 100 simulated capture histories over a 90 day period using a non-constant hazard that, for the first 24 hours, is consistent with a half-normal detection function ($g_0 = 0.01$ and $\sigma = 2400$).

Figure 4.8: Estimated hazard surfaces from the simulation scenarios with an asynchronous spline hazard (K = 8) with a cycle length of either 30 days (top panel) or 90 days (bottom panel).

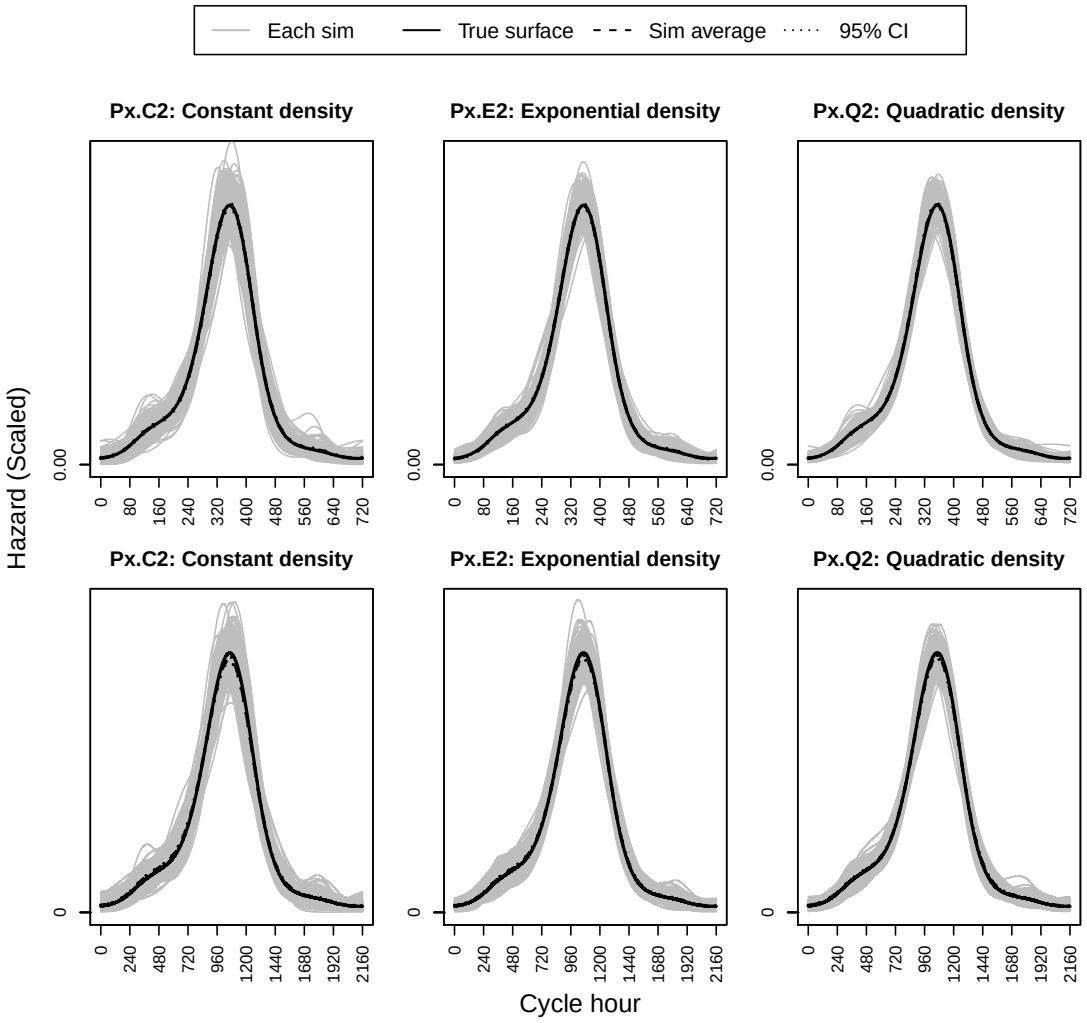

Notes: Each column is for the second scenario of each type of density namely the left hand side plots are for constant density, the middle plots for exponential density, and the right hand side plots for quadratic density. The black line depicts the true hazard function, the grey lines the estimated hazard functions from each simulation, and the dashed black line the average of the simulations.

Figure 4.9: Estimated density surfaces from the proximity detector simulation scenario Px.E2 with an asynchronous spline hazard (K = 8) that has a cycle length of either 30 days (top panel) or 90 days (bottom panel).

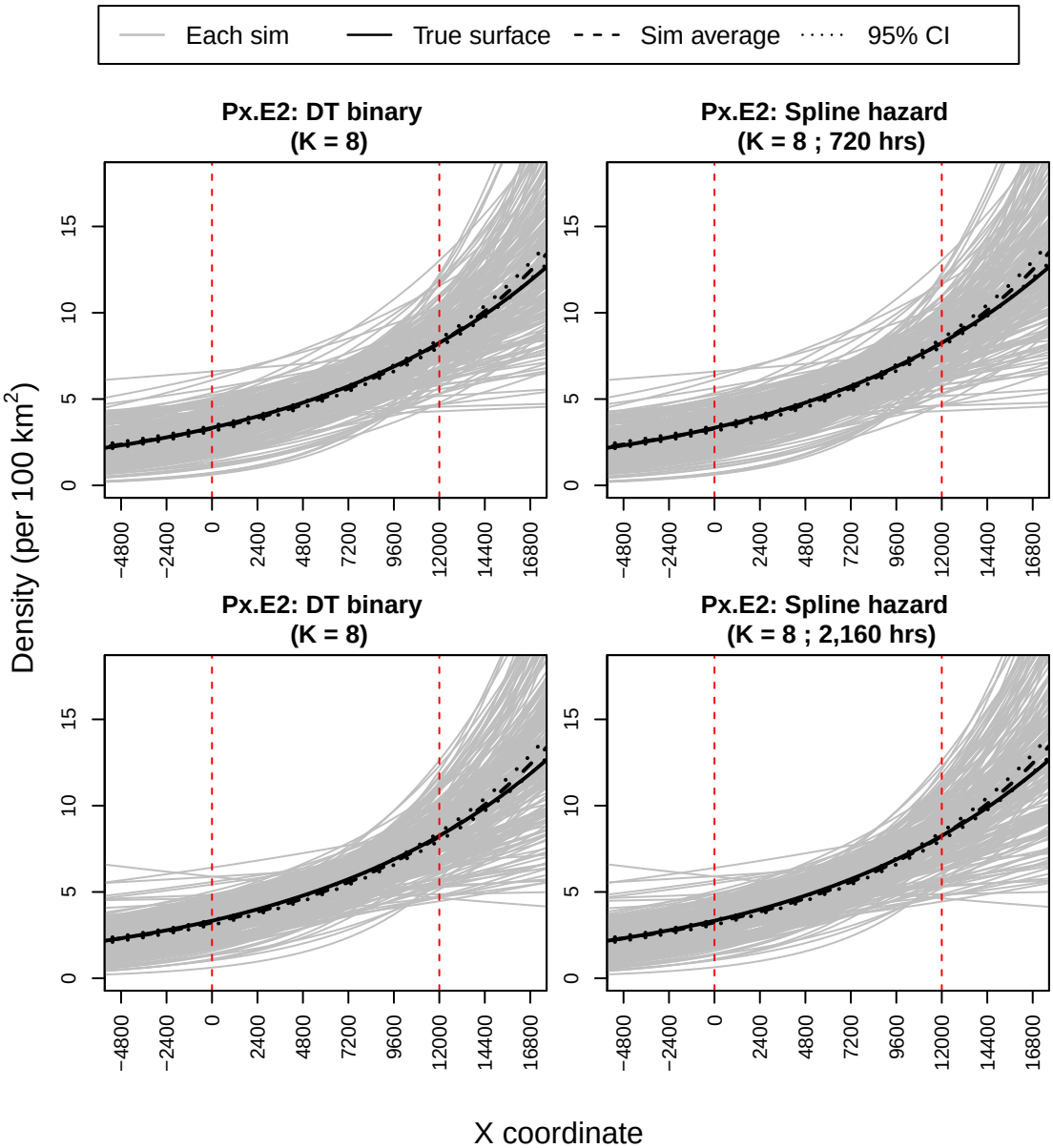

Notes: The black line depicts the true density gradient, the grey lines the estimated density from each simulation, and the dashed black line the average of the simulations.

4.1.3 Jaguar application

CT proximity detector models with a non-constant detection hazard through time are now fitted to the jaguar data. The different hazards that were fitted include the cosine hazard and cyclic spline hazard with three different values for K (4, 6, and 8). The models incorporate different behavioural effects in the form of separate g_0 and/or σ parameters before and after first detection. All models also account for periods of time when the camera traps are not operational for one reason or another. Table 4.3 displays the model selection statistics and Table 4.4 displays the estimates from all the non-constant hazard models. Note that the models from Section 3.1.3 that assume a constant hazard through time have Akaike weights of less than 0.001 if included in Table 4.3.

Figure 4.10 plots the estimated detection hazard from the best fitting model for each hazard type along with the shape that corresponds to the starting values used. In each case the starting values given for the spline hazard estimation correspond to the spline hazard shapes that are plotted in Figure 2.3. Overall, there is support for the spline hazard with K = 6 where the models with and without the g_0 behavioural effect have a combined Akaike weight of almost 90%. The null model (with no behavioural effects) is selected as the best model on the basis of AIC for the splines with both K = 6 and K = 8 whereas a behavioural effect on g_0 is preferred for both the cosine hazard and spline with K = 4.

The best fitting hazard shape (as indicated by AIC) suggests two peaks in detectability, the first one occurring in the early morning (4-5 am) and the second one occurring in the evening (around 8 pm) with the evening peak being higher than the morning peak. The shape of the estimated hazard for K = 8 is similar to the chosen model with K = 6 though it estimates that the morning peak occurs slightly later (around 6 am) and drops off at a faster rate. The AIC_c statistics suggest that the features of the detection hazard are adequately captured by the spline with K = 6. The fit of the best fitting spline hazard to the observed capture times, that are collapsed on to a single cycle, is shown in Figure 4.11. A Kolmogorov-Smirnov goodness-of-fit test statistic was not significant (p-value = 0.43) and so confirms that the estimated hazard fits the jaguar data. The estimated hazard shape for K = 6 remains stable when rerunning the model with starting values corresponding to a flat hazard.

The estimates from models with different non-constant hazards but the same type of behavioural effect are virtually identical to each other. The density point estimate from the best null model increases by approximately 16% after including a behavioural effect on g_0 (2.80 per ha (1.71;4.58) to 3.26 per ha (1.95;5.45)). The nature of the behavioural effect on g_0 is one of "trap happiness" with g_0 doubling

from 0.035 (0.018;0.067) before first capture to 0.075 (0.060;0.094) after first capture. As mentioned in 3.3 this is unlikely to be a true trap happiness effect.

Table 4.3: Model selection summary for the jaguar data and the CT models with cyclic spline hazards for three different values of K. All models specify a constant density.

Hazard	Model	ΔAIC$_c$	wt	npar
CS (K = 6)	D(.) g_0(.) σ(.)	0.00	0.494	5
CS (K = 6)	D(.) g_0(b) σ(.)	0.47	0.390	6
CS (K = 8)	D(.) g_0(.) σ(.)	4.71	0.047	6
CS (K = 6)	D(.) g_0(.) σ(b)	5.44	0.033	7
Cosine	D(.) g_0(b) σ(.)	6.45	0.020	5
Cosine	D(.) g_0(.) σ(.)	8.64	0.007	5
CS (K = 6)	D(.) g_0(b) σ(b)	9.36	0.005	7
CS (K = 8)	D(.) g_0(b) σ(.)	10.63	0.002	6
Cosine	D(.) g_0(.) σ(b)	11.46	0.002	5
Cosine	D(.) g_0(b) σ(b)	11.67	0.001	5
CS (K = 8)	D(.) g_0(.) σ(b)	15.57	< 0.001	7
CS (K = 4)	D(.) g_0(b) σ(.)	26.73	< 0.001	7
CS (K = 8)	D(.) g_0(b) σ(b)	27.95	< 0.001	7
CS (K = 4)	D(.) g_0(.) σ(.)	28.86	< 0.001	7
CS (K = 4)	D(.) g_0(.) σ(b)	31.70	< 0.001	7
CS (K = 4)	D(.) g_0(b) σ(b)	31.96	< 0.001	7

Notes: "CS" in the "Hazard" column refers to a cyclic spline. The brackets in the "Model" column indicate which parameter has a behavioural effect included where "(.)" indicates no effect and "(b)" indicates a behavioural. ΔAIC$_c$ is the difference in AIC$_c$ between the current and the best model (AIC$_c$ is Akaike Information Criterion corrected for small sample size), wt denotes the Akaike weight, npar denotes the number of estimated parameters.

Table 4.4: Estimates (and 95% confidence intervals) from the CT proximity detector models with non-constant detection hazards fitted to the male jaguar data with constant density specified and different behavioural effects. The best model as indicated by AIC for each type of hazard is marked in bold and the best model overall is highlighted in orange.

Model	$\hat{D}$ (95% CI)	$\hat{g}_0$ (95% CI)	$\hat{g}_1$ (95% CI)	$\hat{\sigma}_0$ (95% CI)	$\hat{\sigma}_1$ (95% CI)
			Cosine Hazard		
D(.) g_0(.) σ(.)	2.80 (1.71;4.58)	0.074 (0.058;0.092)	NA	2.95 (2.63;3.31)	NA
D(.) g_0(b) σ(.)	**3.26 (1.95;5.45)**	**0.035 (0.018;0.067)**	**0.075 (0.060;0.094)**	**2.95 (2.63;3.30)**	**NA**
D(.) g_0(.) σ(b)	3.15 (1.88;5.30)	0.073 (0.058;0.091)	NA	2.68 (2.25;3.19)	3.00 (2.66;3.38)
D(.) g_0(b) σ(b)	3.05 (1.78;5.23)	0.027 (0.011;0.063)	0.078 (0.061;0.098)	3.27 (2.53;4.22)	2.90 (2.58;3.27)
			Cyclic spline (K = 4)		
D(.) g_0(.) σ(.)	2.80 (1.71;4.58)	0.074 (0.058;0.092)	NA	2.95 (2.63;3.31)	
D(.) g_0(b) σ(.)	**3.26 (1.95;5.45)**	**0.035 (0.018;0.067)**	**0.075 (0.060;0.094)**	**2.95 (2.63;3.30)**	**NA**
D(.) g_0(.) σ(b)	3.15 (1.88;5.30)	0.073 (0.058;0.091)	NA	2.68 (2.25;3.19)	3.00 (2.66;3.38)
D(.) g_0(b) σ(b)	3.05 (1.78;5.23)	0.027 (0.011;0.064)	0.078 (0.061;0.098)	3.27 (2.53;4.22)	2.90 (2.58;3.27)
			Cyclic spline (K = 6)		
D(.) g_0(.) σ(.)	**2.80 (1.71;4.58)**	**0.074 (0.058;0.092)**	**NA**	**2.95 (2.63;3.31)**	**NA**
D(.) g_0(b) σ(.)	3.26 (1.95;5.45)	0.035 (0.018;0.067)	0.075 (0.060;0.094)	2.95 (2.63;3.31)	NA
D(.) g_0(.) σ(b)	3.15 (1.88;5.30)	0.073 (0.058;0.091)	NA	2.68 (2.25;3.19)	3.00 (2.66;3.38)
D(.) g_0(b) σ(b)	3.05 (1.78;5.23)	0.027 (0.011;0.064)	0.078 (0.061;0.098)	3.27 (2.53;4.22)	2.90 (2.58;3.27)
			Cyclic spline (K = 8)		
D(.) g_0(.) σ(.)	**2.80 (1.71;4.58)**	**0.074 (0.058;0.092)**	**NA**	**2.95 (2.63;3.31)**	**NA**
D(.) g_0(b) σ(.)	3.26 (1.95;5.45)	0.035 (0.018;0.067)	0.075 (0.060;0.094)	2.95 (2.63;3.31)	NA
D(.) g_0(.) σ(b)	3.15 (1.88;5.30)	0.073 (0.058;0.091)	NA	2.68 (2.25;3.19)	3.00 (2.66;3.38)
D(.) g_0(b) σ(b)	3.05 (1.78;5.23)	0.027 (0.011;0.064)	0.078 (0.061;0.098)	3.27 (2.53;4.22)	2.90 (2.58;3.27)

Notes: The DT models use 90 occasions of 24 hours and the CT models a survey duration of T =2,160 hours. The CT models use a cyclic spline hazard with a 24 hour cycle that is consistent with a half-normal detection function shape over an interval of 24 hours. Results are reported on the natural scale. The brackets in the "Model" column indicate which parameter has a behavioural effect included where "(.)" indicates no effect and "(b)" indicates a behavioural effect. Estimated density ($\hat{D}$) is individuals per 100 km^2, $\hat{\sigma}$ is in km, and $\hat{g}_{01}$, $\hat{g}_{02}$, $\hat{\sigma}_1$ and $\hat{\sigma}_2$ are estimated detection function parameters before and after initial detection, respectively.

Figure 4.10: Detection hazard plots with a 24 hour cosine hazard and three 24 hour cyclic cubic spline hazards fitted to the jaguar data.

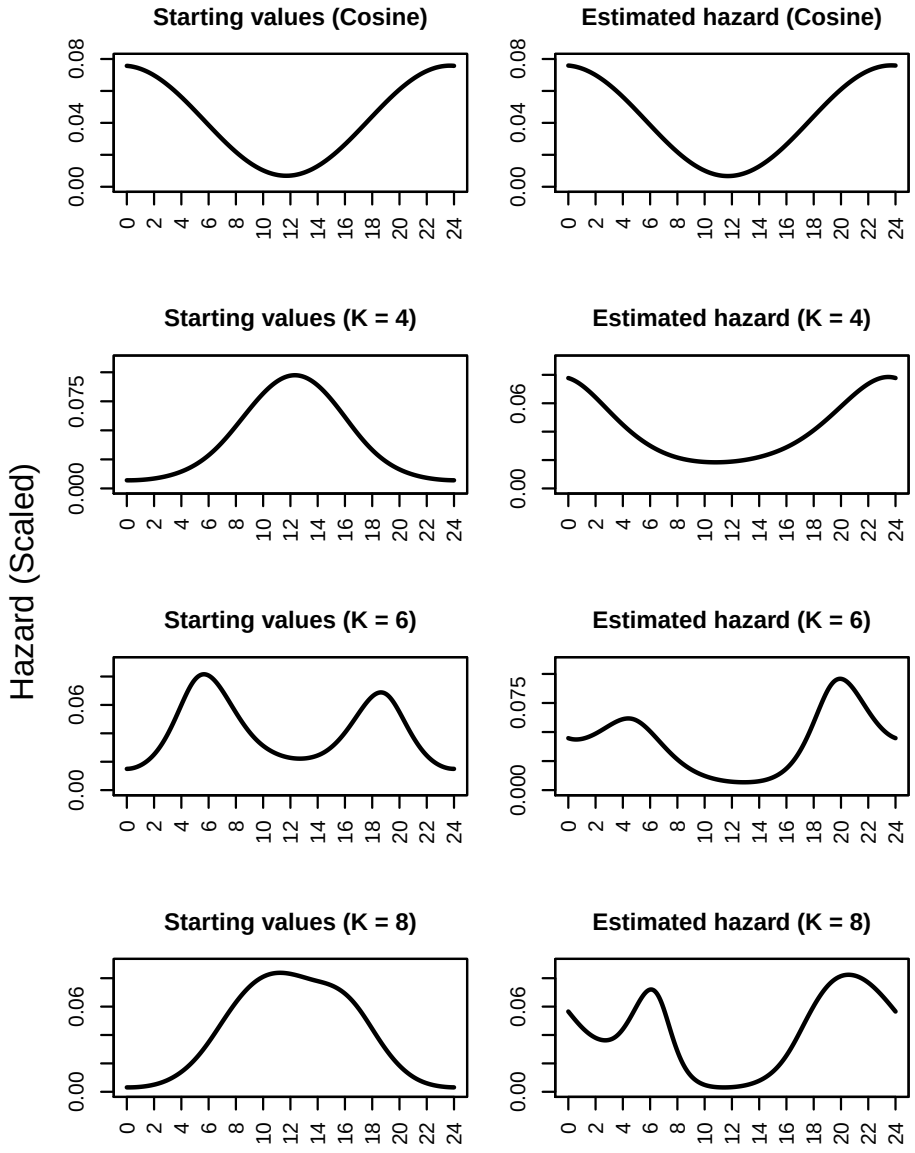

Notes: The plots on the left hand side show the detection hazard shapes that correspond to the starting values supplied in the model fitting. The right hand side plots depict the estimated detection hazard from the best fitting model to the jaguar data for each hazard type.

Figure 4.11: Assessing the goodness-of-fit of the estimated spline hazard from the best CT model to the jaguar capture times

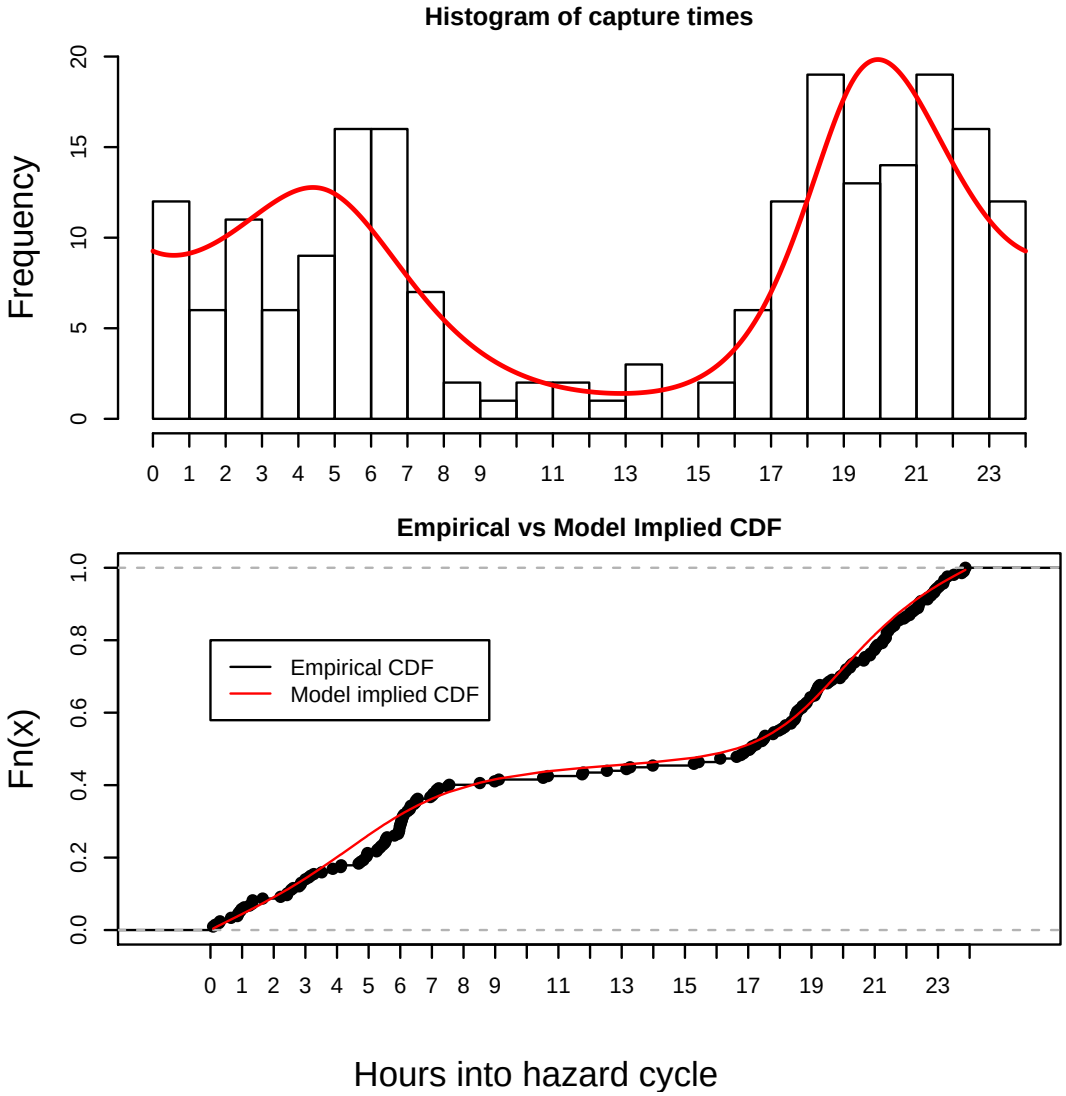

Notes: The top plot depicts the observed capture times that are collapsed on to one cycle with the model estimated detection hazard overlaid in red. The hazard has been scaled to have the same area under the curve as the histogram. The bottom plot is a Q-Q plot.

4.2 Single-catch traps

The performance of the multi-catch and the proposed single-catch trap estimators when fitted to single-catch trap data simulated with a constant detection hazard is explored in Chapter 3. This section runs similar simulation scenarios but where the detection hazard varies in time. The single-catch trap survey simulations here use an asynchronous hazard with a cycle duration of 30 hours and K = 4 and K = 6.

4.2.1 Simulation studies

Except where stated otherwise, all simulations are run for a ten day period (248 hours) with a 5×4 array of traps and use a σ of 100 m, trap spacings of 100 m, and a g_0 of 0.20.

Simulation scenarios

The single-catch estimator takes a long time to converge. The factors that most affect computation time have not been methodically examined but it is clear from initial exploration that apart from model complexity, an increase in the number of traps has a large effect on computation time. The possum study uses 57 traps and takes approximately 30 hours to fit the null model with K = 6 and 130 hours to fit the null model with K = 8. Consequently a smaller subset of scenarios are considered compared to Section 4.1. Three scenarios from the set of scenarios presented in Section 3.2.1 are considered for each type of density model. For constant density scenarios Sc.C2, Sc.C3 and Sc.C4 are used, for exponential density Sc.E1, Sc.E3, and Sc.E4 are used, and for quadratic density the first three scenarios are used (Sc.Q1-3).

Simulating capture times from a cyclic regression spline

With single-catch traps captures between individuals are not independent and capture times cannot be simulated per individual in isolation of what happens with other individuals in the study. Hence as before, the simulated data need to move forward through time rather than generate times per individual. The single-catch trap survey data are simulated using the same general approach given in Section 3.2.1 but in that case a constant hazard was assumed leading to the density of capture times following an exponential distribution.

The CDF for capture times (for each trap and also across all traps) needs to be numerically estimated for the spline hazards by integrating the hazard at each time

point in a fine mesh and using this integrated hazard at each time point t to calculate the cumulative capture probability at time t.

$$P(T < t) = 1 - \exp\left(\int_0^t h(\boldsymbol{s};\boldsymbol{\theta}) \times h(u;\boldsymbol{\psi})\, du\right)$$

The dependence between captures means that this estimation needs to happen before each capture event. In other words the CDF for each individual from which capture times are simulated is recalculated every time an individual is captured and the corresponding trap is occupied and taken out of action, and at each release event when all traps (and individuals) become active. The hazard associated with all time points up to the simulated capture at time t are set to zero each time the CDF is recalculated in order to make it impossible to simulate a capture that happens in the past.

4.2.2 Simulation results

Tables C.12 and C.13 summarise the results from the constant density scenarios, in the first case with the base g_0 of 0.2 and in the second case with a higher g_0 of 0.4 to increase trap saturation levels. The related hazard plots are shown in Figures 4.12 and D.10.

The results from the non-constant density scenarios are summarised in Table C.14 and Table C.15 with the corresponding hazard plots shown in Figures D.11 and D.13. Plots of the estimated density surfaces are given for each non-constant density scenario and for each of the two hazard splines in Figures 4.13, D.12, 4.16 and D.14. In addition, Figure 4.14 plots the sampling distributions for the slope estimates from the exponential density scenarios, and Figures 4.15 and 4.17 plot the RMSB and RMSPE for the exponential and quadratic density scenarios respectively.

The DT multi-catch trap estimator manages to estimate mean density fairly well most of the time, although there is negative bias in mean density over the reduced area for the first two quadratic scenarios and slight negative bias in mean density over the full area for the second exponential scenario. When density follows an exponential gradient the slope estimate is underestimated and the extent of this underestimation is related to the degree of trap saturation as is the estimation of the g_0 parameter. The σ parameter is estimated well apart from slight positive bias for the second quadratic scenario.

The CT single-catch trap estimator is unbiased or nearly so for all parameters of interest, and the underlying hazards are well estimated. It is also clear from the plots of the estimated hazards (here and in the previous section on proximity detectors)

that the variation in the estimated hazards decreases with an increase in sample size. There is slightly more variance in the estimated density surfaces compared to the multi-catch estimator, but Figures 4.15 and 4.17 show that the single-catch estimator is less biased with approximately the same RMSPE or better.

Figure 4.12: Estimated hazard surfaces from the single-catch trap simulation scenarios with constant density and a 30 hour spline hazard (K = 4 in the top panel and K = 6 in the bottom panel).

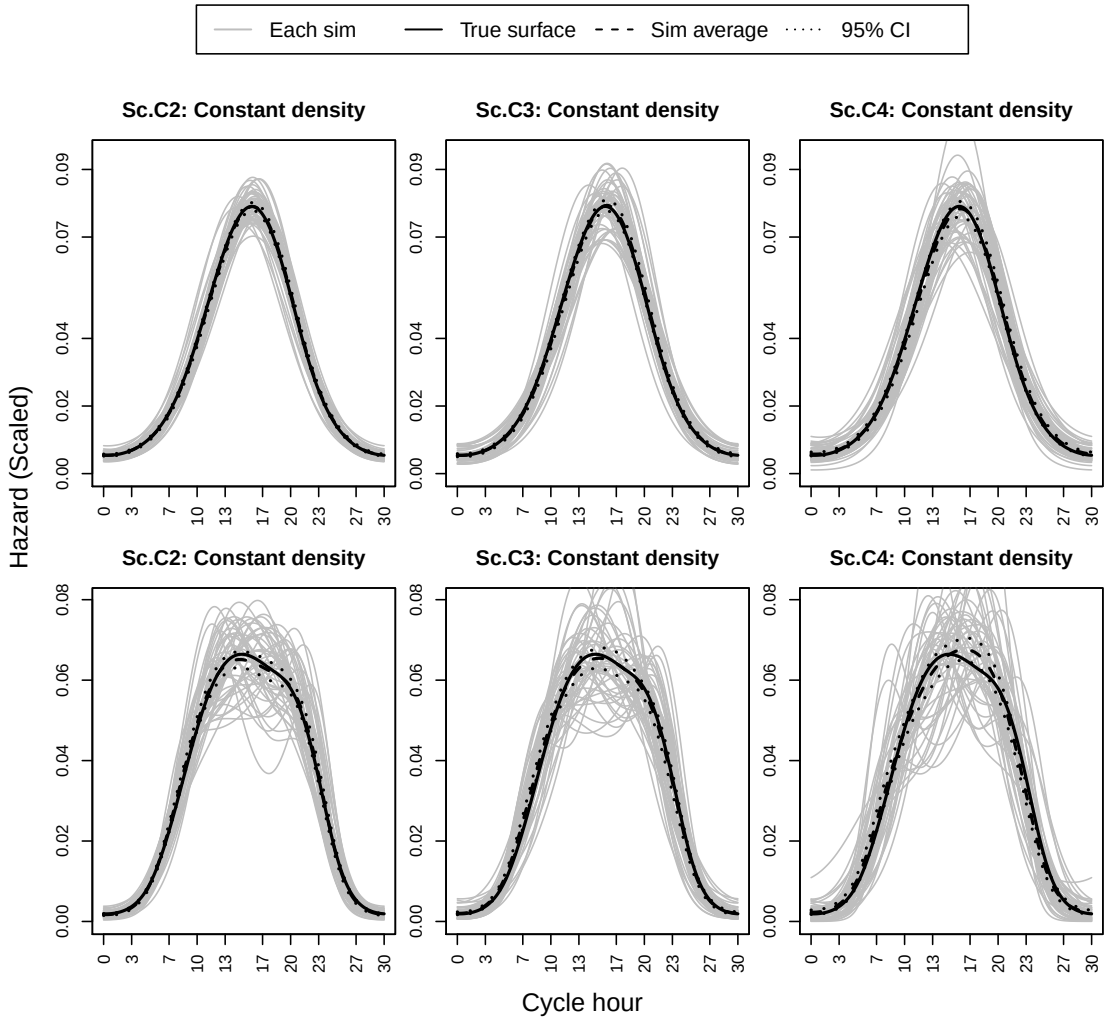

Notes: The black line depicts the true hazard function, the grey lines the estimated hazard functions from each simulation, and the dashed black line the average of the simulations.

Figure 4.13: Estimated density surfaces from the single-catch trap simulation scenarios with exponential density gradients and a 30 hour spline hazard with K = 4.

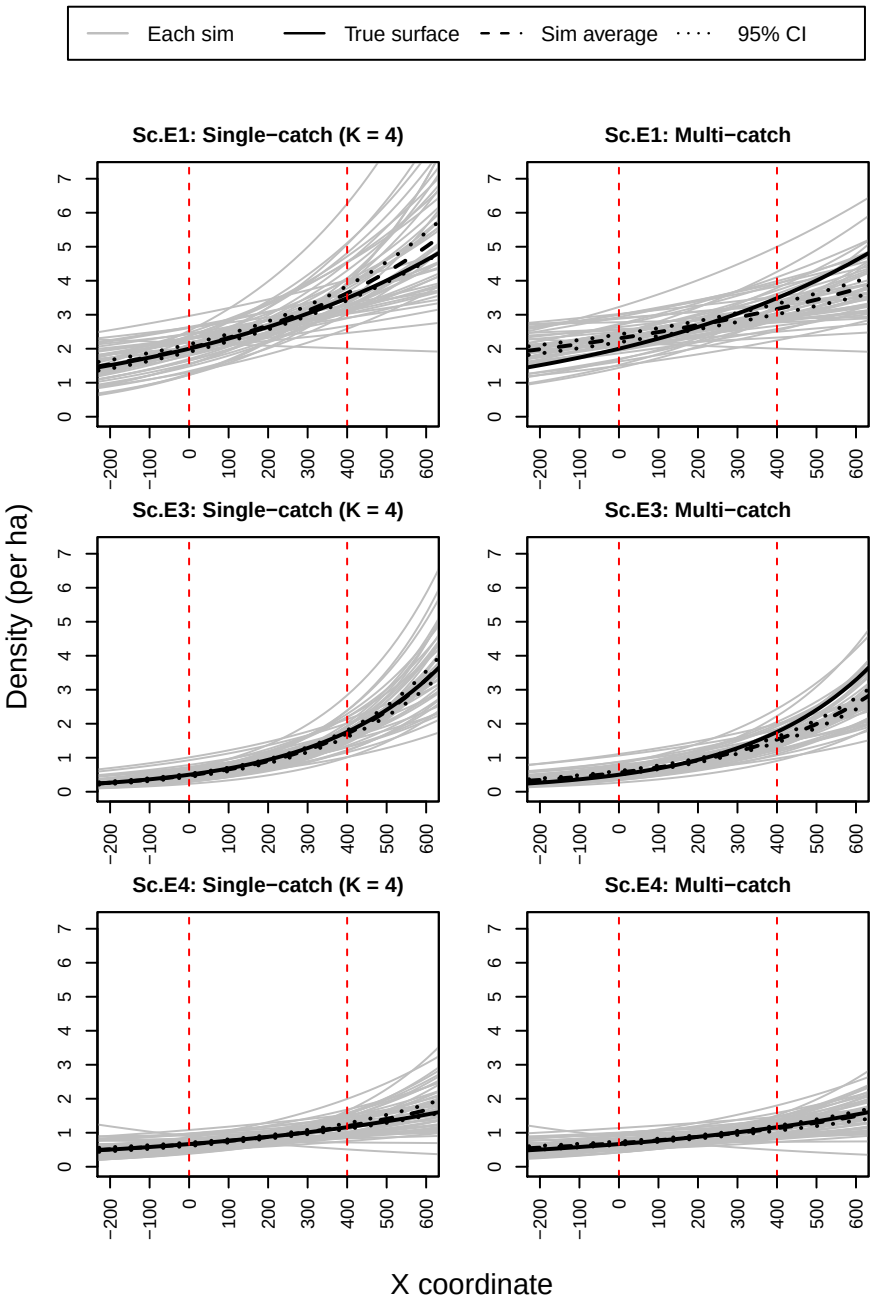

Notes: The black line depicts the true density gradient, the grey lines the estimated density from each simulation, and the dashed black line the average of the simulations.

Figure 4.14: Sampling distributions of the estimates for the slope in the exponential density model for both the multi and single-catch trap estimators, for single-catch trap data with a time-varying hazard.

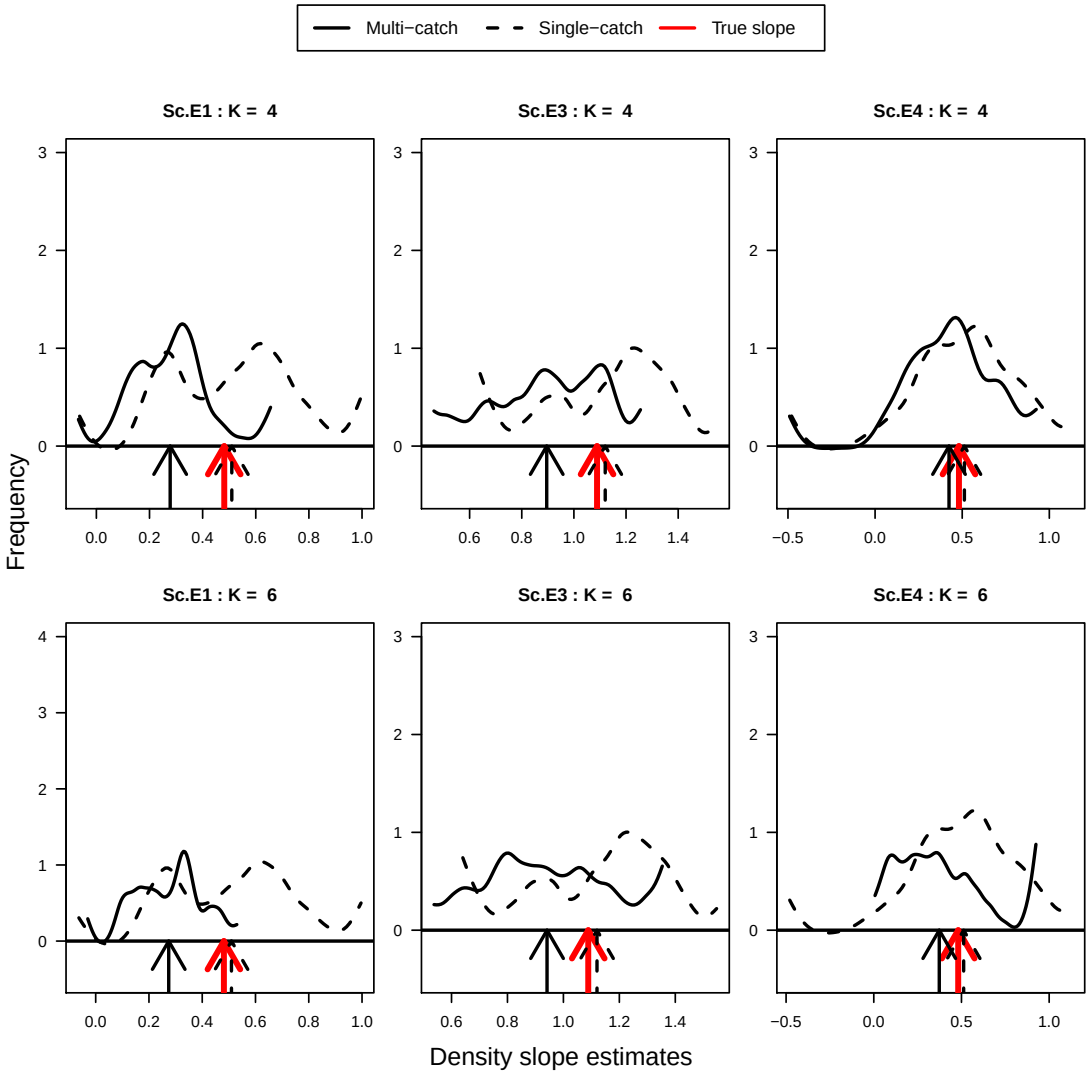

Notes: The arrows mark the position of the mean values for the multi (solid) and single-catch (dashed) estimators, and the red arrows show the true values of the slope parameters.

Figure 4.15: Measures of model performance based on predicted density from the exponential density simulations for single-catch trap data with a 30 hour cyclic spline hazard.

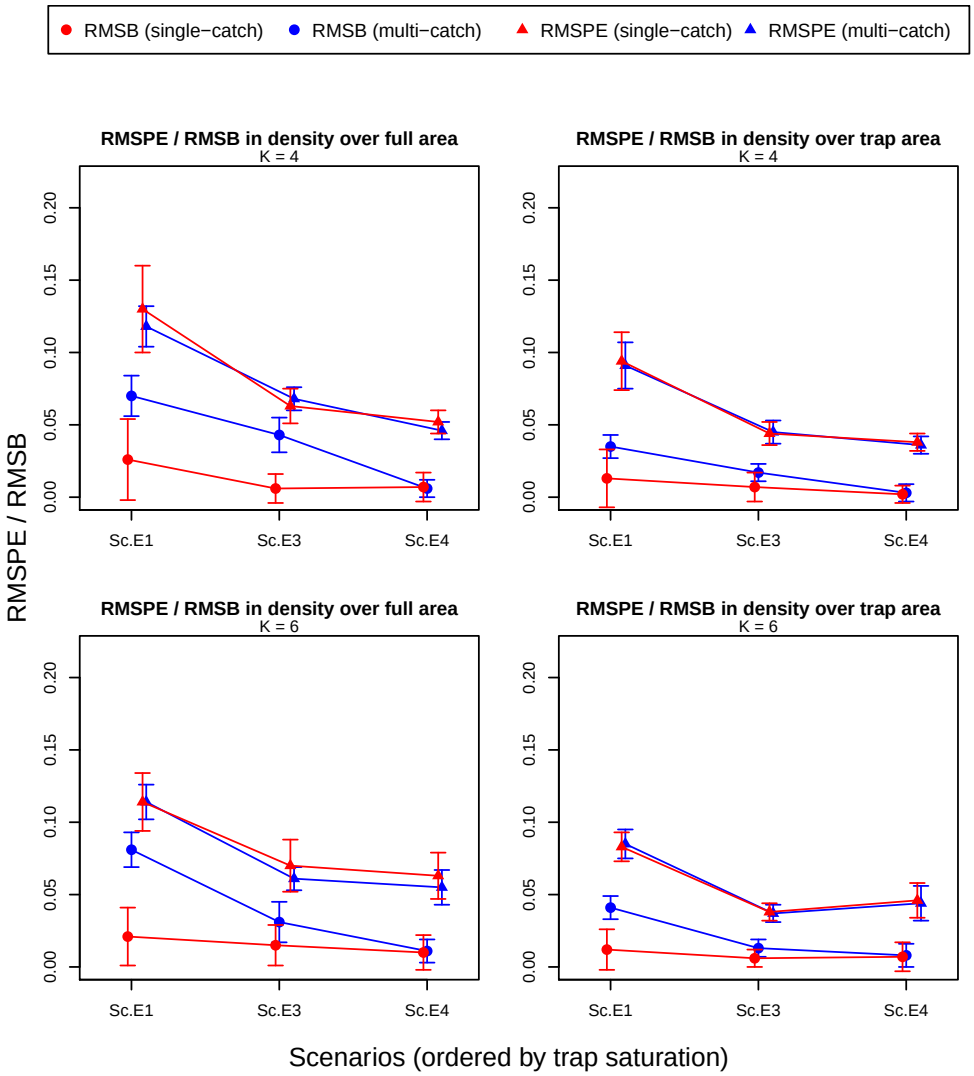

Notes: Results are given for both the full area (top left and bottom left plots) and the area spanning the trap array (top right and bottom right plots). The top row is from simulations using a spline hazard with K = 4, and the bottom row from simulations using K = 6. Standard errors are calculated using the Delta method for the RMSPE and bootstrapping for the RMSB, and error bars are plotted using 2 standard errors. The x-axis is ordered by trap saturation (94%, 61%, 58%)

Figure 4.16: Estimated density surfaces from the single-catch trap simulation scenarios with quadratic density and a 30 hour spline hazard with K = 4.

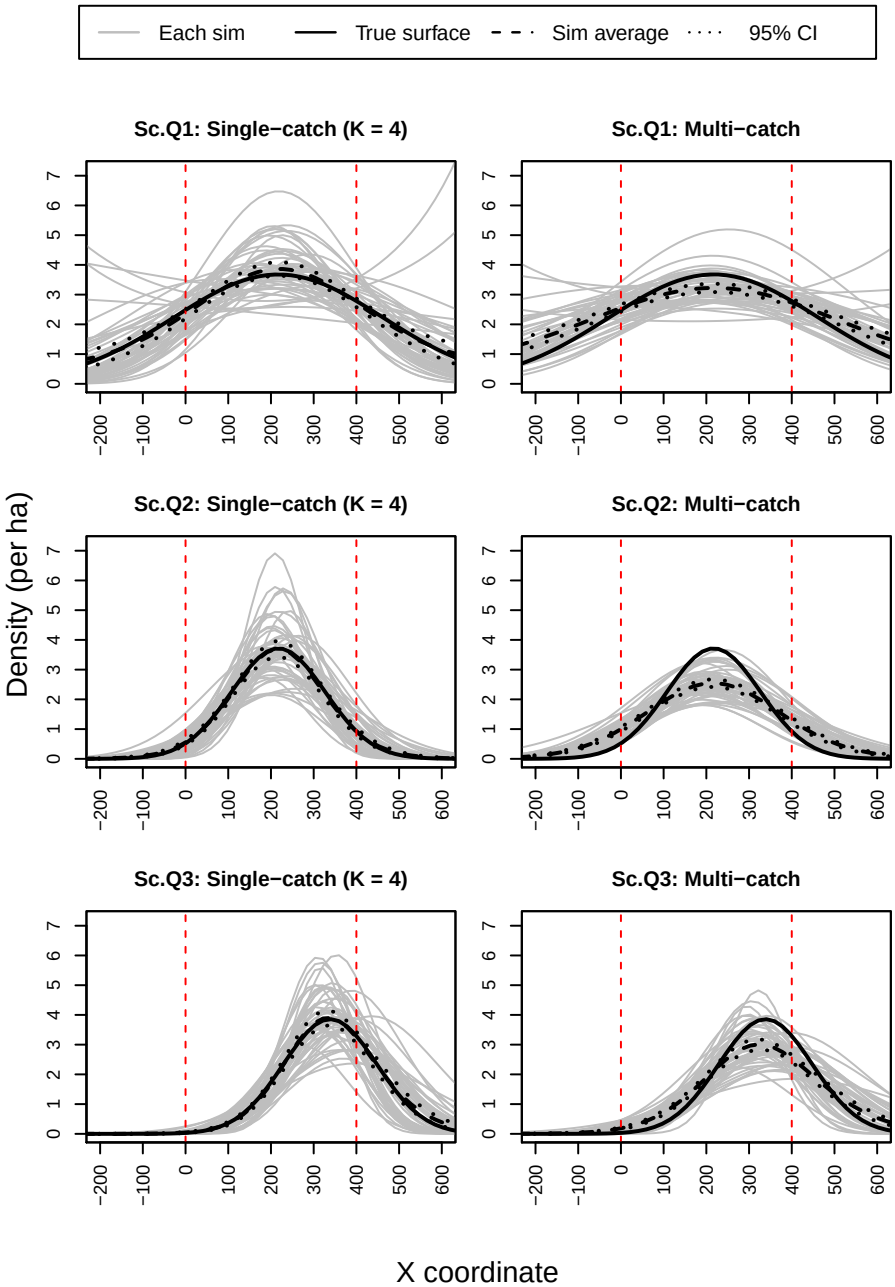

Notes: The black line depicts the true density gradient, the grey lines the estimated density from each simulation, and the dashed black line the average of the simulations.

Figure 4.17: Measures of model performance based on predicted density from the quadratic density simulations for single-catch trap data with a 30 hour cyclic spline hazard.

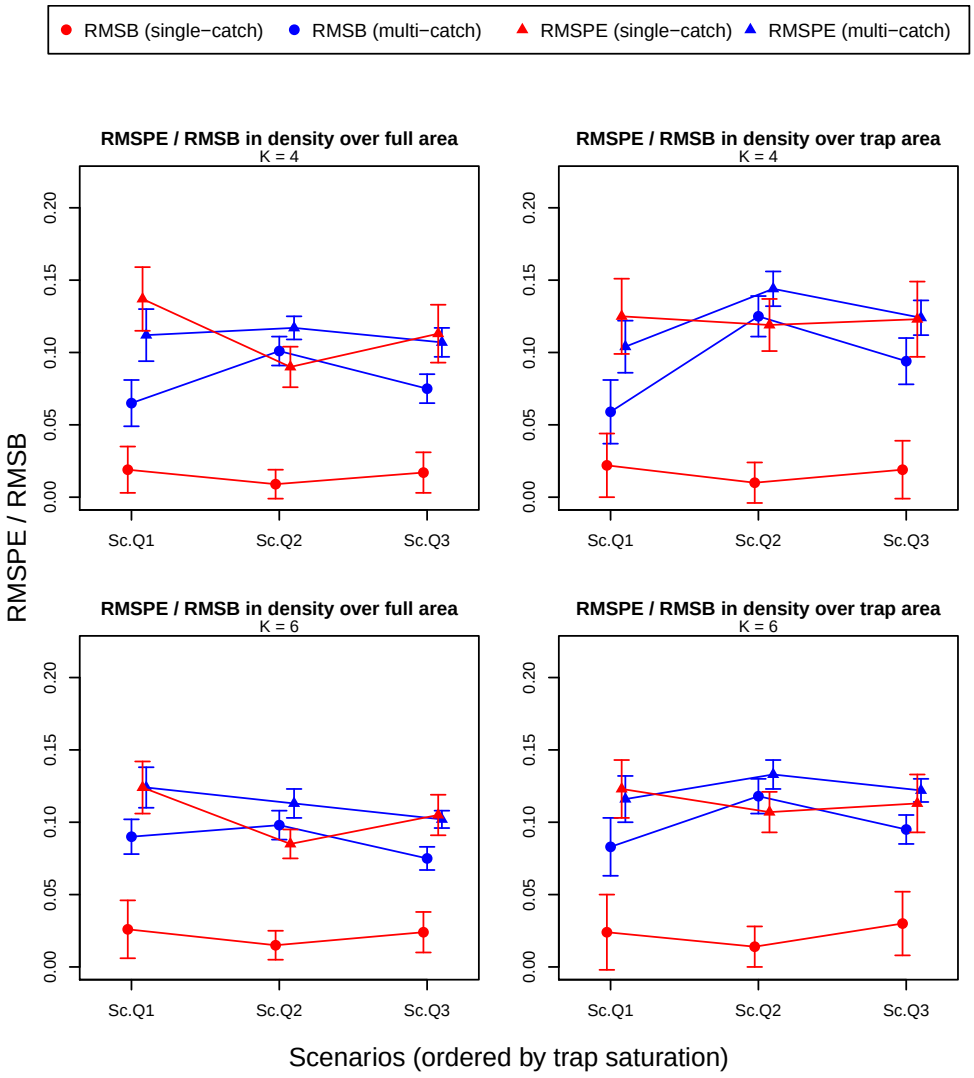

Notes: Results are given for both the full area (top left and bottom left plots) and the area spanning the trap array (top right and bottom right plots). The top row is from simulations using a spline hazard with K = 4, and the bottom row from simulations using K = 6. Standard errors are calculated using the Delta method for the RMSPE and bootstrapping for the RMSB, and error bars are plotted using 2 standard errors. The x-axis is ordered by trap saturation (96%, 82%, 70%)

4.2.3 Possum application

Both the CT models with flexible spline hazards (with K = 4, 6 and 8) and the DT multi-catch trap estimator are fitted to the possum data. As explained in Chapter 1, the traps used in the possum study were sometimes triggered by other non-target animals and the time of the triggering was recorded by the timing device. The CT model is able to accurately account for these "DG" events by setting the detection hazard to zero for the exact time period that the appropriate trap was out of action for. The DT models can account for trap failures by either removing the trap for the entire occasion, or by removing the trap for a proportion of the occasion, or the trap failures can be ignored. The second approach should be the best choice from these options. The sensitivity of the results to the method used to handle trap failures is explored by treating these "DG" events in three different ways when fitting the DT multi-catch trap models.

In the first instance the "DG" events are simply ignored, in the second the trap that had the "DG" event is treated as if it was not operating for the full occasion, and in the third the proportion of time that the trap is out of action for is calculated. The second and third approach requires information on the duration that each trap was active to be associated with each trap, in the form of a "usage matrix" in the `secr` software.

Tables 4.5 and 4.7 show the model selection statistics from the CT and DT models, and Tables 4.6 and 4.8 present the respective estimates. Note that the AIC's for the DT models with different ways of handling the "DG" events cannot be directly compared and so comparisons are made within each of the approaches. Figure 4.18 plots the estimated detection hazard from the best model as indicated by AIC for each hazard type along with the hazard shapes that correspond to the starting values used.

Within the CT models there is overwhelming support (Akaike weight of 1) for the cyclic spline hazard with K = 6 and a behavioural effect on the g_0 parameter. The hazard from the best fitting model based on AIC has a clear and pronounced peak in detectability that rises fairly rapidly from the early evening and has dropped back down to a low level by about 10 pm. The hazard of detection remains low at all other times apart from a very slight bump in the early morning. The hazard with K = 4 has a fairly similar shape but leads to the hazard peak starting earlier in the day, increasing at a slower rate, and decreasing to a low level at a later time. The hazard with K = 4 also lacks the flexibility to model the very slight increase in detectability in the early morning. Increasing K to 8 does not appear to capture any further important features in the detection hazard cycle. The dependence between captures that is induced by single-catch traps changes the detection hazard through

time and makes it much more difficult to assess goodness-of-fit and produce a figure that is similar to Figure 4.11, and this has not been done here. In agreement with the jaguar application above, the estimated hazard shapes are not sensitive to the starting values supplied.

The estimates from models with different non-constant hazards but the same type of behavioural effect are again very similar to each other. Including a behavioural effect on g_0 leads to the density estimate from the null model decreasing by over 20% in the best fitting model with K = 6 (from 8.14 (6.4;10.4) to 6.44 (5.0;8.2) per ha). The corresponding decrease in estimated density is 30% for the model with a behavioural effect on sigma (5.72 (4.4;7.5) per ha) and slightly more when the effect is on both g_0 and σ (5.62 (4.3;7.3) per ha). The nature of the behavioural effect on g_0 is one of "trap shyness" with g_0 decreasing almost 70% from 0.36 (0.26;0.49) before first capture to 0.12 (0.10;0.14) after first capture.

In contrast to the CT models, within each way of handling "DG" events, the DT models all select a behavioural effect on σ (Akaike weights ranging from 0.55 to 0.69) followed by behavioural effects on both the g_0 and σ parameters. The models with a behavioural effect only on g_0 had very little support (Akaike weights < 0.001).

For the DT models with a behavioural effect on σ that fit best according to AIC, the estimate of density ignoring the "DG" events is 4.96 (3.8;6.4) per ha and increases to 5.16 (4.0;6.7) per ha if the events are removed entirely. The intermediate approach that uses the proportion of time that traps are not operating for, results in an estimate for density of 5.04 (3.9;6.6) per ha. The estimate of σ from the third approach is 46.6 m (41.4;52.6) before first capture and 36.4 m (33.0;40.1) after first capture. Note that the models with a behavioural effect on both parameters produce estimates of g_0 that increase after first capture.

Figure 4.18: Detection hazard plots with three 24 hour cyclic cubic spline hazards fitted to the possum data.

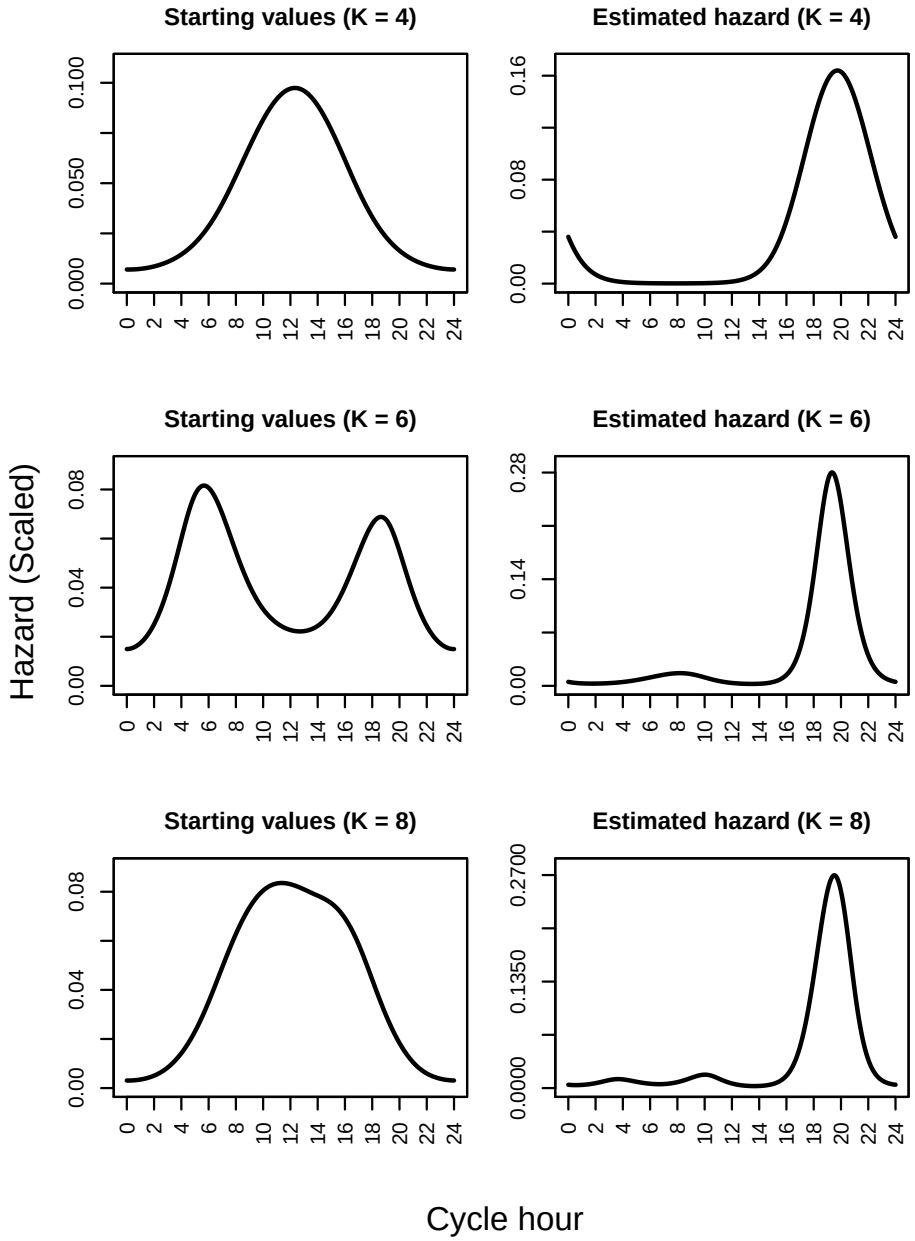

Notes: The plots on the left hand side show the detection hazard shapes that correspond to the starting values supplied in the model fitting. The right hand side plots depict the estimated detection hazard from the best fitting model to the possum data for each hazard type.

Table 4.5: Model selection summary for the possum data and the CT models with cyclic spline hazards for three different values of K. All models specify a constant density.

Hazard	Model	ΔAIC$_c$	wt	npar
K = 6	D(.) g_0(b) σ(.)	0.00	0.999	8
K = 6	D(.) g_0(.) σ(.)	33.35	< 0.001	7
K = 8	D(.) g_0(b) σ(b)	38.26	< 0.001	11
K = 8	D(.) g_0(b) σ(.)	39.93	< 0.001	10
K = 8	D(.) g_0(.) σ(b)	42.29	< 0.001	10
K = 8	D(.) g_0(.) σ(.)	70.61	< 0.001	9
K = 6	D(.) g_0(b) σ(b)	71.74	< 0.001	9
K = 6	D(.) g_0(.) σ(b)	82.78	< 0.001	8
K = 4	D(.) g_0(b) σ(b)	150.24	< 0.001	7
K = 4	D(.) g_0(.) σ(b)	152.89	< 0.001	6
K = 4	D(.) g_0(b) σ(.)	154.34	< 0.001	6
K = 4	D(.) g_0(.) σ(.)	178.35	< 0.001	5

Notes: The brackets in the "Model" column indicate which parameter has a behavioural effect included where "(.)" indicates no effect and "(b)" indicates a behavioural. ΔAIC$_c$ is the difference in AIC$_c$ between the current and the best model (AIC$_c$ is Akaike Information Criterion corrected for small sample size), wt denotes the Akaike weight, npar denotes the number of estimated parameters.

Table 4.6: Estimates (and 95% confidence intervals) from the CT single-catch trap models with non-constant detection hazards fitted to the possum data with constant density specified and different behavioural effects. The best model as indicated by AIC for each type of hazard is marked in bold and the best model overall is highlighted in orange.

Model	$\hat{D}$ (95% CI)	$\hat{g}_0$ (95% CI)	$\hat{g}_1$ (95% CI)	$\hat{\sigma_0}$ (95% CI)	$\hat{\sigma_1}$ (95% CI)
			Cyclic Spline (K = 4)		
D(.) g_0(.) σ(.)	8.08 (6.35;10.29)	0.126 (0.105;0.152)	NA	34.74 (32.06;37.63)	
D(.) g_0(b) σ(.)	6.61 (5.16;8.46)	0.309 (0.217;0.418)	0.119 (0.098;0.144)	34.91 (32.23;37.82)	NA
D(.) g_0(.) σ(b)	5.90 (4.51;7.70)	0.152 (0.125;0.183)	NA	45.74 (40.21;52.04)	31.75 (29.26;34.45)
D(.) g_0(b) σ(b)	**5.97 (4.60;7.75)**	**0.235 (0.154;0.343)**	**0.137 (0.111;0.169)**	**41.17 (35.37;47.93)**	**32.82 (30.03;35.88)**
			Cyclic Spline (K = 6)		
D(.) g_0(.) σ(.)	8.14 (6.40;10.37)	0.126 (0.104;0.151)	NA	34.56 (31.92;37.42)	NA
D(.) g_0(b) σ(.)	**6.44 (5.03;8.24)**	**0.364 (0.256;0.487)**	**0.118 (0.097;0.142)**	**34.82 (32.16;37.70)**	**NA**
D(.) g_0(.) σ(b)	5.72 (4.38;7.49)	0.155 (0.128;0.186)	NA	46.96 (41.19;53.54)	31.34 (28.91;33.96)
D(.) g_0(b) σ(b)	5.62 (4.33;7.29)	0.277 (0.182;0.399)	0.114 (0.092;0.141)	40.97 (35.25;47.62)	33.02 (30.19;36.12)
			Cyclic Spline (K = 8)		
D(.) g_0(.) σ(.)	8.14 (6.39;10.37)	0.126 (0.105;0.152)	NA	34.56 (31.92;37.42)	NA
D(.) g_0(b) σ(.)	6.44 (5.03;8.25)	0.362 (0.255;0.486)	0.118 (0.098;0.143)	34.80 (32.15;37.68)	NA
D(.) g_0(.) σ(b)	5.47 (4.17;7.16)	0.134 (0.111;0.161)	NA	48.62 (42.57;55.53)	31.32 (28.88;33.96)
D(.) g_0(b) σ(b)	**5.82 (4.49;7.55)**	**0.278 (0.181;0.401)**	**0.136 (0.110;0.168)**	**40.93 (35.20;47.59)**	**32.72 (29.94;35.75)**

Notes: The CT models use a cyclic spline hazard with a 24 hour cycle that is consistent with a half-normal detection function shape over an interval of 24 hours. Results are reported on the natural scale. The brackets in the "Model" column indicate which parameter has a behavioural effect included where "(.)" indicates no effect and "(b)" indicates a behavioural effect. Estimated density ($\hat{D}$) is individuals per ha, $\hat{\sigma}$ is in meters, and $\hat{g}_{01}$, $\hat{g}_{02}$, $\hat{\sigma}_1$ and $\hat{\sigma}_2$ are estimated detection function parameters before and after initial detection, respectively.

Table 4.7: Model selection summary for the possum data and the DT multi-catch models for different ways of handling the "DG" events. All models specify a constant density.

Model	ΔAIC$_c$	wt	npar
DG events ignored			
D(.) g_0(.) σ(b)	0.00	0.689	4
D(.) g_0(b) σ(b)	1.59	0.311	5
D(.) g_0(b) σ(.)	14.37	0.001	4
D(.) g_0(.) σ(.)	18.98	< 0.001	3
DG events removed			
D(.) g_0(.) σ(b)	0.00	0.554	4
D(.) g_0(b) σ(b)	0.44	0.445	5
D(.) g_0(b) σ(.)	12.20	0.001	4
D(.) g_0(.) σ(.)	116.12	< 0.001	3
% DG events			
D(.) g_0(.) σ(b)	0.00	0.653	4
D(.) g_0(b) σ(b)	1.27	0.346	5
D(.) g_0(b) σ(.)	13.87	0.001	4
D(.) g_0(.) σ(.)	33.4	< 0.001	3

Notes: The brackets in the "Model" column indicate which parameter has a behavioural effect included where "(.)" indicates no effect and "(b)" indicates a behavioural. ΔAIC$_c$ is the difference in AIC$_c$ between the current and the best model (AIC$_c$ is Akaike Information Criterion corrected for small sample size), wt denotes the Akaike weight, npar denotes the number of estimated parameters.

Table 4.8: Estimates (and 95% confidence intervals) from the DT multi-catch trap estimator, for different ways of handling the "DG" events, fitted to the possum data with constant density specified and different behavioural effects. The best fitting model for each method of handling the trap failures is marked in bold.

Model	$\hat{D}$ (95% CI)	$\hat{g}_0$ (95% CI)	$\hat{g}_1$ (95% CI)	$\hat{\sigma}_0$ (95% CI)	$\hat{\sigma}_1$ (95% CI)
			"DG" events ignored		
D(.) g_0(.) σ(.)	6.04 (4.71;7.75)	0.168 (0.138;0.202)	NA	39.13 (35.55;43.06)	NA
D(.) g_0(b) σ(.)	5.62 (4.37;7.24)	0.254 (0.176;0.353)	0.159 (0.130;0.193)	39.05 (35.55;42.89)	NA
D(.) g_0(.) σ(b)	**4.96 (3.82;6.44)**	**0.189 (0.155;0.228)**	**NA**	**46.86 (41.56;52.83)**	**36.11 (32.70;39.88)**
D(.) g_0(b) σ(b)	4.92 (3.77;6.40)	0.160 (0.102;0.242)	0.198 (0.158;0.244)	48.70 (41.87;56.64)	35.67 (32.17;39.55)
			"DG" events removed		
D(.) g_0(.) σ(.)	6.11 (4.77;7.84)	0.198 (0.163;0.239)	NA	39.11 (35.64;42.91)	NA
D(.) g_0(b) σ(.)	5.81 (4.51;7.48)	0.263 (0.181;0.365)	0.192 (0.157;0.232)	39.07 (35.64;42.83)	NA
D(.) g_0(.) σ(b)	**5.16 (3.98;6.70)**	**0.219 (0.180;0.264)**	**NA**	**45.62 (40.53;51.36)**	**36.57 (33.20;40.29)**
D(.) g_0(b) σ(b)	5.11 (3.92;6.65)	0.167 (0.106;0.253)	0.235 (0.189;0.289)	48.50 (41.73;56.37)	35.87 (32.43;39.67)
			% "DG" events		
D(.) g_0(.) σ(.)	6.14 (4.78;7.88)	0.173 (0.142;0.209)	NA	39.20 (35.64;43.11)	NA
D(.) g_0(b) σ(.)	5.71 (4.43;7.35)	0.261 (0.180;0.362)	0.170 (0.139;0.206)	39.12 (35.63;42.94)	NA
D(.) g_0(.) σ(b)	**5.04 (3.88;6.55)**	**0.20 (0.164;0.241)**	**NA**	**46.64 (41.39;52.56)**	**36.37 (32.97;40.11)**
D(.) g_0(b) σ(b)	4.99 (3.83;6.50)	0.163 (0.104;0.248)	0.211 (0.169;0.261)	48.89 (41.98;56.93)	35.86 (32.39;39.70)

Notes: The DT models use 9 occasions of 24 hours. Results are reported on the natural scale. The brackets in the "Model" column indicate which parameter has a behavioural effect included where "(.)" indicates no effect and "(b)" indicates a behavioural effect. Estimated density ($\hat{D}$) is individuals per ha, $\hat{\sigma}$ is in meters, and $\hat{g}_{01}$, $\hat{g}_{02}$, $\hat{\sigma}_1$ and $\hat{\sigma}_2$ are estimated detection function parameters before and after initial detection, respectively.

4.3 Discussion

4.3.1 Estimator properties

Density

The results from the simulations show that even when the detection hazard varies through time the DT binary proximity detector estimator of density is unbiased or nearly so, and suggest that ignoring actual times of capture does not affect the estimation of density. This result is expected given that the capture times are S-ancillary for the parameters $\boldsymbol{\phi}$ and $\boldsymbol{\theta}$ with respect to the $\boldsymbol{\psi}$ parameters.

In the applications, the CT parameter estimates from models with different hazard shapes but the same behavioural effect are virtually identical in the case of the jaguars and very similar in the case of the possums. It therefore appears as if the estimation of density is robust to misspecification in the hazard function for the observation process component of the model.

The hazard function implies a detection function that is the same for each DT occasion when the hazard cycle length is in agreement with the occasion length. When the duration of the hazard cycle is out of sync with the occasion duration the integrated hazard for different occasions will not be the same, effectively leading to variation in the detection function across the occasions. It is noteworthy that even under these conditions when the DT binary estimator fits a common detection function to all occasions, the estimation of density is still approximately unbiased. Efford et al. (2013) simulated data with temporally varying effort leading to heterogeneity in detection, and compared the results from fitting a null model and the model with an appropriate adjustment to this data. They found that fitting an M_0 model to data generated under an M_t model did not affect the estimation of density although the correctly specified model was chosen on the basis of AIC the vast majority of the time. The authors suggest that the primary benefit from using the correct model may be in preventing unexplained variance being wrongly attributed to some covariate. This is likely the case with the continuous hazard models used here too.

In both the applications the models with the best fitting detection components as indicated by AIC select a different behavioural effect to the models with a worse fitting detection function. For the jaguar dataset the best fitting spline hazard model with K = 6 selects the model with no behavioural effects as does the model with K = 8 that produces a similar detection hazard shape. In contrast the DT model, the constant hazard (count) model, and the model with a cosine hazard shape all select a behavioural effect on g_0. The interpretation of the trap happiness effect on g_0 for jaguars has always been recognised as being unlikely to be a true trap-happiness

effect and more likely to be a mechanism for soaking up some of the heterogeneity in individuals that stems from differential usage of trails. When a more flexible spline hazard is used, the inclusion of the behavioural effect becomes less supported although there is still some support for that model.

The same thing occurs even more clearly with the possum dataset whereby the best fitting CT model overwhelmingly selects a model with a trap-shyness effect on g_0, models with other hazard shapes end up selecting behavioural effects on both detection function parameters, and the DT model selects a model with an effect on σ. A trap-shyness effect is biologically plausible due to the fact that the possums are physically trapped and handled. The discrepancy in the model selection results could be a case of the worse fitting models attributing unexplained variation to the wrong source, especially when one considers that there is a fair amount of support for the DT models with effects on both parameters, including a trap-happiness effect in g_0, whereas all the other models estimate trap-shyness.

For both applications there is a difference in the density point estimates from the best models. The estimate of male jaguar density is 3.60 per 100 km^2(2.14 ; 6.05) from the DT model and 2.80 per 100 km^2 (1.71 ; 4.58) from the best spline hazard model ; for possums the density estimate from the DT model (with the third approach to handling "DG" events) is 5.04 per ha (3.88;6.55) and 6.44 per ha (5.03;8.24) from the best fitting spline hazard model. While I do not have a clear explanation for the fairly big difference in the estimates of possum density, it is known that the DT model does not estimate the correct detection function nor can it handle the DG events as well as the CT model. The possum density estimates from the DT models with the same behavioural effect on g_0 as the CT models (but which have very little support) do bring the estimates closer together.

Broadly speaking, the single-catch trap simulation results from this chapter are in agreement with the simulation results found in Chapter 3. The multi-catch trap estimator of density is unbiased or nearly so when density is constant or does not not vary much (as in exponential scenario Sc.E4). When density varies in space the DT multi-catch trap estimator performs well in most cases with respect to estimating mean density but does not manage to identify areas of high and low density.

Detection process

When the detection hazard is asynchronous relative to the occasion length the DT estimator is biased for g_0. This bias is expected since the detection hazard is set up to produce the specified detection function for the first occasion only, and the DT models are fitting a common detection function to all occasions. For example, it is

clear that the last two asynchronous hazards (with cycle durations of 30 days and 90 days) produce a cumulative or integrated hazard from the first 24 hours that will be very low relative to occasions that occur later on in the hazard cycle. The DT model estimates a single detection function and so ends up estimating the average level of detectability across the study which is significantly higher than the detectability for the first occasion and leads to positive bias in g_0 of around 850%.

Of course one can improve the fit of the DT models by adding occasion-specific detection function parameters or by modelling the effect of time on these parameters (usually by fitting a linear or quadratic trend). Alternatively, the CT framework allows an elegant and fairly parsimonious approach to flexibly model how detectability changes through time. Furthermore, modelling heterogeneity in detectability with the DT models would result in modelling average detectability for an occasion and would not operate at the same resolution as the CT models.

As expected, using the multi-catch trap estimator for single-catch trap data leads to negative bias in g_0 that varies with trap saturation. As discussed in Section 3.3.2 this is due to the multi-catch trap estimator not being able to attribute the correct degree of trap exposure to individuals in the sample. It is probably fairly typical in single-catch trap studies to have trap outages similar to the "DG" events in the possum example that represent another kind of varying trap exposure that the multi-catch trap estimator is not designed to deal with. It is possible that the impact of the violation of the multi-catch assumption is compounded by the existence of these kinds of events.

4.3.2 Modelling activity patterns

Understanding the activity patterns of animals can be used to learn about animal behaviour. Cowan and Forrester (2012) use single-catch traps with timing devices to understand the behavioural response of possums that are caught, and Harmsen et al. (2009) make inference about the hourly activity of jaguars and pumas from the frequency distribution of hourly capture times (397 for jaguars and 413 for pumas). However using a histogram with X bars (a) requires arbitrary decisions about where the intervals start and end for each bar, (b) involves estimating $(X - 1)$ parameters, (c) does not give a smooth estimate of activity pattern change over time, and (d) does not include a rigorous framework for quantifying the associated uncertainty or selecting between alternative models. Using a spline involves no arbitrary decisions about intervals, involves estimating as many or as few parameters as the data support, provides a much more realistic smooth estimate of activity pattern change and a rigorous framework for model selection, uncertainty quantification, and test-

ing hypotheses about activity patterns. The various hazard plots generated from the simulation studies in this chapter show that the CT models are able to estimate the underlying detection hazard cycle well. As one would expect, the variability in these estimates is higher for more complicated hazards that require more parameters, and decreases with more data.

Ridout and Linkie (2009) quantify the overlap in activity patterns between different species from camera trap data. They use kernel density estimation for circular data to estimate the continuous activity pattern distributions, and then look at different measures of overlap. The measures of overlap used in Ridout and Linkie (2009) could also be applied to the estimated activity patterns from the estimated spline hazards.

A crepuscular (active during twilight) hazard shape is deemed most appropriate for modelling detection of jaguars in the Cockscomb Basin Wildlife Sanctuary in Belize. This is in line with Harmsen et al. (2011) who reported a crepuscular peak in activity for jaguars between 6 and 7 pm. On the other hand the estimated detection cycle for possums is more unimodal with a peak in the evening and low levels of detectability at other times, which is again in line with previously published work (Cowan and Forrester, 2012).

A fuller moon leads to brighter hunting conditions and Harmsen et al. (2011) report that the two main prey species of jaguars and pumas both exhibited reduced activity under these conditions, and discuss different potential predator strategies in response to this reduction in activity. The asynchronous hazard with a cycle duration of 720 hours is the type of hazard that could be appropriate if detectability is related to a longer process such as the lunar cycle. However it is likely that if such a process existed it would be on top of a shorter daily detection cycle and both would probably need to be modelled together. The objective in this case is to explore how the misspecification of the binary model affects density estimation and so the combination of both hazard cycles is not implemented here. The CT modelling framework can however easily accommodate this sort of hazard model.

4.3.3 Summary of model performance

When detectability varies through time, using a CT model leads to a model with a better fitting detection component. In addition, the CT framework is able to model heterogeneity in detection in a flexible and parsimonious way as well as being able to model activity patterns and to account for periods of trap outages.

The DT binary proximity detector estimator performs well when the time-varying hazard has the same cycle duration as the occasions used in a DT model. There is

heterogeneity in detection across occasions if the hazard cycle duration is out of sync with the occasion length. In this case the DT estimator for g_0 is biased but the estimator of density is still approximately unbiased.

When the data are from single-catch trap surveys, and the detection hazard varies through time, the performance of the respective models is in agreement with that described in Section 3.3.3.

Chapter 5

Summary, discussion and conclusion

5.1 Summary

In traditional capture-recapture (CR) studies populations are sampled at discrete points in time leading to clear and well defined occasions. This characteristic is reflected in the model development of a wide range of CR models as well as for more recent spatial capture-recapture (SCR) models that incorporate spatial location information and were developed to directly estimate density. However, new types of detectors (such as camera traps) that sample continuously in time are increasingly being used. In order to analyse the resulting data, researchers using traditional methods need to define an appropriate occasion and aggregate their data accordingly.

The continuous-time (CT) framework assumes that detections follow a temporal non homogeneous Poisson process (NHPP) and uses a continuous detection hazard function instead of the usual discrete-time (DT) detection function that has an occasion-specific interpretation. It is straightforward to link the discrete-occasion detection function with an integrated CT hazard for any period of time, and two recent review papers of SCR models (Borchers, 2016; Borchers and Marques, 2016) formulate the detection process in terms of a CT detection hazard. This formulation leads to a general framework that can handle different types of data that are generated by different types of detectors (binary, count, and actual capture times) as well as handle varying exposure.

If one assumes a constant hazard through time then the CT proximity detector likelihood essentially reduces to that of the Poisson SCR count model and there is no information in the actual capture times. Previous work comparing binary and count

models found that reducing counts to binary events led to almost no deterioration in the performance of the estimator (Efford et al., 2009b). The results of the simulations conducted here are in agreement with those conclusions though the initial appearance of bias for simulation scenarios with low trap spacing does suggest that it can be more difficult to maximise the likelihood surface with binary data compared to count data.

If detectability does not change over time the concept of occasions is redundant with Poisson count models. A researcher using a single occasion count model therefore avoids having to make subjective decisions about occasion length. One advantage of aggregating data within occasions is that it reduces any correlation in captures within an individual. One potential problem with using the proposed CT formulation is that of temporal and spatial correlation in capture times. The movement simulations presented in Chapter 3 suggest that this is unlikely to be a problem for the sort of animal that is being monitored by camera trap arrays (like jaguars) that are seen infrequently and routinely move large distances between captures.

A benefit of the CT formulation is that it leads to the construction of a likelihood for single-catch traps with observed capture times. A general single-catch trap likelihood that does not require capture times remains elusive. The DT multi-catch estimator is usually used to analyse data from single-catch trap studies, and while it is known to be the wrong estimator it is considered to be robust to the violation of the multi-catch assumption that traps continue to operate after capturing an individual. The multi-catch estimator compensates for the violation of this assumption by underestimating g_0, i.e. it does not take traps out of action when they are occupied but instead estimates all traps to be less effective than they really are.

The simulations conducted here confirm that the multi-catch estimator is negatively biased for the g_0 parameter and that this bias increases with increasing trap saturation. The simulations also confirm that despite the bias in g_0 the multi-catch estimator is often unbiased in terms of average density estimation. However, there are scenarios when density varies in space that lead to the multi-catch estimator underestimating density in areas of high density and overestimating density in areas of low density. The single-catch trap estimator is unbiased in all these cases.

The CT framework can accommodate any type of detection hazard function. Apart from a constant hazard this work uses hazards with a cosine shape and hazards that are fitted with cyclic cubic regression splines. In both these cases the hazard function is conceptualised as a cyclical function that repeats though time, and hazards that have the same cycle duration as the DT occasion as well as those with a different cycle duration are considered in the simulations.

The DT binary proximity detector estimator for g_0 is biased when the length of

the hazard cycle is out of sync with the occasion and a common detection function is fitted. However, despite the bias in g_0, the estimator is unbiased with regards to density and σ even when detection hazards vary in time. The CT estimators are unbiased or nearly so for all parameters of interest and manage to estimate the underlying hazard cycle well. As expected, the estimators are more precise when there is more data.

5.2 Discussion

5.2.1 Density

Equation 2.20 factorises the probability density function of capture times into two components, one for the frequency of capture events and another for the actual capture times conditional on the frequency. Ignoring capture times means that only the first component is used in the likelihood and suggests that in general there is information in the capture times. However the hazard function used in the simulations conducted here was specified according to Equation 2.22 and hence it is not surprising that there was no significant bias in density when ignoring capture times and using the DT binary proximity detector estimator. The bias in density that is associated with the application of the multi-catch trap estimator to single-catch trap data under certain non-constant density surfaces is due to the violation of the multi-catch trap assumption that traps do not fill up rather than specifically due to using an approach that excludes the times of capture.

Barker et al. (2014) draw similar conclusions for a non-spatial CR model for abundance (N) whereby the MLE for N is the same whether it is based on the full likelihood that includes detection times or the partial likelihood that excludes the times. These conclusions are also in line with other work on CT CR models leading to similar statements by Hwang et al. (2002) and Xi et al. (2007) that the MLE for N is identical under models M_0 and M_t in the first case, and under models M_h and M_{th} in the second. Barker et al. (2014) use the concept of partial ancillarity to explain why there appears to be very little loss of information about abundance when actual capture times are ignored.

Furthermore, Efford et al. (2013) also explored the effect of misspecifying varying temporal effort in DT SCR models and reported that despite a better fitting detection model there was no discernible effect on density estimation from using the correct model that adjusted for the varying effort. The authors make the point that "The primary benefit from effort adjustment may be in controlling for variation that would otherwise be attributed wrongly to other covariates." The fact that, in both the

applications that are used in this work, the best fitting model selected a different behavioural effect to other models gives this assertion some credence.

Implications for trap design

If the multi-catch trap estimator is used in a single-catch trap study, a trap design that lays traps out with trap density roughly proportional to expected animal density in space may avoid higher trap saturation in areas of high density.

It is well-known that extrapolating predictions beyond the range of the model covariates can lead to biased predictions (Conn et al., 2015). The single-catch trap estimator sometimes estimates density with substantial positive bias when extrapolating beyond the range of explanatory variables spanned by the traps (the X coordinate in the simulations). The same thing can be seen in, for example, Figure D.6 from simulations with data from proximity detectors. It is therefore important that traps adequately span the range of any covariate that is included in the density model.

Furthermore, the variance in the single-catch trap estimator for density seems to increase when one extrapolates in this way. For example the RMSPE from the single-catch trap estimator is worse compared to the multi-catch trap estimator in the quadratic simulation scenarios Sc.Q1 and Sc.Q3 with 5 occasions. Both these scenarios are characterised by a sampling design where the trap array does not sample from regions where density is changing. A clustered trap design that spans the range of such covariates would facilitate interpolation rather than extrapolation and ameliorate the high variance in the single-catch trap estimator.

5.2.2 Beyond density

When detectability varies through time there are several different approaches that can be taken with a traditional DT model. The variation across occasions can be ignored and a single detection function fitted to all occasions, which may not lead to biased estimates of density but will limit the inferences that can be drawn from the estimated detection function. At the other extreme, a DT model can estimate separate detection function parameters for every occasion but that approach can lead to a large increase in the number of parameters and an associated increase in variance. An intermediate approach would be to reduce the number of parameters by modelling a parametric trend across time at the resolution of an occasion. A CT model can effectively achieve the same thing without the need for occasions: assuming a constant hazard corresponds to homogeneity in detection while using a flexible spline allows a suitable level of temporal heterogeneity in detection to be

modelled. However, the CT approach provides a flexible modelling framework that allows the data to inform how many parameters are required to model detectability at a finer temporal resolution, and hence allows heterogeneity in detection to be modelled in a more natural, parsimonious and flexible way compared to traditional DT models. Regression splines are able to model hazards with an irregular shape and are likely to be of more practical use then the more rigid cosine hazard shape.

But over and above this, the underlying process occurs in CT and modelling it in CT opens up opportunities to draw inferences about this process. For example, the ability to model detection hazards means that the CT framework can be used as a tool to explore animal activity patterns and learn about both mechanisms of coexistence between sympatric species and predator-prey dynamics (Ridout and Linkie, 2009; Harmsen et al., 2009, 2011). There are benefits to being able to do this, for example Harmsen et al. (2009) say that the mechanisms behind interspecific competition "...are subtle and need further study...". A formal modelling framework allows researchers to evaluate the extent of support for different hypotheses related to animal activity. For example one could model the detection hazard for two different species, for the same species at different locations, or for the same species at different times or seasons, and evaluate the support in the data for common or separate hazard functions in order to make the appropriate inference.

SCR models were developed to primarily solve the problem of estimating density in a non-spatial CR framework. However there is a growing realisation that the addition of a spatial dimension to CR models opens up opportunities to learn about other spatio-temporal processes (Borchers, 2016). In the past few years SCR models have been integrated with resource selection information and with an "ecological distance" metric in order to learn about space usage and landscape connectivity (Royle et al., 2013b,a; Fuller et al., 2015; Sutherland et al., 2015). These models replace the standard Euclidean distance metric with one that is based on distance related to a least cost path that depends on a spatially referenced covariate. A feature of these models is the ability to produce estimated home ranges that are non-stationary and asymmetric as they depend both on where in space the individual lives as well as the surrounding landscape structure. These models also allow a data-driven estimate of the landscape "resistance" parameter (a way of quantifying how environmental factors affect animal movement (Zeller et al., 2012)) that relates directly to landscape connectivity. Another potential area of innovation is to develop models that allow dynamic activity centres and can allow inferences to be drawn about dispersal processes (Royle et al., 2013a; Sutherland et al., 2015). Regardless, the point is that if the aim is to make inference not only about density but also about space usage, movement or some other spatio-temporal process, then the estimation of

the detection function parameters is also of interest in its own right. A CT framework allows the detection process to be modelled on a finer scale than is possible with DT models and there is potential to combine CT models with the sort of models described above.

5.2.3 Further developments

The potential for variation to be wrongly attributed to some covariate when the detection process is misspecified should be examined further. All the simulations conducted here did not involve any covariates and more certainty in this regard would bring a better understanding of the potential benefits to incorporating actual detection times.

Alternative parameterisations of the hazard function can be explored to increase the flexibility of the model and allow richer inferences about space usage through time to be drawn. For example, it is possible to model an interaction between habitat preference and time and see how space use in a particular area changes at a fine temporal scale. It is possible that the effective area used by an individual can remain constant but take on different shapes to reflect different behaviour, i.e. g_0 can drop and σ can increase to reflect faster movement.

Another avenue for development would be to relax the assumption of independence. It is possible to embed a movement model in the SCR model which should be able to model capture times that are spatially and temporally correlated. However, the reality is that from the SCR data alone there will only ever be location information from a very limited number of fixed spatial points (the detector locations) and it is likely that auxillary information (such as telemetry data) would be required to inform the movement model. An approach that uses a detection hazard that is affected by the time and place of an individual's last capture could be more practical to implement. Note that telemetry data have been integrated into SCR models to inform estimates of sigma and space use (Royle et al., 2013b).

Lastly, there is the potential to apply a CT framework in other methodological settings such as traditional CR and occupancy models (where the models use an occasion structure that could be changed to one that uses a continuous-time detection hazard).

5.3 Conclusion

This research into CT SCR models was originally motivated by the growth in the use of camera traps and the fact that camera traps sample populations continuously

in time. However, the realisation that the CT framework also provides a means to obtain a likelihood for single-catch traps meant that the research focus had to be broadened to include single-catch traps.

The single-catch trap simulations suggest that, while the DT SCR multi-catch estimator has been shown to be extremely robust when applied to single-catch trap data, there appear to be scenarios when the estimator is not able to correctly identify areas with varying density. If the focus of interest is only overall density, or if density is reasonably constant, then the multi-catch approximation should perform well. However, this performance deteriorates with high trap saturation and increasing density gradients. Furthermore, the multi-catch trap estimator is poor at estimating the height (but not range) of the detection function and the detection function parameters may be of interest in their own right (for example to inform models of animal movement, space usage and/or landscape connectivity). By contrast the single-catch trap estimators of density, distribution and detection function parameters are found to be unbiased or nearly unbiased in all scenarios considered. If accurate estimation of the detection function is of interest, or if density is expected to vary substantially in space, then there is merit in using the single-catch trap estimator.

In the absence of a single-catch trap likelihood that does not require observed capture times, it is recommended that, where possible, researchers who are using single-catch traps and are interested in modelling variation in density in space incorporate timing devices and use a single-catch trap estimator in preference to a multi-catch trap estimator when trap saturation is expected to be above about 60%.

In terms of estimating density I have not found a clear benefit to using the CT model with data from proximity detector surveys. However the simulations all used a form for the hazard consistent with Equation 2.22, and hence this result is not surprising. The model selection results from the applications are interesting and seem to support the statement by Efford et al. (2013) that there may be indirect benefits for density estimation from having a better fitting detection process. Hence, when detection hazards depend on observable time-varying covariates (time of day, temperature or some other time-varying environmental variables for example) there may be advantage in modelling this using exact detection times even if there is no inherent interest in the nature of the varying hazard, and there is certainly benefit in modelling the effect of time-varying covariates on the detection hazard when there is interest in how the hazard function depends on such covariates. The ability of the CT models to flexibly model detection hazards adds a new dimension to SCR models and has the potential to provide a valuable tool for researchers trying to understand dynamics related to animal activity patterns.

Trap usage in the jaguar example is on a daily scale, i.e. there is data on what

days each trap was operational for, but the CT models can obviously incorporate usage information at a higher resolution (like hours) as well as easily handle other failure events (such as the "DG" events in the possum case study). In addition, using a CT framework avoids having to impose artificial constructs on the data and means that continuous covariates can be included and effects can change smoothly with time rather than being forced to have a step-like nature corresponding to different occasions, for example one could incorporate a trap-happiness or shyness effect that decays smoothly with time.

SCR models are experiencing a rapid growth in both application and method development. The data for both proximity detectors and single-catch traps are actually being generated continuously in time and hence a CT framework provides a natural fit to the data and opens up several opportunities that are not possible with a DT formulation. The work here makes a contribution by developing and exploring the utility of such a CT SCR formulation.

Appendix A

Coding of the survival term

The algebraic expression for the appropriate survival function is given in Equation 2.32. The practical steps taken to implement this expression are outlined below:

1. A file is generated with time intervals for two distinct types of "trap failures". The first kind is a failure in the traditional sense, i.e. times when a particular trap was not operational, and the second type are times when a trap is effectively out of action because it is holding an individual. This second type of failure is extracted from the dataset while the first kind needs to be supplied manually. The "intervals" package (Bourgon, 2015) is used so that the periods of time are treated as intervals and can be checked for partial overlap in a later step.

2. The total amount of exposure for catching an animal is calculated for each trap. This is equal to the full exposure for the study period minus periods of time that a trap is out of action for either of the reasons given above.

3. Once an individual is caught in a particular trap, the exposure to capture for the time period that the individual is held is calculated for all other traps and subtracted from the totals in step 2. If one of these other traps was already out of action over that time period (due to one off the reasons given in step 1) then that amount of exposure will have already been accounted for in step 2 and no additional subtraction is needed. However it is possible that there is partial overlap, i.e. if individual i is caught and held from time 4 to time 6 in trap 1, and trap 2 caught and held another individual from time 5 to time 6, then one only needs to account for the exposure period from trap 2 to individual i from time 4 to time 5 (since the hazard of detection to individual i on trap 2 from time 5 to time 6 is zero). The code takes the full period to be deducted for each trap, and then calculates any overlap between that period and other trap-specific failure periods and removes the overlap from the full amount. No adjustment will be made if a capture period completely overlaps with another failure period.

4. The correct survival term for each individual will be the total trap exposure from step 2 minus the individual adjustments calculated in step 3.

Appendix B

Tables from Chapter 3 single-catch trap simulations

B.1 Simulation I: Comparing the two estimators when density is incorrectly specified

Table B.1: Relative bias (RB) of density and detection parameters estimated by the DT multi and the CT single-catch trap estimators with a constant hazard. All models specify a constant density. The data are simulated for a survey duration of $T = 120$ or 240 hours with constant density and a constant hazard.

Scenario	Model	$RB_{\hat{D}}(\%)$	$RB_{\hat{g}_0}(\%)$	$RB_{\hat{\sigma}}(\%)$
		5 occasions		
Sc.C1 (D = 4)	Multi-catch	9.37 (2.45)	-77.45 (0.59)	-4.19 (1.50)
	Single-catch	10.58 (2.45)	2.95 (2.53)	-3.06 (1.48)
Sc.C2 (D = 2)	Multi-catch	2.38 (2.34)	-55.85 (1.00)	-3.31 (1.27)
	Single-catch	4.06 (2.40)	6.45 (2.28)	-2.52 (1.23)
Sc.C3 (D = 1)	Multi-catch	1.16 (2.24)	-35.83 (1.55)	0.73 (1.47)
	Single-catch	2.77 (2.26)	3.21 (2.60)	1.03 (1.48)
Sc.C4 (D = 0.5)	Multi-catch	5.69 (2.77)	-14.55 (2.34)	-2.73 (1.63)
	Single-catch	7.44 (2.70)	7.64 (2.88)	-3.08 (1.56)
		10 occasions		
Sc.C1 (D = 4)	Multi-catch	-0.72 (1.29)	-77.64 (0.33)	-1.60 (0.80)
	Single-catch	-0.06 (1.30)	1.83 (1.37)	-0.30 (0.79)
Sc.C2 (D = 2)	Multi-catch	0.12 (1.35)	-58.64 (0.55)	-1.44 (0.76)
	Single-catch	0.80 (1.35)	1.29 (1.21)	-0.59 (0.75)
Sc.C3 (D = 1)	Multi-catch	0.93 (1.71)	-38.40 (1.01)	0.60 (0.88)
	Single-catch	1.66 (1.71)	-0.69 (1.52)	1.08 (0.88)
Sc.C4 (D = 0.5)	Multi-catch	-4.71 (2.09)	-19.81 (1.37)	2.21 (1.07)
	Single-catch	-4.14 (2.13)	1.54 (1.67)	2.35 (1.09)

Notes: Relative % bias is shown for each parameter followed by the standard error in parentheses. The DT models use 5 or 10 occasions of 24 hours. Twenty single-catch traps spaced 100 m apart are used for a constant density surface with $g_0 = 0.2$ and $\sigma = 100$. The CT model uses a constant hazard that is consistent with a half-normal detection function shape over an interval of 24 hours. In all cases 100 replications were run and converged and results are reported on the natural scale.

Table B.2: Relative bias (RB) of density and detection parameters estimated by the DT multi and the CT single-catch trap estimators with a constant hazard. All models specify a constant density. The data are simulated for a survey duration of $T = 120$ or 240 hours from different linear density gradients and a constant hazard.

Scenario	Model	$RB_{\hat{D}}(\%)$	$RB_{\hat{g}_0}(\%)$	$RB_{\hat{\sigma}}(\%)$
		5 occasions		
Sc.L1	Multi-catch	-0.97 (2.12)	-76.51 (0.63)	-1.41 (1.41)
	Single-catch	-0.63 (2.12)	8.86 (2.65)	-2.05 (1.31)
Sc.L2	Multi-catch	0.06 (2.20)	-69.36 (0.67)	-2.41 (1.48)
	Single-catch	-0.16 (2.09)	7.10 (2.40)	-2.86 (1.45)
Sc.L3	Multi-catch	-4.53 (1.81)	-56.87 (1.07)	-0.13 (1.44)
	Single-catch	-4.12 (1.80)	6.86 (2.41)	-0.68 (1.36)
Sc.L4	Multi-catch	-4.41 (1.97)	-34.32 (1.59)	0.62 (1.54)
	Single-catch	-3.49 (1.96)	6.79 (2.69)	0.32 (1.48)
		10 occasions		
Sc.L1	Multi-catch	-4.82 (1.11)	-77.51 (0.29)	-0.54 (0.75)
	Single-catch	-4.37 (1.09)	3.84 (1.13)	-1.35 (0.67)
Sc.L2	Multi-catch	-2.73 (1.25)	-70.89 (0.39)	-0.42 (0.85)
	Single-catch	-1.95 (1.23)	3.77 (1.23)	-0.83 (0.81)
Sc.L3	Multi-catch	-4.52 (1.28)	-59.14 (0.57)	0.29 (0.88)
	Single-catch	-3.76 (1.29)	1.88 (1.30)	-0.22 (0.87)
Sc.L4	Multi-catch	-0.58 (1.70)	-37.68 (1.03)	-0.30 (0.94)
	Single-catch	0.17 (1.69)	2.16 (1.37)	-0.50 (0.92)

Notes: Relative % bias is shown for each parameter followed by the standard error in parentheses. The DT models use 5 or 10 occasions of 24 hours. Twenty single-catch traps spaced 100 m apart are used with $g_0 = 0.2$ and $\sigma = 100$. The CT model uses a constant hazard that is consistent with a half-normal detection function shape over an interval of 24 hours. In all cases 100 replications were run and converged and results are reported on the natural scale.

Table B.3: Relative bias (RB) of density and detection parameters estimated by the DT multi and the CT single-catch trap estimators with a constant hazard. All models specify a constant density. The data are simulated for a survey duration of $T = 120$ or 240 hours from different exponential density gradients and a constant hazard.

Scenario	Model	$RB_{\hat{D}}(\%)$	$RB_{\hat{g}_0}(\%)$	$RB_{\hat{\sigma}}(\%)$
		5 occasions		
Sc.E1	Multi-catch	-4.09 (2.01)	-67.25 (0.73)	0.18 (1.44)
	Single-catch	-3.63 (1.92)	5.12 (2.21)	0.01 (1.38)
Sc.E2	Multi-catch	-4.12 (1.89)	-53.57 (1.06)	-1.35 (1.23)
	Single-catch	-3.41 (1.89)	4.11 (2.43)	-2.25 (1.15)
Sc.E3	Multi-catch	-10.58 (2.08)	-43.09 (1.51)	1.39 (1.68)
	Single-catch	-10.88 (1.98)	1.84 (2.39)	-1.02 (1.59)
Sc.E4	Multi-catch	0.59 (2.47)	-32.70 (1.53)	-2.03 (1.45)
	Single-catch	1.47 (2.42)	1.71 (2.12)	-2.02 (1.42)
Sc.E5	Multi-catch	-3.42 (3.39)	-24.63 (2.77)	-2.20 (1.99)
	Single-catch	-4.89 (3.08)	1.70 (3.35)	-4.71 (1.86)
		10 occasions		
Sc.E1	Multi-catch	-3.06 (1.42)	-68.64 (0.44)	-0.27 (0.77)
	Single-catch	-2.37 (1.44)	1.94 (1.19)	-0.09 (0.75)
Sc.E2	Multi-catch	-7.41 (1.22)	-55.12 (0.57)	0.68 (0.84)
	Single-catch	-6.31 (1.21)	2.95 (1.39)	-0.46 (0.79)
Sc.E3	Multi-catch	-9.47 (1.49)	-42.99 (0.82)	-0.39 (0.90)
	Single-catch	-8.63 (1.48)	0.54 (1.45)	-2.18 (0.82)
Sc.E4	Multi-catch	-1.10 (1.63)	-35.41 (0.95)	-0.12 (0.94)
	Single-catch	-0.47 (1.64)	0.44 (1.39)	-0.13 (0.89)
Sc.E5	Multi-catch	-2.76 (2.30)	-27.76 (1.75)	-1.86 (1.07)
	Single-catch	-2.01 (2.27)	-0.64 (2.33)	-4.35 (1.02)

Notes: Relative % bias is shown for each parameter followed by the standard error in parentheses. The DT models use 5 or 10 occasions of 24 hours. Twenty single-catch traps spaced 100 m apart are used with $g_0 = 0.2$ and $\sigma = 100$. The CT model uses a constant hazard that is consistent with a half-normal detection function shape over an interval of 24 hours. In all cases 100 replications were run and converged and results are reported on the natural scale.

Table B.4: Relative bias (RB) of density and detection parameters estimated by the DT multi and the CT single-catch trap estimators with a constant hazard. All models specify a constant density. The data are simulated for a survey duration of $T = 120$ or 240 hours from different quadratic density surfaces and a constant hazard.

Scenario	Model	$RB_{\hat{D}}(\%)$	$RB_{\hat{g}_0}(\%)$	$RB_{\hat{\sigma}}(\%)$
		5 occasions		
Sc.Q1	Multi-catch	9.30 (2.38)	-68.92 (0.75)	1.43 (1.59)
	Single-catch	10.47 (2.40)	4.88 (2.54)	1.54 (1.55)
Sc.Q2	Multi-catch	6.96 (2.34)	-57.95 (0.97)	17.17 (2.92)
	Single-catch	10.30 (2.22)	2.93 (2.34)	9.68 (2.97)
Sc.Q3	Multi-catch	-0.32 (2.24)	-59.09 (1.11)	10.65 (1.79)
	Single-catch	-1.25 (1.89)	16.97 (2.79)	-3.07 (1.20)
Sc.Q4	Multi-catch	9.18 (2.97)	-35.17 (1.71)	5.27 (1.45)
	Single-catch	10.56 (3.01)	4.01 (2.52)	4.14 (1.43)
Sc.Q5	Multi-catch	4.74 (2.89)	-33.21 (1.62)	6.66 (2.07)
	Single-catch	6.30 (2.81)	6.17 (2.50)	4.09 (1.94)
Sc.Q6	Multi-catch	8.69 (3.15)	-26.29 (2.04)	10.02 (2.31)
	Single-catch	10.60 (3.06)	7.23 (3.04)	6.66 (2.22)
Sc.Q7	Multi-catch	8.65 (3.19)	-31.93 (1.73)	13.76 (4.75)
	Single-catch	9.84 (2.98)	4.36 (2.73)	7.45 (3.15)
		10 occasions		
Sc.Q1	Multi-catch	4.84 (1.45)	-69.58 (0.47)	1.78 (0.84)
	Single-catch	5.49 (1.43)	3.88 (1.45)	1.47 (0.83)
Sc.Q2	Multi-catch	2.69 (1.66)	-57.20 (0.66)	10.73 (1.11)
	Single-catch	6.70 (1.64)	2.40 (1.36)	3.06 (0.92)
Sc.Q3	Multi-catch	-0.45 (1.67)	-58.65 (0.65)	5.66 (1.11)
	Single-catch	0.51 (1.55)	9.33 (1.38)	-3.36 (0.85)
Sc.Q4	Multi-catch	3.80 (1.77)	-38.02 (0.83)	4.35 (0.94)
	Single-catch	4.91 (1.74)	1.20 (1.42)	2.76 (0.90)
Sc.Q5	Multi-catch	-0.001 (1.96)	-34.89 (1.01)	3.69 (0.99)
	Single-catch	1.18 (1.97)	3.30 (1.52)	1.88 (0.92)
Sc.Q6	Multi-catch	8.64 (2.49)	-30.38 (1.15)	6.18 (1.76)
	Single-catch	10.63 (2.48)	3.83 (1.62)	2.80 (1.66)
Sc.Q7	Multi-catch	8.53 (2.14)	-31.96 (1.07)	4.38 (1.15)
	Single-catch	10.09 (2.11)	4.48 (1.59)	0.72 (1.03)

Notes: Relative % bias is shown for each parameter followed by the standard error in parentheses. The DT models use 5 or 10 occasions of 24 hours. Twenty single-catch traps spaced 100 m apart are used with $g_0 = 0.2$ and $\sigma = 100$. The CT model uses a constant hazard that is consistent with a half-normal detection function shape over an interval of 24 hours. In all cases 100 replications were run and converged and results are reported on the natural scale.

Table B.5: Relative bias (RB) of density and detection parameters estimated by the DT multi and the CT single-catch trap estimators with a constant hazard. All models specify a constant density. The data are simulated for a survey duration of $T = 120$ hours from various Neyman-Scott distributions (as determined by the μ_c and σ_c parameters) and a constant hazard. The DT models use 5 occasions of 24 hours.

Scenario	μ_c	σ_c	Model	$RB_{\hat{D}}(\%)$	$RB_{\hat{g}_0}(\%)$	$RB_{\hat{\sigma}}(\%)$	Reps
Sc.N1 (D=0.0625)	5	50	Multi-catch	170.80 (24.39)	-4.05 (5.38)	47.71 (32.42)	47
			Single-catch	169.33 (24.73)	14.89 (6.84)	45.55 (31.33)	47
	5	25	Multi-catch	177.28 (26.54)	-13.46 (10.22)	-15.00 (4.12)	49
			Single-catch	175.54 (25.98)	35.73 (11.61)	-18.56 (3.88)	49
	8	50	Multi-catch	184.65 (33.03)	-22.64 (9.87)	28.16 (17.37)	27
			Single-catch	212.81 (37.95)	-2.47 (9.75)	11.64 (14.94)	28
	8	25	Multi-catch	334.04 (44.95)	-28.02 (6.87)	19.22 (25.97)	25
			Single-catch	319.66 (41.32)	2.73 (9.59)	8.23 (22.81)	25
Sc.N2 (D=0.125)	5	50	Multi-catch	82.44 (20.20)	-8.84 (5.34)	7.50 (14.43)	63
			Single-catch	82.14 (17.89)	6.17 (5.94)	-8.64 (5.21)	62
	5	25	Multi-catch	85.61 (14.06)	-11.55 (5.81)	8.04 (6.83)	70
			Single-catch	83.76 (13.26)	9.49 (7.75)	2.75 (6.07)	70
	8	50	Multi-catch	129.85 (26.78)	-13.44 (10.82)	10.63 (18.39)	48
			Single-catch	118.58 (23.08)	12.41 (11.92)	-1.69 (15.76)	48
	8	25	Multi-catch	140.11 (26.59)	-29.72 (5.14)	25.33 (18.98)	42
			Single-catch	121.11 (18.22)	-6.63 (6.47)	4.77 (9.43)	41
Sc.N3 (D=0.5)	5	50	Multi-catch	0.14 (5.17)	-23.37 (2.71)	3.84 (3.14)	99
			Single-catch	0.97 (5.14)	3.47 (3.65)	1.39 (3.10)	99
	5	25	Multi-catch	7.41 (7.16)	-30.24 (2.77)	-0.41 (2.67)	97
			Single-catch	1.85 (4.61)	-4.31 (3.60)	-2.81 (2.41)	96
	8	50	Multi-catch	9.52 (6.17)	-33.21 (2.31)	3.05 (3.28)	93
			Single-catch	8.70 (5.62)	1.98 (3.51)	-4.24 (2.38)	93
	8	25	Multi-catch	32.13 (7.82)	-38.17 (2.35)	6.77 (9.11)	95
			Single-catch	29.60 (7.21)	-3.07 (3.70)	-0.03 (8.78)	95
Sc.N4 (D=2)	5	50	Multi-catch	-0.87 (2.99)	-58.58 (1.10)	0.96 (1.59)	100
			Single-catch	0.42 (2.99)	1.93 (2.21)	-0.38 (1.53)	100
	5	25	Multi-catch	4.75 (3.06)	-60.99 (1.14)	1.54 (1.65)	100
			Single-catch	6.02 (3.06)	-0.22 (2.53)	-0.14 (1.55)	100
	8	50	Multi-catch	-4.71 (3.22)	-62.77 (1.14)	7.46 (1.94)	100
			Single-catch	-3.70 (3.26)	-5.96 (2.30)	3.97 (1.87)	100
	8	25	Multi-catch	3.40 (3.07)	-61.43 (1.20)	0.50 (1.69)	100
			Single-catch	3.31 (2.98)	3.86 (2.75)	-3.33 (1.58)	100
Sc.N5 (D=4)	5	50	Multi-catch	0.79 (2.79)	-77.06(0.66)	-0.21 (1.69)	100
			Single-catch	1.87 (2.81)	2.29 (2.60)	-0.01 (1.63)	100
	5	25	Multi-catch	-0.22 (2.83)	-76.77 (0.70)	0.09 (1.76)	100
			Single-catch	0.77 (2.82)	5.85 (2.98)	-0.04 (1.67)	100
	8	50	Multi-catch	3.88 (3.46)	-77.26 (0.77)	0.10 (1.77)	100
			Single-catch	4.80 (3.48)	1.27 (2.77)	-0.84 (1.64)	100
	8	25	Multi-catch	-0.32 (3.36)	-77.75 (0.70)	3.00 (2.06)	100
			Single-catch	-0.17 (3.27)	-1.00 (2.75)	1.33 (1.97)	100

Notes: Relative % bias is shown for each parameter followed by the standard error in parentheses. Twenty single-catch traps spaced 100 m apart are used with $g_0 = 0.2$ and $\sigma = 100$. The CT model uses a constant hazard that is consistent with a half-normal detection function shape over an interval of 24 hours. Results are reported on the natural scale and "Reps" is number of replications out of 100 where any replications that did not converge or estimated negative or very large variances for any parameter were excluded.

Table B.6: Relative bias (RB) of density and detection parameters estimated by the DT multi and the CT single-catch trap estimators with a constant hazard. All models specify a constant density. The data are simulated for a survey duration of $T = 240$ hours from various Neyman-Scott distributions (as determined by the μ_c and σ_c parameters) and a constant hazard. The DT models use 10 occasions of 24 hours.

Scenario	μ	σ	Model	$\text{RB}_{\hat{D}}(\%)$	$\text{RB}_{\hat{g}_0}(\%)$	$\text{RB}_{\hat{\sigma}}(\%)$	Reps
Sc.N1 (D=0.0625)	5	50	Multi-catch	160.68 (24.05)	-30.94 (4.44)	-6.43 (3.29)	50
			Single-catch	162.57 (23.98)	-19.10 (5.57)	-8.79 (3.19)	50
	5	25	Multi-catch	152.01 (22.39)	-13.59 (5.98)	-11.44 (3.64)	42
			Single-catch	152.93 (21.90)	4.89 (8.34)	-14.13 (3.44)	42
	8	50	Multi-catch	209.28 (18.91)	-32.73 (4.86)	-3.49 (6.06)	35
			Single-catch	210.43 (17.29)	-11.95 (6.48)	-11.13 (3.99)	35
	8	25	Multi-catch	219.61 (26.13)	-33.03 (4.64)	8.80 (9.58)	33
			Single-catch	228.90 (24.41)	-9.52 (6.87)	-6.79 (3.72)	33
Sc.N2 (D=0.125)	5	50	Multi-catch	76.34 (12.16)	-26.35 (2.99)	-5.29 (2.76)	76
			Single-catch	75.58 (11.80)	-9.39 (3.96)	-7.86 (2.63)	76
	5	25	Multi-catch	77.98 (13.31)	-30.00 (3.32)	-5.31 (3.24)	78
			Single-catch	77.90 (13.11)	-13.07 (4.22)	-9.12 (2.79)	78
	8	50	Multi-catch	98.75 (12.84)	-25.45 (2.97)	-2.12 (5.59)	68
			Single-catch	98.64 (12.63)	-0.21 (4.14)	-5.94 (5.82)	68
	8	25	Multi-catch	120.90 (16.47)	-37.64 (4.27)	-1.18 (14.69)	56
			Single-catch	130.97 (20.20)	-19.70 (5.43)	-6.57 (14.32)	57
Sc.N3 (D=0.5)	5	50	Multi-catch	3.84 (4.04)	-29.43 (1.89)	-0.62 (1.67)	100
			Single-catch	4.54 (4.05)	-2.55 (2.42)	-2.75 (1.58)	100
	5	25	Multi-catch	11.48 (6.46)	-40.83 (1.82)	-0.78 (2.09)	98
			Single-catch	12.03 (6.50)	-16.02 (2.77)	-3.84 (1.95)	98
	8	50	Multi-catch	1.98 (5.04)	-34.78 (1.91)	-1.51 (1.77)	98
			Single-catch	2.30 (5.01)	-4.00 (2.56)	-5.53 (1.60)	98
	8	25	Multi-catch	28.76 (10.34)	-45.48 (1.59)	-0.98 (2.35)	98
			Single-catch	27.89 (9.06)	-15.20 (2.65)	-6.35 (2.06)	98

Notes: Relative % bias is shown for each parameter followed by the standard error in parentheses. Twenty single-catch traps spaced 100 m apart are used with $g_0 = 0.2$ and $\sigma = 100$. The CT model uses a constant hazard that is consistent with a half-normal detection function shape over an interval of 24 hours. Results are reported on the natural scale and "Reps" is number of replications out of 100 where any replications that did not converge or estimated negative or very large variances for any parameter were excluded.

Table B.7: Relative bias (RB) of density and detection parameters estimated by the DT multi and the CT single-catch trap estimators with a constant hazard. All models specify a constant density. The data are simulated for a survey duration of $T = 120$ or 240 hours from various Neyman-Scott distributions with a higher value for μ_c (15) and a constant hazard.

Scenario	μ_c	σ_c	Model	$\text{RB}_{\hat{D}}(\%)$	$\text{RB}_{\hat{g}_0}(\%)$	$\text{RB}_{\hat{\sigma}}(\%)$	Reps
5 occasions							
Sc.N3 (D=0.5)	15	50	Multi-catch	39.31 (9.04)	-44.47 (2.49)	-2.55 (3.59)	85
			Single-catch	35.57 (8.56)	-4.74 (4.41)	-11.94 (2.79)	85
	15	25	Multi-catch	54.37 (12.06)	-53.13 (2.04)	13.88 (7.66)	84
			Single-catch	44.99 (9.90)	-8.36 (3.73)	-3.62 (5.35)	84
	15	15	Multi-catch	59.59 (15.51)	-53.51 (2.26)	16.89 (7.92)	72
			Single-catch	55.0 (13.34)	-5.22 (5.20)	-7.14 (3.62)	72
Sc.N4 (D=2)	15	50	Multi-catch	-0.06 (4.56)	-62.29 (1.55)	3.38 (2.07)	99
			Single-catch	-1.10 (4.40)	-0.22 (2.88)	-3.27 (1.75)	99
	15	25	Multi-catch	7.32 (5.28)	-67.12 (1.14)	6.03 (2.93)	100
			Single-catch	4.74 (4.92)	-10.33 (2.99)	-1.31 (3.06)	100
	15	15	Multi-catch	-1.05 (4.68)	-68.25 (0.96)	10.33 (2.67)	100
			Single-catch	-2.64 (4.39)	-7.50 (2.94)	-0.16 (2.29)	100
10 occasions							
Sc.N3 (D=0.5)	15	50	Multi-catch	19.66 (6.60)	-54.28 (1.72)	-1.66 (2.68)	91
			Single-catch	18.76 (6.37)	-22.62 (3.35)	-9.11 (2.09)	91
	15	25	Multi-catch	39.13 (8.24)	-57.07 (1.44)	1.26 (2.85)	80
			Single-catch	38.44 (8.00)	-18.15 (3.53)	-8.32 (2.29)	80
	15	15	Multi-catch	40.95 (7.53)	-60.75 (1.65)	3.09 (4.86)	79
			Single-catch	38.55 (6.72)	-23.65 (3.97)	-9.95 (3.22)	79
Sc.N4 (D=2)	15	50	Multi-catch	7.81 (3.92)	-66.89 (0.96)	2.01 (1.18)	100
			Single-catch	8.59 (3.86)	-5.75 (1.95)	-3.61 (1.01)	100
	15	25	Multi-catch	9.18 (3.70)	-68.29 (0.76)	3.96 (1.46)	99
			Single-catch	10.36 (3.63)	-7.45 (1.82)	-2.77 (1.16)	99
	15	15	Multi-catch	5.41 (4.06)	-70.24 (0.83)	6.57 (1.69)	100
			Single-catch	6.29 (4.09)	-11.16 (1.98)	-1.93 (1.35)	100

Notes: Relative % bias is shown for each parameter followed by the standard error in parentheses. The DT models use 5 or 10 occasions of 24 hours. Twenty single-catch traps spaced 100 m apart are used with $g_0 = 0.2$ and $\sigma = 100$. The CT model uses a constant hazard that is consistent with a half-normal detection function shape over an interval of 24 hours. Results are reported on the natural scale and "Reps" is number of replications out of 100 where any replications that did not converge or estimated negative or very large variances for any parameter were excluded.

B.2 Simulation II: Comparing the two estimators with density correctly specified

Table B.8: Relative bias (RB) of density and detection parameters estimated by the DT multi and the CT single-catch trap estimators with a constant hazard. All models specify an exponential density model. The data are simulated for a survey duration of $T = 120$ or 240 hours from different exponential density gradients and a constant hazard.

Scenario	Model	$RB_{\hat{D}_{slope}}(\%)$	$RB_{\hat{g}_0}(\%)$	$RB_{\hat{\sigma}}(\%)$	$RB_{\hat{D}_F}(\%)$	$RB_{\hat{D}_R}(\%)$
		5 occasions				
Sc.E1	Multi-catch	-62.29 (1.22)	-66.84 (0.37)	-0.77 (0.65)	-2.09 (0.96)	0.71 (0.99)
	Single-catch	2.54 (2.43)	3.18 (1.04)	0.43 (0.65)	4.30 (1.08)	2.98 (1.03)
Sc.E2	Multi-catch	-42.18 (1.11)	-53.79 (0.46)	0.23 (0.63)	-4.59 (0.95)	0.99 (1.02)
	Single-catch	2.53 (1.76)	1.67 (0.98)	0.64 (0.62)	4.29 (1.11)	2.44 (1.06)
Sc.E3	Multi-catch	-27.56 (1.16)	-40.08 (0.67)	0.56 (0.67)	-6.13 (1.01)	0.84 (1.10)
	Single-catch	2.66 (1.56)	6.21 (1.12)	0.58 (0.65)	3.74 (1.27)	1.03 (1.14)
Sc.E4	Multi-catch	-21.04 (2.61)	-32.72 (0.72)	-0.58 (0.67)	1.61 (1.14)	1.79 (1.14)
	Single-catch	4.00 (3.40)	3.96 (1.06)	-0.27 (0.65)	5.39 (1.21)	2.95 (1.14)
Sc.E5	Multi-catch	-8.40 (1.33)	-18.55 (1.20)	1.93 (1.15)	2.73 (2.26)	7.21 (2.02)
	Single-catch	5.45 (1.53)	9.36 (1.60)	0.42 (1.14)	14.72 (2.79)	7.12 (2.06)
		10 occasions				
Sc.E1	Multi-catch	-47.76 (1.24)	-68.23 (0.20)	-0.79 (0.36)	-2.58 (0.57)	-0.28 (0.59)
	Single-catch	2.00 (2.05)	0.84 (0.57)	0.21 (0.35)	1.92 (0.61)	1.06 (0.60)
Sc.E2	Multi-catch	-32.75 (1.05)	-54.80 (0.27)	-0.19 (0.35)	-4.84 (0.64)	-0.31 (0.70)
	Single-catch	-0.09 (1.44)	0.86 (0.54)	-0.16 (0.33)	1.83 (0.72)	1.01 (0.71)
Sc.E3	Multi-catch	-20.08 (0.95)	-43.61 (0.36)	0.63 (0.39)	-5.31 (0.76)	0.19 (0.86)
	Single-catch	2.33 (1.18)	0.54 (0.63)	-0.11 (0.37)	2.73 (0.88)	1.16 (0.88)
Sc.E4	Multi-catch	-11.67 (2.41)	-35.14 (0.43)	0.00 (0.41)	-0.78 (0.80)	-0.88 (0.82)
	Single-catch	7.27 (2.88)	1.28 (0.65)	0.19 (0.40)	1.78 (0.83)	-0.06 (0.83)
Sc.E5	Multi-catch	-5.32 (1.27)	-22.77 (0.83)	0.77 (0.62)	-2.39 (1.26)	2.18 (1.50)
	Single-catch	5.09 (1.40)	4.40 (1.10)	-0.91 (0.59)	5.74 (1.41)	2.21 (1.51)

Notes: Relative % bias is shown for each parameter followed by the standard error in parentheses. The DT models use 5 or 10 occasions of 24 hours. Twenty single-catch traps spaced 100 m apart are used with $g_0 = 0.2$ and $\sigma = 100$. $RB_{\hat{D}_{slope}}$ is the relative bias in the slope parameter from the exponential density model, $RB_{\hat{D}}$ is the relative bias in mean density over a defined area where F refers to the full area (with $2 \times \sigma$) and R to the area spanned by the trap array. The CT model uses a constant hazard that is consistent with a half-normal detection function shape over an interval of 24 hours. In all cases, except the last scenario, 500 replications were run and converged (scenario 5 had 497 and 496 replications for 5 and 10 occasions respectively). Results are reported on the natural scale.

Table B.9: Relative bias (RB) of density and detection parameters estimated by the DT multi and the CT single-catch trap estimators with a constant hazard. All models specify a quadratic density model. The data are simulated for a survey duration of $T = 120$ or 240 hours from different quadratic density surfaces and a constant hazard.

Scenario	Model	$RB_{\hat{g}_0}(\%)$	$RB_{\hat{\sigma}}(\%)$	$RB_{\hat{D}_F}(\%)$	$RB_{\hat{D}_R}(\%)$	Reps
		5 occasions				
Sc.Q1	Multi-catch	-69.54 (0.33)	1.80 (0.66)	5.50 (0.98)	-10.04 (0.86)	500
	Single-catch	3.19 (1.01)	1.28 (0.62)	4.95 (0.97)	1.78 (1.10)	500
Sc.Q2	Multi-catch	-57.22 (0.47)	6.98 (0.69)	1.59 (0.90)	-16.56 (0.67)	500
	Single-catch	4.68 (1.05)	-0.77 (0.51)	2.98 (0.86)	0.56 (0.87)	481
Sc.Q3	Multi-catch	-59.58 (0.46)	4.62 (0.74)	-5.02 (0.88)	-5.95 (0.95)	486
	Single-catch	3.68 (1.09)	1.16 (0.68)	4.79 (1.07)	0.00 (1.24)	457
Sc.Q4	Multi-catch	-36.06 (0.67)	1.34 (0.64)	2.69 (1.02)	-5.38 (0.97)	500
	Single-catch	3.56 (1.05)	-0.06 (0.60)	3.18 (1.00)	2.18 (1.12)	497
Sc.Q5	Multi-catch	-33.91 (0.74)	2.10 (0.69)	0.47 (1.02)	-5.19 (1.07)	499
	Single-catch	4.19 (1.12)	1.06 (0.66)	2.86 (1.06)	0.09 (1.20)	495
Sc.Q6	Multi-catch	-27.90 (0.81)	2.26 (0.72)	2.20 (1.08)	-6.45 (1.03)	473
	Single-catch	7.28 (1.16)	-0.94 (0.67)	4.49 (1.13)	0.09 (1.20)	432
Sc.Q7	Multi-catch	-28.98 (0.84)	1.70 (0.75)	2.72 (1.11)	-6.24 (1.11)	462
	Single-catch	6.78 (1.32)	-0.81 (0.76)	5.37 (1.19)	-1.63 (1.27)	417
		10 occasions				
Sc.Q1	Multi-catch	-70.41 (0.20)	0.80 (0.37)	3.31 (0.66)	-7.88 (0.61)	500
	Single-catch	0.72 (0.58)	0.17 (0.35)	2.48 (0.63)	1.11 (0.73)	500
Sc.Q2	Multi-catch	-59.20 (0.28)	7.38 (0.37)	-1.09 (0.63)	-14.70 (0.52)	500
	Single-catch	0.95 (0.53)	0.33 (0.29)	1.25 (0.62)	0.26 (0.65)	500
Sc.Q3	Multi-catch	-60.36 (0.29)	3.89 (0.42)	-5.12 (0.63)	-6.85 (0.72)	500
	Single-catch	2.62 (0.61)	-0.43 (0.36)	1.46 (0.71)	0.24 (0.85)	498
Sc.Q4	Multi-catch	-38.01 (0.41)	1.72 (0.37)	0.64 (0.80)	-5.84 (0.80)	500
	Single-catch	1.38 (0.62)	0.46 (0.35)	1.21 (0.79)	0.41 (0.91)	500
Sc.Q5	Multi-catch	-36.07 (0.47)	1.37 (0.39)	-1.59 (0.77)	-5.48 (0.84)	500
	Single-catch	1.31 (0.66)	-0.08 (0.37)	0.30 (0.79)	-0.11 (0.95)	500
Sc.Q6	Multi-catch	-31.70 (0.52)	4.03 (0.45)	-0.66 (0.87)	-6.85 (0.84)	495
	Single-catch	2.15 (0.71)	0.82 (0.41)	1.48 (0.90)	-0.49 (0.95)	486
Sc.Q7	Multi-catch	-32.21 (0.49)	2.58 (0.44)	0.50 (0.87)	-4.95 (0.88)	493
	Single-catch	2.56 (0.70)	0.02 (0.42)	2.92 (0.92)	0.79 (1.01)	478

Notes: Relative % bias is shown for each parameter followed by the standard error in parentheses. The DT models use 5 or 10 occasions of 24 hours. Twenty single-catch traps spaced 100 m apart are used with $g_0 = 0.2$ and $\sigma = 100$. $RB_{\hat{D}}$ is the relative bias in mean density over a defined area where F refers to the full area (with $2 \times \sigma$) and R to the area spanned by the trap array. The CT model uses a constant hazard that is consistent with a half-normal detection function shape over an interval of 24 hours. Results are reported on the natural scale and "Reps" is number of replications out of 500 where any replications that did not converge or estimated negative or very large variances for any parameter were excluded.

Appendix C

Tables from Chapter 4 simulations

C.1 Proximity detectors

C.1.1 Synchronous cosine simulations

Table C.1: Relative bias (RB) of density and detection parameters estimated by the DT binary and the CT proximity detector models with a constant hazard and a 24 hour cosine hazard. All models specify constant density. The data are simulated for a survey duration of T = 2,160 hours with constant density and a 24 hour cosine hazard.

Scenario	Model	$RB_{\hat{D}}(\%)$	$RB_{\hat{g}_0}(\%)$	$RB_{\hat{\sigma}}(\%)$	$RB_{\psi_1}(\%)$	$RB_{\psi_2}(\%)$	Reps
Px.C1: D = 8	DT	0.10 (0.79)	0.48 (0.45)	-0.17 (0.20)	NA	NA	498
	Constant hazard	0.08 (0.79)	0.51 (0.44)	-0.20 (0.20)	NA	NA	500
	Cosine hazard	0.08 (0.79)	0.51 (0.44)	-0.20 (0.20)	0.77 (5.48)	-0.14 (0.34)	500
Px.C2: D = 4	DT	0.58 (1.17)	0.80 (0.71)	-0.30 (0.31)	NA	NA	494
	Constant hazard	0.41 (1.16)	0.44 (0.68)	-0.25 (0.31)	NA	NA	500
	Cosine hazard	0.83 (1.16)	0.47 (0.68)	-0.23 (0.31)	4.26 (7.99)	0.26 (0.48)	493
Px.C3: D = 2	DT	2.66 (1.82)	1.03 (1.03)	-1.24 (0.56)	NA	NA	494
	Constant hazard	2.43 (1.81)	0.94 (1.02)	-1.22 (0.56)	NA	NA	500
	Cosine hazard	3.26 (1.88)	1.15 (1.02)	-1.19 (0.58)	8.89 (13.98)	0.71 (0.70)	470

Notes: Relative % bias is shown for each parameter followed by the standard error in parentheses. The DT models use 90 occasions of 24 hours. Twenty proximity detectors spaced 3,000m apart are used with $g_0 = 0.05$ and $\sigma = 2,400$. The CT model uses either a constant or a cosine hazard that is consistent with a half-normal detection function shape over an interval of 24 hours. Results are reported on the natural scale and "Reps" is number of replications out of 500 where any replications that did not converge or estimated negative or very large variances for any parameter were excluded.

Table C.2: Relative bias (RB) of density and detection parameters estimated by the DT binary and the CT proximity detector models with a constant hazard and a 24 hour cosine hazard. All models specify constant density. The data are simulated for a survey duration of T = 2,160 hours with a constant density of 4 per 100 km^2 and a 24 hour cosine hazard with 3 levels for g_0.

Scenario	Model	RB$_{\hat{D}}$(%)	RB$_{\hat{g}_0}$(%)	RB$_{\hat{\sigma}}$(%)	RB$_{\psi_1}$(%)	RB$_{\psi_2}$(%)	Reps
Px.C2 ($g_0 = 0.5$)	DT	-0.18 (0.93)	-0.05 (0.16)	-0.21 (0.09)	NA	NA	492
	Constant hazard	2.27 (0.98)	-5.39 (0.45)	-2.29 (0.23)	NA	NA	470
	Cosine hazard	2.45 (1.00)	-4.66 (0.42)	-2.10 (0.21)	0.69 (3.90)	0.30 (0.25)	478
Px.C2 ($g_0 = 0.2$)	DT	0.09 (0.95)	0.30 (0.30)	0.22 (0.14)	NA	NA	489
	Constant hazard	-0.02 (0.93)	0.17 (0.29)	0.14 (0.14)	NA	NA	500
	Cosine hazard	-0.02 (0.93)	0.17 (0.29)	0.14 (0.14)	3.13 (3.70)	0.24 (0.21)	500
Px.C2 ($g_0 = 0.1$)	DT	-1.79 (1.02)	-0.06 (0.44)	-0.02 (0.21)	NA	NA	488
	Constant hazard	-2.11 (1.01)	0.00 (0.42)	-0.04 (0.21)	NA	NA	500
	Cosine hazard	-2.07 (1.01)	0.01 (0.42)	-0.05 (0.21)	-5.05 (5.76)	0.47 (0.36)	498

Notes: Relative % bias is shown for each parameter followed by the standard error in parentheses. The DT models use 90 occasions of 24 hours. Twenty proximity detectors spaced 3,000m apart are used with $\sigma = 2,400$. The CT model uses either a constant or a cosine hazard that is consistent with a half-normal detection function shape over an interval of 24 hours. Results are reported on the natural scale and "Reps" is number of replications out of 500 where any replications that did not converge or estimated negative or very large variances for any parameter were excluded.

Table C.3: Relative bias (RB) of density and detection parameters estimated by the DT binary and the CT proximity detector models with a constant hazard and a 24 hour cosine hazard. All models specify exponential density. The data are simulated for a survey duration of T = 2,160 hours from different exponential density gradients and a 24 hour cosine hazard.

Scenario	Model	$\text{RB}_{\hat{D}_{slope}}(\%)$	$\text{RB}_{\hat{g}_0}(\%)$	$\text{RB}_{\hat{\sigma}}(\%)$	$\text{RB}_{\hat{D}_F}(\%)$	$\text{RB}_{\hat{D}_R}(\%)$	Reps
Px.E1	DT	2.06 (2.70)	0.36 (0.41)	-0.43 (0.21)	2.03 (0.81)	0.71 (0.82)	491
	Constant hazard	2.11 (2.70)	0.41 (0.40)	-0.40 (0.20)	1.99 (0.81)	0.63 (0.81)	500
	Cosine hazard	1.77 (2.68)	0.43 (0.40)	-0.39 (0.20)	2.01 (0.81)	0.69 (0.81)	499
Px.E2	DT	-2.48 (2.11)	-0.48 (0.54)	-0.02 (0.26)	1.17 (0.94)	0.07 (0.96)	488
	Constant hazard	-1.55 (2.11)	-0.42 (0.52)	0.11 (0.25)	0.67 (0.94)	-0.58 (0.97)	500
	Cosine hazard	-1.52 (2.12)	-0.52 (0.52)	0.12 (0.26)	0.85 (0.94)	-0.40 (0.97)	497
Px.E3	DT	-2.55 (3.69)	2.00 (0.59)	-0.52 (0.28)	0.97 (0.99)	-0.91 (1.00)	493
	Constant hazard	-2.78 (3.67)	1.93 (0.58)	-0.43 (0.28)	0.77 (0.98)	-1.11 (1.00)	500
	Cosine hazard	-2.21 (3.67)	2.01 (0.58)	-0.39 (0.28)	0.94 (0.98)	-0.96 (1.00)	497

Notes: Relative % bias is shown for each parameter followed by the standard error in parentheses. The DT models use 90 occasions of 24 hours. Twenty proximity detectors spaced 3,000 m apart are used with $g_0 = 0.05$ and $\sigma = 2,400$. $\text{RB}_{\hat{D}_{slope}}$ is the relative bias in the slope parameter from the exponential density model, $\text{RB}_{\hat{D}}$ is the relative bias in mean density over a defined area where $_F$ refers to the full area (with $2 \times \sigma$) and $_R$ to the area spanned by the trap array. The CT model uses either a constant or a cosine hazard that is consistent with a half-normal detection function shape over an interval of 24 hours. Results are reported on the natural scale and "Reps" is number of replications out of 500 where any replications that did not converge or estimated negative or very large variances for any parameter were excluded.

Table C.4: Relative bias (RB) of density and detection parameters estimated by the DT binary and the CT proximity detector models with a constant hazard and a 24 hour cosine hazard. All models specify quadratic density. The data are simulated for a survey duration of T = 2,160 hours from different quadratic density surfaces and a 24 hour cosine hazard.

Scenario	Model	$RB_{\hat{g}_0}(\%)$	$RB_{\hat{\sigma}}(\%)$	$RB_{\hat{D}_F}(\%)$	$RB_{\hat{D}_R}(\%)$	Reps
Px.Q1	DT	0.17 (0.41)	-0.05 (0.19)	-0.29 (0.78)	-0.48 (0.90)	491
	Constant hazard	0.20 (0.40)	-0.06 (0.19)	-0.44 (0.77)	-0.60 (0.89)	500
	Cosine hazard	0.20 (0.40)	-0.06 (0.19)	-0.44 (0.77)	-0.60 (0.89)	500
Px.Q2	DT	0.04 (0.46)	0.20 (0.21)	0.04 (0.96)	-0.78 (0.98)	481
	Constant hazard	0.02 (0.46)	0.20 (0.21)	-0.27 (0.95)	-0.99 (0.96)	495
	Cosine hazard	0.07 (0.46)	0.19 (0.21)	-0.15 (0.95)	-0.87 (0.96)	493
Px.Q3	DT	-0.14 (0.49)	-0.38 (0.24)	0.05 (0.89)	-0.33 (1.00)	463
	Constant hazard	-0.28 (0.47)	-0.26 (0.23)	0.28 (0.87)	0.06 (0.98)	486
	Cosine hazard	-0.26 (0.47)	-0.27 (0.23)	0.37 (0.88)	0.10 (0.98)	484

Notes: Relative % bias is shown for each parameter followed by the standard error in parentheses. The DT models use 90 occasions of 24 hours. Twenty proximity detectors spaced 3,000 m apart are used with $g_0 = 0.05$ and $\sigma = 2,400$. $RB_{\hat{D}_{slope}}$ is the relative bias in the slope parameter from the exponential density model, $RB_{\hat{D}}$ is the relative bias in mean density over a defined area where $_F$ refers to the full area (with $2 \times \sigma$) and $_R$ to the area spanned by the trap array. The CT model uses either a constant or a cosine hazard that is consistent with a half-normal detection function shape over an interval of 24 hours. Results are reported on the natural scale and "Reps" is number of replications out of 500 where any replications that did not converge or estimated negative or very large variances for any parameter were excluded.

C.1.2 Synchronous spline simulations

Table C.5: Relative bias (RB) of density and detection parameters estimated by the DT binary and the CT proximity detector models with a 24 hour cyclic cubic spline hazard with K = 4 or K = 8. All models specify constant density. The data are simulated for a survey duration of T = 2,160 hours with constant density and a 24 hour cyclic cubic spline hazard with K = 4 or K = 8.

Scenario	Model	$RB_{\hat{D}}(\%)$	$RB_{\hat{g}_0}(\%)$	$RB_{\hat{\sigma}}(\%)$
		K = 4		
Px.C1: D = 8	DT	0.45 (1.27)	-0.03 (0.66)	-0.16 (0.30)
	Spline hazard	0.44 (1.26)	-0.15 (0.65)	-0.14 (0.30)
Px.C2: D = 4	DT	3.19 (1.70)	0.54 (1.03)	-0.63 (0.49)
	Spline hazard	3.18 (1.70)	0.47 (1.01)	-0.60 (0.49)
Px.C3: D = 2	DT	0.01 (2.42)	-1.39 (1.48)	-1.18 (0.72)
	Spline hazard	-0.01 (2.42)	-1.32 (1.48)	-1.18 (0.72)
		K = 8		
Px.C1: D = 8	DT	1.25 (1.30)	0.00 (0.64)	-0.02 (0.34)
	Spline hazard	1.27 (1.30)	0.03 (0.64)	-0.04 (0.34)
Px.C2: D = 4	DT	2.29 (1.94)	1.92 (0.95)	-0.95 (0.55)
	Spline hazard	2.28 (1.93)	1.88 (0.93)	-0.97 (0.54)
Px.C3: D = 2	DT	3.48 (2.48)	1.70 (1.67)	-1.07 (0.77)
	Spline hazard	3.37 (2.48)	1.28 (1.68)	-0.92 (0.76)

Notes: Relative % bias is shown for each parameter followed by the standard error in parentheses. The DT models use 90 occasions of 24 hours. Twenty proximity detectors spaced 3,000 m apart are used with $g_0 = 0.05$ and $\sigma = 2,400$. The CT model uses a time-varying spline hazard that is consistent with a half-normal detection function shape over an interval of 24 hours. In all cases 200 replications were run and converged and results are reported on the natural scale.

Table C.6: Relative bias (RB) of density and detection parameters estimated by the DT binary and the CT proximity detector models with a 24 hour cyclic cubic spline hazard with K = 4 or K = 8. All models specify exponential density. The data are simulated for a survey duration of T = 2,160 hours from different exponential density gradients and a 24 hour cyclic cubic spline hazard with K = 4 or K = 8.

Scenario	Model	$\text{RB}_{\hat{D}_{slope}}(\%)$	$\text{RB}_{\hat{g}_0}(\%)$	$\text{RB}_{\hat{\sigma}}(\%)$	$\text{RB}_{\hat{D}_F}(\%)$	$\text{RB}_{\hat{D}_R}(\%)$
				K = 4		
Px.E1	DT	-0.54 (4.30)	-0.33 (0.59)	-0.09 (0.30)	-1.60 (1.12)	-2.68 (1.15)
	Spline hazard	-0.50 (4.30)	-0.30 (0.58)	-0.09 (0.30)	-1.60 (1.12)	-2.69 (1.15)
Px.E2	DT	-0.48 (3.16)	0.12 (0.89)	-0.24 (0.42)	-1.69 (1.46)	-3.05 (1.48)
	Spline hazard	-0.51 (3.16)	0.28 (0.88)	-0.28 (0.42)	-1.67 (1.46)	-3.03 (1.48)
Px.E3	DT	5.88 (6.12)	0.36 (0.96)	-0.10 (0.46)	3.68 (1.79)	0.92 (1.82)
	Spline hazard	5.90 (6.12)	0.27 (0.95)	-0.08 (0.46)	3.66 (1.78)	0.90 (1.81)
				K = 8		
Px.E1	DT	-4.90 (4.10)	-0.17 (0.69)	-0.45 (0.33)	1.32 (1.19)	0.46 (1.17)
	Spline hazard	-4.91 (4.10)	-0.31 (0.67)	-0.41 (0.33)	1.30 (1.19)	0.44 (1.17)
Px.E2	DT	3.96 (3.42)	1.28 (0.87)	0.33 (0.39)	-1.06 (1.56)	-3.25 (1.61)
	Spline hazard	4.04 (3.42)	1.31 (0.86)	0.29 (0.39)	-1.03 (1.56)	-3.24 (1.60)
Px.E3	DT	1.74 (6.67)	1.54 (0.95)	0.00 (0.48)	-0.81 (1.78)	-3.47 (1.80)
	Spline hazard	1.73 (6.68)	1.50 (0.94)	0.00 (0.47)	-0.80 (1.78)	-3.47 (1.81)

Notes: Relative % bias is shown for each parameter followed by the standard error in parentheses. The DT models use 90 occasions of 24 hours. Twenty proximity detectors spaced 3,000 m apart are used with $g_0 = 0.05$ and $\sigma = 2,400$. $\text{RB}_{\hat{D}_{slope}}$ is the relative bias in the slope parameter from the exponential density model, $\text{RB}_{\hat{D}}$ is the relative bias in mean density over a defined area where $_F$ refers to the full area (with $2 \times \sigma$) and $_R$ to the area spanned by the trap array. The CT model uses a time-varying spline hazard that is consistent with a half-normal detection function shape over an interval of 24 hours. In all cases 200 replications were run and converged and results are reported on the natural scale.

Table C.7: Relative bias (RB) of density and detection parameters estimated by the DT binary and the CT proximity detector models with a 24 hour cyclic cubic spline hazard with K = 4 or K = 8. All models specify quadratic density. The data are simulated for a survey duration of T = 2,160 hours from different quadratic density surfaces and a 24 hour cyclic cubic spline hazard with K = 4 or K = 8.

Scenario	Model	$\text{RB}_{\hat{g}_0}(\%)$	$\text{RB}_{\hat{\sigma}}(\%)$	$\text{RB}_{\hat{D}_F}(\%)$	$\text{RB}_{\hat{D}_R}(\%)$
		K = 4			
Px.Q1	DT	-0.23 (0.62)	-0.02 (0.30)	-1.11 (1.27)	-0.98 (1.26)
	Spline hazard	-0.15 (0.61)	-0.08 (0.29)	-1.08 (1.27)	-0.91 (1.26)
Px.Q2	DT	1.52 (0.64)	-0.14 (0.28)	1.09 (1.36)	0.27 (1.38)
	Spline hazard	1.49 (0.63)	-0.15 (0.28)	1.09 (1.36)	0.29 (1.38)
Px.Q3	DT	-1.03 (0.68)	0.74 (0.34)	-2.50 (1.56)	-2.22 (1.60)
	Spline hazard	-1.04 (0.68)	0.75 (0.34)	-2.50 (1.56)	-2.21 (1.61)
		K = 8			
Px.Q1	DT	0.65 (0.65)	-0.34 (0.33)	0.10 (1.23)	-1.21 (1.38)
	Spline hazard	0.64 (0.66)	-0.34 (0.33)	0.10 (1.23)	-1.20 (1.38)
Px.Q2	DT	0.46 (0.71)	-0.01 (0.33)	1.32 (1.38)	0.86 (1.42)
	Spline hazard	0.64 (0.71)	-0.07 (0.33)	1.34 (1.38)	0.85 (1.42)
Px.Q3	DT	1.28 (0.72)	-0.23 (0.32)	0.96 (1.38)	0.67 (1.55)
	Spline hazard	1.23 (0.72)	-0.21 (0.32)	0.96 (1.38)	0.63 (1.55)

Notes: Relative % bias is shown for each parameter followed by the standard error in parentheses. The DT models use 90 occasions of 24 hours. Twenty proximity detectors spaced 3,000 m apart are used with $g_0 = 0.05$ and $\sigma = 2,400$. $\text{RB}_{\hat{D}}$ is the relative bias in mean density over a defined area where $_F$ refers to the full area (with $2 \times \sigma$) and $_R$ to the area spanned by the trap array. The CT model uses a time-varying spline hazard that is consistent with a half-normal detection function shape over an interval of 24 hours. In all cases 200 replications were run and converged and results are reported on the natural scale.

C.1.3 Asynchronous spline simulations

Table C.8: Relative bias (RB) of density and detection parameters estimated by the DT binary and the CT proximity detector models with a 30 hour cyclic cubic spline hazard with K = 4 or K = 8. All models specify constant density. The data are simulated for a survey duration of T = 2,160 hours with constant density and a 30 hour cyclic cubic spline hazard with K = 4 or K = 8.

Scenario	Model	$RB_{\hat{D}}(\%)$	$RB_{\hat{g}_0}(\%)$	$RB_{\hat{\sigma}}(\%)$
		K = 4		
Px.C1: D = 8	DT	0.63 (1.30)	-15.10 (0.61)	0.03 (0.36)
	Spline hazard	0.64 (1.30)	-0.04 (0.72)	0.04 (0.36)
Px.C2: D = 4	DT	0.88 (1.60)	-14.88 (0.90)	0.28 (0.57)
	Spline hazard	0.90 (1.59)	0.09 (1.07)	0.30 (0.57)
Px.C3: D = 2	DT	5.56 (2.64)	-14.51 (1.45)	-1.70 (0.81)
	Spline hazard	5.56 (2.63)	0.13 (1.66)	-1.63 (0.81)
		K = 8		
Px.C1: D = 8	DT	-0.90 (1.37)	-14.50 (0.63)	-0.33 (0.37)
	Spline hazard	-0.87 (1.37)	1.99 (0.75)	-0.34 (0.37)
Px.C2: D = 4	DT	1.56 (1.73)	-14.84 (0.94)	-0.33 (0.51)
	Spline hazard	1.57 (1.73)	1.40 (1.09)	-0.32 (0.51)
Px.C3: D = 2	DT	5.05 (2.61)	-15.81 (1.51)	-1.42 (0.84)
	Spline hazard	4.83 (2.61)	0.15 (1.73)	-1.24 (0.83)

Notes: Relative % bias is shown for each parameter followed by the standard error in parentheses. The DT models use 90 occasions of 24 hours. Twenty proximity detectors spaced 3,000 m apart are used with $g_0 = 0.05$ and $\sigma = 2,400$. The CT model uses a time-varying spline hazard that is consistent with a half-normal detection function shape over for the first 24 hour occasion. In all cases 200 replications were run and converged and results are reported on the natural scale.

Table C.9: Relative bias (RB) of density and detection parameters estimated by the DT binary and the CT proximity detector models with a 30 hour cyclic cubic spline hazard with K = 4 or K = 8. All models specify exponential density. The data are simulated for a survey duration of T = 2,160 hours from different exponential density gradients and a 30 hour cyclic cubic spline hazard with K = 4 or K = 8.

Scenario	Model	$RB_{\hat{D}_{slope}}(\%)$	$RB_{\hat{g}_0}(\%)$	$RB_{\hat{\sigma}}(\%)$	$RB_{\hat{D}_F}(\%)$	$RB_{\hat{D}_R}(\%)$
				K = 4		
Px.E1	DT	1.47 (3.99)	-14.78 (0.59)	0.68 (0.38)	0.80 (1.24)	-0.30 (1.26)
	Spline hazard	1.40 (3.98)	0.35 (0.71)	0.75 (0.38)	0.76 (1.24)	-0.33 (1.26)
Px.E2	DT	13.24 (3.70)	-14.14 (0.81)	-0.55 (0.47)	4.20 (1.61)	-0.24 (1.62)
	Spline hazard	13.25 (3.70)	0.97 (0.93)	-0.48 (0.47)	4.16 (1.61)	-0.28 (1.62)
Px.E3	DT	5.79 (7.20)	-15.87 (0.82)	-1.58 (0.49)	4.77 (1.78)	1.50 (1.86)
	Spline hazard	5.65 (7.18)	-1.20 (0.97)	-1.49 (0.49)	4.72 (1.77)	1.47 (1.85)
				K = 8		
Px.E1	DT	-0.20 (3.83)	-15.84 (0.58)	-0.26 (0.34)	2.13 (1.16)	1.15 (1.16)
	Spline hazard	-0.22 (3.83)	0.31 (0.68)	-0.21 (0.34)	2.11 (1.16)	1.14 (1.16)
Px.E2	DT	0.08 (3.49)	-16.35 (0.81)	0.39 (0.45)	1.36 (1.48)	-0.27 (1.54)
	Spline hazard	0.05 (3.49)	-0.49 (0.94)	0.41 (0.44)	1.38 (1.48)	-0.25 (1.54)
Px.E3	DT	-0.96 (6.72)	-16.39 (0.81)	-0.12 (0.55)	3.46 (1.79)	0.81 (1.83)
	Spline hazard	-0.90 (6.72)	-0.52 (0.96)	-0.06 (0.55)	3.42 (1.78)	0.77 (1.83)

Notes: Relative % bias is shown for each parameter followed by the standard error in parentheses. The DT models use 90 occasions of 24 hours. Twenty proximity detectors spaced 3,000 m apart are used with $g_0 = 0.05$ and $\sigma = 2,400$. $RB_{\hat{D}_{slope}}$ is the relative bias in the slope parameter from the exponential density model, $RB_{\hat{D}}$ is the relative bias in mean density over a defined area where $_F$ refers to the full area (with $2 \times \sigma$) and $_R$ to the area spanned by the trap array. The CT model uses a time-varying spline hazard that is consistent with a half-normal detection function shape over for the first 24 hour occasion. In all cases 200 replications were run and converged and results are reported on the natural scale.

Table C.10: Relative bias (RB) of density and detection parameters estimated by the DT binary and the CT proximity detector models with a 30 hour cyclic cubic spline hazard with K = 4 or K = 8. All models specify quadratic density. The data are simulated for a survey duration of T = 2,160 hours from different quadratic density surfaces and a 30 hour cyclic cubic spline hazard with K = 4 or K = 8.

Scenario	Model	$\text{RB}_{\hat{g}_0}(\%)$	$\text{RB}_{\hat{\sigma}}(\%)$	$\text{RB}_{\hat{D}_F}(\%)$	$\text{RB}_{\hat{D}_R}(\%)$
		K = 4			
Px.Q1	DT	-14.11 (0.58)	0.07 (0.33)	-0.11 (1.25)	-2.15 (1.30)
	Spline hazard	0.90 (0.68)	0.12 (0.33)	-0.13 (1.25)	-2.13 (1.30)
Px.Q2	DT	-15.52 (0.59)	0.43 (0.35)	0.91 (1.36)	-0.26 (1.35)
	Spline hazard	-0.49 (0.69)	0.38 (0.35)	1.18 (1.34)	0.00 (1.33)
Px.Q3	DT	-13.63 (0.68)	-0.74 (0.37)	0.40 (1.44)	0.25 (1.59)
	Spline hazard	1.64 (0.79)	-0.69 (0.37)	0.41 (1.44)	0.25 (1.59)
		K = 8			
Px.Q1	DT	-15.95 (0.59)	-0.03 (0.30)	0.81 (1.31)	-2.07 (1.45)
	Spline hazard	0.10 (0.67)	0.03 (0.30)	0.77 (1.31)	-2.09 (1.45)
Px.Q2	DT	-15.93 (0.60)	-0.09 (0.33)	0.33 (1.33)	-0.60 (1.39)
	Spline hazard	0.08 (0.71)	0.00 (0.33)	0.30 (1.33)	-0.60 (1.39)
Px.Q3	DT	-15.17 (0.68)	-0.54 (0.33)	-0.32 (1.40)	-1.16 (1.60)
	Spline hazard	1.25 (0.82)	-0.55 (0.33)	-0.30 (1.40)	-1.17 (1.61)

Notes: Relative % bias is shown for each parameter followed by the standard error in parentheses. The DT models use 90 occasions of 24 hours. Twenty proximity detectors spaced 3,000 m apart are used with $g_0 = 0.05$ and $\sigma = 2,400$. $\text{RB}_{\hat{D}}$ is the relative bias in mean density over a defined area where $_F$ refers to the full area (with $2 \times \sigma$) and $_R$ to the area spanned by the trap array. The CT model uses a varying hazard that is consistent with a half-normal detection function shape over for the first 24 hour occasion. In all cases 200 replications were run and converged and results are reported on the natural scale.

Table C.11: Relative bias (RB) of density and detection parameters estimated by the DT binary and the CT proximity detector models with either a 30 day or 90 day cyclic cubic spline detection hazard with K = 4 or K = 8. All models specify the correct density surface. The data are simulated for a survey duration of T = 2,160 hours from different density surfaces with either a 30 day or 90 day cyclic cubic spline detection hazard with K = 4 or K = 8.

Scenario	Model	$\text{RB}_{\hat{D}/D_{slope}}(\%)$	$\text{RB}_{\hat{g}_0}(\%)$	$\text{RB}_{\hat{\sigma}}(\%)$	$\text{RB}_{\hat{D}_F}(\%)$	$\text{RB}_{\hat{D}_R}(\%)$
		30 day cyclic hazard with 3 cycles				
Px.C2	DT	2.07 (1.45)	834.76 (5.51)	1.09 (0.31)	NA	NA
	Spline hazard	2.43 (1.46)	3.27 (4.20)	-0.31 (0.30)	NA	NA
Px.E2	DT	6.76 (3.24)	848.01 (6.07)	1.47 (0.28)	0.80 (1.27)	-1.54 (1.41)
	Spline hazard	7.14 (3.25)	-6.21 (2.83)	0.09 (0.28)	1.18 (1.28)	-1.24 (1.41)
Px.Q2	DT	NA	848.43 (3.63)	1.44 (0.22)	-0.88 (1.35)	-1.53 (1.37)
	Spline hazard	NA	0.04 (2.48)	0.03 (0.22)	-0.63 (1.35)	-1.35 (1.37)
		90 day cyclic hazard with 1 cycle				
Px.C2	DT	1.20 (1.60)	849.51 (6.66)	1.06 (0.33)	NA	NA
	Spline hazard	1.46 (1.60)	6.33 (3.99)	-0.13 (0.31)	NA	NA
Px.E2	DT	6.06 (3.04)	847.33 (5.15)	1.10 (0.26)	0.04 (1.30)	-2.45 (1.28)
	Spline hazard	6.29 (3.04)	2.97 (3.03)	-0.14 (0.26)	0.39 (1.30)	-2.15 (1.28)
Px.Q2	DT	NA	846.11 (3.65)	1.07 (0.19)	-1.95 (1.31)	-2.31 (1.39)
	Spline hazard	NA	5.97 (2.78)	-0.23 (0.19)	-1.72 (1.32)	-2.10 (1.39)

Notes: Relative % bias is shown for each parameter followed by the standard error in parentheses. The DT models use 90 occasions of 24 hours. Twenty proximity detectors spaced 3,000 m apart are used with $g_0 = 0.05$ and $\sigma = 2,400$. $\text{RB}_{\hat{D}_{slope}}$ is the relative bias in the slope parameter from the exponential density model, $\text{RB}_{\hat{D}}$ is the relative bias in mean density over a defined area where $_F$ refers to the full area (with $2 \times \sigma$) and $_R$ to the area spanned by the trap array. The CT model uses a time-varying spline hazard that is consistent with a half-normal detection function shape over for the first 24 hour occasion. In all cases 200 replications were run and converged and results are reported on the natural scale.

C.2 Single-catch traps

Table C.12: Relative bias (RB) of density and detection parameters estimated by the DT multi and the CT single-catch trap estimators with a 30 hour cyclic cubic spline hazard with K = 4 or K = 6. All models specify constant density. The data are simulated for a survey duration of $T = 240$ hours with constant density and a 30 hour cyclic cubic spline hazard with K = 4 or K = 6.

Scenario	Model	$RB_{\hat{D}}(\%)$	$RB_{\hat{g}_0}(\%)$	$RB_{\hat{\sigma}}(\%)$
		K = 4		
Sc.C2: D = 2	Multi-catch	0.71 (2.33)	-59.90 (0.82)	-2.00 (1.14)
	Single-catch	1.43 (2.31)	3.87 (1.86)	-1.02 (1.12)
Sc.C3: D = 1	Multi-catch	-0.06 (2.59)	-43.14 (1.06)	0.91 (1.17)
	Single-catch	0.57 (2.60)	1.84 (2.13)	1.33 (1.15)
Sc.C4: D = 0.5	Multi-catch	-0.81 (3.19)	-30.84 (1.63)	0.29 (1.87)
	Single-catch	-0.22 (3.18)	0.25 (2.71)	0.12 (1.83)
		K = 6		
Sc.C2: D = 2	Multi-catch	-2.20 (2.06)	-60.22 (0.84)	-0.72 (1.00)
	Single-catch	-1.65 (2.05)	2.24 (1.75)	-0.07 (0.96)
Sc.C3: D = 1	Multi-catch	3.47 (2.02)	-43.54 (0.93)	-2.66 (1.10)
	Single-catch	4.03 (2.06)	-0.51 (1.55)	-2.11 (1.12)
Sc.C4: D = 0.5	Multi-catch	10.90 (4.20)	-30.66 (1.68)	-2.58 (1.75)
	Single-catch	10.68 (4.27)	0.53 (2.64)	-1.95 (1.74)

Notes: Relative % bias is shown for each parameter followed by the standard error in parentheses. The DT models use 10 occasions of 24 hours. Twenty single-catch traps spaced 100 m apart are used with $g_0 = 0.2$ and $\sigma = 100$. The CT model uses a time-varying spline hazard that is consistent with a half-normal detection function shape over an interval of 24 hours. In all cases 50 replications were run and converged. Results are reported on the natural scale.

Table C.13: Relative bias (RB) of density and detection parameters estimated by the DT multi and the CT single-catch trap estimators with a 30 hour cyclic cubic spline hazard with K = 4 or K = 6. All models specify constant density. The data are simulated for a survey duration of T = 240 hours with constant density, a 30 hour cyclic cubic spline hazard with K = 4 or K = 6, and a higher value for g_0 (0.4).

Scenario	Model	$\text{RB}_{\hat{D}}(\%)$	$\text{RB}_{\hat{g}_0}(\%)$	$\text{RB}_{\hat{\sigma}}(\%)$
		K = 4		
Sc.C2: D = 2	Multi-catch	4.41 (1.59)	-77.29 (0.44)	-3.52 (0.94)
	Single-catch	4.84 (1.59)	-0.69 (1.46)	-0.90 (0.94)
Sc.C3: D = 1	Multi-catch	1.42 (2.70)	-57.07 (1.01)	-1.65 (1.04)
	Single-catch	2.59 (2.74)	1.25 (1.60)	-0.13 (1.03)
Sc.C4: D = 0.5	Multi-catch	-1.67 (2.98)	-40.01 (1.35)	-0.08 (1.13)
	Single-catch	-1.37 (3.02)	0.54 (1.97)	0.97 (1.13)
		K = 6		
Sc.C2: D = 2	Multi-catch	0.78 (1.96)	-76.26 (0.56)	-3.13 (0.93)
	Single-catch	1.63 (1.98)	0.89 (1.44)	-0.78 (0.92)
Sc.C3: D = 1	Multi-catch	0.41 (2.56)	-58.09 (0.67)	-0.45 (1.15)
	Single-catch	1.09 (2.54)	0.67 (1.72)	1.28 (1.10)
Sc.C4: D = 0.5	Multi-catch	3.04 (2.99)	-38.91 (1.17)	-2.75 (1.22)
	Single-catch	3.26 (3.06)	2.42 (1.79)	-1.65 (1.26)

Notes: Relative % bias is shown for each parameter followed by the standard error in parentheses. The DT models use 10 occasions of 24 hours. Twenty single-catch traps spaced 100 m apart are used with $g_0 = 0.4$ and $\sigma = 100$. The CT model uses a time-varying spline hazard that is consistent with a half-normal detection function shape over an interval of 24 hours. In all cases 50 replications were run and converged. Results are reported on the natural scale.

Table C.14: Relative bias (RB) of density and detection parameters estimated by the DT multi and the CT single-catch trap estimators with a 30 hour cyclic cubic spline hazard with K = 4 or K = 6. All models specify an exponential density model. The data are simulated for a survey duration of $T = 240$ hours from different exponential density gradients and a 30 hour cyclic cubic spline hazard with K = 4 or K = 6.

Scenario	Model	$RB_{\hat{D}_{slope}}(\%)$	$RB_{\hat{g}_0}(\%)$	$RB_{\hat{\sigma}}(\%)$	$RB_{\hat{D}_F}(\%)$	$RB_{\hat{D}_R}(\%)$
				K = 4		
Sc.E1	Multi-catch	-42.28 (4.27)	-70.15 (0.65)	-0.05 (1.13)	-0.92 (2.23)	1.17 (2.30)
	Single-catch	5.91 (6.83)	-1.10 (1.62)	1.15 (1.12)	0.68 (0.52)	3.43 (2.46)
Sc.E3	Multi-catch	-17.73 (2.68)	-47.73 (1.24)	1.69 (1.50)	-8.84 (2.63)	-3.94 (3.02)
	Single-catch	2.88 (3.03)	0.94 (2.61)	1.19 (1.47)	0.52 (0.62)	-2.44 (2.88)
Sc.E4	Multi-catch	-11.86 (7.47)	-40.94 (1.54)	-0.45 (1.75)	0.00 (2.83)	-0.14 (2.85)
	Single-catch	6.47 (8.72)	1.82 (2.35)	-0.06 (1.76)	2.08 (2.97)	0.28 (2.89)
				K = 6		
Sc.E1	Multi-catch	-43.05 (3.65)	-69.20 (0.69)	-0.09 (1.05)	-4.88 (1.94)	-2.72 (2.05)
	Single-catch	12.84 (6.53)	1.78 (2.07)	0.90 (1.01)	0.00 (2.09)	-1.63 (2.07)
Sc.E3	Multi-catch	-13.53 (2.81)	-48.84 (1.17)	1.42 (1.35)	-6.37 (2.32)	-2.86 (2.41)
	Single-catch	8.23 (3.47)	0.07 (2.01)	0.54 (1.32)	0.83 (2.64)	-2.76 (2.43)
Sc.E4	Multi-catch	-22.43 (7.11)	-40.70 (1.36)	-0.92 (1.51)	3.29 (3.54)	3.80 (3.47)
	Single-catch	-4.57 (8.83)	2.89 (2.30)	-0.38 (1.46)	5.64 (3.73)	4.45 (3.51)

Notes: Relative % bias is shown for each parameter followed by the standard error in parentheses. The DT models use 10 occasions of 24 hours. Twenty single-catch traps spaced 100 m apart are used with $g_0 = 0.2$ and $\sigma = 100$. $RB_{\hat{D}_{slope}}$ is the relative bias in the slope parameter from the exponential density model, $RB_{\hat{D}}$ is the relative bias in mean density over a defined area where $_F$ refers to the full area (with $2 \times \sigma$) and $_R$ to the area spanned by the trap array. The CT model uses a constant hazard that is consistent with a half-normal detection function shape over an interval of 24 hours. In all cases 50 replications were run and converged. Results are reported on the natural scale.

Table C.15: Relative bias (RB) of density and detection parameters estimated by the DT multi and the CT single-catch trap estimators with a 30 hour cyclic cubic spline hazard with K = 4 or K = 6. All models specify a quadratic density model. The data are simulated for a survey duration of $T = 240$ hours from different quadratic density surfaces and a 30 hour cyclic cubic spline hazard with K = 4 or K = 6.

Scenario	Model	$\text{RB}_{\hat{g}_0}(\%)$	$\text{RB}_{\hat{\sigma}}(\%)$	$\text{RB}_{\hat{D}_F}(\%)$	$\text{RB}_{\hat{D}_R}(\%)$
		K = 4			
	Multi-catch	-71.43 (0.57)	1.92 (1.38)	0.63 (2.00)	-8.36 (1.83)
Sc.Q1	Single-catch	1.16 (1.92)	0.88 (1.25)	-0.11 (1.94)	1.74 (2.27)
	Multi-catch	-60.97 (0.96)	7.83 (1.55)	-2.05 (2.38)	-15.26 (1.97)
Sc.Q2	Single-catch	1.93 (1.86)	1.57 (1.16)	-0.28 (2.38)	-1.80 (2.37)
	Multi-catch	-62.64 (0.99)	4.66 (1.47)	-4.95 (1.93)	-6.91 (2.21)
Sc.Q3	Single-catch	4.01 (2.30)	0.59 (1.28)	0.77 (2.15)	0.71 (2.57)
		K = 6			
	Multi-catch	-71.02 (0.69)	2.19 (1.12)	0.53 (1.86)	-11.89 (1.74)
Sc.Q1	Single-catch	1.94 (1.97)	1.95 (1.14)	-0.34 (1.82)	-3.67 (2.33)
	Multi-catch	-59.18 (0.72)	2.45 (1.03)	0.50 (1.80)	-13.38 (1.49)
Sc.Q2	Single-catch	6.07 (1.75)	-2.46 (0.92)	1.79 (1.74)	-1.12 (1.90)
	Multi-catch	-63.69 (0.70)	2.94 (1.21)	-1.33 (1.91)	-0.76 (2.19)
Sc.Q3	Single-catch	-0.36 (2.08)	-0.70 (1.08)	4.51 (2.10)	6.27 (2.58)

Notes: Relative % bias is shown for each parameter followed by the standard error in parentheses. The DT models use 10 occasions of 24 hours. Twenty single-catch traps spaced 100 m apart are used with $g_0 = 0.2$ and $\sigma = 100$. $\text{RB}_{\hat{D}}$ is the relative bias in mean density over a defined area where $_F$ refers to the full area (with $2 \times \sigma$) and $_R$ to the area spanned by the trap array. The CT model uses a spline hazard that is consistent with a half-normal detection function shape over an interval of 24 hours. In all cases 50 replications were run and converged. Results are reported on the natural scale.

Appendix D

Figures from Chapter 4 simulations

D.1 Synchronous spline simulations

Figure D.1: Estimated hazard surfaces from the proximity detector simulation scenarios with exponential density and a 24 hour spline hazard (K = 4 in the top panel and K = 8 in the bottom panel).

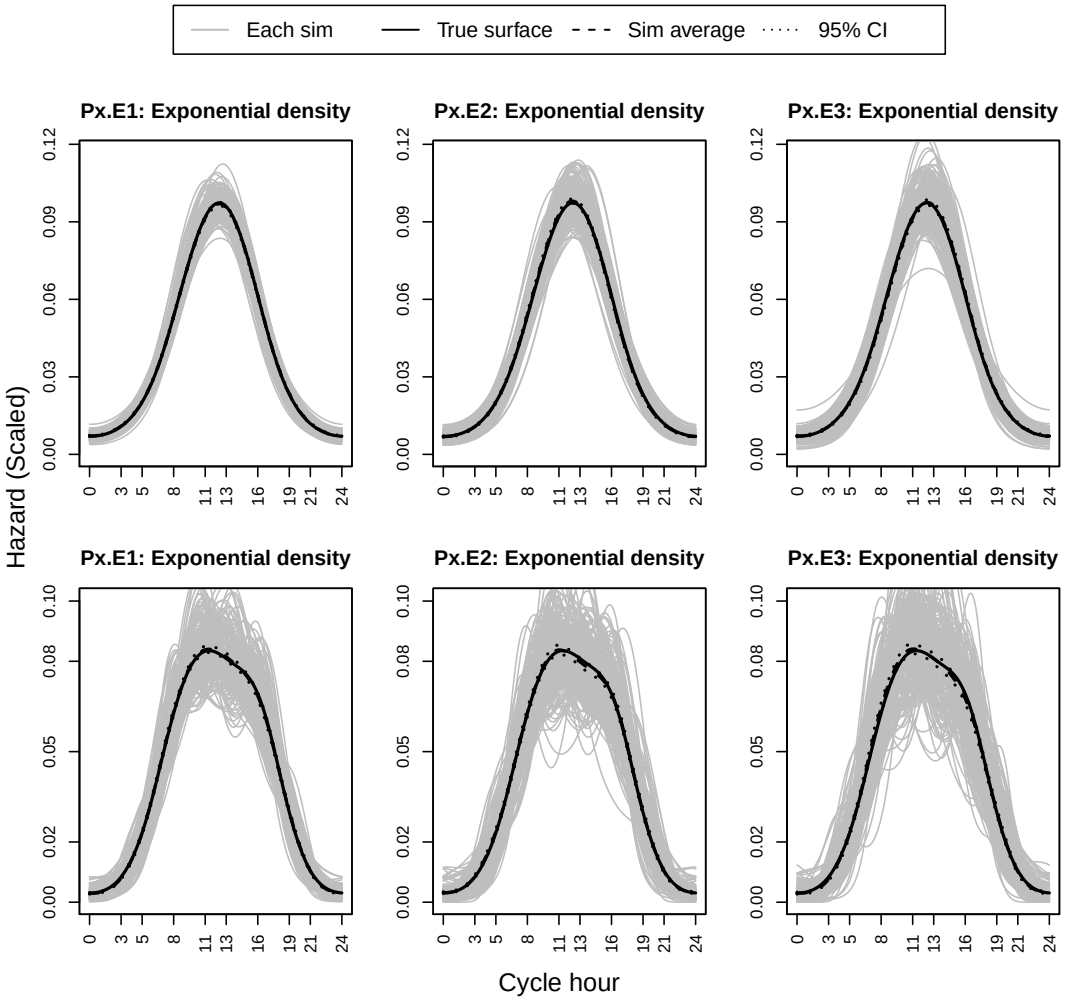

Notes: The black line depicts the true hazard function, the grey lines the estimated hazard functions from each simulation, and the dashed black line the average of the simulations.

Figure D.2: Estimated hazard surfaces from the proximity detector simulation scenarios with quadratic density and a 24 hour spline hazard (K = 4 in the top panel and K = 8 in the bottom panel).

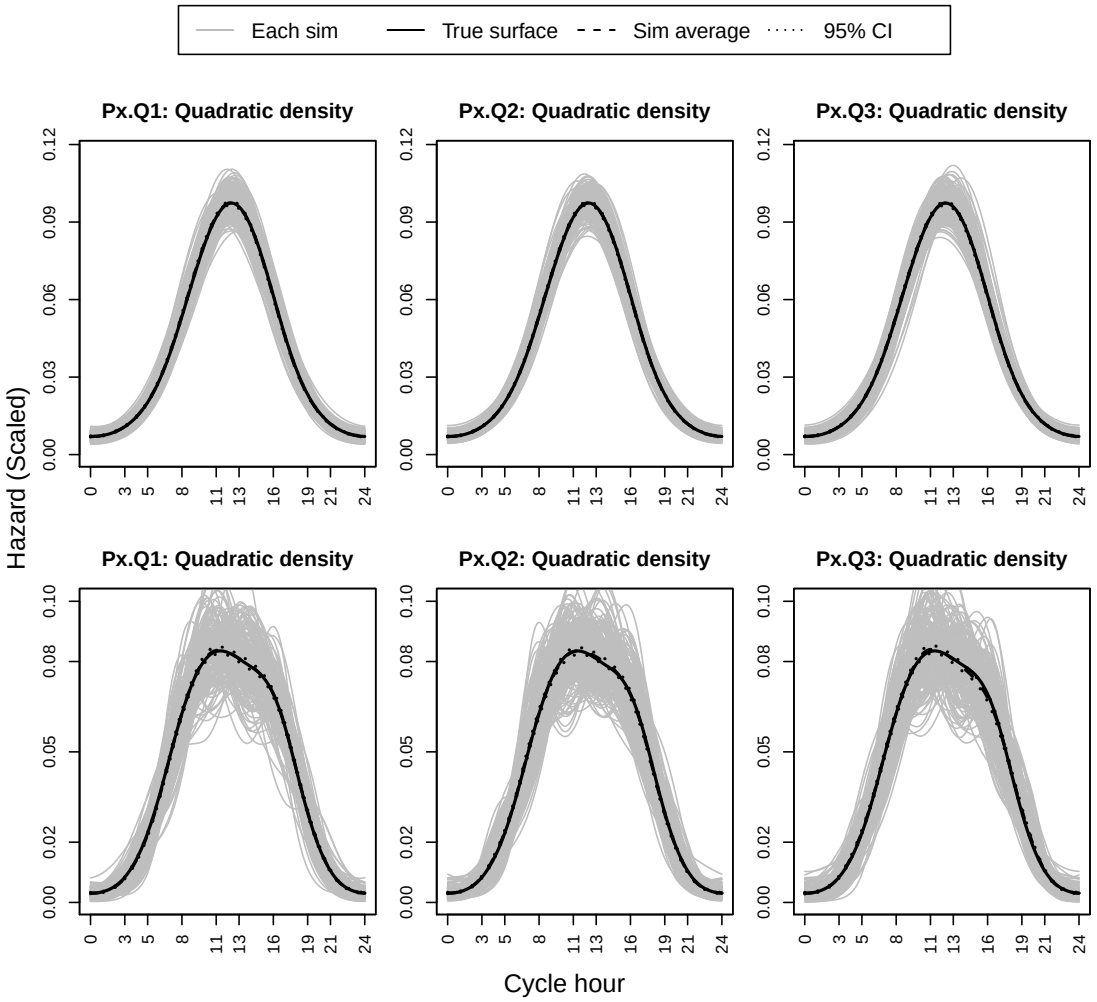

Notes: The black line depicts the true hazard function, the grey lines the estimated hazard functions from each simulation, and the dashed black line the average of the simulations.

Figure D.3: Estimated density surfaces from the proximity detector simulation scenario Px.Q1 with a 24 hour spline hazard (K = 4 in the top panel and K = 8 in the bottom panel).

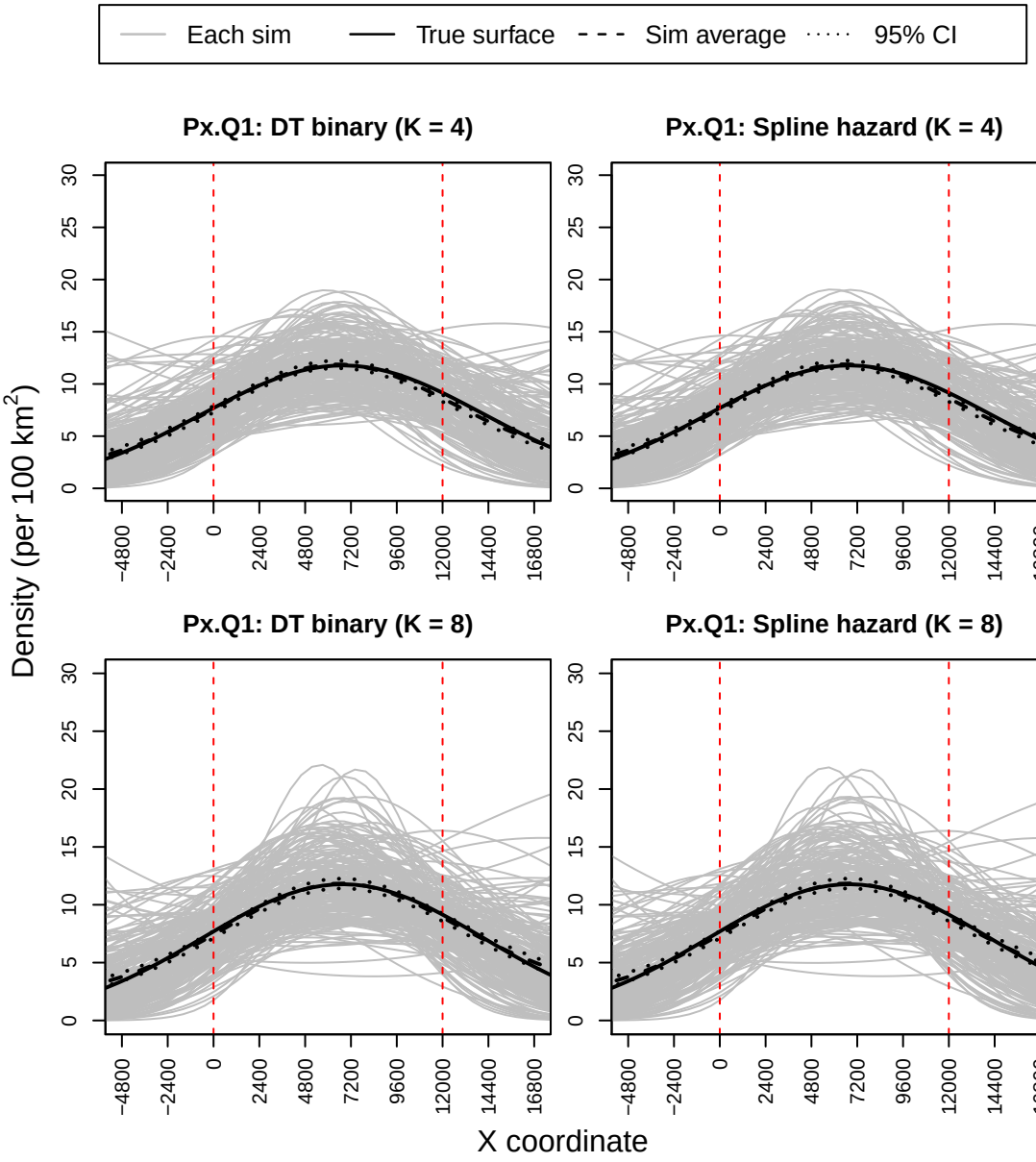

Notes: The black line depicts the true density gradient, the grey lines the estimated density from each simulation, and the dashed black line the average of the simulations.

Figure D.4: Estimated hazard surfaces from the proximity detector simulation scenarios with constant density and a 30 hour spline hazard (K = 4 in the top panel and K = 8 in the bottom panel).

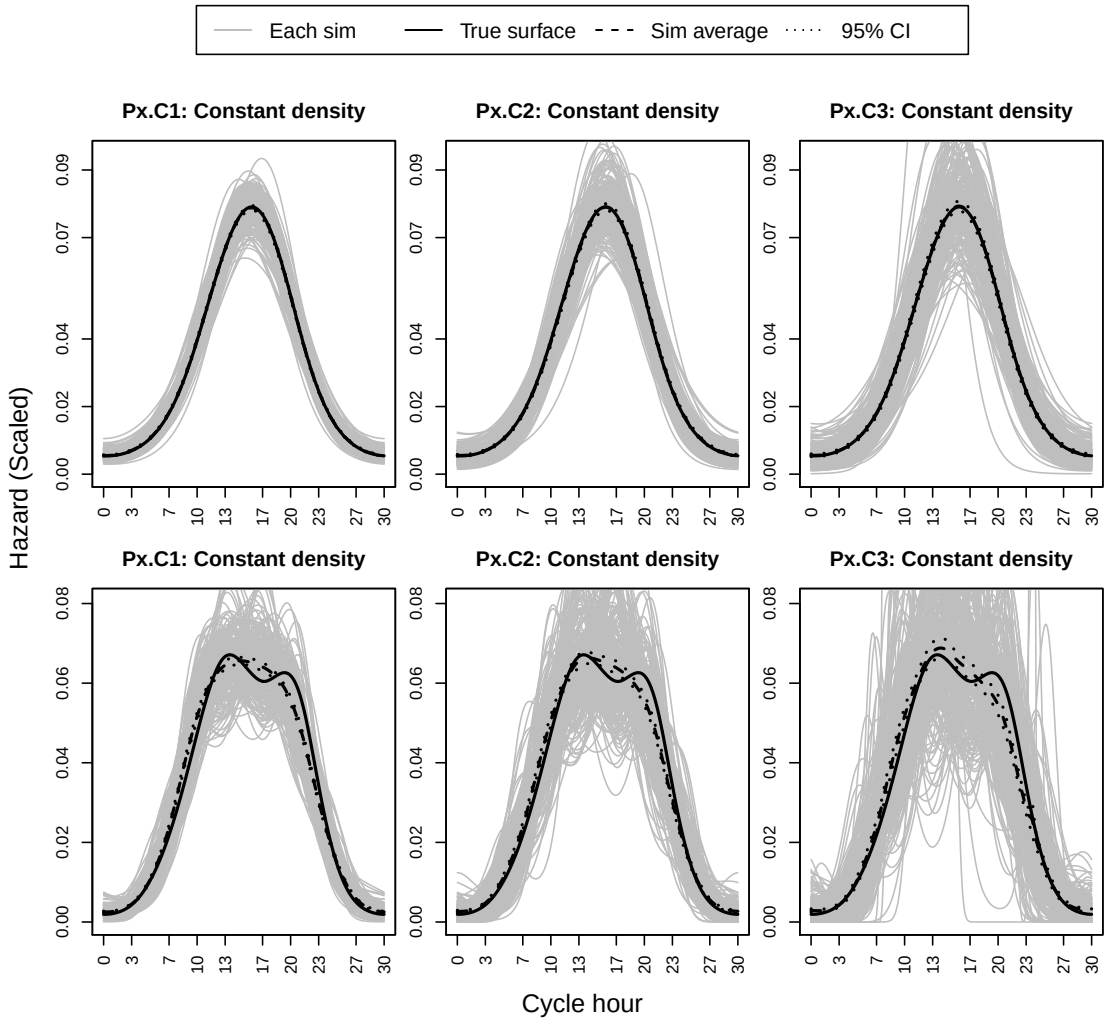

Notes: The black line depicts the true hazard function, the grey lines the estimated hazard functions from each simulation, and the dashed black line the average of the simulations.

Figure D.5: Estimated hazard surfaces from the proximity detector simulation scenarios with exponential density and a 30 hour spline hazard (K = 4 in the top panel and K = 8 in the bottom panel).

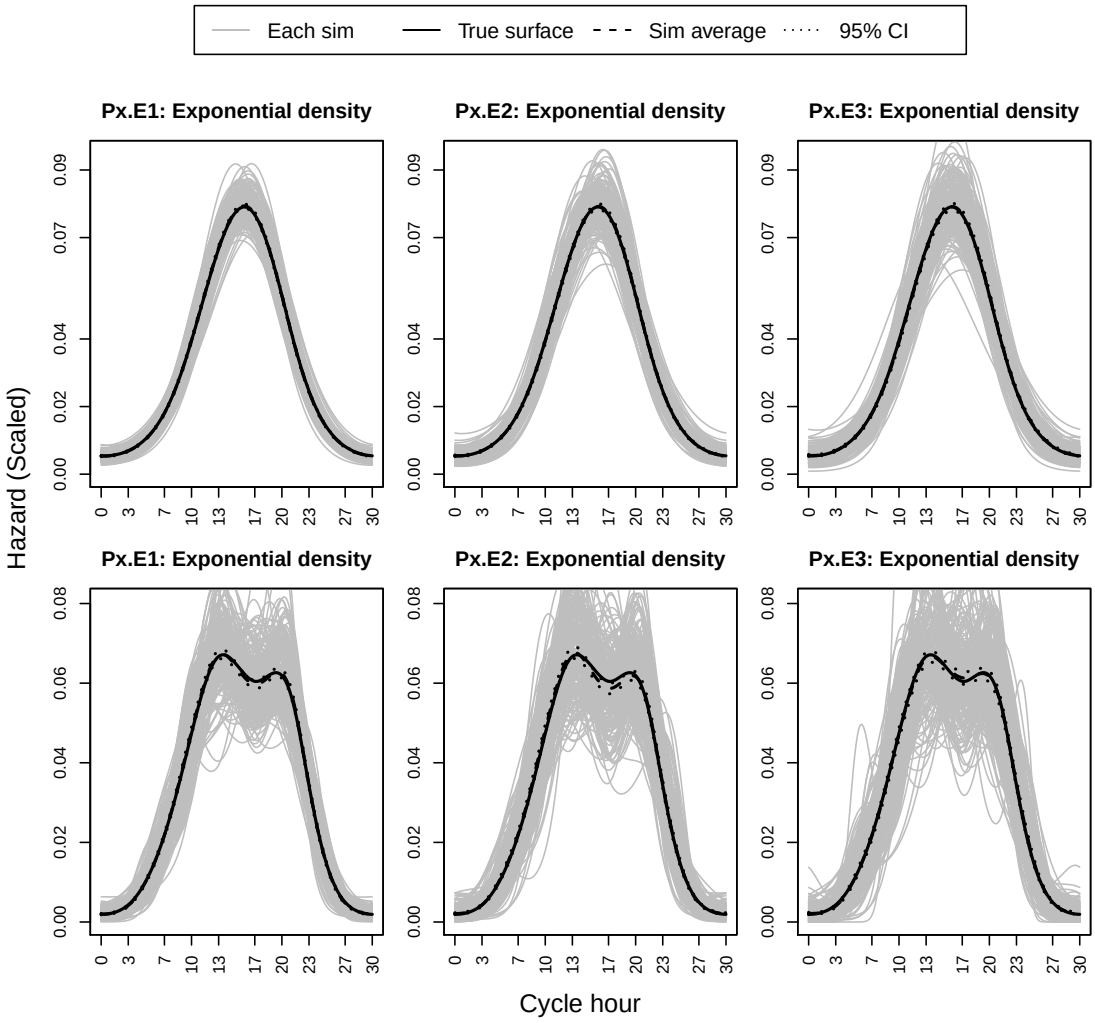

Notes: The black line depicts the true hazard function, the grey lines the estimated hazard functions from each simulation, and the dashed black line the average of the simulations.

Figure D.6: Estimated density surfaces from the proximity detector simulation scenario Px.E2 with a 30 hour spline hazard (K = 4 in the top panel and K = 8 in the bottom panel).

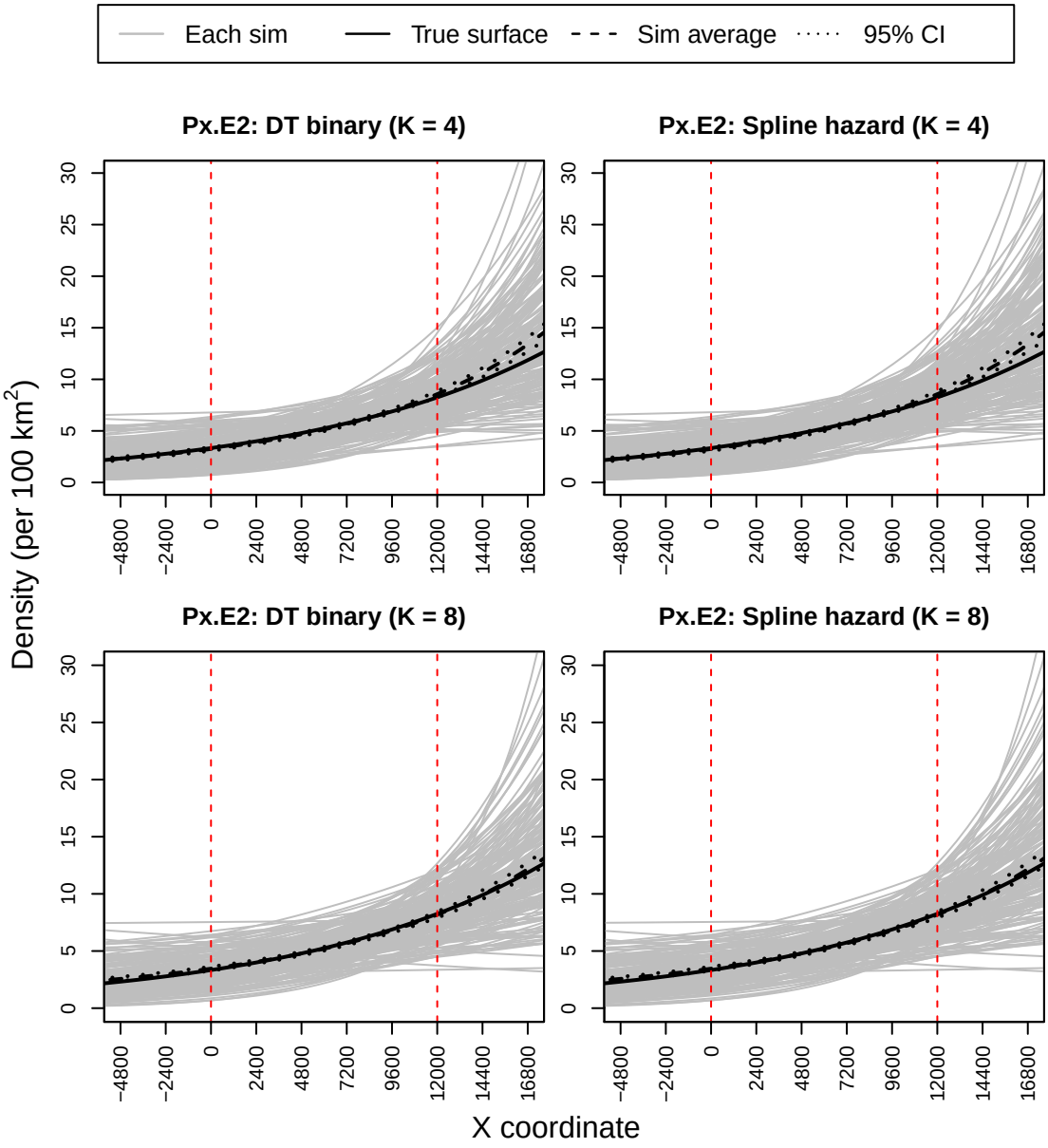

Notes: The black line depicts the true density gradient, the grey lines the estimated density from each simulation, and the dashed black line the average of the simulations.

Figure D.7: Estimated hazard surfaces from the proximity detector simulation scenarios with quadratic density and a 30 hour spline hazard (K = 4 in the top panel and K = 8 in the bottom panel).

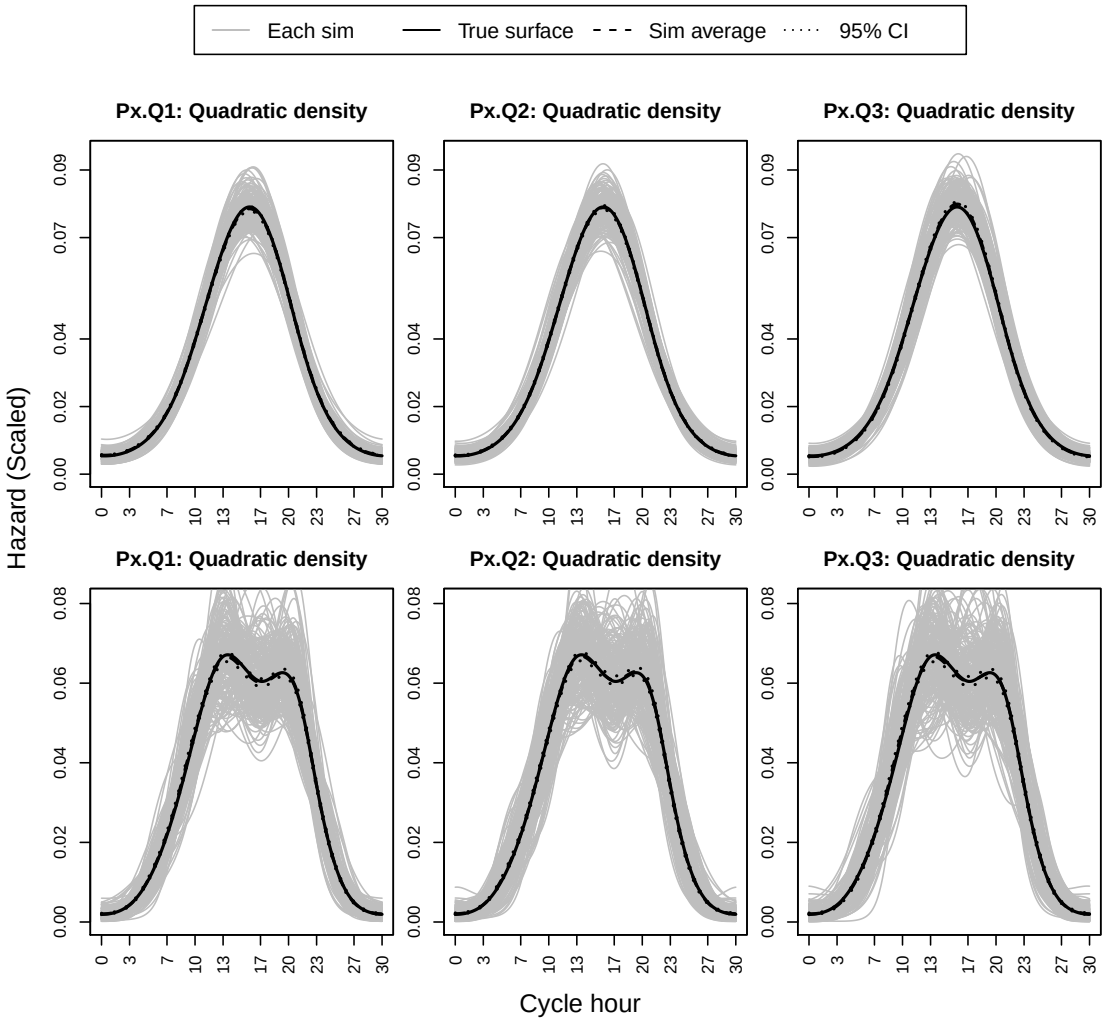

Notes: The black line depicts the true hazard function, the grey lines the estimated hazard functions from each simulation, and the dashed black line the average of the simulations.

Figure D.8: Estimated density surfaces from the proximity detector simulation scenario Px.Q1 with a 30 hour spline hazard (K = 4 in the top panel and K = 8 in the bottom panel).

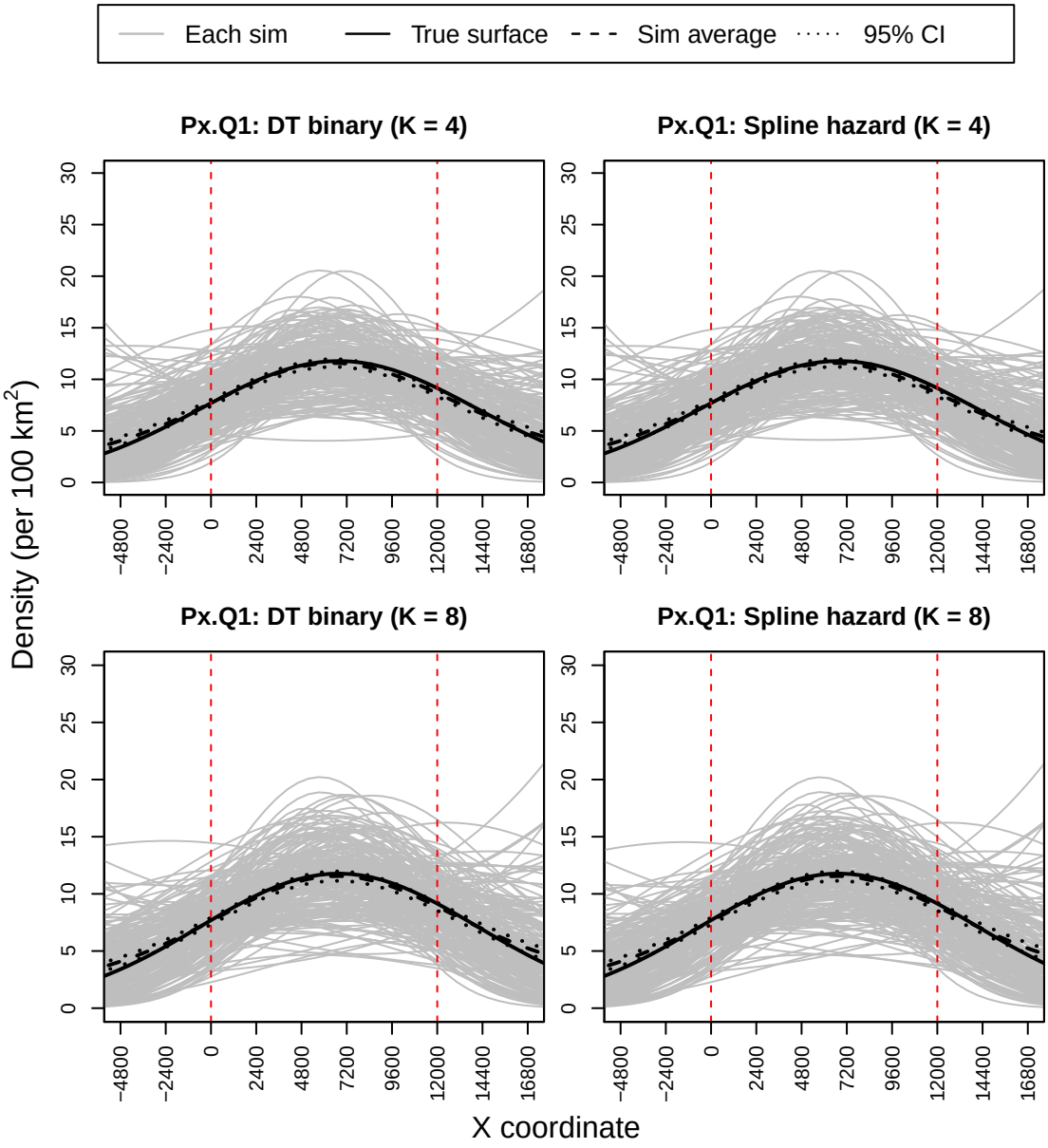

Notes: The black line depicts the true density gradient, the grey lines the estimated density from each simulation, and the dashed black line the average of the simulations.

Figure D.9: Estimated density surfaces from the proximity detector simulation scenario Px.Q2 with an asynchronous spline hazard (K = 8) that has a cycle length of either 30 days (top panel) or 90 days (bottom panel).

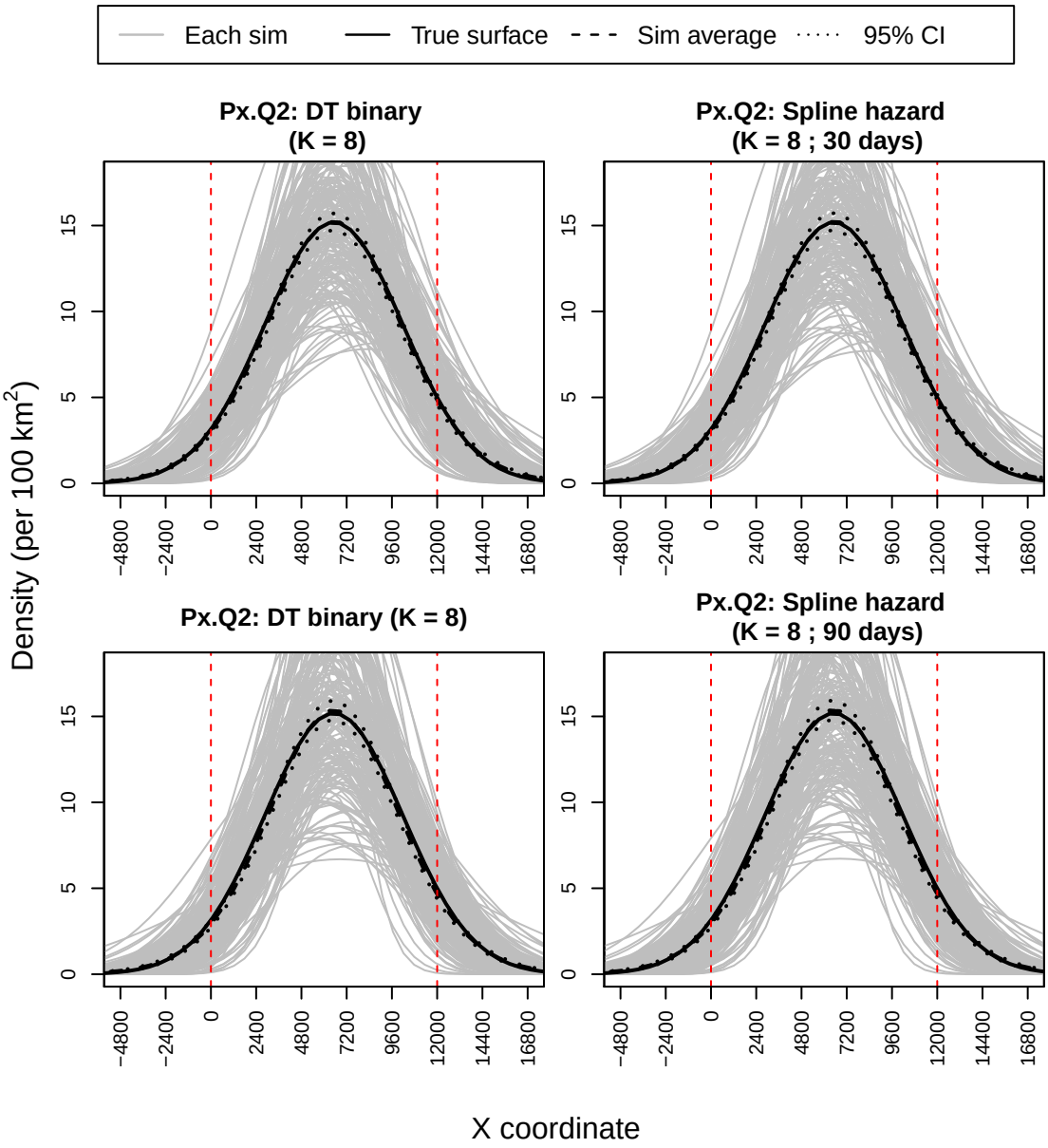

Notes: The black line depicts the true density gradient, the grey lines the estimated density from each simulation, and the dashed black line the average of the simulations.

D.2 Single-catch traps

Figure D.10: Estimated hazard surfaces from the single-catch trap simulation scenarios with constant density, a higher value for g_0 (0.4), and a 30 hour spline hazard (K = 4 in the top panel and K = 6 in the bottom panel).

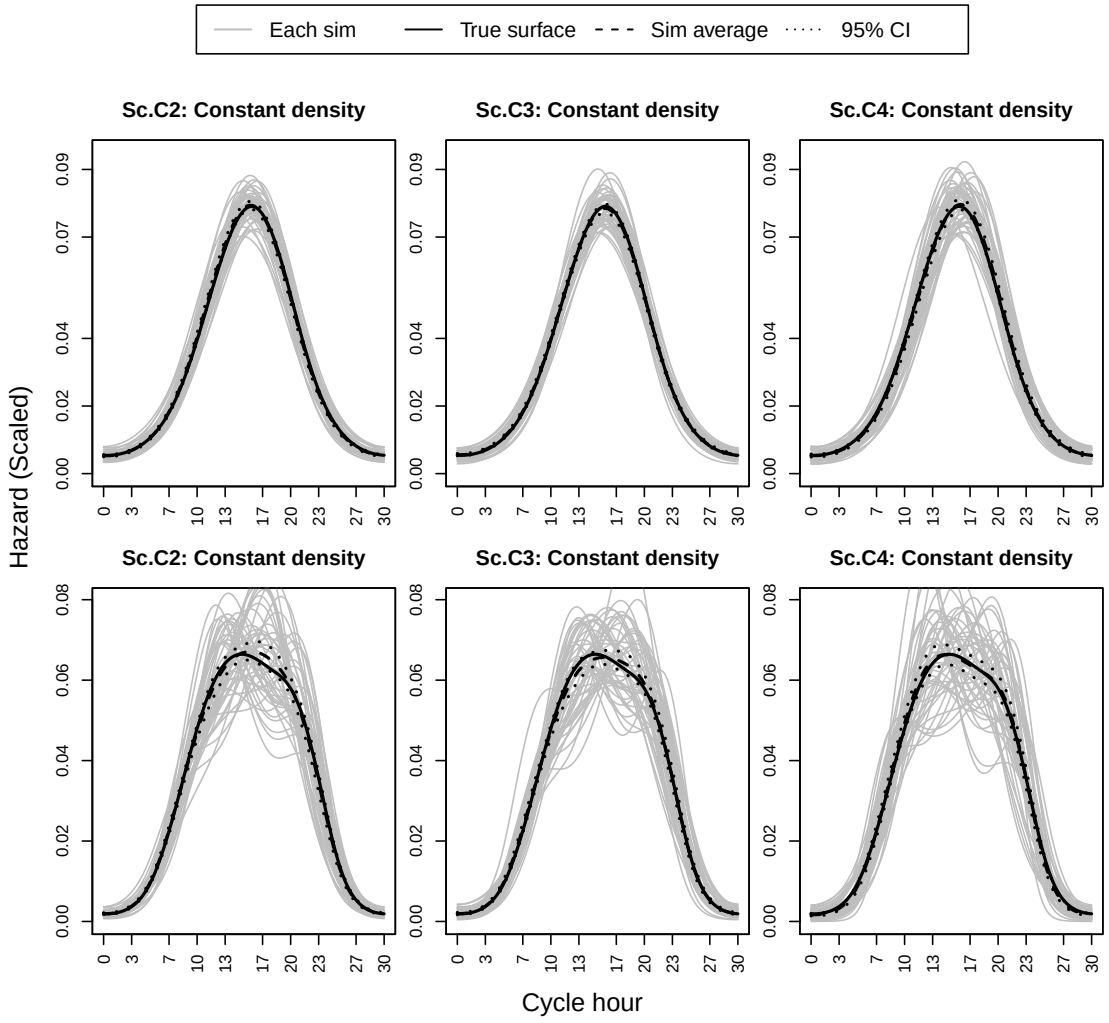

Notes: The black line depicts the true hazard function, the grey lines the estimated hazard functions from each simulation, and the dashed black line the average of the simulations.

Figure D.11: Estimated hazard surfaces from the single-catch trap simulation scenarios with exponential density and a 30 hour spline hazard (K = 4 in the top panel and K = 6 in the bottom panel).

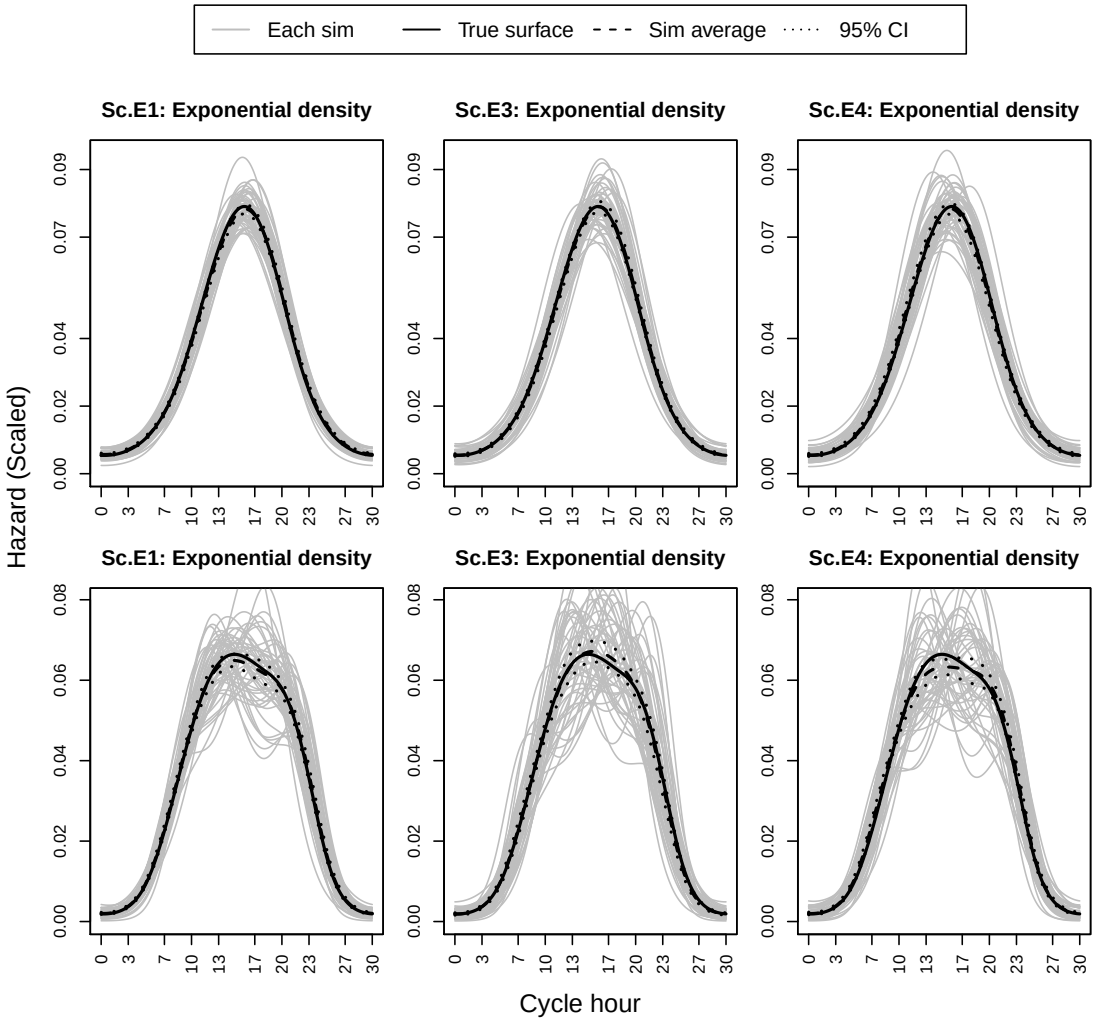

Notes: The black line depicts the true hazard function, the grey lines the estimated hazard functions from each simulation, and the dashed black line the average of the simulations.

Figure D.12: Estimated density surfaces from the single-catch trap simulation scenarios with exponential density gradients and a 30 hour spline hazard with K = 6.

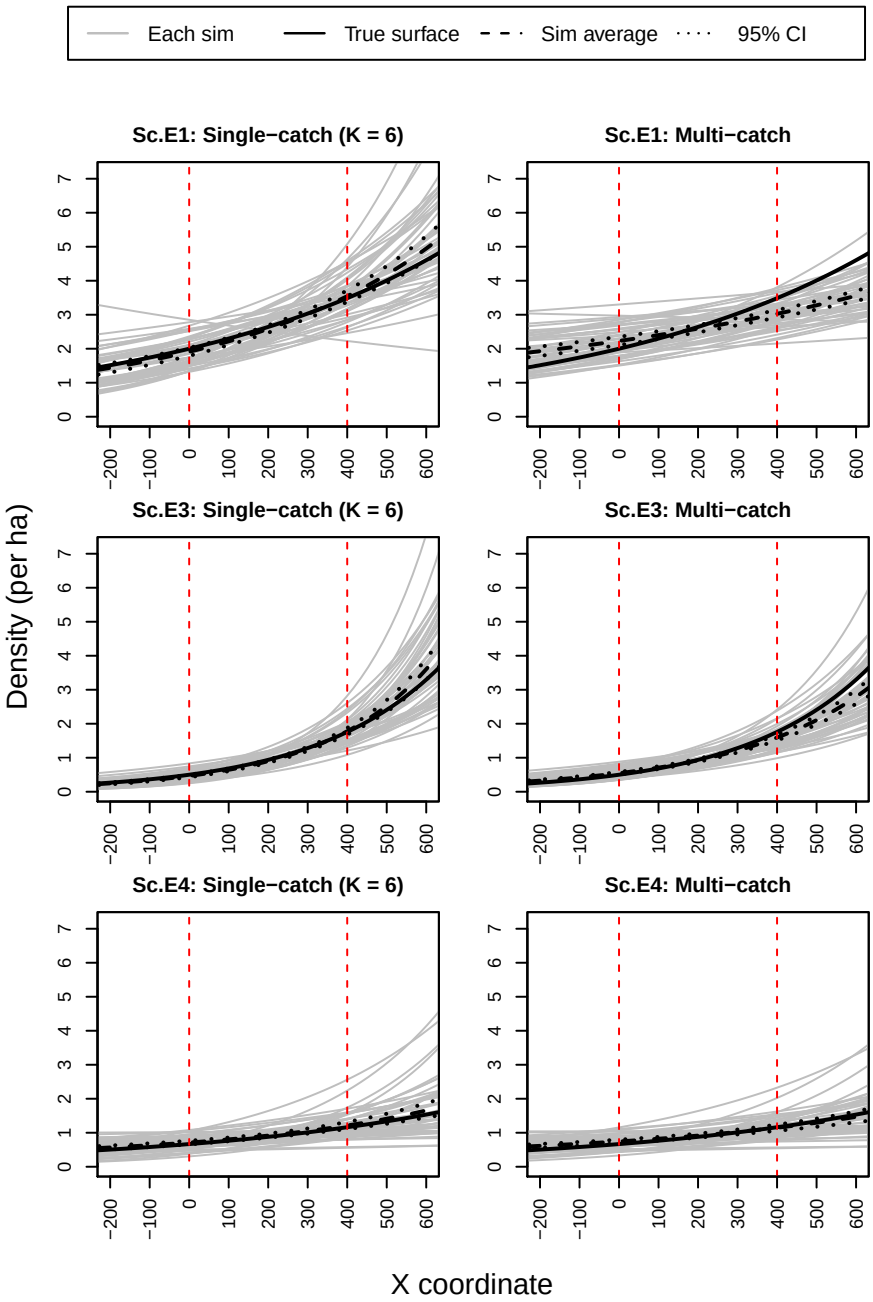

Notes: The black line depicts the true density gradient, the grey lines the estimated density from each simulation, and the dashed black line the average of the simulations.

Figure D.13: Estimated hazard surfaces from the single-catch trap simulation scenarios with quadratic density and a 30 hour spline hazard (K = 4 in the top panel and K = 6 in the bottom panel).

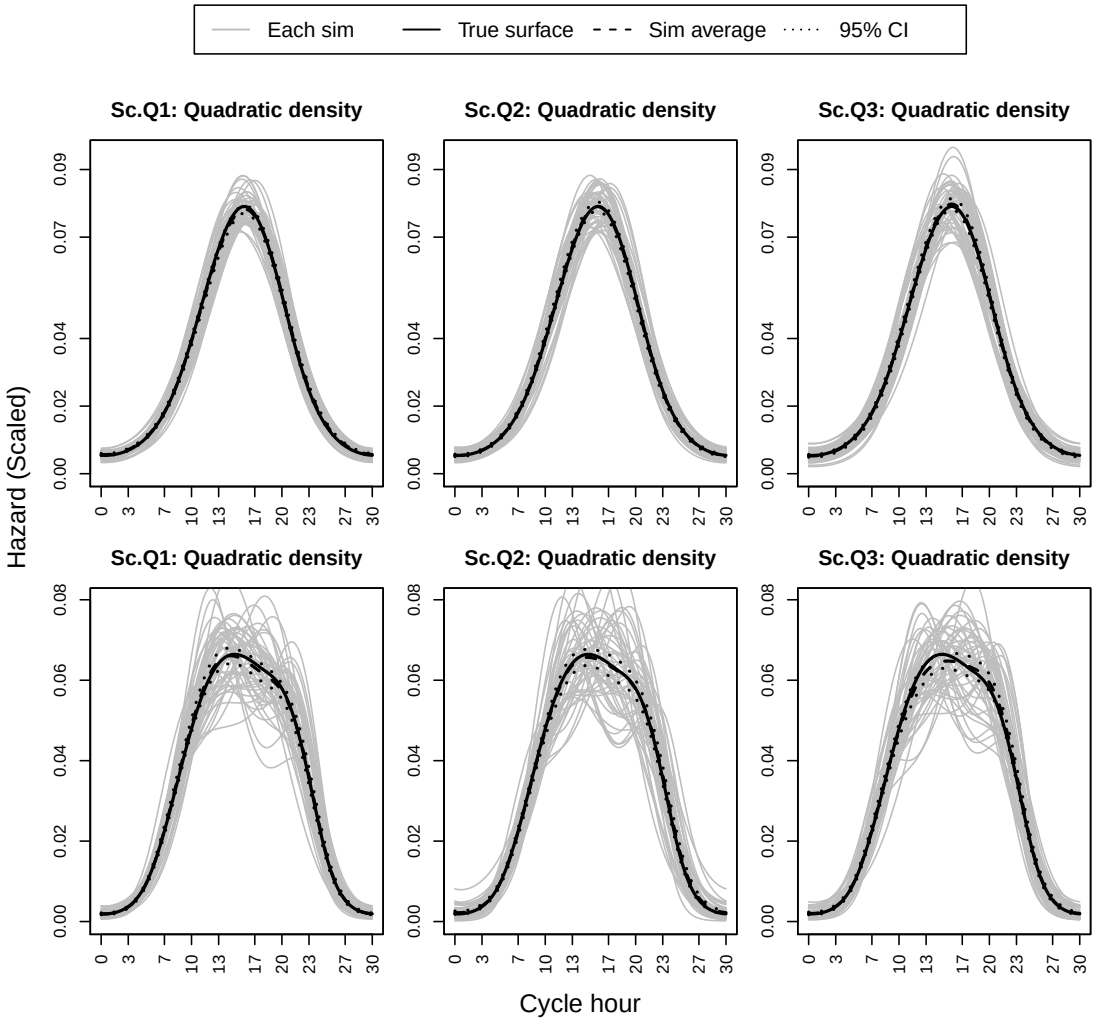

Notes: The black line depicts the true hazard function, the grey lines the estimated hazard functions from each simulation, and the dashed black line the average of the simulations.

Figure D.14: Estimated density surfaces from the single-catch trap simulation scenarios with quadratic density and a 30 hour spline hazard with K = 6.

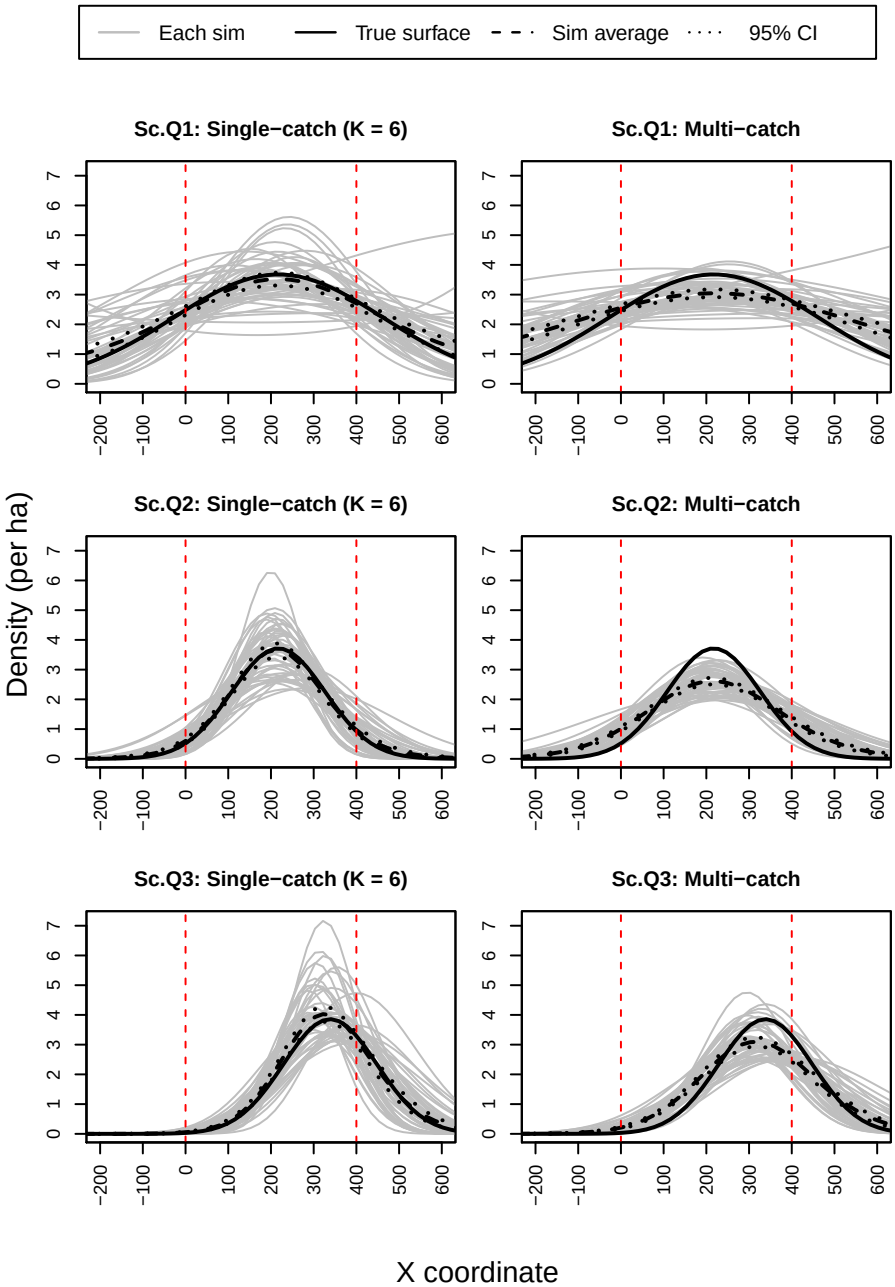

Notes: The black line depicts the true density gradient, the grey lines the estimated density from each simulation, and the dashed black line the average of the simulations.

Bibliography

Balme, G. A., Hunter, L. T. B., and Slotow, R. (2009). Evaluating methods for counting cryptic carnivores. *Journal of Wildlife Management*, 73(3):433–441.

Barbour, A. B., Ponciano, J. M., and Lorenzen, K. (2013). Apparent survival estimation from continuous mark-recapture/resighting data. *Methods in Ecology and Evolution*, 4(9):846–853.

Barker, R., Schofield, M., Wright, J., Frantz, A., and Stevens, C. (2014). Closed-population capture-recapture modeling of samples drawn one at a time. *Biometrics*, 70:775–782.

Becker, N. G. (1984). Estimating population size from capture-recapture experiments in continous time. *Australian Journal of Statistics*, 26:1–7.

Becker, N. G. and Heyde, C. C. (1990). Estimating population size from multiple recapture experiments. *Stochastic Processes and their Applications*, 36:77–83.

Beyersmann, J., Latouche, A., Buchholz, A., and Schumacher, M. (2009). Simulating competing risks data in survival analysis. *Statistics in Medicine*, 28:956–971.

Borchers, D. (2012). A non-technical overview of spatially explicit capture-recapture models. *Journal of Ornithology*, 152(2):435–444.

Borchers, D. (2016). Spatial capture-recapture models. *Statistical Science*.

Borchers, D. and Efford, M. (2008). Spatially explicit maximum likelihood methods for capture-recapture studies. *Biometrics*, 64:377–385.

Borchers, D. and Marques, T. (2016). A review of spatial capture-recapture and distance sampling models. *Advances in Statistical Analysis, Ecological Statistics Special Issue*, in press.

Bourgon, R. (2015). *intervals: Tools for Working with Points and Intervals*. R package version 0.15.1.

Boyce, M. S., Mackenzie, D. I., Manly, B. F., Haroldson, M. A., and Moody, D. (2001). Negative binomial models for abundance estimation of multiple closed populations. *Journal of Wildlife Management*, 65(3):498–509.

Buckland, S., Anderson, D. R., Burnham, K., and Laake, J. (1993). *Distance sampling: estimating abundance of biological populations.* Chapman and Hall.

Campbell, D. (1990). Changes in the structure and composition of a New Zealand lowland forest inhabited by brushtail possums. *Pacific Science*, 44:277–96.

Carbone, C., Christie, S., Conforti, K., Coulsen, T., Franklin, N., Ginsberg, J. R., Griffiths, M., Holden, J., Kawanishi, K., Kinnaird, M., Laidlaw, R., Lynam, A., Macdonald, D. W., Martyr, D., McDougal, C., Nath, L., O'Brien, T., Seidensticker, J., Smith, D. J. L., Sunquist, M., Tilson, R., and Shahruddin, W. N. W. (2001). The use of photographic rates to estimate densities of tigers and other cryptic mammals. *Animal Conservation*, 4:75–79.

Caso, A., Lopez-Gonzalez, C., Payan, E., Eizirik, E., de Oliveira, T., Leite-Pitman, R., Kelly, M., and Valderrama, C. (2008). Panthera onca. In *The IUCN Red List of Threatened Species.* Version 2013.2 (www.iucnredlist.org) Downloaded on 21 November 2013.

Chao, A. (2001). An overview of closed capture-recapture models. *Journal of Agricultural, Biological, and Environmental Statistics*, 6(2):158–175.

Chao, A. and Huggins, R. (2005). Modern closed-population capture-recapture models. In Amstrup, S. C., McDonald, T. L., and Manly, B. F. J., editors, *Handbook of capture-recapture analysis*, chapter 4, pages 58–87. Princeton University Press.

Chao, A. and Lee, S. M. (1993). Estimating population size for continuous-time capture-recapture models via sample coverage. *Biometrical Journal*, 35:29–45.

Codling, E. A., Plank, M. J., and Benhamou, S. (2008). Random walks in biology. *Journal of the Royal Society Interface*, 5:813–834.

Conn, P., Johnson, D., and Boveng, P. (2015). On extrapolating past the range of observed data when making statistical predictions in ecology. *Plos ONE*, 10(10).

Cook, R. and Lawless, J. (2007). *The statistical analysis of recurrent events.* Springer.

Cormack, R. (1965). Estimates of survival from the sighting of marked animals. *Biometrika*, 51:429–438.

Cowan, P. and Forrester, G. (2012). Behavioural responses of brushtail possums to live trapping and implications for trap-catch correction. *Wildlife Research*, 39:343–349.

Craig, C. C. (1953). On the utilization of marked specimens in estimating populations of flying insects. *Biometrika*, 40(1):170–176.

Darroch, J. (1958). The multiple-recapture census: I. estimation of a closed population. *Biometrika*, 45(3/4):343–359.

Dice, L. R. (1938). Some census methods for mammals. *Journal of Wildlife Management*, 2:119–130.

Dillon, A. (2005). Ocelot density and home range in Belize, Central America: camera-trapping and radio telemetry. Master's thesis, Virginia Polytechnic Institute and State University, Blacksburg, Virginia.

Dillon, A. and Kelly, M. J. (2007). Ocelot leopardus pardalis in Belize: the impact of trap spacing and distance moved on density estimates. *Oryx*, 41(4):469–477.

Efford, M. (2004). Density estimation in live-trapping studies journal. *Oikos*, 106:598–610.

Efford, M. (2016). *secr: Spatially explicit capture-recapture models*. R package version 2.10.2.

Efford, M. and Cowan, P. (2004). Long-term population trend of the common brushtail possum trichosurus vulpecula in the Orongorongo Valley, New Zealand. In Goldingay, R. and Jackson, S., editors, *The biology of Australian possums and gliders.*, chapter 39. Surrey Beatty and Sons, Chipping Norton, Sydney.

Efford, M. G., Borchers, D. L., and Byrom, A. E. (2009a). Density estimation by spatially explicit capture-recapture: Likelihood-based methods. In Thomson, D., Cooch, E., and Conroy, M., editors, *Modeling Demographic Processes in Marked Populations*, pages 255–269. Springer, New York, New York, USA.

Efford, M. G., Borchers, D. L., and Mowat, G. (2013). Varying effort in capture-recapture studies. *Methods in Ecology and Evolution*, 4(7):629–636.

Efford, M. G., Dawson, D. K., and Borchers, D. L. (2009b). Population density estimated from locations of individuals on a passive detector array. *Ecology*, 90(10):2676–2682.

Fewster, R. and Buckland, S. (2004). Assessment of distance sampling estimators. In Buckland, S., Anderson, D., Burnham, K., Laake, J., Borchers, D., and Thomas, L., editors, *Advanced Distance Sampling*, chapter 10, pages 281–306. Oxford University Press, Oxford, UK.

Foster, R. J. and Harmsen, B. J. (2012). A critique of density estimation from camera-trap data. *The Journal of Wildlife Management*, 76:224–236.

Foster, R. J., Harmsen, B. J., and Doncaster, C. P. (2010). Habitat use by sympatric jaguars and pumas across a gradient of human disturbance in Belize. *Biotropica*, 42(6):724–731.

Fuller, A., Sutherland, C., Royle, J., and Hare, M. (2015). Estimating population density and connectivity of american mink using spatial capture-recapture. *Ecological Applications*.

Gardner, B., Reppucci, J., Lucherini, M., and Royle, J. A. (2010). Spatially explicit inference for open populations: estimating demographic parameters from camera-trap studies. *Ecology*, 11:3376–3383.

Gardner, B., Royle, J. A., and Wegan, M. T. (2009). Hierarchical models for estimating density from dna mark-recapture studies. *Ecology*, 90(4):1106–1115.

Gaston, K. (2003). *The structure and dynamics of geographic ranges.* Oxford University Press, Oxford.

Gerber, B. D., Karpanty, S. M., and Kelly, M. J. (2012). Evaluating the potential biases in carnivore capture-recapture studies associated with the use of lure and varying density estimation techniques using photographic-sampling data of the malagasy civet. *Population Ecology*, 54:43–54.

Gerber, B. D. and Parmenter, R. R. (2015). Spatial capture-recapture model performance with known small-mammal densities. *Ecological Applications*, 25(3):695–705.

Goldberg, J., Tempa, T., Norbu, N., Hebblewhite, M., Mills, S., Wangchuk, T., and Lukacs, P. (2015). Examining temporal sample scale and model choice with

spatial capture-recapture models in the common leopard panthera pardus. *PLoS One*, 10(11).

Griffiths, M. and van Schaik, C. P. (1993). The impact of human traffic on the abundance and activity periods of sumatran rain forest wildlife. *Conservation Biology*, 7(3):623–626.

Harmsen, B., Foster, R., Silver, S., Ostro, L., and Doncaster, C. (2009). Spatial and temporal interactions of sympatric jaguars and pumas in a neotropical forest. *Journal of Mammalogy*, 90(3):612–620.

Harmsen, B., Foster, R., Silver, S., Ostro, L., and Doncaster, C. (2011). Jaguar and puma activity patterns in relation to their main prey. *Mammalian Biology*, 76(3):320–324.

Harmsen, B. J., Foster, R. J., Silver, S., Ostro, L., and Doncaster, C. P. (2010a). Differential use of trails by forest mammals and the implications for camera-trap studies: A case study from Belize. *Biotropica*, 42(1):126–133.

Harmsen, B. J., Foster, R. J., Silver, S. C., Ostro, L. E., and Doncaster, C. P. (2010b). The ecology of jaguars in the Cockscomb Basin Wildlife Sanctuary, Belize. In MacDonald, D. W. and Loveridge, A. J., editors, *The Biology and Conservation of Wild Felids*, chapter 18, pages 403–416. Oxford University Press.

Hwang, W. and Chao, A. (2002). Continuous-time capture-recapture models with covariates. *Statistica Sinica*, 12:1115–1131.

Hwang, W., Chao, A., and Yip, P. (2002). Continuous-time capture-recapture models with time variation and behavioural response. *Australian and New Zealand Journal of Statistics*, 44:41–54.

Ivan, J. S., White, G. C., and Shenk, T. M. (2013a). Using auxiliary telemetry information to estimate animal density from capture-recapture data. *Ecology*, 94:809–816.

Ivan, J. S., White, G. C., and Shenk, T. M. (2013b). Using simulation to compare methods for estimating density from capture-recapture data. *Ecology*, 94:817–826.

Jolly, G. (1965). Explicit estimates from capture-recapture data with both death and immigration: stochastic model. *Biometrika*, 52:225–247.

Jordan, M., Barrett, R., and Purcell, K. (2011). Camera trapping estimates of density and survival of fishers (Martes pennanti). *Wildlife Biology*, 17:266–276.

Karanth, K. U. (1995). Estimating tiger panthera tigris populations from camera trap data using capture-recapture models. *Biological Conservation*, 71:333–338.

Karanth, K. U., Chundawat, R. S., Nichols, J. D., and Kumar, N. S. (2004). Estimation of tiger densities in the tropical dry forests of panna, central india, using photographic capture–recapture sampling. *Animal Conservation*, 7:285–290.

Karanth, K. U. and Nichols, J. D. (1998). Estimation of tiger densities in india using photographic captures and recaptures. *Ecology*, 79(8):2852–2862.

Karanth, K. U., Nichols, J. D., Kumar, N. S., and Hines, J. E. (2006). Assessing tiger population dynamics using photographic capture-recapture sampling. *Ecology*, 11:2925–2937.

Kery, M., Gardener, B., Stoeckle, T., and Weber, D. (2011). Use of spatial capture-recapture modeling and DNA data to estimate densities of elusive animals. *Conservation Biology*, 25(2):356–364.

Krebs, C. J., Boonstra, R., Gilbert, S., Reid, D., Kenney, A. J., and Hofer, E. J. (2011). Density estimation for small mammals from livetrapping grids: rodents in northern canada. *Journal of Mammalogy*, 92(5):974–981.

Langrock, R., King, R., Matthiopoulos, J., Thomas, L., Fortin, D., and Morales, J. M. (2012). Flexible and practical modeling of animal telemetry data: hidden markov models and extensions. *Ecology*, 93(11):2336–2342.

Lin, D. Y. and Yip, P. S. F. (1999). Parametric regression models for continuous time removal and recapture studies. *Journal of the Royal Statistical Society: Series B*, 61(2):401–411.

Linkie, M., Dinata, Y., Nugroho, A., and Achmad Haidir, I. (2007). Estimating occupancy of a data deficient mammalian species living in tropical rainforests: Sun bears in the kerinci seblat region, sumatra. *Biological Conservation*, 137(1):20–27.

Maffei, L., Cuellar, E., and Noss, A. (2004). One thousand jaguars (panthera onca) in bolivia's chaco? camera trapping in the kaa-iya national park. *Journal of Zoology*, 262:295–304.

Maffei, L. and Noss, A. (2008). How small is too small? camera trap survey areas and density estimates for ocelots in the bolivian chaco. *Biotropica*, 40(1):71–75.

Marques, T., Thomas, L., Martin, S., Mellinger, D., Ward, J., Moretti, D., Harris, D., and Tyack, P. (2013). Estimating animal population density using passive acoustics. *Biological Reviews*, 88(2):287–309.

Morales, J. M., Haydon, D. T., Frair, J., Holsinger, K. E., and Fryxell, J. M. (2004). Extracting more out of relocation data: building movement models as mixtures of random walks. *Ecology*, 85(9):2436–2445.

Nayak, T. (1988). Estimating population size by recapture sampling. *Biometrika*, 75:113–120.

Noss, A. J., Gardner, B., Maffei, L., Cuellar, E., Montano, R., Romero-Munoz, A., Sollman, R., and O'Connell, A. F. (2012). Comparison of density estimation methods for mammal populations with camera traps in the kaa-iya del gran chaco landscape. *Animal Conservation*, doi: 10.1111/j.1469-1795.2012.00545.x.

Obbard, M. E., Howe, E. J., and Kyle, C. J. (2010). Empirical comparison of density estimators for large carnivores. *Journal of Applied Ecology*, 47:76–84.

R Core Team (2015). *R: A Language and Environment for Statistical Computing*. R Foundation for Statistical Computing, Vienna, Austria.

Reich, B. and Gardner, B. (2014). A spatial capture-recapture model for territorial species. *Environmetrics*, 25:630–637.

Ridout, M. S. and Linkie, M. (2009). Estimating overlap of daily activity patterns from camera trap data. *Journal of Agricultural, Biological, and Environmental Statistics*, 14(3):322–337.

Rowcliffe, J. and Carbone, C. (2008). Surveys using camera traps: are we looking to a brighter future? *Animal Conservation*, 11(3):185–186.

Royle, J., Chandler, R., Gazenski, K., and Graves, T. (2013a). Spatial capture-recapture models for jointly estimating population density and landscape connectivity. *Ecology*, 94(2):287–294.

Royle, J., Chandler, R., Sun, C., and Fuller, A. (2013b). Integrating resource selection information with spatial capture-recapture. *Methods in Ecology and Evolution*, 4:520–530.

Royle, J., Chandler, R. B., Sollmann, R., and Gardner, B. (2013c). *Spatial Capture-Recapture*. Academic Press.

Royle, J. A., Karanth, K. U., Gopalaswamy, A. M., and Kumar, N. S. (2009a). Bayesian inference in camera trapping studies for a class of spatial capture-recapture models. *Ecology*, 11:3233–3244.

Royle, J. A., Nichols, J. D., Karanth, K. U., and Gopalaswamy, A. M. (2009b). A hierarchical model for estimating density in camera-trap studies. *Journal of Applied Ecology*, 46:118–127.

Royle, J. A. and Young, K. V. (2008). A hierarchical model for spatial capture-recapture. *Ecology*, 89(8):2281–2289.

Sadleir, R. (2000). Evidence of possums as predators of native animals. In Montague, T., editor, *The brushtail possum: : biology, impact and management of an introduced marsupial.*, pages 126–31. Manaaki Whenua Press, Christchurch, New Zealand.

Seber, G. (1965). A note on the multiple-recapture census. *Biometrika*, 52:249–259.

Silver, S. C., Ostro, L. E. T., Marsh, L. K., Maffei, L., Noss, A. J., Kelly, M. J., Wallace, R. B., Gomez, H., and Ayala, G. (2004). The use of camera traps for estimating jaguar panthera onca abundance and density using capture/recapture analysis. *Oryx*, 38(2):148–154.

Smouse, P. E., Focardi, Moorcroft, P. R., Kie, J. G., Forester, J. D., and Morales, J. M. (2010). Stochastic modelling of animal movement. *Philosophical Transactions of the Royal Society B*, 365:2201–2211.

Soisalo, M. K. and Cavalcanti, S. M. C. (2006). Estimating the density of a jaguar population in the Brazilian pantanal using camera-traps and capture-recapture sampling in combination with gps radio-telemetry. *Biological Conservation*, 129:487–496.

Stuart, S. N., Chanson, J., Cox, N., Young, B., Rodrigues, A., Fischmann, D., and Waller, R. (2004). Status and trends of amphibian declines and extinctions worldwide. *Science*, 306:1783–1786.

Sutherland, C., Fuller, A., and Royle, J. (2015). Modelling non-euclidean movement and landscape connectivity in highly structured ecological networks. *Methods in Ecology and Evolution*, 6:169–177.

Thompson, W. L. (2004). *Sampling rare or elusive species: concepts, designs, and techniques for estimating population parameters.* Island Press, Washington, D.C., USA.

Tobler, M., Carrillo-Percastegui, S. E., Leite Pitman, R., Mares, R., and Powell, G. (2008). An evaluation of camera traps for inventorying large- and medium-sized terrestrial rainforest mammals. *Animal Conservation*, 11(3):169–178.

Tobler, M. W. and Powell, G. V. N. (2013). Estimating jaguar densities with camera traps: Problems with current designs and recommendations for future studies. *Biological Conservation*, 159:109–118.

Trolle, M., Noss, A. J., Lima, E. D. S., and Dalponte, J. C. (2007). Camera-trap studies of maned wolf density in the cerrado and the pantanal of brazil. *Biodiversity and Conservation*, 16:1197–1204.

White, G. C., Anderson, D. R., Burnham, K. P., and Otis, D. L. (1982). Capture-recapture and removal methods for sampling closed populations. Technical Report LA 8787-NERP, Los Alamos National Laboratory, Los Alamos.

Williams, B. K., Nichols, J. D., and Conroy, M. J. (2002). *Analysis and Management of Animal Populations.* Academic Press.

Wilson, K. R. and Anderson, D. R. (1995). Continuous-time capture-recapture population estimation when capture probabilities vary over time. *Environmental and Ecological Statistics*, 2:55–69.

Wood, S. (2016). *mgcv: Mixed GAM computation vehicle with GCV / AIC / REML smoothness estimation.* Version 1.8.1.

Xi, L., Yip, P., and Watson, R. (2007). A unified likelihood-based approach for estimating population size in continuous-time capture-recapture experiments with frailty. *Biometrics*, 63:228–236.

Yip, P. (1989). An inference procedure for a capture and recapture experiment with time-dependent capture probabilities. *Biometrics*, 45(2):471–479.

Yip, P., Zhou, Y., Lin, D., and Fang, X. (1999). Estimation of population size based on additive hazards models for continuous-time recapture experimets. *Biometrics*, 55:904–908.

Yip, P. S. F., Huggins, R. M., and Lin, D. Y. (1995). Inference for capture-recapture experiments in continuous time with variable capture rates. *Biometrika*, 83(2):477–483.

Yip, P. S. F. and Wang, Y. (2002). A unified regression model for recapture studies with random removals in continuous time. *Biometrics*, 58:192–199.

Zeller, K., McGarigal, K., and Whiteley, A. (2012). Estimating landscape resistance to movement: a review. *Landscape Ecology*, 27(6):777–797.